

# Self-Assembling Behaviour of the Peptide Hormone PYY<sub>3-36</sub> and its Lipidated Conjugates for Future Applications in Controlling Satiety Levels



**Samuel Burholt**

Submitted in accordance with the requirements for the degree of  
Doctor of Philosophy

University of Reading  
Department of Chemistry  
October 2019

The candidate confirms that the work submitted is his own, except where work which has formed part of jointly authored publications has been included. The contribution of the candidate and the other authors to this work has been explicitly indicated below. The candidate confirms that appropriate credit has been given within the thesis where reference has been made to the work of others. Details of the jointly authored publications and the contributions of the candidate and the other authors to the work are outlined on the page iii.

This copy has been supplied on the understanding that it is copyright material and that no quotation from the thesis may be published without proper acknowledgement.

The right of Samuel Burholt to be identified as author of this work has been asserted by him in accordance with the Copyright, Designs and Patents Act 1988.

© 2021 The University of Reading and Samuel Burholt.

Details of joint published publications and the contributions made by the candidate to these publications that relate to this thesis are as set out below (see list of numbered publications on the next page, denoted in square brackets).

**Samuel Burholt** conducted the experimental measurements, data analysis and data interpretation, for all the 17PYY<sub>3-36</sub> data. This included CD, FTIR, SAXS and the fluorescence studies. Further to this, he conducted all the experiments and completed the related analysis for the gels section within the PYY paper [4]. He assisted in the data acquisition and processing of the SANS data for the shear alignment paper [3], and moreover, he assisted in the acquisition of SAXS and fluorescence data for the nanosheet formation paper [1] as well as supporting the writing of the review [2].

**Ian Hamley** supervised the overall organisation of all papers and assisted in the experimental design of all the experiments. Further to this, he provided the writing of key sections of the papers and gave feedback on all papers. As a corresponding author, he was also responsible for the writing of the rebuttal letters to the reviewers.

**Jessica Hutchinson** conducted the experimental measurements, data analysis and interpretation for all the 11 and 23PYY<sub>3-36</sub> investigations. This included CD, FTIR, SAXS and the fluorescence studies. Further to this, she collated and proofread the review [2] and PYY paper [4]. She also helped in providing the response to the reviewer's comments on these papers. Further to this, she assisted in acquiring data for other papers, including SANS data, and pH studies [1, 3].

**Steven Kirkham** and **Valeria Castelletto** assisted in the training for all the lab-based experiments and also assisted with the collection of the synchrotron data for two papers [1, 3].

**Rodrigo da Silva, E.; Alves, W.; Gutfreund, P.; Porcar, L.; Dattani, R.; Hermida-Merino, D.; Newby, G.:** Although not referenced within this thesis, these authors completed analysis and work on the shear alignment paper [3].

**Reza, M.; Ruokolainen, J.; Stasiak, J.:** These authors were collaborators that completed the cryo-TEM images for various studies and papers [1, 3]. Subsequent analysis and identification of the cryo-TEM images has been carried out by authors, Samuel Burholt, Ian Hamley, Jessica Hutchinson, Steven Kirkham, and Valeria Castelletto, listed above in this section.

**Lundback, A.; Uddin, S.; Gomes Dos Santos, A.:** These authors were the collaborators from MedImmune Ltd and assisted in providing direction and giving feedback on the paper [4] before submission.

## Publications

[1] Hamley, I.W.; Hutchinson, J.A.; Kirkham, S.; Castelletto, V.; Kaur, A.; Reza, M.; Ruokolainen, J., “Nanosheet Formation by an Anionic Surfactant-like Peptide and Modulation of Self-Assembly through Ionic Complexation.” *Langmuir* **32** (40) (2016): 10387-10393. This article does not relate to any chapter.

Note; although not a co-author, I contributed to this paper by assisting with the collection and visualisation of the fluorescence data and additionally assisted in the collection of the small angle x-ray scattering data (see paper acknowledgements).

[2] Hutchinson, J.A.; Burholt, S.; Hamley, I.W., “Peptide hormones and lipopeptides: from self-assembly to therapeutic applications.” *Journal of Peptide Science* **23** (2017): 82-94. This review relates to Chapters 1, 3, and 4.

Note: I helped with writing the manuscript and provided support during the reviewer stage. The review was based on both the first year PhD study reports of Jessica Hutchinson and that of mine.

[3] Hamley, I.W.; Burholt, S.; Hutchinson, J.; Castelletto, V.; Rodrigo da Silva, E.; Alves, W.; Gutfreund, P.; Porcar, L.; Dattani, R.; Hermida-Merino, D.; Newby, G.; Reza, M.; Ruokolainen, J.; Stasiak, J., “Shear Alignment of Bola-Amphiphilic Arginine-Coated Peptide Nanotubes.” *Biomacromolecules* **18** (1) (2017): 141-149. This review relates to Chapters 1, 3, and 4.

Note: I collected and analysed the small angle neutron scattering data for the arginine-coated peptide nanotubes that was used to show the isotropic alignment.

[4] Hutchinson, J. A.; Burholt, S.; Hamley, I. W.; Lundback, A.; Uddin, S.; Gomes Dos Santos, A.; Reza, M.; Seitsonen, J.; Ruokolainen, J., “The Effect of Lipidation on the Self-Assembly of the Gut-Derived Peptide Hormone PYY<sub>3-36</sub>.” *Bioconjugate Chemistry* **29** (7) (2018): 2296-2308. This article relates to Chapters 1, 2, 3, and 4.

Note: I assisted in all the studies concerning one lipopeptide, termed 17PYY<sub>3-36</sub>, further to this I completed the full analysis of the structures and formation of all the gels formed from all 3 lipopeptides.

## Acknowledgements

I would like to thank my primary supervisor Prof Ian Hamley for giving me this opportunity to study for this PhD and for sharing his significant wealth of specialist knowledge of self-assembled systems. Additionally, I would thank my secondary supervisor Prof Wayne Hayes for his support during the synthesis project within my second year. I am also grateful to Jessica Hutchinson for joining me on the PhD journey and enduring the lengthy beamtime sessions with me. I would also thank Dr Ste Kirkham for teaching me many of the techniques that I am continuing to enjoy the process of mastering. I would also like to recognise Ste's qualities as a worthy squash opponent.

Having moved into a new office mid PhD, I would like to thank all those who made it enjoyable during my time there. My thanks go to Hannah, Jessi, Iain, Oli, Tahkur, Jasraj, Charlotte, Adam, Alex, Sarah, and Zoe. Your happiness and positive personalities brightened up many of my days.

I would like to thank all the University of Reading Chemical Analysis Facility (CAF) team, including the Electron Imaging team, who helped facilitate my studies. Without them this PhD would not have been completed. Other mentions of thanks should go to all the collaborators and beamline staff at the European Synchrotron Radiation Facility (ESRF), Institute Laue-Langevin (ILL) and Diamond Light Source facilities that provided highly experienced support and shared their passion of X-ray science with me.

Latterly, I am extremely thankful to Prof Nick Terrill (Diamond Light Source) and Prof Michael Rappolt (Leeds University), for their time and expertise in providing a detailed review of my work. Their input and understanding of my dyslexia have been instrumental in improving the quality of this revision of my thesis.

## Abstract

Obesity is a global health issue with nations struggling to deal with its treatment and economic impacts. Modified peptide hormones have already been shown to be effective at improving the treatment of other chronic conditions such as lymphoma or anaemia. However, peptide hormones, especially those targeted in treating obesity, are known to suffer from short drug lifetimes and thus requiring frequent administration. For the drug to take effect over a longer period requires a gel matrix-based drug carrier or a modification to the peptide itself. This thesis looks at how to use peptide modifications to potentially improve the delivery methods and efficacy of drugs used to control satiety levels.

A novel lipopeptide, based on Peptide Tyrosine-Tyrosine (PYY<sub>3-36</sub>), was characterised by using circular dichroism spectroscopy (CD), small angle X-ray scattering, critical aggregation concentration experiments, and cryo-TEM. Studies were completed to investigate the secondary structures and the self-assembly processes over a range of physiological pHs and temperatures. While native PYY<sub>3-36</sub> failed to form gels, PYY lipopeptides formed into gels with elongated fibre-like structures with a secondary structural change from  $\alpha$ -helical to  $\beta$ -sheet. Gels formed from natural peptides and water offer the potential for a highly biocompatible gel with a slow release profile.

Using the same analytical techniques, the thesis goes on to investigate co-aggregation of PYY<sub>3-36</sub> with  $\beta$ -cyclodextrin to establish if this common low-cost drug carrier can be used as an alternative delivery method. The results showed that  $\beta$ -cyclodextrin did show aggregation around the twisted sheet structure of the self-assembled PYY<sub>3-36</sub> but did not show co-assembly or encapsulation, rendering it ineffective as a delivery mechanism.

Lipidated PYY<sub>3-36</sub> was mixed with lipopolysaccharide (LPS), providing some insight into how lipidated PYY<sub>3-36</sub> could interact with amphiphilic molecules such as bacteria endotoxins. The results show that LPS do co-assemble with lipidated PYY<sub>3-36</sub>, however, unexpectedly the lipidated PYY<sub>3-36</sub> elongated fibre structure remains largely unchanged following the co-assembly. The implications of this observation warrant further analysis.

Ultimately, the findings of this thesis could be applied to the development of drug formulations for other conditions, such as lymphoma or anaemia, which would benefit from the lipidation of large peptides that enable slow release mechanisms. Additionally, the results within this thesis add knowledge to the fundamental research of self-assembly and clarifies the effects of lipidation on larger peptides that allow gelation to occur.

## Table of Contents

Publications	iv
Acknowledgements	v
Abstract	vi
Table of Contents	1
List of Figures	3
List of Tables	5
Abbreviations	6
Commonly used symbols and physical constants	8
<b>1. Introduction</b>	<b>9</b>
1.1 Research Motivation	9
1.2 Peptides	10
1.3 Primary, Secondary and Tertiary Structure	12
1.4 Bioactive Peptides	13
1.5 Uses of Natural and Synthetic Bioactive Peptides	14
1.6 Limitations and Methods to Improve Peptide Drug Delivery	17
1.7 Lipopeptides and Peptide Amphiphiles	18
1.8 Self-Assembly	19
1.9 Applications of Self-Assembling Peptide Systems	21
1.10 Hydrogels	24
1.11 Endocrine Peptides	27
1.12 Peptide YY	29
1.13 Research Aims and Objectives	31
<b>2. Materials and Methods</b>	<b>33</b>
2.1 Materials and Sample Preparation	33
2.1.1 Materials	33
2.1.2 Sample Preparations	34
2.2 Applied Methodologies	
2.2.1 Transmission Electron Microscopy (TEM)	36
2.2.2 Small Angle X-Ray Scattering (SAXS)	41
2.2.3 Circular Dichroism (CD)	49
2.2.4 UV Absorbance Concentration Measurements	52
2.2.5 Zeta Potential Measurements	54
2.2.6 Critical Aggregation Concentration (CAC) Experiments	55
2.2.7 BODIPY TR Cadaverine LPS Displacement Assay	57
2.3 Rational of Applied Methods	58
<b>3. PYY<sub>3-36</sub> and 17PYY<sub>3-36</sub>, the Effects of Lipidation</b>	<b>59</b>
3.1 Introduction to Peptide Hormone PYY <sub>3-36</sub> and 17PYY <sub>3-36</sub>	59
3.2 Cryo-TEM, Visualising Self-Assembled Structures	60
3.3 Small Angle X-Ray Scattering of PYY <sub>3-36</sub> and 17PYY <sub>3-36</sub> Structures	64
3.4 Secondary Structure Investigation of 17PYY <sub>3-36</sub> by Circular Dichroism	68

3.5 Critical Aggregation Concentration (CAC) Determination of 17PYY <sub>3-36</sub> Self-Assembled Structures	74
3.6 Comparison of 17PYY <sub>3-36</sub> to 11PYY <sub>3-36</sub> and 23PYY <sub>3-36</sub>	76
3.7 Conclusions of the Lipidation of PYY <sub>3-36</sub> at Position 17	78
<b>4. Lipopeptide PYY<sub>3-36</sub> Gels</b>	<b>80</b>
4.1 Introduction to Lipopeptide and Peptide Gels	80
4.2 Formation of Hydrogels	81
4.3 Gel Concentration Determination using A280 nm	83
4.4 Transmission Electron Microscopy to Visualise Hydrogel Structure	84
4.5 Small Angle X-Ray Scattering Investigation into Hydrogel Fibres	87
4.6 Secondary Structure Investigation of Fibres using Circular Dichroism	89
4.7 11, 17 and 23PYY <sub>3-36</sub> Gel Conclusions	92
<b>5. 17PYY<sub>3-36</sub>, PYY<sub>3-36</sub> and A9R interactions with Lipopolysaccharide.</b>	<b>94</b>
5.1 Introduction to A9R and LPS	94
5.2 17PYY <sub>3-36</sub> complexation to LPS Cryo-TEM Observations	95
5.3 SAXS Investigation of 17PYY <sub>3-36</sub> and LPS Aggregation Structures	97
5.4 Circular Dichroism Study of 17PYY <sub>3-36</sub> and LPS Aggregates	100
5.5 Further Investigations with PYY <sub>3-36</sub> and A9R Complexing to LPS	101
5.6 Cryo-TEM Investigation of the interaction between A9R and LPS	102
5.7 A9R with LPS, SAXS Investigation	104
5.8 Circular Dichroism Study PYY <sub>3-36</sub> and A9R with LPS	105
5.9 A280/A200 Absorbance Studies of PYY <sub>3-36</sub> and A9R with LPS	108
5.10 LPS Specific Dye Absorbance Study using PYY <sub>3-36</sub> and A9R	110
5.11 Zeta Potentials of A9R/PYY <sub>3-36</sub> and LPS Complexes	113
5.12 Conclusion of LPS interaction with comparison of 17PYY <sub>3-36</sub> and A9R	115
<b>6. Synthesis and Inclusion Potential for Polysaccharide with PYY<sub>3-36</sub> using <math>\beta</math>-cyclodextrin</b>	<b>117</b>
6.1 Introduction to Synthesis and Inclusion of PYY <sub>3-36</sub> with $\beta$ -cyclodextrin	117
6.2 Polysaccharide Conjugate Synthesis	119
6.3 Circular Dichroism for Complexation of PYY <sub>3-36</sub> and $\beta$ -cyclodextrin	120
6.4 Small Angle X-Ray Scattering Study of PYY <sub>3-36</sub> with $\beta$ -cyclodextrin	121
6.5 Cryo-TEM Visualisation of PYY <sub>3-36</sub> with $\beta$ -cyclodextrin	123
6.6 A280 nm Study of $\beta$ -cyclodextrin aggregation with PYY <sub>3-36</sub>	125
6.7 Zeta Potentials of PYY <sub>3-36</sub> and $\beta$ -cyclodextrin Ratios	126
6.8 Conclusions of PYY <sub>3-36</sub> with $\beta$ -cyclodextrin	128
<b>7. Conclusions and Future Work</b>	<b>130</b>
7.1 Thesis Conclusions	130
7.2 Future Work	132
<b>References</b>	<b>135</b>

## List of Figures

<b>Figure 1:</b> Scheme explaining the structure of peptides. ....	11
<b>Figure 2:</b> The structural formula of the anti-microbial peptide daptomycin. Stereocenters defined using R (D) and S (L).....	15
<b>Figure 3:</b> Lipopeptide amphiphiles. ....	19
<b>Figure 4:</b> Image showing the process of self-assembly to materials. ....	26
<b>Figure 5:</b> Diagram showing the main peptides involved in the control of hunger. ....	27
<b>Figure 6:</b> Illustrations of binding sites for Y1 and Y2 with hPYY + hPYY <sub>(3-36)</sub> .....	29
<b>Figure 7:</b> Visual colour shift, from pink to blue, from the complexation of LPS and the LPS specific dye BODIPY TR. ....	35
<b>Figure 8:</b> Overall structure of a TEM machine with images of common studied samples.....	37
<b>Figure 9:</b> Two types of TEM sample discs used.....	38
<b>Figure 10:</b> Sample preparation for the Cryo-TEM method. ....	40
<b>Figure 11:</b> Diagram illustrating SAXS measurements and a fitted form factor over experimental data. ....	43
<b>Figure 12:</b> Different simulated fits of used models in this study. The scattered intensity, $I(\text{a.u.})$ , is illustrated for the examples of diluted core shell cylinder, cylinders, and bilayer fits.....	44
<b>Figure 13:</b> Scheme illustrating the principle of CD data recording. ....	50
<b>Figure 14:</b> Photos showing the use of a nanodrop to produce a small path length, which is useful for low concentration or low fluorescing molecules, and the application of a small amount of sample to the stage.....	53
<b>Figure 15:</b> Diagram showing what zeta potential is and what this relates to, given a charged particle in solution.....	54
<b>Figure 16:</b> Scheme showing monomers in solution below and above the CAC. The CAC being useful information for when the formation of aggregates can occur. ....	55
<b>Figure 17:</b> Schemes explaining the process for using pyrene as a CAC probe. ....	56
<b>Figure 18:</b> Chemical Structure of BODIPY TR Cadaverine. ....	57
<b>Figure 19:</b> Full Structure of PYY <sub>3-36</sub> and linker unit, with locations of lipidations. Top: Chemical structure with positions of lipidation on the amino acid chain shown by the arrows. Left to right of the arrow positions being 11PYY <sub>3-36</sub> , 17PYY <sub>3-36</sub> , and finally 23PYY <sub>3-36</sub> . ....	60
<b>Figure 20:</b> Cryo-TEM images showing the $\alpha$ -helical based twisted sheet self-assembled structures of 0.5 wt% PYY <sub>3-36</sub> prepared in H <sub>2</sub> O at pH 2 (A), 4 (B), 6 (C), and 8 (D).....	61
<b>Figure 21:</b> Cryo-TEM Images showing the $\alpha$ -helical self-assembled elongated fibre structures of 17PYY <sub>3-36</sub> , in water, at pH 2 (A), pH 4 (B), pH 6 (C) and pH 8 (D). ....	62
<b>Figure 22:</b> All SAXS curves and form factor fitting curves for PYY <sub>3-36</sub> at four different pH values (2, 4, 6 and 8). All samples were prepared in H <sub>2</sub> O at room temperature. Figure taken from authored paper 4. <sup>298</sup> .....	64
<b>Figure 23:</b> SAXS curves for 17PYY <sub>3-36</sub> at three different pH values, prepared in H <sub>2</sub> O, 2, 4 and 8 including the long cylinder shell fitted curves.....	66
<b>Figure 24:</b> CD spectrum comparing 0.5 wt% PYY <sub>3-36</sub> at pH 3.30, 4.55, and 6.81 to 17PYY <sub>3-36</sub> at pH values, 4.43, 5.99, and 8.20.....	69
<b>Figure 25:</b> CD spectra for a 0.5 wt% PYY <sub>3-36</sub> sample prepared in H <sub>2</sub> O at pH 4.6. Temperature study of 20-60 °C.....	71
<b>Figure 26:</b> <b>A</b> - CD spectra for 0.5 wt% 17PYY <sub>3-36</sub> , pH 4.43 H <sub>2</sub> O. Temperature Study (20 -70 °C). <b>B</b> - CD spectra for 0.5 wt% 17PYY <sub>3-36</sub> , pH 8.20 H <sub>2</sub> O. Temperature Study (20-70 °C). <b>C</b> - Temperature CD study of 0.5 wt% 17PYY <sub>3-36</sub> pH 5.99 (20-70 °C). ....	72
<b>Figure 27:</b> Pyrene fluorescence vs. concentration of 17PYY <sub>3-36</sub> at pH 2.12, 4.35, 6.73 and 8.21. ....	75
<b>Figure 28:</b> Four photos demonstrating the inverted vial tests for gel formation. ....	82

<b>Figure 29:</b> Overall diagram showing the method of thin layer gel formation, showing the preparation (left), deposition (middle) and layer (right) formation. ....	84
<b>Figure 30:</b> Drop coating method used for gel TEM.....	85
<b>Figure 31:</b> Three TEM Images showing highly elongated and entwined fibres from different lipopeptides hydrogels at pH 8. i) 11PYY <sub>3-36</sub> ii) 17PYY <sub>3-36</sub> iii) 23PYY <sub>3-36</sub> .....	86
<b>Figure 32:</b> Small Angle X-Ray Scattering comparison graph showing al pH 8 gels of 11, 17 and 23PYY <sub>3-36</sub> . ....	87
<b>Figure 33:</b> CD Spectra for 11, 17 and 23PYY <sub>3-36</sub> hydrogels at pH 8. ....	89
<b>Figure 34:</b> Temperature CD studies on the 17PYY <sub>3-36</sub> pH 8 gel (A) and on the 23PYY <sub>3-36</sub> pH 8 gel (B) from 20-70 °C. ....	91
<b>Figure 35:</b> Visual turbidity from the mixing of LPS and 17PYY <sub>3-36</sub> . Left to right: 0.5 wt% LPS, mix 0.5:0.5 wt% LPS:17PYY <sub>3-36</sub> and 0.5 wt% 17PYY <sub>3-36</sub> . ....	95
<b>Figure 36:</b> Cryo-TEM images showing the odd co-assembly of 17PYY <sub>3-36</sub> and the bacteria endotoxin LPS.....	96
<b>Figure 37:</b> Comparison spectrum of SAXS patterns for 17PYY <sub>3-36</sub> , fitted with a long cylindrical shell (2.2.2 Eq. 2), LPS, fitted with a bilayer and long cylindrical model (2.2.2 Eq 2 and 5) and 1:1 mixture, which was fitted with a bilayer model (2.2.2 Eq 5). ....	97
<b>Figure 38:</b> CD spectrum of 0.5 wt% 17PYY <sub>3-36</sub> (black), 0.5 wt% LPS (red), and a 1:1 mixture of the two samples (green). ....	100
<b>Figure 39:</b> Chemical Structure of A9R. A9R is a known anti-bacterial peptide and readily self-assembles and forms gels.....	101
<b>Figure 40:</b> Cryo-TEM showing the formation of two distinct self-assembly structures of 0.5 wt%: 0.5 wt% A9R: LPS in H <sub>2</sub> O. ....	103
<b>Figure 41:</b> SAXS patterns for 0.1 wt% A9R, 0.1 wt% LPS and 0.1: 0.1, 0.2: 0.1, 0.1: 0.2 wt% mixtures in H <sub>2</sub> O. ....	104
<b>Figure 42:</b> Comparison CD spectra of PYY <sub>3-36</sub> , 17PYY <sub>3-36</sub> and mixtures with LPS.....	106
<b>Figure 43:</b> UV fluorescence experiment showing the A280 Nanodrop concentration results combined with the predicted results. ....	108
<b>Figure 44:</b> Showing the results for the A205 nm experiment on the Nanodrop. ....	110
<b>Figure 45:</b> Chemical structure drawing of BODIPY <sup>TM</sup> TR cadaverine.....	111
<b>Figure 46:</b> Comparison of BODIPY <sup>TM</sup> TR cadaverine release with complexation of A9R and PYY <sub>3-36</sub> to Lipopolysaccharide. Intensity values at 620 nm were recorded with the addition of 10 µL of each solution. Both solutions were the same molarity. The intensity values were then fitted linearly to show a trend line and help show the gradient of increase. ....	112
<b>Figure 47:</b> Example saccharide unit, n denoting chain possibility. n=1 is glucose, n=2 disaccharide, n>3 oligosaccharides, n>5 polysaccharides. ....	117
<b>Figure 48:</b> Summary of synthesis path. ....	118
<b>Figure 49:</b> Mesh diagram of β-cyclodextrin showing pocket formed by the 7 membered ring. ....	119
<b>Figure 50:</b> Circular Dichroism comparison of PYY <sub>3-36</sub> , β-cyclodextrin and a 1:1 Mixture. ....	121
<b>Figure 51:</b> SAXS patterns comparing PYY <sub>3-36</sub> , β-cyclodextrin, and 1:1, 1:2, and 2:1 ratios ..... .....	122
<b>Figure 52:</b> Cryo-TEM images showing the β-cyclodextrin aggregation around that of the α-helical twisted sheets of PYY <sub>3-36</sub> . ....	124
<b>Figure 53:</b> Absorbance values for mixtures of PYY <sub>3-36</sub> and β-cyclodextrin.....	125
<b>Figure 54:</b> Zeta-potential diagram explaining the possible shielding effects of β-cyclodextrin on the charged twisted sheet structure of PYY <sub>3-36</sub> . ....	127

## List of Tables

<b>Table 1:</b> Overview of applied methods. ....	58
<b>Table 2:</b> Gaussian coil and gaussian bilayer form factor fitting parameters for the PYY <sub>3-36</sub> samples at pH values 2, 4, 6 and 8. ....	65
<b>Table 3:</b> Fitting parameters used to fit the long cylinder shell model for the 3 different pH samples of 17PYY <sub>3-36</sub> . ....	67
<b>Table 4:</b> Summary of self-assembly structures. Secondary structures are colour coded: $\alpha$ -helix (light orange background) and $\beta$ -sheet (grey-blue background). ....	78
<b>Table 5:</b> Summary of lipidated PYY <sub>3-36</sub> samples that formed gels for given pH values. ....	83
<b>Table 6:</b> Summary of all three long cylindrical shell model (Chapter 2.2.2 Eq. 2) fitting parameters resulting from the 11, 17 and 23PYY <sub>3-36</sub> hydrogels SAXS patterns. ....	88
<b>Table 7:</b> SAXS form factor fitting parameters for LPS, 17PYY <sub>3-36</sub> and a 0.5:0.5 wt% mixture. ....	99
<b>Table 8:</b> Ellipticities values at 190, 210 and 222 nm wavelength for CD spectrums of 0.5 wt% PYY <sub>3-36</sub> , 17PYY <sub>3-36</sub> , LPS and 1:1 mixture. ....	106
<b>Table 9:</b> Difference in ellipticities values at 190, 210 and 222 nm wavelength for CD spectrums of PYY <sub>3-36</sub> , 17PYY <sub>3-36</sub> , LPS and 1:1 mixture. ....	107
<b>Table 10:</b> Zeta potential, Mobility, and Conductivity results for PYY <sub>3-36</sub> , A9R and mixtures with LPS. ....	114
<b>Table 11:</b> Zeta potentials for Various Ratios of PYY <sub>3-36</sub> and $\beta$ -cyclodextrin. ....	127

## Abbreviations

Ala – A – Alanine

AMP – Anti-microbial peptide

Arg – R – Arginine

Asn – N – Asparagine

Asp – D – Aspartic Acid

BODIPY-TR – 4,4-difluoro-4-bora-3a,4a-diaza-s-indacene

C18 – Octadecylsilane

CAC – Critical Aggregation Concentration

CAF – Chemical Analysis Facility

CD – Circular Dichroism

CMC – Critical Micelle Concentration

Cryo-TEM – Cryogenic Transmission Electron Microscopy

Cys – C – Cysteine

DDP-4 – Enzyme Dipeptidyl Peptidase 4

DNA – Deoxyribonucleic acid

DSC – Differential scanning calorimetry

ECM – Extracellular Matrix

ESI – MS – Electrospray ionization - mass spectrometry

eV – Electronvolt

Gln – Q – Glutamine

GLP-1 – Glucagon-Like Peptide 1

Glu – E – Glutamic Acid

Gly – G – Glycine

H<sub>2</sub>O - Water

HCL – Hydrochloric acid

His – H – Histidine

Ile – I – Isoleucine

Leu – L – Leucine

LPS – Lipopolysaccharide

Lys – K – Lysine  
MALDI – MS – Matrix-assisted laser desorption/ionisation - mass spectrometry  
Met – M – Methionine  
MLV – Multilamellar Vesicle  
NaOH – Sodium Hydroxide  
NMR – Nuclear Magnetic Resonance  
NPY – Neuropeptide Y  
PA – Peptide Amphiphile  
PEG – Polyethylene Glycol  
Phe – F – Phenylalanine  
pHEMA – Poly(2-hydroxyethyl methacrylate)  
pI – Isoelectric point  
PP – Proline  
Pro – P – Proline  
PVA – Poly(vinyl alcohol)  
Pyl – O – Pyrrolysine  
PYY – Peptide Tyrosine-Tyrosine  
PYY<sub>3-36</sub> – Enzyme-Truncated Peptide Tyrosine-Tyrosine  
RNA – Ribonucleic acid  
SAPNS – Self-assembling peptide scaffold nanofibre  
SAXS – Small Angle X-ray Scattering  
SDS – Sodium Dodecyl Sulphate  
Sec – U – Selenocysteine  
Ser – S - Serine  
SOP – Standard operating procedure  
TAT – GRKKRRQRRRPQ  
TEM – Transmission Electron Microscopy  
Thr – T – Threonine  
TLC – Thin Layer Chromatography  
Trp – W – Tryptophan

Tyr – Y – Tyrosine

ULV – Unilamellar Vesicle

UV – Ultraviolet

Val – V – Valine

$\beta$ -sheet - Beta-sheet

## **Commonly used Symbols and Physical Constants**

D – Right Chirality

g/mol-1 – Molecular weight

L – Left Chirality

m – Milli

n – Nano

$^{\circ}\text{C}$  – Degree Celsius

pH – logarithmic scale of "hydrogen potency"

R – Right Chirality

S – Left Chirality

sec – Second

wt% - Weight Percent

$\alpha$  – Alpha

$\beta$  – Beta

$\mu$  – Micro

# 1. Introduction

## 1.1 Research Motivation

Obesity is a global health issue, caused by the over accumulation of fat within the human body that leads to negative health and economic outcomes. Obesity has been linked to an increased risk of cardiovascular disease, diabetes, cancer, and strokes.<sup>1</sup> Nonetheless, the percentage of the global population that is considered obese is still increasing. In the UK, for example, the percentage of the population that is obese has almost doubled from 15% to 29%, from 1993 to 2016.<sup>2</sup> USA and Mexico follow the same trend, 30% to 42% from 1999 to 2018, and 18% to 29% from 1995 to 2016, respectively.<sup>3-4</sup> With this chronic medical condition becoming more prevalent, various scientific, private, and governmental organisations have taken a keen interest in finding solutions to reduce this trend. The approaches taken towards the different solutions to the problem of obesity are varied, from understanding the method of fat storage through to the development of novel weight loss treatments. All of this work is being undertaken to reduce the long-term financial burden that an overly obese population places upon its national healthcare systems.

For these reasons, there has been a large increase in research and development activities within the pharmaceutical sector for the development of anti-obesity or “weight-loss” drugs. Given the large numbers of the population that are obese in many developed and developing countries, a successful remedy could have far reaching societal impacts and deliver lucrative drug sales and development incomes for any company that can treat obesity successfully. There are only four approved drugs available in the USA: Orlistat (Alli, Xenical), Phentermine and Topiramate (Qsymia), Bupropion and Naltrexone (Contrave), and finally Liraglutide (Saxenda, Victoza). Only Orlistat (Alli, Xenical) is approved for use in the UK. All these drugs do state that their effects can vary from person to person, and close monitoring is needed for anyone taking them.

The most common causes for obesity in children and adults worldwide are overeating and physical inactivity, which leads to a calorie surplus that the body stores in the form of subcutaneous fat.<sup>1, 5</sup> In 1980 a peptide hormone was discovered which controls the body’s satiety levels through the creation of a feeling of being full and not hungry.<sup>6</sup> This peptide hormone is called Peptide Tyrosine-Tyrosine (PYY<sub>3-36</sub>) and is formed from small units referred to as amino acids. This specific PYY chain (a peptide sequence) achieves this by

interacting with a receptor in the brain (neuroreceptor Y1-5), which in turn causes the feeling of being full.

However, peptide hormones, especially those targeted in treating obesity, are known to suffer from short drug lifetimes (typically between 4 to 6 hours), as they are removed through the biological processes of the body. This short drug lifetime therefore leads to frequent administration, making it less practical for the patient. For the drug to take effect over a longer period requires a gel matrix-based drug carrier or a superior modification of the peptide structure. This thesis looks at how to use peptide modifications to potentially improve the delivery methods and efficacy of peptide drugs used to control satiety levels.

## 1.2 Peptides

Peptides are a group of biological polymers formed from amino acid monomers joined by covalent amide bonds. Amide bonds are formed between the carboxyl group (-COOH) and the amino group (-NH<sub>2</sub>) of another corresponding amino acid. There are 20 different amino acids, but each contains the same backbone HOOC-C(R)H-NH<sub>2</sub>, as seen in Figure 1. These amino acids vary by the R group constituent. Of the 20 amino acids found in organisms, 9 are classed as essential with the further 11 being non-essential. They are classed this way because of the necessity for the human body to obtain them. The common proteinogenic amino acids cannot be synthesised by the human body, so they need to be consumed. These are Histidine (H), Methionine (M), Threonine (T), Lysine (K), Tryptophan (W), Phenylalanine (F), Isoleucine (I), Leucine (L) and Valine (V). The non-essential amino acids are produced by the body, so do not need to be ingested. These include Alanine (A), Arginine (R), Asparagine (N), Aspartic Acid (D), Cysteine (C), Glutamic Acid (E), Glutamine (Q), Glycine (G), Proline (P), Serine (S) and Tyrosine (Y). Each amino acid has its own name, abbreviation, as well as its own letter. The latter is a useful nomenclature, especially when describing longer amino acids chains.

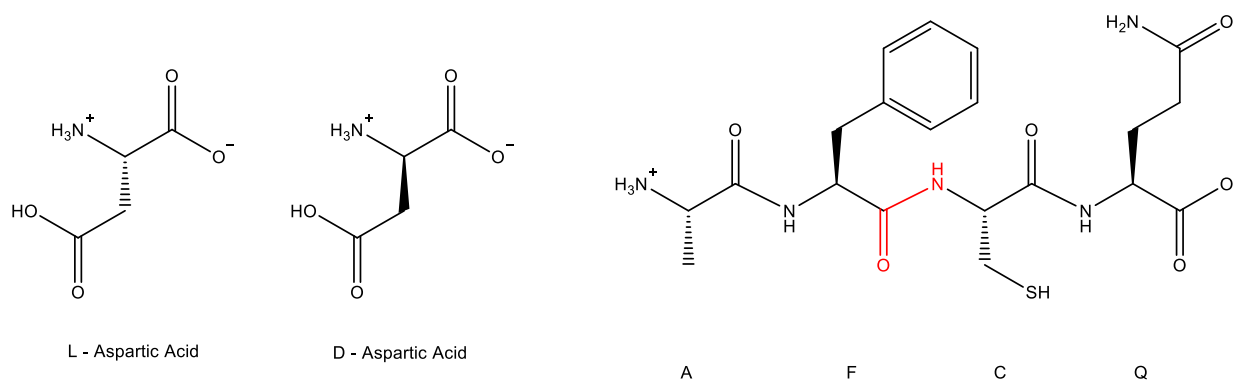


**Figure 1:** Scheme explaining the structure of peptides. Left and Middle: The structure of an amino acid, aspartic acid, with both its L (Left) and D (Right) chiral forms are shown. Right: Structural scheme showing a peptide chain formed of 4 amino acids; Alanine (A), Phenylalanine (F), Cysteine (C) and Glutamine (Q). The amide bond between the carboxylic acid and amino acid groups of different amino acids is highlighted in red. All structural formulas are drawn as zwitterions and were made with ChemDraw Professional.

The amino acid R groups range from being hydrophilic to hydrophobic. They can also be inherently basic or acidic due to variation in R groups. The amino acid group can also be further diversified by having a chiral centre, meaning they can be either right- (D) or left-handed (L). When considering amino acids for their receptor binding role in drug efficacy it is important to note that the proteins found throughout the body mainly exist in the (L) configuration, with only cysteine having a different absolute stereochemistry, while still being (L), and glycine being exempt due to its non-chirality (two hydrogens).<sup>7</sup> Different R groups can also be protonated or deprotonated, which gives rise to zwitterions. A zwitterion is where the amines of an amino acid's functional groups become protonated and the carboxylic acids become deprotonated respectively at a specific pH.<sup>8</sup>

Proteins are typically formed by more than 50 amino acids that are covalently bonded in a polymer like structure, and which exhibit a specific function that is derived from its sequence. Examples of these functions include protease that breaks down polypeptides and proteins in shorter fragments, or DNA helicase that destabilises the DNA helix so that the separate strands can be replicated by other proteins.<sup>9-13</sup> Dipeptides and tripeptides define peptides with two and three amino acids, respectively. A polypeptide or short peptide is defined as having 4 to 50 amino acids within its structure.<sup>14-15</sup> Peptides and proteins are found within every cell and tissue throughout the human body. In the body they function as enzymes, messenger hormones or antioxidants. The ability to maintain peptide levels in the human body is extremely important and without proper control can cause serious medical issues, such as hypoglycaemia (low blood

sugar levels, from increased insulin production), high blood pressure (from loss of oxytocin production that helps regulate blood pressure), and hyper-fight or flight responses (triggered by the overproduction of epinephrine). Peptides form the sub-unit for most human hormones produced in various glands, including the stomach, intestine, and brain. A few examples of peptide hormones include, insulin, Glucagon-Like-Peptide (GLP-1) and ghrelin. Target cells contain hormone specific receptors located in their cell membranes and respond to the binding of specific hormones, causing cascading biological events in the cell, which enable the hormone to produce its effect on the body. An example of this would be GLP-1 that causes  $\beta$  cells in the pancreas to release insulin.<sup>16-22</sup>

### 1.3 Primary, Secondary and Tertiary Structure

A peptide can have four distinct levels of structure. The *primary structure* describes the individual amino acid sequence forming the peptide. This sequence can be described in various ways, but the most common approach is using single letters, such as KKVF, which would describe a Lysine-Lysine-Valine-Phenylalanine chain.

The three main *secondary structures* of peptides are  $\alpha$ -helices,  $\beta$ -sheets, and turns or loops.<sup>23</sup>  $\alpha$ -helices are a right-handed spiral configuration of amino acids, where a backbone electropositive NH moiety electrostatically bonds a hydrogen atom to an electronegative, lone pair available C=O group, four amino acids away from the NH moiety along the primary sequence.  $\beta$ -Sheets are regular strands of polypeptides connected laterally, between strands, by hydrogen bonding. There is normally between three to ten amino acids per strand, with one intramolecular hydrogen bond per amino acid on the strand.<sup>24</sup> The  $\beta$ -sheets can be in parallel or anti-parallel form, meaning the primary strand runs in the same/or alternating direction to each other respectively. Turns and loops are strands of amino acids that allow the peptide chain to bend and change its direction. These turns or loops are also known as random coil formations as they display no structural order. The secondary structure of peptides are caused by the intrapolymeric bonding via hydrogen bonds, disulphide bridges or in some cases by  $\pi$ - $\pi$  stacking.<sup>25-</sup>  
<sup>27</sup> Hydrogen bonds can be formed between several polar amino acid moieties (for instance Glu, Asp, Ser, Asn and Lys) as these contain negatively charged oxygen ( $O^-$ ) as proton acceptors and positively charged hydrogens ( $H^+$ ) as proton donors, required for this interaction. Disulphide bridges occur when two thiol groups of cysteines oxidise to form a covalent sulphur bridge (-S-S-). Aromatic stacking can also influence the secondary structure as it is weaker when compared to hydrogen bonding. Aromatic stacking is found with the amino acids Phe, Trp, Tyr

and His. Electrostatic interactions, mainly caused by solvents, can also cause changes to the secondary structure, such as is seen between water (polar) and benzene or diethyl ether (non-polar), or by changes in pH.<sup>28-33</sup> The bonding methods listed above are responsible for peptides having different secondary structures.

The *tertiary structure* defines the 3D arrangement of all the secondary and primary structures in space. This definition includes the orientation, location, and any further bonding between all the secondary structure components and other amino acids in the peptide chain. The further bonding between the secondary structures gives rise to its final 3D arrangement. These form via hydrogen bonds, disulphide bridges, electrostatic interactions, and aromatic stacking but only on the edges of the secondary structures for the free peptide chains. This intermolecular bonding (bonding between different molecules) leads to more structural changes until the peptide, or protein, has reached a specific conformation that typically occurs at the peptide's lowest energy state.

Finally, the *quaternary structure* refers the assemblies of proteins, e.g., dimers and trimers, which is crucial for the protein complex to function properly.<sup>34-40</sup>

## 1.4 Bioactive Peptides

Bioactive peptides refer to the peptides found throughout the body that are vital for the human body's well-being. These peptides have a range of functions from homeostatic, anti-fungal, anti-viral and anti-tumour properties. Bioactive peptides control many of the human body's functions as they serve as transporters across membranes and act as hormones for a variety of glands and organs. Examples of the use of bioactive peptides in the body include helping to maintain the ion concentration within cells (through ion channels), cell-penetrating peptides facilitating cellular uptake of an agent into the cell, such as short fragments of DNA, and to help the growth of lean muscle mass.<sup>41-43</sup> A few notable named examples include: Oxytocin, a nine amino acid peptide hormone that is essential in social bonding, reproduction, and childbirth.<sup>44-45</sup> Glutathione, a tripeptide that is found throughout most organisms and is an important antioxidant.<sup>46-47</sup> Finally, Somatostatin that is a cyclic 14 amino acid peptide hormone which regulates the endocrine system, also known as the growth hormone-inhibiting hormone.<sup>48-49</sup>

## 1.5 Uses of Natural and Synthetic Bioactive Peptides

As mentioned above, there are many native peptides that have important functions within the human body and, since their discovery, some bioactive peptides have been employed as anti-microbial agents. These peptides have become the basis for a new and powerful field in the pharmaceutical industry. These peptides can be formed naturally by the body or synthetically, although many synthetic peptides are based on the structure of naturally occurring peptides. Over 60 peptide drugs are now available on the market which combat a range of conditions from advanced prostate cancer (e.g. Goserelin by AstraZeneca, or Degarelix by Ferring), hypertension (e.g. Enalapril by Merck & Co), glycaemic control (e.g. Exenatide from Amylin/Lilly) to severe infections (e.g. Neosporin<sup>TM</sup> which is a combination of three antibiotics, neomycin (polysaccharide), polymyxin B (cyclic polypeptide), and bacitracin (cyclic polypeptide), produced by Johnson & Johnson).<sup>50-60</sup>

***Anti-Microbial Peptides (AMPs).*** As part of the innate human immune system, small cationic peptides have been used to combat microbial infections throughout the body, such as daptomycin (Figure 2).<sup>61-65</sup> Similar to daptomycin, bacitracin is another commercial cyclic anti-microbial peptide. Given topically, it interferes with the cell wall and causes cell death, like that seen by daptomycin.<sup>66-67</sup> Another AMP, specifically a glycopeptide, is vancomycin. This medication is given intravenously and has been shown to block the construction of the cell wall.<sup>68-69</sup> Applications of AMPs is receiving growing interest as common molecule-based anti-microbial drugs are experiencing growing bacterial resistance and consequently are requiring higher doses or are completely losing their ability to function. Investigation into these anti-microbiological peptides is, unsurprisingly, a rapidly developing field and, with over 90 years of history, has the potential to help combat the bacteria resistance problem facing the current world's population.<sup>70</sup>

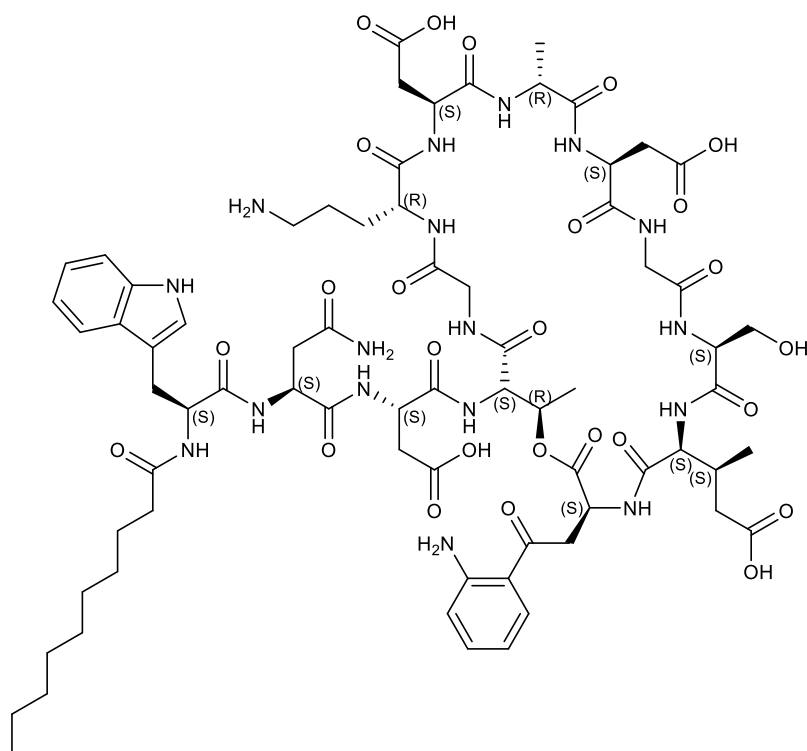


**Figure 2:** The structural formula of the anti-microbial peptide daptomycin. Stereocenters defined using R and S. The scheme shows the lipid tail, the amino acid building blocks, and the cyclic peptide nature that has been demonstrated to be important in its anti-microbial properties (the structural formula was made with ChemDraw Professional).

**Peptides in Healing.** The ability to heal is another innate process of the human body and one that is sometimes taken for granted, yet it is a critical aspect in homeostasis. The body's healing capabilities, which copes with a variety of internal and external damage to the body, contains a small number of peptides that enable the healing to occur. A few have a variety of functions, from growth hormones (stimulating muscle formation) to bone formation. These peptides make an interesting prospect for new healing methods that hijack the body's innate healing methods to improve and speed up healing.<sup>71-72</sup> A readily available human growth hormone drug that is sold under many brand names, is Somatropin, and a drug developed by Æterna Zentaris for growth hormone deficiency is Macimorelin.

**Peptide Drugs and Diet.** As has been seen, many functions in the body are regulated by peptides and their role in such functions as hormone release, memory retention, hunger and homeostasis. This ability for peptides to be multi-functional allows for the adaptation and implementation of these peptides for the creation of novel drugs. As per previous uses, novel drug development using peptides will have the inherent benefits of them being biologically accepted and recognisable by the body and extremely biologically specific in their targeted function.

Peptide hormones are a sub-set of the body's messaging systems. Many of these systems relate to the gut-brain interaction that is involved in controlling important mechanisms such as glucose levels and satiety (hunger levels).<sup>73-74</sup> Ghrelin, for example, is produced in the stomach and stimulates the hypothalamus in the brain to produce a feeling of hunger.<sup>75</sup> This messenger hormone is always present in the blood and its level controls its efficacy and hunger simulation. More of it increases hunger, less the opposite. Glucagon-Like Peptide 1 (GLP-1), oxyntomodulin, uroguanylin, and finally the Peptide Tyrosine-Tyrosine (PYY) are all peptide hormones produced in the small bowel and interact with a variety of neuro-receptors in the brain reducing appetite.<sup>21, 74, 76-83</sup> From a structural perspective, they contain a different amount of amino acids, 30 for GLP-1, 37 for oxyntomodulin, 16 for uroguanylin and 36 for PYY, respectively. There are many drugs based on GLP-1, however the majority are currently undergoing clinical trials, examples of such include Dulaglutide and Cpd86 from Lilly, ZPGG-72 and ZP3022 from Zealand Pharma, ITCA by Intarcia, and MOD-6030 by Prolor.

PYY is of particular interest as it was found to reduce appetite in rodents and primates when injected or used as a nasal spray.<sup>84</sup> This effect was analysed further in human studies which showed a decrease of caloric intake by 30% when PYY was given orally.<sup>85</sup> The study also compared obese subjects alongside non-obese subjects which demonstrated the same level of caloric intake decrease. Leptin, another peptide under study for obesity treatment, shows decreased effectiveness in obese subjects as a resistance was gained.<sup>86</sup> This observation was not observed in the case of PYY, making it an extremely promising drug candidate for obesity treatment.

PYY is produced in L-cells of the gastrointestinal tract and circulates through the blood stream to neuropeptide Y-receptors in the brain. PYY is cleaved in the blood circuit by the enzyme Dipeptidyl Peptidase 4 (DDP-4), eliminating two amino acids leading to the truncated PYY<sub>3-36</sub> form. Both PYY and PYY<sub>3-36</sub> act upon the Y-receptors, but the majority of interacting peptides are found in the 34 amino acid form. There are five known Y-receptors, named Y<sub>1</sub> to Y<sub>5</sub>, which are understood to be linked with appetite, anxiety, and blood pressure. PYY and PYY<sub>3-36</sub> have different selectivity for these five receptors with PYY<sub>3-36</sub> being highly selective to receptor Y<sub>2</sub>.<sup>87</sup> At the time of writing, there are currently no drugs on the market using PYY<sub>3-36</sub> as its base.

## 1.6 Limitations and Methods to Improve Peptide Drug Delivery

Many peptide drugs have suffered from a disadvantage that, during the evolution of the human species, the body has developed to be very efficient at removing peptide messengers from its system. The body, in responding this way to peptides messengers, ensures that key triggers, such as hunger and growth are regulated and managed. This means that the body will remove a bioactive peptide drug faster than a synthetic drug as these are not as readily known to the body and its biological protection mechanisms. The body uses proteins, enzymes, and pathways to cleave, neutralise, or remove the peptide from the human body, which will be less efficient against a synthetic drug. Another important effect is that peptide drugs need to be designed extremely precisely to a particular receptor, or set of receptors, to guarantee a very a very targeted and specific binding relationship. Any treatment, amendment or change to the structure of the peptide, if primary, secondary, or tertiary, could have a detrimental effect on the efficacy of the drug.

The body's protection mechanisms reduce the time the peptide is retained in the body and increases the chance of enzyme cleavage. There are three main ways of improving body retention time and reducing enzyme cleavage. The first method is to ***co-administer the drug with a stabilising molecule***, this hinders enzyme attack and also might help to reduce the effects of pH on the molecule. A commercial example of co-administering with a stabilising molecule is the modified cyclodextrin ring marketed under the trade name of Captisol. This stabilising molecule has been shown to improve solubility, stability, and bioavailability of the co-administered drugs.<sup>88-95</sup> Another way is to form or use a ***gel to encapsulate the peptide drug***.<sup>96-106</sup> This allows for a slow release mechanism as well as protects the drug from enzyme attack. There are a few commercial examples of these gels on the market, including Geloil, Gelucire, and Peceol. Finally, a ***peptide can be lipidated, forming a lipopeptide***, or similarly, polyethylene glycol (PEG) chains that can covalently be bound to peptides, forming a so-called PEGylated peptide. These treatments increase the molecular weight that in turn reduces the peptide's clearance rate from the body, as well as hindering specific enzyme binding that consequently lowers enzyme cleavage.<sup>107-110</sup> One highly valuable side effect of this lipidation is the formation of self-assembled structures that are thought to help reduce clearance and enzyme attack.<sup>111-113</sup> Lipidation has been used for the commercial anti-bacterial drug Daptomycin, though all methods (co-administration, gel, or lipidation) are still being researched with a number of new drugs and drug formulations currently undergoing preclinical and clinical trials. It should also be noted that lipidation can prevent the binding of a drug

molecule to a receptor. Therefore cell, preclinical, and clinical studies are extremely important to ensure the lipidation, or PEG-lation, has not affected the drug efficacy.

### 1.7 Peptide Amphiphiles and Lipopeptides

Peptide amphiphile (PA) describes a broad range of peptides with amphiphilic (having both hydrophilic, water-loving, and hydrophobic, water-fearing) properties. PAs fall in to three different classes of peptides. The first class are peptides containing polar and non-polar sections arising from its amino acid's segments that are *pure peptide amphiphiles*. The second class are hydrophilic peptides attached to hydrophobic alkyl chains. These *lipopeptides* also give rise to amphiphilic properties. The third class concerns *peptide co-polymers*. These are polymers partially consisting of a peptide backbone which is covalently bound to a conventional polymer. As a result, the design of PAs inherently allows to produce an amphiphilic molecule, as both the conventional polymer and the peptide can be tuned to have hydrophilic and/or hydrophobic properties.<sup>108, 114-117</sup>

There are many molecules in the human body which owe their functionality to their amphiphilic properties such as phospholipids in bilayers, membrane proteins and various fatty acids. For instance, the amphiphilic nature of fatty acid is an extremely important property that supports continued body functions such as cell signalling, energy storage and providing some of the building blocks for cell membranes.<sup>118-120</sup> The coexisting hydrophobic and hydrophilic segments allows an amphiphilic surfactant molecule to exist at water and oil interface as well as, more importantly for this research, self-assemble in an aqueous environment into ordered structures (Figure 3).<sup>121-122</sup>

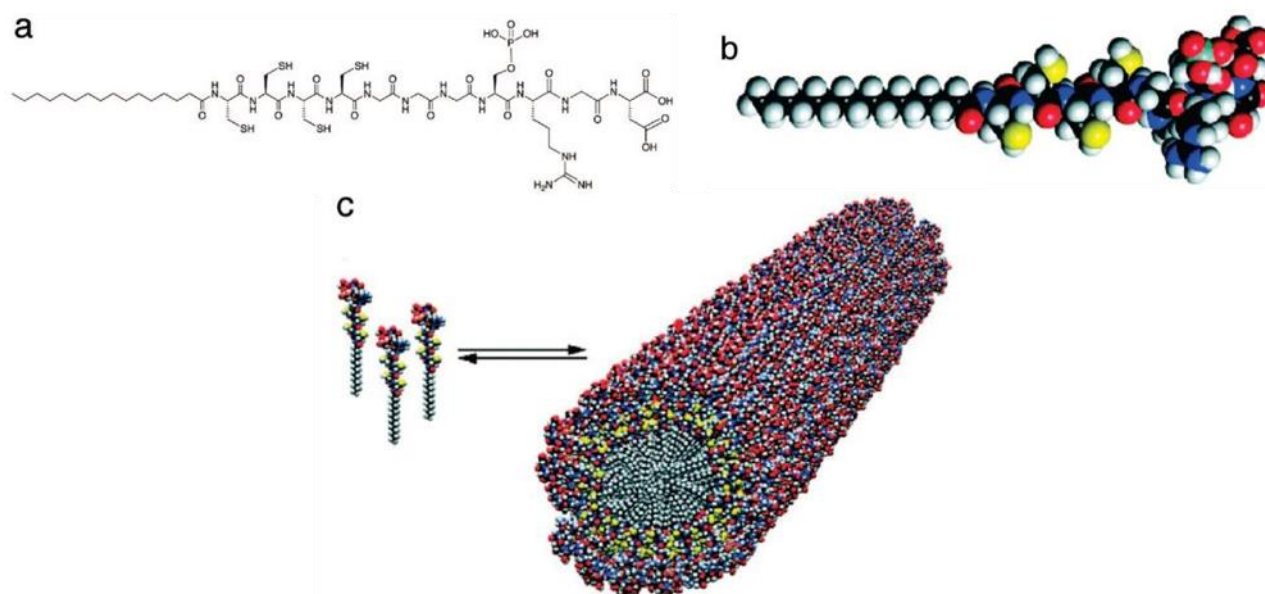


**Figure 3:** Lipopeptide amphiphiles. A) and B) display the chemical formula and calotte model of the lipopeptide pentadecenoyl-CCCCGGGS(phosphorylated)RGD. C) Self-assembled rod-like aggregate of the lipopeptide pentadecenoyl-CCCCGGGS(phosphorylated)RGD in aqueous environment. Note, the polar groups RGD of the peptide are in contact with water, while the hydrophobic hydrocarbon chains are shielded from the water phase and located in the core of the aggregate. This figure has been adapted from reference 122.<sup>122</sup>

## 1.8 Self-Assembly

**Methods of Self-Assembly.** Self-assembly is a relatively old research area (>100 years)<sup>123</sup> that carries with it a vast amount of literature on theoretical, experimental and applied research.<sup>23, 33, 115, 123-157</sup>

Self-assembly occurs through the intermolecular forces causing a favourable structural change to an ordered system. This effect is dependent on many variables, including surfactant concentration, pH, ionic strengths, temperature, hydrophobic and hydrophilic interactions, intermolecular bonding types, (such as hydrogen bonding or van der Waals forces), electric and magnetic fields. Self-assembly can also be assisted by 2D or 3D templates.<sup>158-161</sup> All these forces take some effect on either the enthalpy and/or entropy of aggregation.

Amphiphilic molecules such as PAs and lipopeptides self-assemble at a critical concentration, known as the Critical Aggregation Concentration (CAC).<sup>162</sup> Similarly, the Critical Micelle Concentration (CMC) defines the concentration at which surfactant-like molecules start to form

micelles. It should be noted that CMC is not applicable to all self-assembling molecules, as structures other than micelles can be formed.

Lipopeptides and PAs self-assembly has been investigated under various conditions, including their concentration, pH, temperature and ionic strength characteristics.<sup>116, 146, 163-166</sup> In aqueous solutions the hydrophobic section, the alkyl chain predominantly for lipopeptides and the hydrophobic amino acid groups or the co-polymer in PAs, aggregate to form different self-assembled structures, where the hydrophobic moieties are found in the core of the aggregates due to the hydrophobic effect. This results in a screened hydrophobic environment with the hydrophilic, sometimes bioactive, peptide located at the polar and apolar interface. The reverse occurs when PAs are immersed into a hydrophobic environment (non-polar solvents), resulting in the hydrophilic moieties being located at the core of the aggregate.<sup>167-169</sup> This reverse process is not investigated extensively, since the human body, being made up of 60% water, provides a predominately aqueous environment for lipopeptides and PAs.

**3D Self-Assembled Structures.** The self-assembled structures of PAs and lipopeptides are defined by a number of structural categories. These include micelles, liposomes, nanotubes, nanotapes, fibrils, ribbons, and bilayers. Micelles are often spherically shaped organisations of molecules. In aqueous solutions the hydrophobic tail sections point inwards forming a hydrophobic pocket protected by the hydrophilic head groups or segments on the outside. If the hydrophilic parts are formed of bioactive segments, this will form very bioactive external surface.<sup>152, 170</sup>

Nanotubes and tapes are distinct structures that can be formed by specific PAs and lipopeptides. These tapes and tubes are able to transfer oxygen, encapsulate carbon particles and are able to be aligned by shear force.<sup>171-174</sup>

Fibrils is a term used to describe a fibre-like structure that can have various linkages and off-shoots.<sup>175-176</sup> They are normally tubular in shape and can have various thicknesses. There are specific detrimental types of  $\beta$ -sheet secondary structure fibrils, called amyloid fibrils that are heavily associated with neurodegenerative diseases, such as Alzheimer's disease.<sup>176-180</sup> Ribbons, or nanoribbons, are 2D planar regularly ordered structures that can be flat or twisted along their main axis, and in the case of twists, they may exhibit a variety of different spacings between them.

Bilayers are composed by two sheets of amphiphiles, where the surfaces are commonly polar, and its core is hydrophobic.<sup>181-184</sup> These structures can then become building blocks for further structures.

Liposomes refer to vesicle formation, which are normally spherical in shape, and can contain a differing solvent inside their body. This gives them the potential transporting various substances.<sup>185-186</sup> Liposomes can either be multilamellar vesicles (MLV) formed from many bilayers stacked in radial direction or are unilamellar vesicles (ULV) which have only one bilayer. Solid supported films are multilamellar bilayers being typically formed on a solid-supported wafer, e.g. on a silica wafer.

All the self-assemblies described above can be formulated with lipopeptide and peptide amphiphiles, equipping them with the benefits of increasing the bioavailability of the drug, supporting the administration of regenerative medicine and the potential treatments for diseases.

## 1.9 Applications of Self-Assembling Peptide Systems

*Skincare.* PAs and lipopeptides have found many applications with some pertinent examples being discussed within this section. A commercially available lipopeptide with the trade name Matrixyl™ (C<sub>16</sub>-KTTKS) has been used in anti-wrinkle creams. This lipopeptide has been shown to self-assemble into a  $\beta$ -sheet, fibrillary-like superstructure via CD and TEM. Hamley et al. investigated this fibrillar structure and found it to have a bilayer spacing of 5.3 nm using small angle X-ray scattering (SAXS).<sup>108</sup> Further investigations using human dermal fibroblasts suggest that the KTTKS polypeptide increase the skin's collagen production by forming a similar self-assembled structure to that of the skins extracellular matrix (ECM), but the mechanism for the anti-wrinkle effect is not fully understood.<sup>187</sup> ECM is the outer region of a cell, which supports the cell and those around it. This ECM has also shown to form parallel arrays of polydisperse fibrils, similar in structure to that of the lipopeptide. The combined KTTKS peptide motif with the C<sub>16</sub> chain has also shown to assist the skin permeability, and further, the self-assembled structures produce a highly peptide-rich surface. The combination of this similar parallel structure and the increase skin permeability, all add to the increased collagen production, making it a highly effective skincare additive. This lipopeptide's effect happens at a low concentration, which is close to its CAC, 0.002 wt%.<sup>188</sup> Other lipopeptides, such as C<sub>16</sub>-GHK or C<sub>16</sub>-KT, also have been reported, on an experimental basis, to have

collagen stimulating effects with similar  $\beta$ -sheet nanostructures, but were not as highly ordered or as long as those of C<sub>16</sub>-KTTKS.<sup>108</sup> This observation has not been fully understood but does lend evidence to the self-assembled structure being important in allowing increased collagen production. However, the high order and length of the fibrillar structures do not seem to be as important as the secondary structure in collagen stimulating effects.

**Tissue Scaffolds.** Various research groups have investigated the use of PA and lipopeptides as scaffolds to produce tissue or other cells. For instance, the linear RGD amino acid sequence was linked with dialkyl lipid chains. This scaffold allowed for spreading of melanoma and endothelial cells when it was carboxyl-coupled but inhibited spreading with amino-attached PAs. It was concluded that the resultant amino-attached PA self-assembled structure was poorly packed and the RGD active peptide head was less accessible to the cells.<sup>189</sup> Another group managed to encapsulate cells within nano-fibrils made up of PAs with the IKVAV peptide group.<sup>190</sup> These PAs were shown to be effective at treating spinal cord injury in mice. This was due to the nano-fibrils inhibiting scar formation which helped to lessen the injury. Guo et al. suggest this is because of the nano-fibrils allowing for robust migration of host repair cells, growth of blood vessels and axons (nerve fibre cells). This migration of host repair cells shows that this self-assembled peptide nanofibre scaffold (SAPNS) mimicked a friendly 3D cell environment. This observation invites further research as it could lead to a greater use of SAPNSs in healing and the reduction of scar formation.<sup>190</sup>

**Antimicrobial Applications.** The area of antimicrobial and antibacterial materials and agents has probably received most of the research attention with regards to PA and lipopeptide self-assembly. Lipidation of peptides has shown to improve the uptake of the peptide into the cell wall. This was investigated with a range of gram-negative or positive bacteria and two common fungal strains. This improved uptake into the cell wall and subsequent disruption of the cell membrane was found to be an efficient mode of action, causing bacterial leakage and cell death.<sup>61</sup> An amphiphilic TAT peptide was found to work as an effective antimicrobial agent in a similar way. It was further demonstrated that the PA can also be transported across the blood-brain barrier, potentially having brain infection combating potential.<sup>191</sup> Possibly one of the best-known lipopeptides used in treating infections is daptomycin. Daptomycin has been so successful in its ability to combat systemic and life-threatening infections that it is now marketed under the trademarked name of Cubicin®. It is a cyclic peptide group joined by an amide linkage to a lipid chain (Figure 2). The mechanism by which daptomycin acts on bacteria has been investigated quite extensively.<sup>61, 64-65, 192-198</sup> It works by using the lipid chain to insert into

the cell wall. The daptomycins then aggregate within the cell membrane causing pores to form, leaking internal cell ions. This in turn causes cell depolarization, resulting in the inhibition of various syntheses, including that of DNA, RNA and protein. These effects combine to cause cell death. The self-assembly of daptomycin was studied in aqueous conditions, outside the cell, and was shown to form micelles.<sup>65</sup> This aggregation process in the bacterial cell membrane makes it one of the best lipopeptide drugs to treat gram-positive organisms; it also causes limited side effects when not administered in the right dosages. The common side-effects include hypotension (low blood pressure), insomnia and dyspnoea (shortness of breath), making it vital to monitor patients going through daptomycin therapy as well as controlling the dosages.<sup>199-200</sup> Caspofungin and amphotericin B are other commercial antimicrobial drugs that have had very high success rates on fungal infections.<sup>201-202</sup> Both work in different ways, caspofungin by inhibiting glucan synthesis, while amphotericin B works by ion leakage coupled with oxidative stress production inside the cell. The examples given here represent a small sample of the lipopeptide drugs that are commercially available, with many more currently undergoing trials.<sup>196, 203-204</sup>

***Drug Delivery.*** Drug delivery has been investigated with PAs and lipopeptides.<sup>113, 142, 205-223</sup> In this thesis the two main approaches of drug delivery were looked at. The first approach makes use of the self-assembled structure of PAs and loading hydrophobic drug molecules in the hydrophobic core of the self-assembled structures such as micelles, uni/multilamellar vesicles or fibres. This method allows for the transport of the drug in highly aqueous environments to reach the target cells. An instructive example is TAT PA, a single layer fibre nanostructure with a hydrophobic inner core that is due to the high number of octanoic acid (hydrophobic) groups and the high length to head group ratio. It was shown that the PAs with the highest amount of octanoic acid groups could encapsulate and retain the drug paclitaxel, to help with the treatment of oesophageal, breast and lung cancer. This PA is still under research, but looks very promising for drug formulation for the treatment of cancer.<sup>224</sup> The high hydrophobicity of the octanoic acid groups made this drug delivery system highly efficient because it was able to protect the hydrophobic drug in an aqueous environment. The other main use of PA for drug delivery concerns the lipidation of specific peptide head groups. While the peptide head groups define their binding capacity to specific receptors, the attached lipid group allows the PA to cross various membranes, thereby increasing its bioactivity as well as reducing the probability of it becoming metabolised. A good example of this is an amphiphilic design of the commercial anti-cancer drug dalargin, which forms nanofibres.<sup>100</sup> These fibres displayed high blood

circulation times, and more importantly, they were able to cross the blood-brain barrier. This allowed the normally hydrophobic cancer drug to reach cancer-tumours within the brain.

In summary, lipopeptides and peptides have many useful applications that include (i) additives to skin care products, helping with collagen stimulation, (ii) tissue scaffolds, differentiating stem cells before injection, (iii) anti-microbial peptide drugs, most notably Daptomycin or Caspofungin and finally, (vi) promising drug-carrier developments, with promising cases increasing the circulation times in the body and improvements in delivery of drugs across the blood brain barrier.<sup>65, 187, 193, 196, 201, 217, 225-230</sup>

Even though some of the applications of lipopeptides and peptides are clearly less clinically critical than others, they all make use of the two different but important aspects of peptide amphiphiles and lipopeptides; namely the ability of amino acids to be tuneable to specific functions and their ability to self-assemble.

## 1.10 Hydrogels

**Structure and Functions.** Hydrogel is a term used to define hydrophilic (water-loving) polymer chain networks that are highly water-absorbent with some hydrogel configurations allowing for over 90% water retention. The polymers are classified homopolymer, copolymer or multi-polymer gels which defines the monomer base unit, i.e. it contains one, two or more monomers, respectively. These polymer networks can be natural or synthetic and are held together by covalent bonds and/or crosslinks, van der Waals' forces and hydrogen bonding.<sup>142, 231</sup> Due to the hydrophilic nature of the polymer chains they also contain charged species that are either anionic, cationic and ampholytic (both charges present). Hydrogels are commonly amorphous polymers, meaning that its overall structure has a random organisation, though some hydrogels can be cross-linked which does impart some crystallinity to the hydrogel. Furthermore, semi-crystalline polymers have local areas of order but the overall structure is still random. Lastly, crystalline polymers are typically highly ordered systems with only a small fraction of amorphous material.

Hydrogels are highly susceptible to environmental factors such as pH, temperature and pressure.<sup>232</sup> To tailor a hydrogel in a specific function, all three factors can be exploited for the drug delivery by, for example, triggering the drug release through a change in pH or pressure.

The ability to vary hydrophilic and hydrophobic polymers, along with their individual properties, allows for hydrogels to be used in an extensive range of applications.

***Applications of Hydrogels.*** There is a growing interest in the use of hydrogels as scaffolds for tissue engineering. A study carried out in 2014 used a biodegradable thermosensitive hydrogel to mimic microenvironments for the differentiation of stem cells, with the potential to improve *in vivo* (human) injection.<sup>233</sup> The stem cells injected would already be selective to the location needed, thus having higher acceptance and success rates when injected.<sup>233</sup> Apart from applying responsive hydrogels under variable environmental conditions, they are widely used for their capacity to absorb large quantities of liquid. Biodegradable cellulose-based hydrogels are being designed to combat the ever-increasing use of disposable nappies, hopefully leading to a sustainable way of degradation, and the returning of substances to landfills in a non-toxic way. Another use for hydrogels is given in the production of water-gel explosives. These water-gel explosives are composed of a mixture of aqueous ammonium nitrate solution in a gel-like mixture, normally polyvinyl alcohol, dextran gums, or urea-formaldehyde. These water-gel explosives have almost completely taken over the use of dynamite as they are cheaper to make, can be manufactured to be less toxic and are substantially less hazardous to produce, transport and store.<sup>234</sup> Recent research efforts have focused on the use of hydrogels to potentially function as an artificial cornea scaffold.<sup>235</sup> Hydrogels guarantee good retention of liquid, thus reducing the probability of the artificial cornea from drying out and it allows the polymer to be customised, being able to create varied segments. These can be used to protect the eye from sunlight or to prevent bacterial growth.<sup>235-236</sup> A few variants have been developed, including, PHEMA (poly(HEMA-co-methacrylic acid copolymers), PVA based co-polymers, collagen polymer variants and interpenetrating polymer networks, the last of which are hydrogels with two entangled non-covalent bonded polymeric systems.<sup>237</sup> Gels have also been made for the cholesterol lowering drug Atorvastatin that is injected intramuscularly (into deep muscle tissue) as a *in situ* gel.<sup>238</sup> Gels can also be injected subcutaneously (under the skin layer, but above the muscular layers), such as with the cholesterol lowering drug Simvastatin, which uses a chitosan and  $\beta$ -glycerol phosphate disodium salt hydrate-based hydrogel.<sup>239</sup>

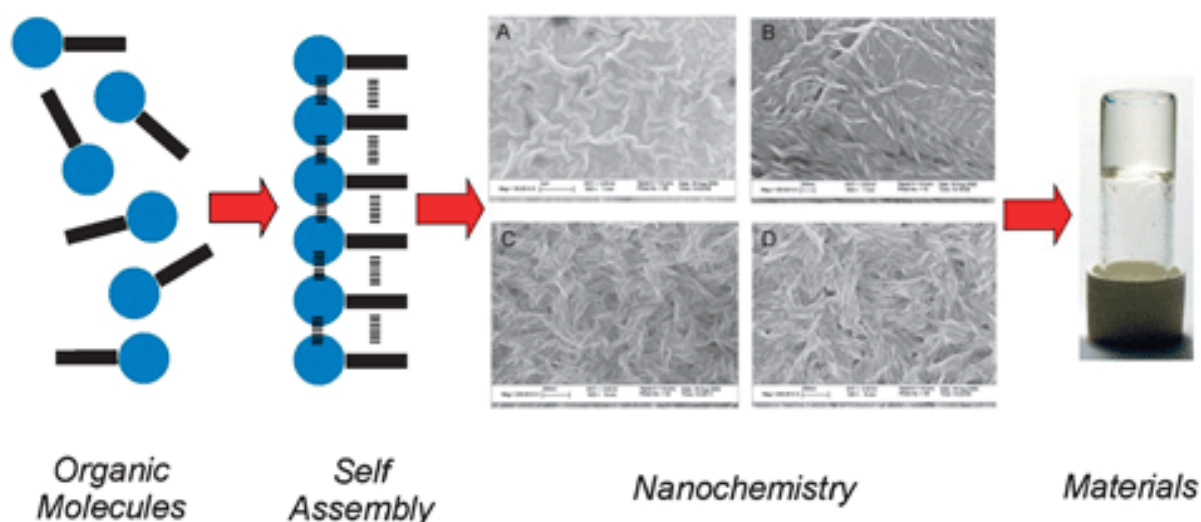


**Figure 4:** Image showing the process of self-assembly to materials. Left – Individual organic molecules, which could be either peptide amphiphiles, lipopeptides or any amphiphilic molecule with an organic base self-assemble. Second and third from left – Larger nano-scale formation of layers or films as observed by TEM. Fourth from left – A stiff gel in a vial produced by the self-assembly and nano-scale ordering. The figure is taken from reference.<sup>240</sup>

**Gels from Self-Assembly.** Gel formation of self-assembling systems is a promising research field, finding applications in hydrogen bond donors and acceptor systems and novel fibril formations. In particular, lipidation of peptides and PAs can be used for the formation of hydrogels (Figure 4).<sup>232, 241</sup> Hydrogels formed from self-assembly show similar structures to those of common polymeric hydrogels and exhibit similar responses to pH, temperature and light.<sup>242-245</sup> Generally, drug delivery has to cope with a delicate balance of sustained release, efficacy and stability. It has been demonstrated that the incorporation of a biological molecule into a large self-assembled structure leads to slow and sustained release profiles (slow release over a long time) and drug stability.<sup>212, 246-250</sup> The main issue with self-assembled systems is the potential for loss of drug effectiveness. This issue can be caused by self-assembly limiting the drug's interactions with blood proteins, i.e. potentially limiting its ability to get to its active site by retention within the self-assembled drug carrier. Another reason for a reduction in efficacy is that the drug candidate needs the ability to self-assemble or to be held within the self-assembled drug carrier, which could mean a modification to the bioactive drug molecule itself. These modifications, through the addition of a lipid, polysaccharide, or other molecule, could change the efficacy of the molecule. Any decrease or increase in charge, amino acid sequence, secondary structure, or tertiary structure could also have a large impact on the efficacy of the drug molecule.<sup>251-254</sup> Thus, hydrogels can be considered a highly useful material with bioactive

properties, as long as the drug molecule is not modified beyond its ability to create the necessary bio-response.

## 1.11 Endocrine Peptides

**Figure 5:** Diagram showing the main peptides involved in the control of hunger. The figure has been taken from reference<sup>255</sup>.

The endocrine system is a large network of glands within the body that creates a multitude of peptide hormones, helping to control moods, growth and development of cells, metabolism and reproduction.<sup>256-260</sup> A few of the glands involved in this network are the hypothalamus, pituitary, pineal gland, thyroid gland, adrenal glands, pancreas and ovaries or testes. One area that the endocrine system controls is the satiety level (hunger). As shown in Figure 5, there are different peptides produced by the human body for the control of satiation and glucose homeostasis.<sup>255, 261</sup>

Produced in the oxyntic glands within the stomach, Ghrelin is a 28-amino acid peptide that has the ability to stimulate calorie intake. Studies have shown within rats that were injected via their cerebrospinal fluid (to by-pass the blood brain barrier), they were resistant to induced obesity when fed a high-fat diet. This was related to the rats eating less and therefore utilising stored triglycerides and lipids as the main energy source.<sup>262</sup>

Leptin, another well-known peptide hormone, is produced by the adipose cells that control many biological mechanisms that are linked with inflammatory responses, wound healing, and

bone formation. Another valuable effect is that leptin limits food intake by binding to key regulatory centres within the brain. This helps maintain the energy balance within the body and overall homeostasis. Various studies show leptin activity is linked strongly to the hypothalamus that controls the expression of various appetite-stimulating and suppressing peptide hormones.<sup>263</sup>

Glucagon-Like Peptide 1 (GLP-1) is a 30-amino acid peptide that stimulates insulin secretion. Further to this, GLP-1 has been linked to inhibiting gastric emptying and reducing appetite. Produced in the L-cells within the small bowel and colon, GLP-1 circulates within the body and is cleaved by the enzyme Dipeptidyl Peptidase IV (DDP-4), making it inactive.<sup>73</sup> DDP-4 is produced by the body in large quantities, thus making the half-life of GLP-1 limited to a few minutes. Even with the poor half-life, developments towards a GLP-1 drug and formation have been heavily researched. The GLP-1 receptor is also of great interest for targeted drug design as it can be activated by an agonist that leads to the same satiety increasing effects, as seen when activated with the peptide hormone GLP-1.<sup>22</sup> Various GLP-1 receptor agonist drugs have been on the market since 2014, with one under the trade name of Semaglutide<sup>TM</sup> showing a 20% body mass reduction.<sup>264-267</sup>

Pancreatic Polypeptide (PP) is a 36 amino acid peptide that belongs to the PP-fold family.<sup>268</sup> Pancreatic polypeptide, in a similar manner to GLP-1, is released after consumption of food and is linked to the modulation of gastric acid secretion and gastric emptying.<sup>269</sup> Further studies have shown the level of PP is dependent on the blood glucose levels, insulin levels and on the digestive state the body is in. This shows that pancreatic polypeptide could play an important role in energy homeostasis and feeding behaviour, leading to a potential drug candidate for the control of appetite.

## 1.12 Peptide YY

**Structure and Activity.** Polypeptide YY, or Peptide YY (PYY), as it is more commonly known, is a gastrointestinal hormone belonging to the neuropeptide family. The primary structure of its various forms is described as follows:

PYY - YPIKPEAPGEDASPEELNRYRYASLRHYLNLVTRQRY

PYY<sub>3-36</sub> - IKPEAPGEDASPEELNRYRYASLRHYLNLVTRQRY

This peptide family includes PYY as well as the Neuropeptide Y (NPY) and Pancreatic Polypeptide (PP).<sup>268</sup> The PP-fold motif is found throughout this family and is formed through the incorporation of certain residues that are predominately Pro2, Pro5, Pro8, Gly9 and Tyr20 and Tyr27 (Figure 20). This PP-fold has been found to protect the peptide against enzyme attack as well as producing a hydrophobic pocket that reduces the hydrophobic residues interaction to the aqueous environment.<sup>270</sup> As well as containing the PP-fold motif, PYY and its derivative PYY<sub>3-36</sub> also have a high C-terminal  $\alpha$ -helix proportion that has been suggested to be extremely important for structural integrity of PYY.<sup>271</sup>

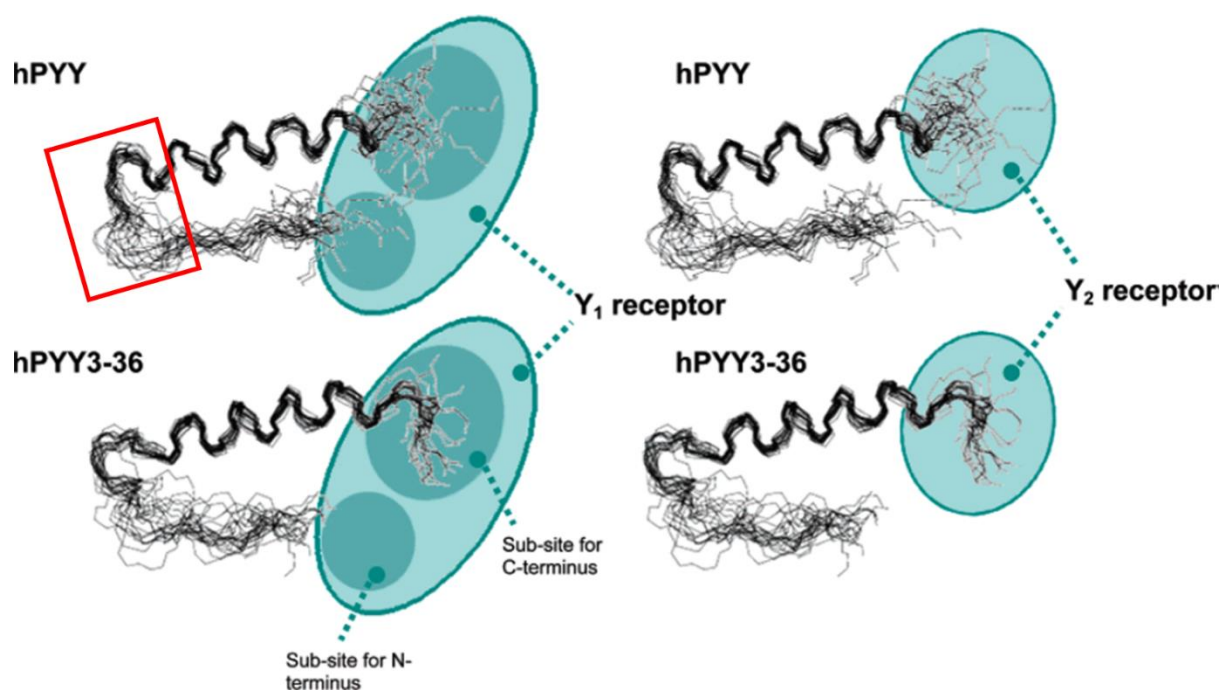


**Figure 6:** Illustrations of binding sites for Y1 and Y2 with hPYY + hPYY<sub>(3-36)</sub>. Red box highlights the PP-fold, characteristic for the neuropeptide family. For further details, refer to the main text. The image has been taken from reference.<sup>271</sup>

PYY is a native peptide produced predominately by the colon after food intake. After secretion into the body, the 36-amino acid PYY is cleaved by the Dipeptidyl Peptidase IV (DPP-IV) protein, leading to PYY<sub>3-36</sub>, i.e. losing the Tyrosine-Proline residues from the N-terminus. Both, the PYY and its 3-36 form act on a certain set of G-protein coupled receptors that are

large proteins that detect molecules on the outside of the cell and produce an internal cell response, termed the neuropeptide Y receptors. There are currently five known Y receptors, Y<sub>1</sub>, Y<sub>2</sub>, Y<sub>3</sub>, Y<sub>4</sub> and Y<sub>5</sub>. Only four receptors (1, 2, 4, and 5) have been found to have significant effects on the human body.<sup>272-273</sup> These receptors have varied actions including reducing appetite, controlling circadian rhythm, and influencing anxiety levels. NPY, PYY and PYY<sub>3-36</sub> have varied binding affinities to these Y receptors. PYY binds to all Y receptors with equal affinity but PYY<sub>(3-36)</sub> binds selectively to the Y<sub>2</sub> receptor.<sup>87, 271</sup> This change in binding affinity has been hypothesised to be due to the structural loss of the tyrosine and proline amino acids.<sup>271</sup> It is thought that the Y<sub>1</sub> receptor requires both the C-terminus and N-terminus for recognition, binding and subsequent activation. The Y<sub>2</sub> receptor is thought to have a smaller receptor site and only requires the C-terminus for recognition (as shown in Figure 6). This could explain the reduced affinity for PYY<sub>3-36</sub> for any other Y receptor than Y<sub>2</sub>.<sup>271</sup> Other studies that replaced the amide bonds with ester bonds also confirm the role of the end section and its significance in binding and activation.<sup>274</sup>

***Effects on the Human Body.*** Research into the PYY and PYY<sub>3-36</sub> effects on the body have been completed, although predominately in the food and biological science fields.<sup>84, 275-278</sup> A study in 2002 commented on the potential for acute peripheral administration of PYY<sub>3-36</sub> to inhibit food intake.<sup>279</sup> PYY<sub>3-36</sub> was injected into fasted (for 24 hr) rats' hypothalamuses and showed a significant decrease in food intake, even at low 100 fmol doses.<sup>280</sup> This effect was initially controversial with only a very few other researchers being able to repeat the results.<sup>281</sup> A theory behind the proposed controversy was that the mice used in the repeat tests were unaccustomed to a laboratory environment and as such they experienced increased their stress levels. Stress inherently reduces baseline food intake and, as such, it makes any investigations on anorectic (appetite suppressing) agents difficult to assess.<sup>281</sup> Further research into its use in human studies has found that obese subjects showed normal levels of sensitivity to the appetite reducing effects of PYY<sub>3-36</sub>, meaning PYY<sub>3-36</sub> is a good candidate for use in the reduction of appetite for obese patients.<sup>282</sup>

***Potential Applications and Problems.*** The ability of PYY and PYY<sub>3-36</sub> to reduce food intake has made it of great interest as an anti-obesity or chronic eating disorder medication. A few studies have shown that even though it works as an appetite suppressant, it does have some drawbacks that need to be overcome. Studies that used high doses of PYY have reported taste aversion in animals and caused humans to be nauseous.<sup>283</sup> This effect was compounded however by rapid dose administration. These side effects were combated by issuing low doses

at a steady and controlled infusion rate mainly through intravenous injections.<sup>284</sup> The two main problems with the administration of PYY seem to be both the dosage and how it is administered; low doses intravenously administered seem to be the optimum dose path.<sup>285</sup> This however is inconvenient for patients, as they must inject themselves with low doses multiple times during the program and this can cause irritation and/or damage to the veins; it can also build up patient reluctance to keep injecting regularly. Oral and nasal dosage overcome these issues, but with both methods the efficacy drops off as the nose or stomach drug barriers limit uptake into the body.

Peptide lipidation and gelation, with their ability to better protect the drug within the human body, could overcome the issues of the efficacy drop off, and therefore allow for the application of PYY<sub>3-36</sub> as an effective satiety drug. The development of a greater understanding of PYY<sub>3-36</sub> lipidation could potentially advance the field of the use of large peptides and lipidation for drug delivery, which in turn, would expand the potential drug candidate list for the treatment of a greater number of health issues.

### **1.13 Research Aims and Objective**

The overall aims of this project are to investigate the effects of (i) *lipidation on structure the hunger-suppressing hormone PYY<sub>3-36</sub>* and (ii) to investigate strategies for the *development of prolonged release methods*. Applied methods embrace different approaches such as the formation of a gel, the complexation of PYY<sub>3-36</sub> to another moiety such as  $\beta$ -cyclodextrin and incorporation of other stabilisers used within the formulation research area. While there is already an extensive body of research going on in PYY in the fields of medicine and biology, investigations have still not been carried out on lipopeptide conjugates, making these studies novel and highly interesting to many fundamental and applied research fields. The first set of studies in this body of work were planned to compare the structural differences between the novel lipidated versions and the un-lipidated version.

The first set of planned studies were:

- Investigate the secondary structure changes caused by the addition of a lipid to the peptide hormone at room temperature using Circular Dichroism spectroscopy (CD) (Methodology in Chapter 2.2.3).

- Investigation of the differences in position of lipidation on the secondary structure and the differences in self-assembled structure formed, using Cryo-TEM and SAXS methods (Methodology in Chapter 2.2.1 and 2.2.2).
- Once determined at room temperature, to investigate their stability to temperature by completing a thermal denaturation experiment (Methodology in Chapter 2.2.3).
- Investigate the effect of a selection of physiological pHs on the secondary structure and self-assembled structure of the lipidated PYY<sub>3-36</sub>, using a combination of CD and SAXS techniques (Methodology in Chapter 2.2.2 and 2.2.3).
- Using critical aggregation concentration methods to understand the concentrations at which the determined self-assembled structures form (Methodology in Chapter 2.2.6).
- Further investigation of pH effects on the critical aggregation concentrations (Methodology in Chapter 2.2.6).
- Investigate the potential for the formation of gels using the lipidated peptide hormone self-assembled structures (Methodology in Chapter 2.1.2).
- If hydrogels form, investigate the macro-structure using transmission electron microscopy (TEM) (Methodology in Chapter 2.2.1).
- Investigate, using SAXS, the self-assembled structure with comparison to the non-gel structure (Methodology in Chapter 2.2.2).
- Investigations of the secondary structure changes between the gel and non-gel form by CD (Methodology in Chapter 2.2.3).

With these differences determined and the potential hydrogel investigated, this allowed further research into the potential use of these lipidated hormones as potential drug candidates. This second research section was planned to focus on the structural investigation of these novel lipopeptides, using a variety of scientific methods to explore new avenues of drug design and formulation.

The second set of planned studies were:

- Investigate a synthesis route for a sugar complexation to the peptide hormone PYY<sub>3-36</sub>.
- Investigate the known complexation properties of  $\beta$ -cyclodextrin and improve its drug formulation and delivery potential of PYY<sub>3-36</sub> (Methodology in Chapters 2.2.1 to 2.2.7).

Wider investigations of the interaction of the lipidated peptide hormone with a well-researched bacterial cell wall endotoxin LPS, including co-self-assembly studies, and comparisons to a known anti-bacterial agent A9R.

## 2. Materials and Methods

This chapter details the materials and methods applied throughout this thesis. This includes explaining in detail the experimental design and the experimental strategy for the subsequent result chapters. Methods that will be covered are Transmission Electron Microscopy (TEM), with a particular focus on Cryo-TEM, Small Angle X-ray Scattering (SAXS), with the showing of SAXS fitting methods, Circular Dichroism (CD), Pyrene Critical-aggregation Concentration (CAC) experiments, lipopolysaccharide specific dye 4,4-difluoro-4-bora-3a,4a-diaza-s-indacene (BODIPY-TR) experiment, UV absorbance concentration measurements and zeta potential experiments.

### 2.1 Materials and Sample Preparations

#### 2.1.1 Materials

PYY<sub>3-36</sub>, 11PYY<sub>3-36</sub>, 17PYY<sub>3-36</sub> and 23PYY<sub>3-36</sub> acetate salts were custom synthesised by Bachem, Bubendorf, Switzerland. The design and specific location of the lipidation was determined by the industrial sponsor MedImmune Ltd prior the commencement of this thesis. The molecular mass was measured using matrix-assisted laser desorption/ionisation - mass spectrometry (MALDI-MS) by the supplier using a Axima-CFR instrument (Shimadzu, Kyoto, Japan) and found to be 4049.61, 4458.19, 4389.13, 4389.27 g mol<sup>-1</sup>, respectively, with error values of  $\pm 0.10$  g mol<sup>-1</sup> for all acetates (theoretical expected value, via chemical structure: 4047.07, 4454.37, 4387.32, and 4387.32, respectively g mol<sup>-1</sup>). The molecular mass was checked by Electrospray Ionization – mass spectrometry (ESI-MS) separately by the University of Reading Chemical Analysis Facility (CAF) team using an LTQ-Orbitrap XL instrument (ThermoFisher Scientific, Waltham, MA, USA) and found to be 4049.07, 4458.41, 4389.32, and 4389.33 g mol<sup>-1</sup>, respectively, with error values of  $\pm 1-3$  ppm for all measurements. The purity was 96.9, 95.4, 97.8, and 98.3%, respectively, with error values of  $\pm 0.1\%$  for all measurements, as determined using a Dionex UltiMate 3000 HPLC (ThermoFisher Scientific, Waltham, MA, USA) system with Vydac C18 column (Hesperia, CA, USA).

All water used throughout these preparations and experiments was ultrapure water (18 M $\Omega$  Barnstead Nanopure, ThermoFisher Scientific, USA). All pH changes were completed using micropipette additions of 1 M HCl or 1 M NaOH, purchased reagent grade from Sigma-Aldrich (MO, USA). pH was determined by electronic pH meter, more details in Chapter 2.1.2.

All Lipopolysaccharide (LPS) used within this thesis was sourced from Sigma Aldrich (St. Louis, Missouri, USA). The LPS was biologically obtained from *Escherichia coli* 0111:B4 and was supplied purified by phenol extraction. Batches of 100 mg powder were purchased when required. It should be noted that LPS is extremely heterogeneous and, as this material was obtained from a biological source, its purity would be under question. This issue of LPS purity is addressed within Chapter 5.

$\beta$ -cyclodextrin and maltoheptaose used throughout this these was purchased from Sigma Aldrich (St. Louis, Missouri, USA). The  $\beta$ -cyclodextrin obtained was of 25 g and was supplied with greater than 97% purity, determined by the supplier. The maltoheptaose was purchased at the highest purity available, 60% determined by the supplier.

The pyrene used for all CAC measurements was purchased from Sigma Aldrich (St. Louis, Missouri, USA). It was supplied at 98% purity.

### **2.1.2 Sample Preparations**

#### ***Gel Sample Preparation***

Gels were prepared by making up 1–2 wt% peptide solutions in ultrapure water (18 M $\Omega$  Barnstead Nanopure, ThermoFisher Scientific, USA), and changing the pH accordingly using 1 M HCl or 1 M NaOH (ThermoFisher Scientific, USA). The pH was recorded using an electronic pH meter, more details of the equipment used is provided below. The solutions were heated to 60 °C for approximately 2–10 h and then left to stand for 3 to 24 hours for the gelation to occur. The concentration of the gels was determined by Nanodrop experiments (Chapter 2.24) and ranged from 1.6 to 2.4 wt%. The pH range studied was pH 2–8.

#### ***Solution Sample Preparation***

Solutions were prepared using ultrapure water (18 M $\Omega$  Barnstead Nanopure, ThermoFisher Scientific, USA), and changes to the solutions pH values were completed using reagent grade 1M HCL and 1M NaOH (ThermoFisher Scientific, USA). The pH values were recorded using an electronic lab-based pH meter, with a glass pH electrode and an internal calibrated electrode. The pH meter was calibrated before each experiment by using two buffer solutions of known pH. The pH meter can produce pH values for the samples to two decimal places, with an error of  $\pm 0.01$ , however pH values are given to one decimal place.

### ***Pyrene Sample Preparation***

Peptide concentrations of  $1.3 \cdot 10^{-3}$  to 0.13 wt% were used with a constant  $2.167 \cdot 10^{-5}$  wt% of pyrene within each sample. A 0.05 wt% pyrene in ethanol stock solution was prepared. 0.046 mL of this stock solution was evaporated, confirmed to be completed by visual precipitation, on the inside edge of a glass vial then made up to 100 mL with water. This provided a concentration of  $2.167 \cdot 10^{-5}$  wt% of pyrene in water. This concentration is at the upper threshold of pyrene's dispersion within water. A higher concentration above this value would show the presence of precipitation of pyrene crystals and can affect the CAC measurements.

### ***BODIPY-TR Cadaverine and Lipopolysaccharide Sample Preparation***

The plan for these samples was make two peptides solutions, PYY<sub>3-36</sub> and A9R, made up to the same molarity, and have a solution of LPS and BODIPY-TR Cadaverine to which they were added. To complete this 1 mg sample of BODIPY TR (Invitrogen™, ThermoFisher, Waltham, MA, USA) was dissolved in a 200 mL volumetric flask with water (supplier mentioned previously), giving the solution a bright pink colouring (Figure 7A). A 20 mL aliquot was taken and to this 1 mg of Lipopolysaccharide (Sigma-Aldrich, Missouri, USA) was added, changing the solution to blue colour, as seen in Figure 7B. This solution was then used as the starting solution for all fluorescence readings, to which the same molarity peptide solutions were added.

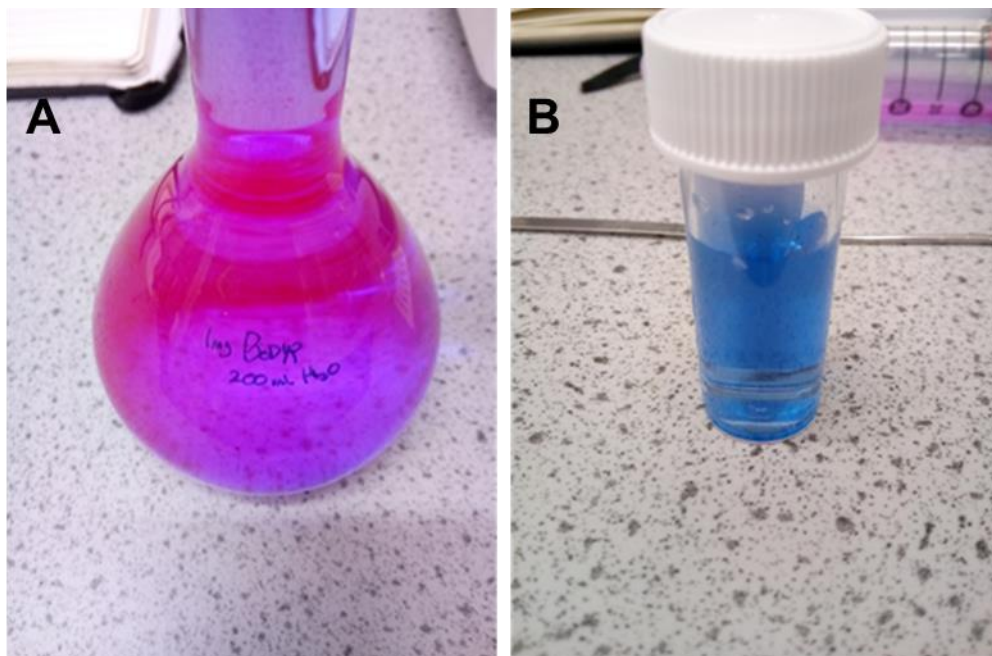


**Figure 7:** Visual colour shift, from pink to blue, from the complexation of LPS and the LPS specific dye BODIPY TR. A – Showing 1 mg of BODIPY TR in 200 mL H<sub>2</sub>O, giving a strong pink colour. B – Small aliquot of A with the addition of 1 mg of LPS, changing the colour to a blue.

The effect of pH and the peptide concentration is extremely important in the determination of precise and reliable results for all the applied methods used in this thesis. A good example of this would be the CD methods as the results can be highly affected by both variables. For this method, if the pH is incorrectly recorded then the results cannot be confidently used to determine the secondary structure of the peptide. Though there are several reasons for a potential variation in pH e.g. pH variation through sample, and incorrectly calibrated electrodes, the risk of variation can be minimised by measuring the pH of a thoroughly mixed sample in solution, and not the solution before the sample was added.

Another factor that can affect the accuracy of the applied methods would be if the lipopeptide provided was not purified correctly to remove reagents, such as the acid trifluoroacetic acid used in the manufacturing of the peptide. The presence of reagents can impact the purity and as a result can change the calculated concentration of the peptide in solution. To mitigate both issues, the pH was monitored by a doubly calibrated electronic pH meter and the lipopeptides studied were analysed by ESI-MS after delivery. The lowest purity of the measured lipopeptides was 95%. Even with the pH calibrations and measurement process used, and the high purity of the lipopeptides supplied, it is not possible to completely rule out pH or concentration variations in the results. However, with all the steps above in place, it is believed all parameters can be given with a high level of certainty. Further to this, any place where concentration or pH is not known, the data, processing, and discussion, is limited to only what can be verified, rather than relying on inference.

## **2.2 Applied Methods**

### **2.2.1 Transmission Electron Microscopy**

Transmission Electron Microscopy (TEM) is a well-established technique, originally demonstrated in 1931 by Max Knoll and Ernst Ruska, followed by a commercial development of a first TEM apparatus in 1939.<sup>286</sup> TEM utilises the scattering properties of electrons to obtain structural images with a nanometre scale resolution. A few instructive examples for the use of this technique are the visualisation of the structure of bacteria, pollen products or silica nano particles.<sup>287-289</sup> This technique is particularly suitable at visualising self-assembled structures that do not need to be dissolved, which limits the technique of conventional TEM to solid self-assembled systems.

In Figure 8 an electron microscope diagram details the main TEM instrument components.<sup>290</sup> TEM instruments contain a set of lenses that confine the beam of electrons produced by the electron gun as described below. The complete instrument is under a high vacuum of  $1 \cdot 10^{-6}$  Pa, minimizing the scattering produced by the electrons colliding with air molecules. The conventional TEM used for experiments on gel samples for this thesis (see Chapter 4), was a JEM 2100 plus (JEOL Ltd., Akishima-Tokyo, Japan). The TEM instrument is fitted with a lanthanum hexaboride ( $\text{LaB}_6$ ) crystal filament producing current density of  $10 \text{ A/cm}^2$  @ 1800 K within a narrow energy spread of 1-2 eV.<sup>291-292</sup> Emitted electrons are accelerated at 200 kV and passed through the condenser lens. All lenses used in a typical TEM instrument are electromagnetic, meaning they use a magnetic field to deflect or correct the beam of electrons. The condenser lens focusses the beam of electrons onto the sample stage which are scattered by the sample structures present and afterwards focused by the objective lens. Finally, they are enlarged and projected onto the viewing stage. This image is then projected on to a fluorescent screen for focusing and alignment which is then replaced with a specialised 4.0-megapixel AMT XR-401 camera (Amtimaging, Woburn, MA, USA) set a range of different magnifications. The use of the camera allows for images to be taken and analysed, allowing for different parameters such as shape, size and weight of the structures to be recorded.

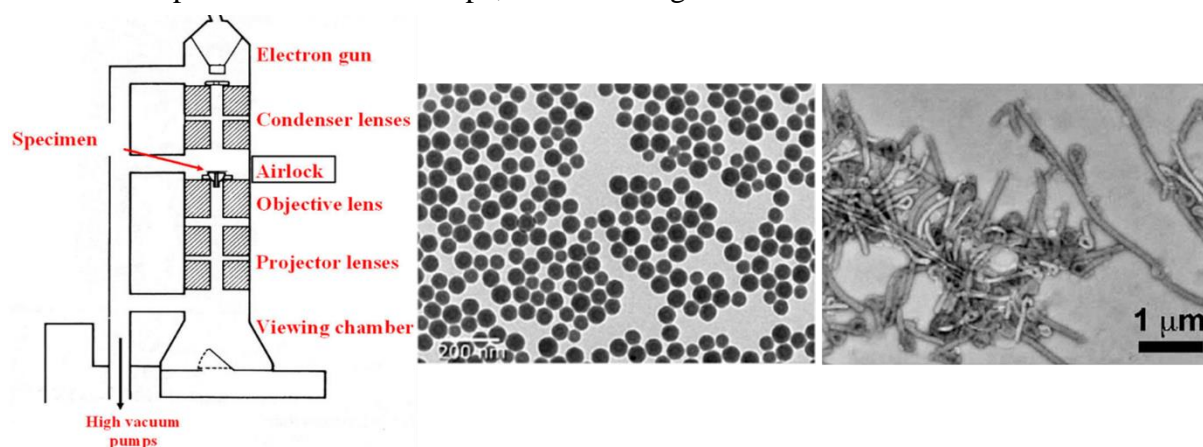


**Figure 8:** Overall structure of a TEM machine with images of common studied samples. Left – Constructional diagram of a conventional TEM machine, showing the electron gun, the various lenses and their positions, sample airlock, and viewing chamber. Centre – Silica nanoparticles with an average diameter of 70 nm. Right – Ebola virus, negative stained with methylamine tungstate. From left to right images are taken from references <sup>290, 293-294</sup>.

The sample, which is placed into the TEM via an airlock, is fixed on a 3 mm diameter grid. There were two types of grids used, (i) a thin film carbon (Agar Scientific Ltd, Essex, UK) and (ii) silicon nitride grid (Agar Scientific Ltd, Essex, UK). Carbon film grids are made of a thin hexagonally perforated carbon film covering a copper frame, while the other grid is composed from a continuous silicon nitride film covering a silicon frame. The images in Figure 9 show

the two designs in more detail. Carbon grids were used for any experiment in which the sample was dry. The silicon nitride frames were only used for a single spin-coated gel sample. The use of carbon grids having troughs can give rise to large areas of dense material that the electron beam cannot pass through. Silicon nitride frames on the other hand do not have this issue but are more prone to damage and breaking.

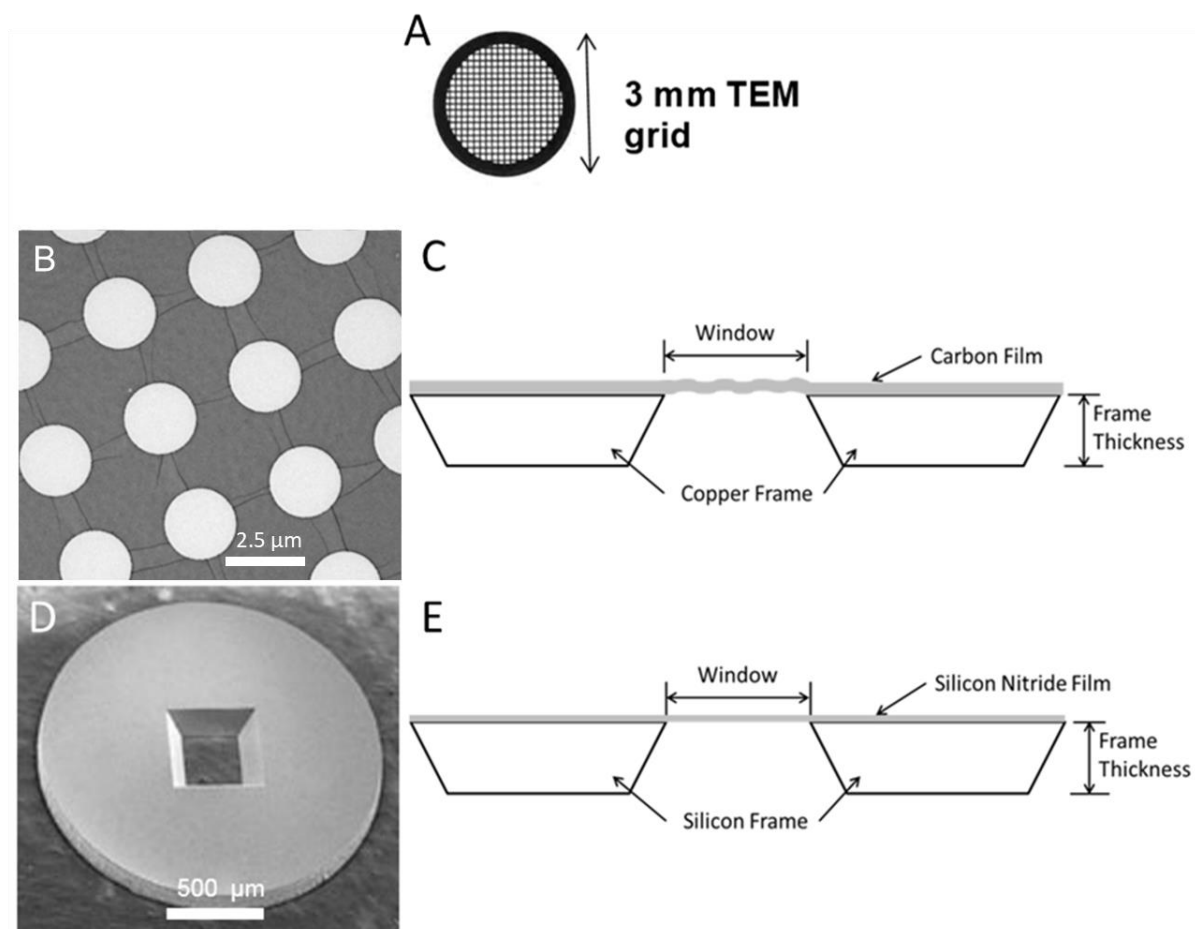


**Figure 9:** Two types of TEM sample discs used. A - Overall size and shape of a TEM grid or frame, B – A magnified “holey” carbon grid without film, C – Cross-section diagram of a carbon holey grid and the issue of varied window thickness. D – A magnified silicon frame without silicon nitride film window. E – Cross-section diagram of a silicon nitride frame with a thin continuous nitride film, making the gel cross-section thinner and the gel samples more TEM applicable. Image B amended from reference <sup>295</sup> and image D is amended from reference <sup>296</sup>.

For the precise control of the electron energy (eV) and reducing in scattering of the electron beam, the samples and optical path need to be set under a minimum vacuum of  $1 \cdot 10^{-6}$  Pa. This is problematic with samples that require the presence of counter ions or solvents, as they will

evaporate and potentially destroy alignment and/or structure, leading to incorrect images and interpretations.<sup>297</sup>

The grids were prepared by allowing a concentrated solution of the sample to be dried on the grid. This process is explained in further detail in section 4.4, including the spin-drying method as well.

**Cryo-TEM** is a variant of traditional TEM using cryogenic temperatures to “freeze” the solution, allowing for visualisation of dissolved or dispersed structures in its natural environment.<sup>156, 298-302</sup> Cryo-TEM is extremely useful for imaging biological samples that can be unstable or destroyed without solvent, given the ultra-low vacuum conditions. Cryo-TEM is like that of conventional TEM except that this method is equipped with a modified airlock allowing for frozen samples to be loaded. The preparation steps of samples for Cryo-TEM are explained in Figure 9 below.<sup>303</sup> After loading the sample onto the holey carbon grid the excess solution is removed with a filter paper. Thereafter the sample is shock frozen in liquid ethane ( $T = -188\text{ }^{\circ}\text{C}$ ), and then finally transferred to the airlock of the Cryo-TEM. While the Cryo-TEM images have been taken by collaborators, Mehedi Reza, Jani Seitsonen, and Janne Ruokolainen from the Nanomicroscopy Center in The Aalto University in Finland, the analysis of the images was completed independently, unless clarification on technical imaging and processing details were required.

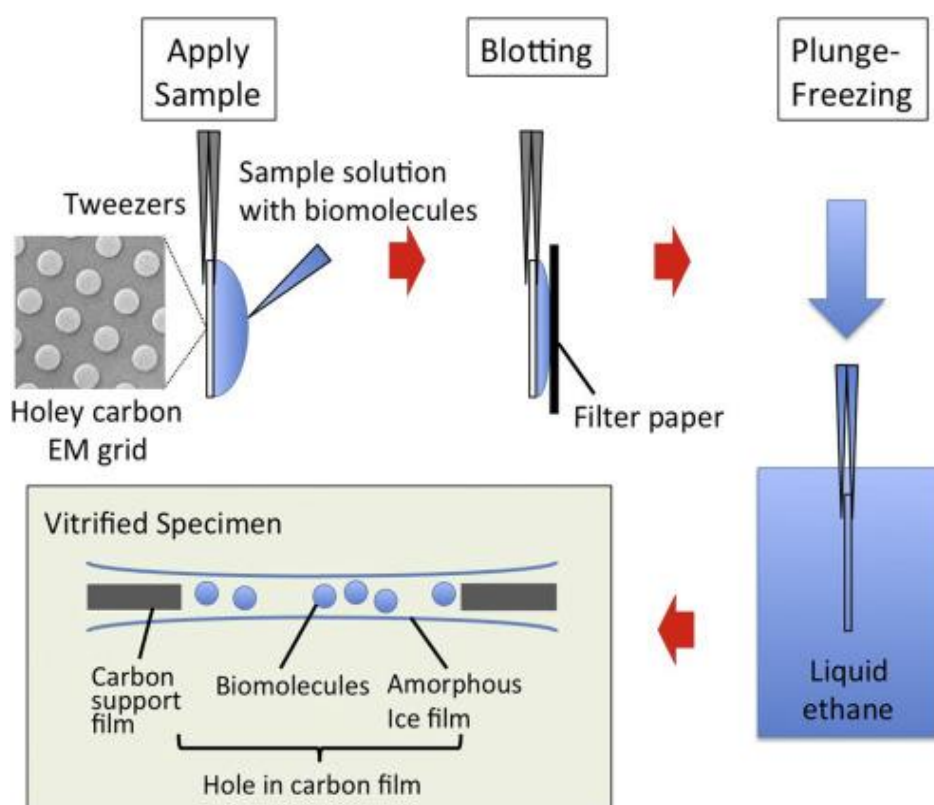


**Figure 10:** Sample preparation for the Cryo-TEM method. Top left – first the sample is applied to the holey carbon grid, then excess solution is removed via blotting with filter paper, and finally the solution is frozen with liquid ethane at  $-188\text{ }^{\circ}\text{C}$ . Bottom left – schematic showing frozen biomolecules, allowing for TEM visualization of samples with solvent. For further details please refer to the main text.<sup>303</sup> Image was taken from ref<sup>303</sup>.

In detail, imaging was carried out using a field emission cryo-electron microscope (JEOL JEM-3200FSC) operating at 200 kV. Images were taken using bright-field mode and zero loss energy filtering (omega type) with a slit width of 20 eV. Micrographs were recorded using a CCD camera (Gatan Ultrascan 4000, USA). The specimen temperature was maintained at  $-187\text{ }^{\circ}\text{C}$  during the imaging. Vitrified specimens were prepared using an automated FEI Vitrobot device using Quantifoil 3.5/1 holey carbon copper grids, with a  $3.5\text{ }\mu\text{m}$  hole sizes. Grids were cleaned using a Gatan Solarus 9500 plasma cleaner just prior to use and then transferred into the environmental chamber of a FEI Vitrobot at room temperature and 100% humidity. Following this,  $3\text{ }\mu\text{L}$  of sample solution at 0.5 wt% concentration was applied on the grid, blotted once for 1 s, and then vitrified in a 1:1 mixture of liquid ethane and propane at  $-180\text{ }^{\circ}\text{C}$ . Grids with vitrified sample solutions were maintained in a liquid nitrogen atmosphere and then cryo-transferred into the microscope.

### 2.2.2 Small Angle X-ray Scattering

Small Angle X-ray Scattering (SAXS) is another analysis methodology used extensively throughout this thesis for the characterisation of self-assembled structures or for the identification of potential complexation. SAXS is a widely used and useful technique that enables the understanding of structure at the nano-level. Uses include determining shape, size and distribution of macromolecules, determining pore sizes in porous material, and visualising and measuring partially ordered materials.<sup>304-310</sup> Solution SAXS experiments within this report were completed at the beamlines B21 at the Diamond Light Source in Didcot, UK or at the BioSAXS BM29 beamline at the European Synchrotron Radiation Facility in Grenoble, France (Chapters 3, 5, and 6). The hydrogel SAXS experiments were completed at I22 and B21 at Diamond Light Source (Chapter 4).

For solution SAXS experiments at the ESRF BM29 the sample-detector distance was 2.84 m, X-ray wavelength was 0.99 Å, and used a Pilatus 1M detector (Dectris Ltd, Switzerland). At Diamond B21, data was collected with a fixed sample-detector distance of 3.9 m with an X-ray wavelength of 1 Å, using a Pilatus 2 M detector (Dectris Ltd, Switzerland). Silver behenate was used as a calibration standard in both cases. All peptide solutions with given concentrations of 0.1, 0.2 and 0.5 wt% of peptide in water were loaded into Fisherbrand™ 0.2 mL polypropylene tubes (Fisher Scientific, UK) in an automated sample changer (designed by the EMBL team in Grenoble) and fed through a single 100 µm thick quartz cell capillary via vacuum. This sample changer allowed for 8 to 16 samples to be run via an automated script, limiting the need for continual manual sample changing. The automatic sample changer is a standard part of the B21 and BM29 operation. A solvent was run before and after the sample, allowing for background scattering subtraction. This process was the same for both beamlines. As only a single quartz capillary was used throughout each experiment it was cleaned between the different samples and solvents. These cleaning steps were completed at both beamlines B21 and BM29.

On the B21, a custom-made gel holder using Kapton windows designed by Charlotte Edwards-Gayle was used.<sup>311</sup> The gel holder was 3D printed allowing for a “packet” of sample to be sandwiched between Kapton tape (used for its high transmittance of X-rays, as well as its stability to samples and temperatures). This 3D printed device can then be placed with repeated precision in the X-ray beam, allowing for both SAXS and WAXS (wide angle X-ray scattering) to be completed with consistency. The device can then be removed, cleaned and reused for other samples. SAXS patterns were recorded using a Pilatus 2 M detector at a camera length

of 3.9 m with a wavelength of 1 Å. Experiments on I22 used modified DSC pans with windows of Teflon or Kapton to allow for X-ray transmission through the DSC pan, while also being able to contain the gel sample. The sample to detector distance was 7.483 m and collected on Pilatus P3-2M detector (Dectris Ltd, Switzerland). Any Teflon or Kapton used for the DSC windows was corrected for with background subtraction as explained below.

Two software packages DAWN (Data Analysis Software group, Diamond Light Source Ltd) and ScÅtter (Rob Rambo, Diamond Light Source Ltd) were used for data processing (subtraction and reduction).<sup>312-313</sup> For all SAXS data gathered for solutions and gels, a direct beam scattering pattern and a cell scattering pattern were collected. Additionally, a scattering pattern for the background was also completed which, for the gels and solutions, was water. Both the empty cell and the background (water) scattering were subtracted from the sample scattering pattern. This produces a scattering pattern specifically for the sample and does not include any artefact scattering from the cell used (for example if Kapton is used) or the background. Once subtracted then the data was reduced by converting the large 2D detector scattering pattern to one pattern averaged in all directions around the beam position. This technique is explained in more detail below. Taking this approach allows the scattering pattern for the sample to be obtained and visualised. All these steps were and can be completed within Dawn and ScÅtter.

The Figure 11 below illustrates the process by which a one-dimensional SAXS pattern is produced. When a monochromatic X-ray beam hits the sample part of the light is scattered producing a two-dimensional scattering pattern. Scattering can be isotropic (no specific alignment of scattering, scattering equally in all directions) or anisotropic (alignment in scattering, producing specific areas of scatter rather than radially equal). Typically, solution SAXS is isotropic as the molecules or self-assembled structures are randomly orientated. This is the case for all the samples analysed in this thesis.

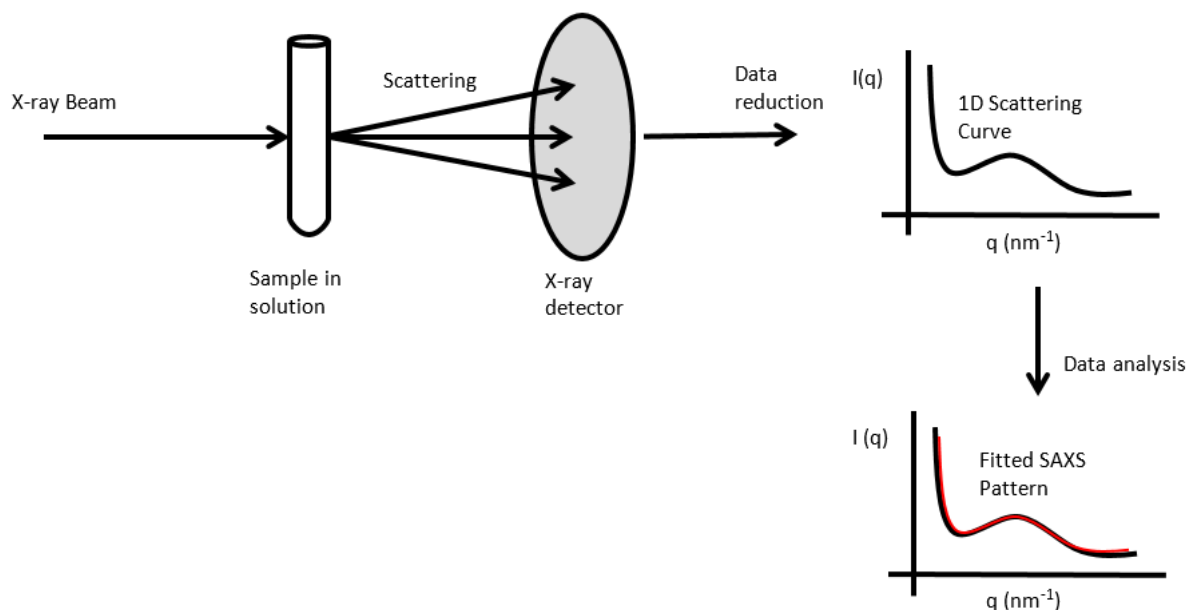


**Figure 11:** Diagram illustrating SAXS measurements and a fitted form factor over experimental data. Clockwise from top left: After recording a full detector image with a 2D X-ray detector, the image is radially integrated, resulting a 1D scattering curve. After background subtraction the scattered intensity (black curve) is fitted by a form-factor model function (red curve) to understand the underlying structure of the sample.

With randomly orientated self-assembled structures the scattering can be radially averaged around the beam from the 2D scattering pattern recorded by the detector to produce a 1D pattern. This produces an “average” 1D scattering curve representing scattering intensity as a function of wave-vector,  $q$ , which is characteristic of the structure within the solution. The equation for  $q$  can be seen below, where  $\lambda$  is the wavelength of the incident beam and  $\theta$  is half the angle of incidence (the difference between the incident and scattered radiation). The unit of  $q$  is nm<sup>-1</sup> or Å<sup>-1</sup>.

$$q = \frac{4\pi \sin\theta}{\lambda} \quad (\text{Eq. 1})$$

The  $q$ -range ( $q$ -min equals the value closest to beam centre and  $q$ -max furthest from beam centre) is determined by the experiment set up, including the wavelength of X-ray used, pixel size of detector, sample-detector distance and the position of the X-ray beam upon the detector (note, a centrally placed beam will result in a smaller  $q$ -range, when compared to one placed in the corner).

Another critical step for a SAXS experiment is the collection of a separate pure solvent scattering curve. This allows for the removal of the solvent’s scattering from that of the dissolved particle, molecule or self-assembled structure. It is common practice to subtract the

background data before completing any further analysis of the data as some lightly scattering structures, such as small proteins, can only be seen when the background is removed. Background noise can be a problem with solution SAXS, therefore the correct setting of all the SAXS parameters such as sample-detector distance, the concentration of the sample, buffer choice and sample environment set up (air or all vacuum) are important to obtain to reduce the noise and scattering of the background.

Many self-assembled structures give characteristic 1D scattering patterns, the simulated fits of which are shown below in Figure 12. The 1D scattering pattern is also known as a form factor, which is a pattern of interference showing each scattered wave by the atoms within the structure.

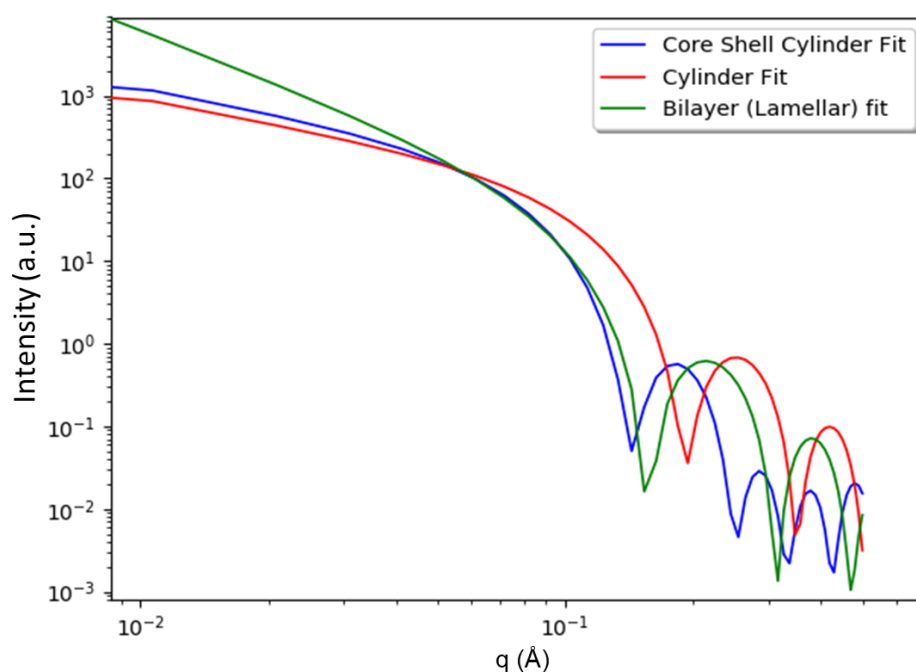
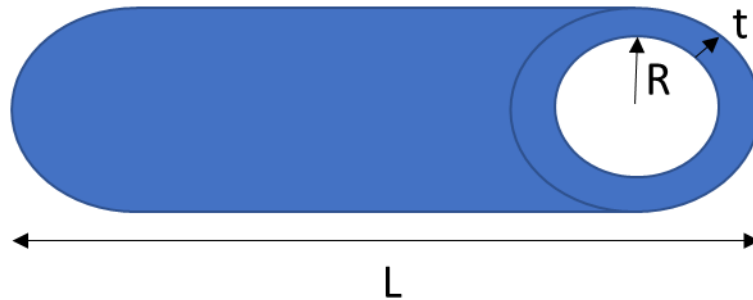


**Figure 12:** Different simulated fits of used models in this study. The scattered intensity,  $I(\text{a.u.})$ , is illustrated for the examples of diluted core shell cylinder, cylinders, and bilayer fits. Each having a 20 nm radius or thickness, and 1000 nm in length. Models simulated using the fitting software SasView.

Using mathematical modelling, a form factor, such as sphere, hollow sphere, long or flat cylinder can be defined and its scattering pattern discerned. This allows for the comparison of a model's scattering curve, fitted to user defined parameters, to that produced experimentally by the sample. Overall, this technique can provide further information on the structure such as size, length, electron density of the core or shell and the polydispersity of the structure. There are many form factors which have been mathematically modelled, including spheres, shells, rods, cylinders, bilayers, and dumbbells. All these models can be found within all fitting software, such as SASfit or SasView.

The samples within this thesis were novel and, as such, their structures were unknown. However, after visualisation by TEM, all samples, including the gels, were then analysed by SAXS and found to be largely fibre or sheet like in nature. The form factors applied to the data are listed below.

**Long Cylindrical Shell (References <sup>314-315</sup>):**



$$I_{LongCylindricalShell}(q) = P'(q)P_{cs}(q) \quad (\text{Eq. 2})$$

$$P'(q) = 2 \frac{Si(qL)}{qL} - \left( \frac{\sin(\frac{qL}{2})}{qL/2} \right)^2 \quad (\text{Eq. 2b})$$

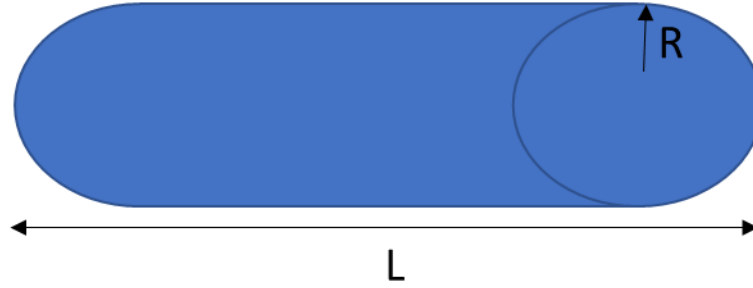
$$Si(x) = \int_0^x \frac{\sin(t)}{t} dt \quad (\text{Eq. 2c})$$

$$P_{cs}(q) = \left( 2 \frac{J_1(qR)}{qR} (\rho_{core} - \rho_{shell}) R^2 L \pi + 2 \frac{J_1(q(R+t))}{q(R+t)} (\rho_{shell} - \rho_{solv}) (R+t)^2 L \pi \right)^2 \quad (\text{Eq. 2d})$$

where  $R$  = radius of core,  $t$  = thickness of shell,  $L$  = length of cylinder,  $q$  = scattering vector,  $\rho_{core}$  = electron density of the core,  $\rho_{shell}$  = electron density of the shell,  $\rho_{solv}$  = electron density of the solvent. This equation only holds true for cylinders of greater length than radius.

This form factor is used for SAXS results within Chapters 4 and 5.

**Long Cylinder (Reference <sup>316</sup>):**



$$I_{long\ cylinder}(q, R, L) = (\Delta\rho\pi R^2 L)^2 \frac{2}{qL} \left\{ Si_{\frac{x}{2}}(qL) \Lambda_1^2(qR) - \frac{\omega(2qR)}{qL} - \frac{\sin(qL)}{(qL)^2} \right\} \quad (\text{Eq. 3})$$

$$Si_{\frac{x}{2}}(x) = \left( Si(x) + \frac{\cos x}{x} + \frac{\sin x}{x^2} \right) \quad (\text{Eq. 3a})$$

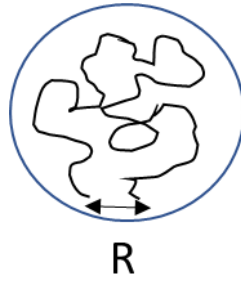
$$\Lambda_1(x) = \frac{2}{x} J_1(x) \quad \Lambda_2(x) = \frac{8}{x^2} J_2(x) \quad (\text{Eq. 3b})$$

$$\omega(x) = \frac{8}{x^2} (3J_2(x) + J_0(x) - 1) \quad (\text{Eq. 3d})$$

where  $J_n(x)$  = are the regular cylindrical Bessel function of order n, R = radius and L is length of the cylinder and  $\Delta\rho$  is the electron density contrast of the cylinder with respect to the solvent. The equation is only valid when L is greater than 2R.

This form factor is applied to samples in Chapter 3.

**Gaussian Coil (Reference <sup>317-318</sup>):**



$$I_{\text{Gaussian Coil}}(q) = I_0 \left( \frac{1}{vU^{2v}} \gamma \left( \frac{1}{2v}, U \right) - \frac{1}{vU^v} \gamma \left( \frac{1}{v}, U \right) \right) \quad (\text{Eq. 4})$$

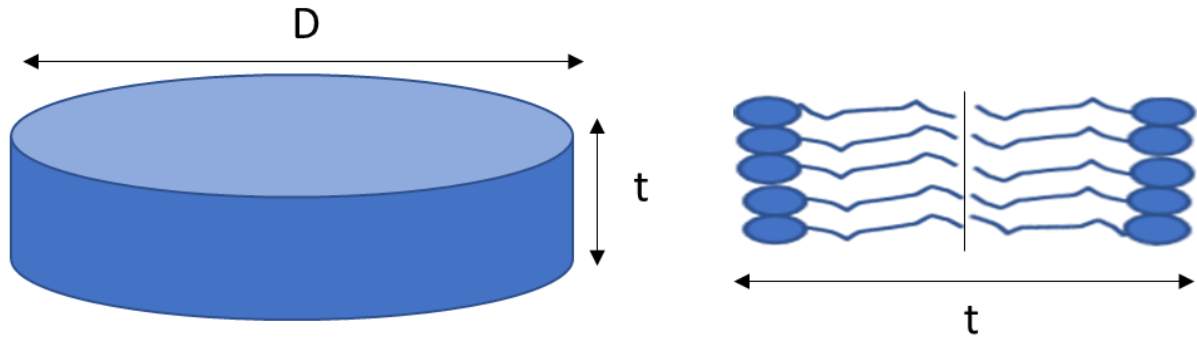
$$U = (2v + 1)(2v + 2) \frac{q^2 R_G^2}{6} \quad (\text{Eq. 4a})$$

$$\text{Gamma Function } \gamma(a, x) = \int_0^x dt t^{a-1} \exp(-t) \quad (\text{Eq. 4b})$$

where  $R_G$  = radius of gyration.  $v$  = excluded volume parameter and  $I_0$  = forward scattering. Note, the excluded volume parameter  $v = 1/3$  for partially precipitate in poor solvents,  $v = 1/2$  for thermally relaxed in "theta" solvent and  $v = 3/5$  for swollen in good solvents. The specific volume parameter used is stated within each model's parameter table.

This model was used within Chapter 3. Fitting a twisted sheet-like structure.

**Bilayer Gaussian (References <sup>319-320</sup>):**



$$\eta(r) = p_{out} \left[ \exp\left(-\frac{(r-\frac{t}{2})^2}{2\sigma_{core}^2}\right) + \exp\left(-\frac{(r+\frac{t}{2})^2}{2\sigma_{out}^2}\right) \right] + p_{core} \exp\left(-\frac{r^2}{2\sigma_{core}^2}\right) \quad (\text{Eq. 5})$$

$$\mu_{out} = Q\sigma_{out} = \pm t/2 \quad \mu_{core} = Q\sigma_{core} = \pm t/2 \quad (\text{Eq. 5a})$$

$$F_{out} = \sqrt{2\pi} \sigma_{out} p_{out} \exp(-\mu_{out}^2/2) \cos(Qt/2) \quad (\text{Eq. 5b})$$

$$F_{core} = \sqrt{2\pi} \sigma_{core} p_{core} \exp(-\mu_{core}^2/2) \quad (\text{Eq. 5c})$$

$$P_{cs}(q) = (F_{core}(q) + 2F_{out}(q))^2 \quad (\text{Eq. 5d})$$

Where:  $\eta(r)$  = electron density profile of bilayer.  $\sigma_{out}$  = scattering length of outer Gaussians.  $p_{out}$  = electron density of the outer gaussians.  $\sigma_{core}$  = scattering length of inner gaussian,  $p_{core}$  = electron density of inner gaussians.  $t$  = bilayer thickness.  $D$  = diameter of disc (defines the unit cell), with  $P_{cs}(q)$  = scattering length density for the cross-section form factor.

This model was used in Chapters 3 and 5, to fit the twisted sheets structures and coiled fibre structures from the co-assembly of two molecules.

A simulated fit is found to be close to the experimental data by assessment through a residuum chi ( $\chi$ ) square test (Eq. 6). This compares the experimental data to that of the fit over all the points of the experimental data. A good  $\chi^2$  fit value should be as close to 1 as possible. For all fits within this thesis the  $\chi^2$  was 0.9-1, indicating a high degree of coherence to the experimental data. Once a good fit was confirmed, the parameters (for which the simulated pattern was optimised) are recorded and can be compared with other models. These structural parameters are given above and vary from model to model.

$$\chi^2 = \frac{1}{N-m} \sum_{i=1}^N \left( \frac{I_{exp}(q_i) - I_{th}(q_i)}{\Delta I(q_i)} \right)^2 \quad (\text{Eq. 6})$$

where  $N$  = number of data points,  $m$  is the number of fit parameters,  $I_{exp}(q_i)$  and  $I_{th}(q_i)$  being the experimental data and fitting function, respectively.

It should be noted that there are a few other methods available to analyse scattering patterns, such as the power law (that looks at overall dimensionality of the particles: for instance, 1D-cylinders, 2D-planes and 3D-spheres) and Guinier analysis (approximations for size, interactions and the presence of oligomers). However only detailed form factor model fitting can provide such a large range of parameters for analysis for the formed structures. For this reason, detailed form factor modelling has been the prominent method used through all chapters of this thesis. All the fitting within the following chapters have been fitted using software called SASfit. There is other fitting software available, such as SasView, ScÅtter or FibreFix. SASfit was selected as it allows for greater control of the background and easier combination of form factors (which is used within this thesis for one co-assembly structure).

### 2.2.3 Circular Dichroism Spectroscopy

Circular Dichroism (CD) spectroscopy is an extremely useful technique in the field of biophysical chemistry as it can identify  $\alpha$ -helical,  $\beta$ -sheet, random coil secondary structure as well as provide percentages of these structures within a polypeptide or protein. This is important in enabling an understanding of the physical structure of a peptide or protein and can give additional structural information about active sites or secondary structure specific binding areas of a peptide drug. This technique has other uses including investigating isomers and chirality in molecules, but within this thesis it was specifically used for the identification and percentage of secondary structure within PYY<sub>3-36</sub> and 17PYY<sub>3-36</sub> in all experimental Chapters 3 to 6.

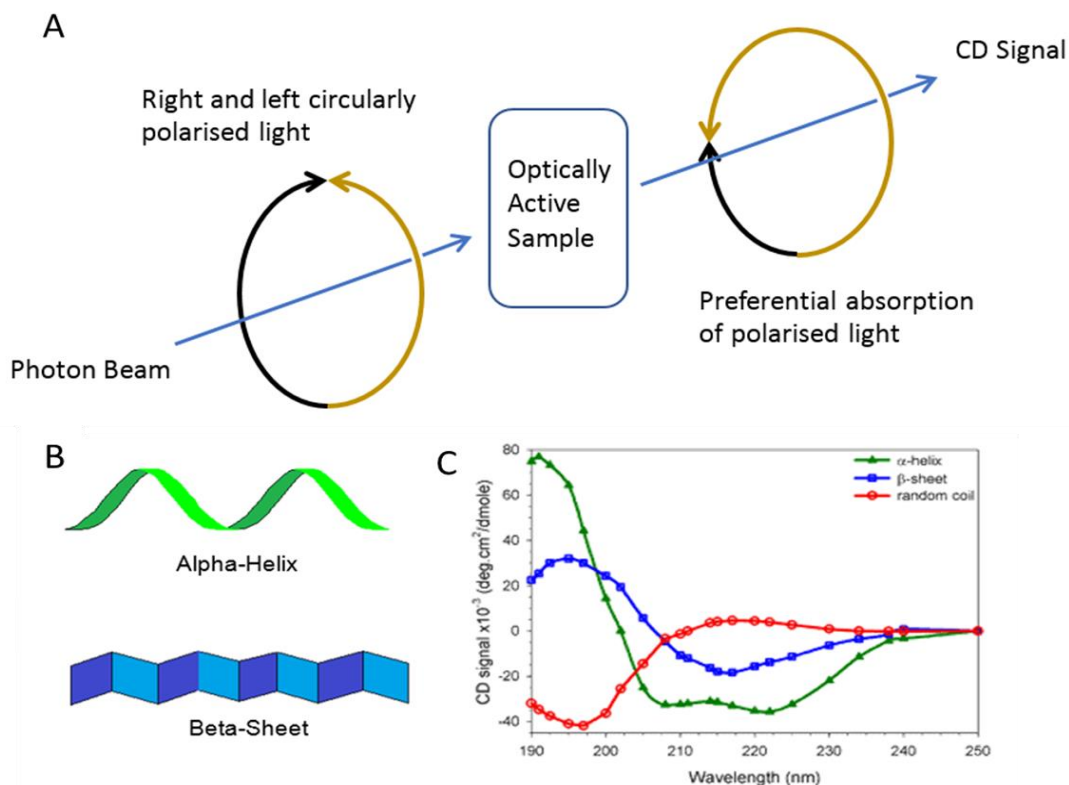


**Figure 13:** Scheme illustrating the principle of CD data recording. A – Scheme illustrating the preferential absorption of a circularly polarized photon beam. B - Diagrams of  $\alpha$  helical and  $\beta$ -sheet secondary structures. C-Specific CD spectra for the  $\alpha$ -helix,  $\beta$ -sheet, and random coil. Image taken from ref <sup>321</sup>

Secondary structure of a peptide produces a specific spectrum of the polarised light (Figure 13 A) that allows for identification of  $\alpha$ -helical,  $\beta$ -sheet or random coil secondary structures (Figure 13 B and C).<sup>321</sup> Information about the secondary structure is extremely important as proteins and other chiral soft matter molecules produce these types of structure upon aggregation, assembly, or denaturation. CD thus allows for the visualisation of the intramolecular effects, structure, stability, monomer-oligomers and binding.

Circular Dichroism works by the specific differential absorption of right and left handed circularly polarised light passing through the sample, as shown in Figure 13. If the sample is optically active, this means it will preferentially absorb the right or left circularly polarised light. This difference can be measured which produces a characteristic CD-spectrum as a function of wavelength from which conclusions on the secondary structure can be drawn.

A Photophysics Chirascan Circular Dichroism Spectrometer (Applied Photophysics, UK) was used to obtain all the CD data used throughout this thesis. Temperature studies were completed using a temperature controller and heated stage, the controller being an A-Omega Instruments Series 800 temperature controller (A-Omega Instruments, Houston, TX, USA). Temperature

ramps from 20 to 70 °C with recording a CD spectrum every 5 °C were carried out. Before each measurement, the sample was equilibrated for 2 mins. After the maximum temperature of 70 °C was reached the sample was cooled back to 20 °C, investigating the reversibility of the temperature effects on the sample. The Chirascan software (Applied Photophysics, UK) was used to control the variables of the experiment with the Pro Data Viewer (Applied Photophysics, UK) to visualise, in real-time, the data produced. Once the data was collected it was exported to Origin (OriginLab, Northampton, MA, USA) to complete the data manipulation following using Eq. 9. Some experimental results for CD have been smoothed using the Fast Fourier Transform function, which is available through the Chirascan software.<sup>322-324</sup> When this function has been applied it will be noted and the number of points the data smoothed by will also be defined.

Liquid samples were all run in Quartz Suprasil cells from Hellma Analytics (Southend-on-Sea, UK). The cells used are 0.1 mm or 0.01 mm in path length. The 0.1 mm quartz plaques were used for solutions and the 0.01 mm for gels. The reason for this variation in plate pathlength was to limit the absorbance to below 2. All samples were prepared with maximum absorbance values below 2 due to the limitations of the photomultiplier within the machine which records the light. The absorbance can be calculated via measuring the intensity of the light before and after the sample, according to:

$$A = \text{Log}_{10} \left( \frac{I_0}{I} \right) \quad (\text{Eq. 7})$$

with  $A$  = absorbance (unit-less),  $I_0$  = the intensity of the incident light, and  $I$  is intensity of that light after it passed through the sample. Further, we have:

$$A = \epsilon cl \quad (\text{Eq. 8})$$

with  $A$  = absorbance (unit-less),  $\epsilon$  = molar attenuation coefficient ( $\text{L mol}^{-1} \text{ cm}^{-1}$ ), and  $l$  = pathlength of cell (cm).

Three separate runs were completed and then averaged to a single spectrum, but only if the scans and absorbance values did not change, showing a non-evaporating, stable sample. A 0.5 nm step was used, with 1 nm bandwidth and a 1s collection time per step, for all samples. All samples within this thesis were recorded from 190-260 nm. The small step size was to obtain a larger set of data points (60 for 1s collection time versus 120 for 0.5s). The data was collected and exported to Origin Pro 61 (OriginLab, Massachusetts, USA). All samples have been

background subtracted, removing water and quartz cell contributions from the data. The degree of ellipticity,  $\theta$ , was then recorded for all CD samples and used to determine the molar ellipticity value, if the molar concentration of the sample was known.

The CD method is only able to provide one molar ellipticity of the sample under test, given one unique molarity (Eq. 9). However, when the sample is a mixture that contains two or more components, one single molarity cannot be applied meaning that it is not possible to calculate or estimate the molar ellipticity of the mixture, or any of its components. The graphs have therefore been left as ellipticity (deg) to allow for a comparison with similar weight percentages.

The equation used to calculate molar ellipticity is given by:

$$\text{Molar Ellipticity (deg cm}^2 \text{ mol}^{-1}) = \frac{\theta \text{ (deg)}}{10 \cdot \text{Molarity (mol dm}^{-3}) \cdot \text{Pathlength of Cell (cm)}} \quad (\text{Eq. 9})$$

Note, molar ellipticity is universal parameter, allowing for the comparison of different CD spectra completed on different machines, with different path length and concentrations.

A theoretical based 100%  $\alpha$ -helical peptide, of the same length, with a molar ellipticity of -37,400 deg cm<sup>2</sup> dmol<sup>-1</sup> can be simulated using Eq. 9. This spectrum can then be compared to the molar ellipticity recorded and a percentage of the  $\alpha$ -helical structure obtained for each recorded peptide or lipopeptide. This can then allow for quantification of the  $\alpha$ -helical content and better comparison between lipidated and native, along with any temperature dependencies.

#### 2.2.4 Ultraviolet (UV) Absorbance Concentration Measurements

A small section of this thesis makes use of the Nanodrop One instrument (ThermoScientific, Massachusetts, USA) for the analysis of peptide concentrations and its function is described here briefly. The molar absorbance coefficient of a peptide with tyrosine (Y), tryptophan (W), and cysteine (C) can be calculated with the following equation:

$$\varepsilon = (nW \times 5500) + (nY \times 1490) + (nC \times 125) \quad (\text{Eq. 10})$$

This gives the weighted sum of the 280 nm molar absorption concentrations for these amino acids. Given that there are four tyrosine residues in each peptide the molar absorption coefficient becomes 5960 L mol<sup>-1</sup> cm<sup>-1</sup>. Combined with the Beer-Lambert law (Eq. 8) this allows for a concentration to be determined. With the known molecular weights and volumes enables this concentration value to be converted to weight percentages (wt%). The benefits of

the use of the Nanodrop One instrument, compared to other spectrofluorometers, are the minimal sample used, approximately 2  $\mu\text{L}$ , and a reduced path length of 0.03 to 1.0 mm that allows for more accurate measurements. These two advantages enable the measurement of extremely low sample concentrations with detection limits of 2  $\text{ng}/\mu\text{L}$ . Furthermore, it reduces the experimental time to 8 secs for each sample.

Further studies on tyrosine (Y), tryptophan (W), and cysteine (C) free peptides were completed with a wavelength 205 nm. The 205 nm wavelength arises from the absorbance band of the amino acid backbone bond and using the commonly used molar absorption coefficient of 31  $\text{mL mg}^{-1} \text{cm}^{-1}$  a concentration can be determined, via the Beer-Lambert law (Eq. 8).<sup>325-326</sup>

All gel samples for the Nanodrop measurements were prepared using ultra-pure water (18 M $\Omega$  Barnstead Nanopure, ThermoScientific, USA). After cleaning the pedestal, running a blank and finally running a water sample, the samples were run using approx. 2  $\mu\text{L}$  of sample (part of this sample preparation being shown in Figure 14). After each sample the sample pedestal (which creates the experiment's pathlength) was cleaned and a new sample was placed on the pedestal via micropipette. This is all in accordance with the standard operating procedure (SOP) of the Nanodrop One found within the manual.



**Figure 14:** Photos showing the use of a nanodrop to produce a small path length, which is useful for low concentration or low fluorescing molecules, and the application of a small amount of sample to the stage. Modified from ThermoFisher Nanodrop website, reference <sup>327</sup>.

Data for pure samples was used to predict the experimental values of mixtures. This was done by simple addition (for example A1 - 0.33, B1 – 0.52, Theoretical value of 1:1 A1: B1 mixture – 0.85), and if they are referenced, they will be titled as a theoretical value.

### 2.2.5 Zeta Potential Measurements

Studies were completed using zeta potentials to observe the double layer charge of the particles within the solution, as shown in Figure 15. All studies were completed in the same manner following the experimental method detailed below. The zeta potential of a particle is an indicator of stability within the solution. A large zeta potential, greater than 60 mV, shows excellent stability, lower zeta potentials show reduced stability, with above 5 mV being the smallest magnitude for a stable molecule. With values below 5 mV particles are considered to only be briefly coagulating or flocculating and are not considered stable.<sup>328-330</sup>

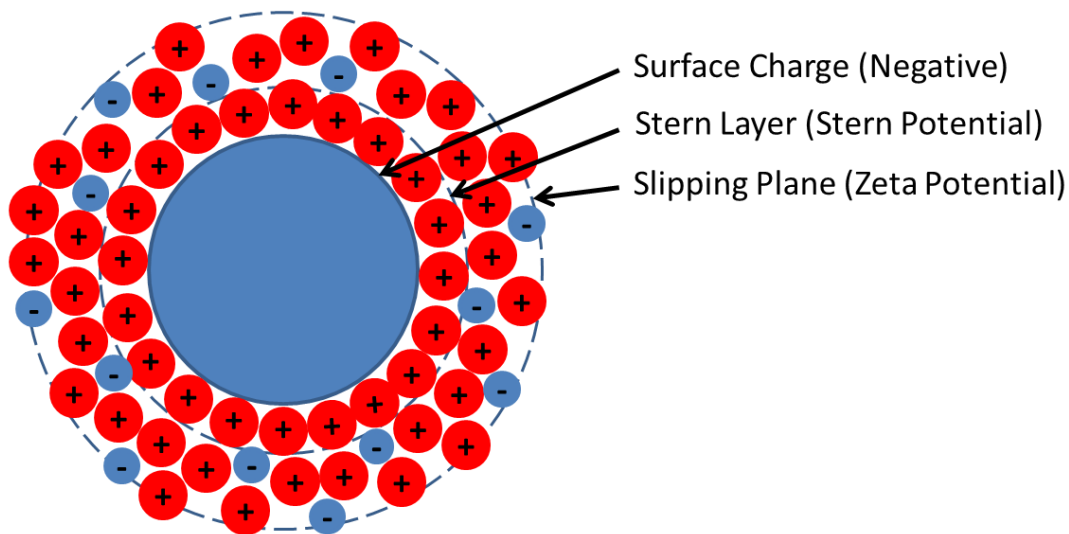


**Figure 15:** Diagram showing what zeta potential is and what this relates to, given a charged particle in solution.

All experiments used a Zetasizer Nano series Nano-ZS machine (Malvern Instruments, Malvern (UK)). 1 mL samples were made up within water (18 M $\Omega$  Barnstead Nanopure, ThermoFisher Scientific, USA) and put into Malvern Nano series disposable folded capillary cells (DTS1070). These were placed within the instrument and allowed to equilibrate for 120 secs before 3 separate runs were completed to produce an average reading. The standard 50.0 V was applied to each solution of molecules, the voltage of which defines the strength of electrical field ( $E$ ). This voltage causes the molecules to move with a velocity related to their zeta potential. This particle velocity ( $v$ ) is measured using a laser interferometric technique called M3-PALS (Phase analysis Light Scattering). This enables the calculation of electrophoretic mobility ( $\frac{v}{E}$ ) and conductivity ( $\sigma$ ) (via resistivity ( $\Omega m$ )), and from this the zeta potential ( $\zeta$ ). All values in the equations below are measured or calculated by the Zetasizer:

$$\zeta \approx 4\pi\eta \left( \frac{v}{E} \right) / \epsilon \quad (\text{Eq. 10})$$

$$\sigma = \frac{1}{\rho} \quad (\text{Eq. 11})$$

with  $\zeta$  = zeta potential (mV),  $\eta$  = viscosity (N s/m<sup>2</sup>),  $v$  = particle velocity (cm/s),  $E$  = strength of electrical field (V/m),  $\epsilon$  = dielectric constant (F/m), with  $\frac{v}{E}$  = electrophoretic mobility. The conductivity equation (with measurements of constant cross-sectional area and length) is given with  $\sigma$  = conductivity (S/m) and  $\rho$  = resistivity ( $\Omega$ m).

### 2.2.6 Critical Aggregation Concentration (CAC) Experiments

To determine the critical concentration at which a self-assembling molecule, such as a lipopeptide or peptide amphiphiles, aggregates, the aromatic probe pyrene was used. The assembly of these molecules is shown simply in Figure 16, with black and red denoting hydrophilic and hydrophobic sections respectively in an aqueous environment.

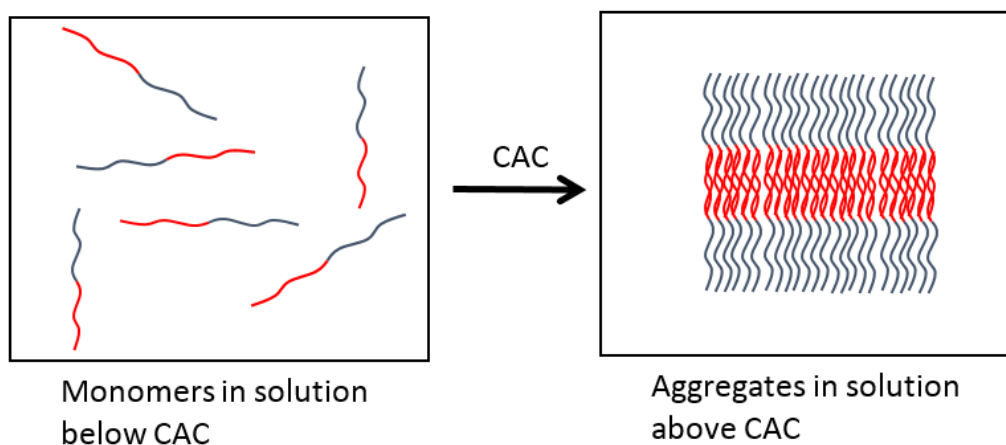


**Figure 16:** Scheme showing monomers in solution below and above the CAC. The CAC being useful information for when the formation of aggregates can occur.

Pyrene can function as a probe for this aggregation and allow for the identification of the concentration at which this occurs. Pyrene has a characteristic emission spectrum with 3 strong emission bands between 360-500 nm when excited at 339 nm. This emission spectra changes depending on environmental factors. If the pyrene is located within a largely hydrophobic or hydrophilic environment the emission spectra will change. Locations of hydrophobic nature, within an aqueous environment, occur when self-assembling amphiphilic monomers aggregate. The hydrophobic pocket could be located within a micelle sphere, in the wall of a vesicle, in the inner tube of a fibre or in the inner portion of a  $\beta$ -sheet. With pyrene present in the same solution as the self-assembling monomer there are two specific pyrene emission peaks which

show this effect namely,  $I_1$ (373 nm) and  $I_3$  (383 nm). An  $I_1/I_3$  intensity ratio versus concentration plot of the monomer with a constant pyrene concentration can be obtained. An increase in  $I_3$  and reduction in  $I_1$  intensities occur when pyrene is in a more hydrophobic environment and will reduce the  $I_1/I_3$  ratio for that concentration of self-assembling monomer (From Figure 17 B to C). When measured across a large concentration range two linear lines of best fit can be used to show a “break point” that is when the environment changes from hydrophilic to hydrophobic, indicating the presence of self-assembly aggregates in the solution (Figure 17 D).

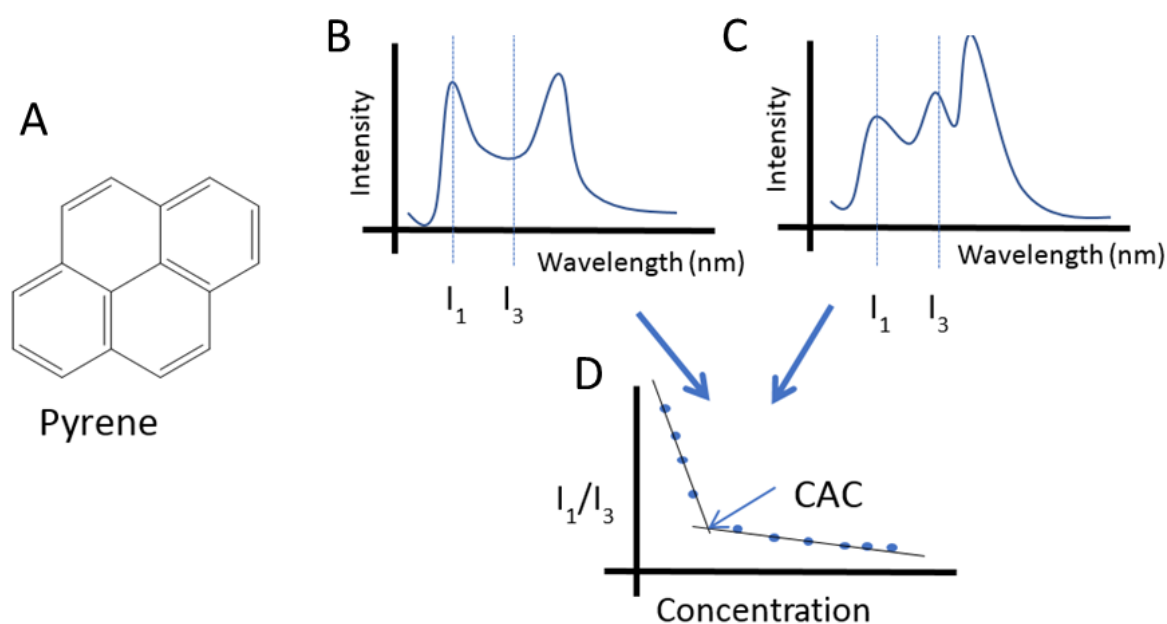


**Figure 17:** Schemes explaining the process for using pyrene as a CAC probe. A – Chemical structure of pyrene. B – Simplified emission spectrum of pyrene in a hydrophilic aqueous environment. C – Simplified emission spectrum of pyrene in a hydrophobic environment, aggregated amphiphilic molecules. D – Ratios of the intensity at pyrene peak  $I_1$  and  $I_3$  versus concentration, showing the “break point” of aggregation by using two linear lines of best fit. The pyrene emission spectra will shift from an B spectrum to a C spectrum with self-assembly, and an increase in the hydrophobic environment.

All the fluorescence spectra were recorded with a Varian Cary Eclipse FLR fluorescence spectrophotometer (Agilent, Santa Clara, CA) within the Reading University Chemical Analysis Facility. Samples were run within 4 mm inner-diameter quartz cuvettes (Hellma Analytics, Southend-on-Sea, UK).

### 2.2.7 BODIPY TR Cadaverine Lipopolysaccharide Displacement Assay

An experiment to investigate the potential aggregation of Lipopolysaccharides (LPS) to two different peptides was completed within this thesis, using the LPS specific dye BODIPY TR Cadaverine. The fluorescence methodology is similar to that used for CAC measurements, but instead of a ratio of peak intensities (such as 373/383 nm for pyrene), this technique uses the emission peak height of BODIPY TR Cadaverine (which is 620 nm) to determine if the BODIPY TR Cadaverine is being displaced from LPS. A higher intensity value relates to a free molecule, with a suppressed and reduced peak relating to a complexed molecule.

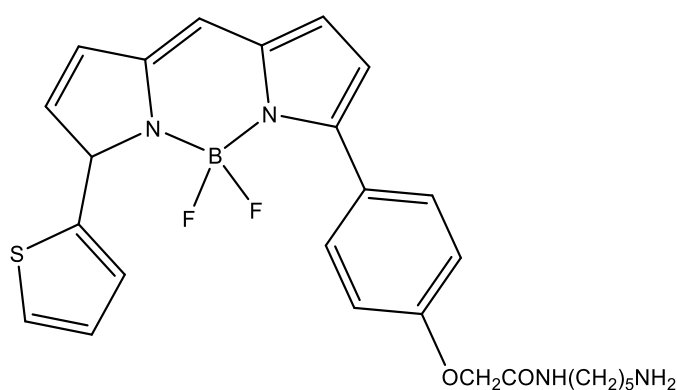


**Figure 18:** Chemical Structure of BODIPY TR Cadaverine.

This method used a Varian Cary Eclipse FLR fluorescence spectrophotometer (Agilent, Santa Clara, CA) within the Reading University Chemical Analysis Facility. 1 mL of the BODIPY TR Cadaverine and LPS complex sample was taken and placed within the 4 mm inner diameter quartz cuvette (Hellma Analytics, Southend-on-Sea, UK). For all measurements, an excitation wavelength of 583 nm was used, with an emission range of 590-680 nm. The peak of interest is at 620 nm, which is the only emission peak of BODIPY, and within the range specified above.

To this LPS and BODUPY TR solution 10  $\mu$ L of the A9R or PYY<sub>3-36</sub> peptide solution was added. The combined sample within the cuvette (Hellma Analytics, Southend-on-Sea, UK) was then allowed to equilibrate for 5 mins. This mixture was then placed within the Varian Cary Eclipse fluorescence spectrometer (Agilent, Santa Clara, CA) and a spectrum was recorded using the excitation (583 nm) and emission range (590-680 nm) stated above. This additional process was completed 10 times adding a total of 100  $\mu$ L to the solution for each peptide PYY<sub>3-36</sub> and A9R. The peak maximum at 620 nm was taken from the fluorescence spectra at the beginning (pre-addition, only LPS – BODIPY TR) then for each 10  $\mu$ L addition. This intensity value at 620 nm was then plotted against the amount of peptide solution added.

An increase in peak intensity shows displacement of the BODIPY TR dye and incorporation with the peptide of interest. The BODIPY TR Cadaverine dye is highly specific to the lipid A section of LPS (lower segment).<sup>331</sup> This would show a complexation between a peptide and the lower segment of LPS. A range of studies that have used LPS-BODIPY TR complexes and fluorescence have an estimated a ratio of 1:1.5 to 1:5 LPS to BODIPY TR probe.<sup>332</sup>

### 2.3 Rational of Applied Methodologies

This chapter has covered all the applied and complementary methodologies. For these studies the use of multiple complementing methodologies helps to provide a full picture of the self-assembled systems or complexing solutions. This multiple method approach is an extremely important one and it is suggested that it be carried forward into further research into the molecular effects (CACs and  $\beta$ -sheets) of macro formations (such as gels). Below is a method overview table summarising the method, key parameter, sample type and which sections of this thesis it was used in.

**Table 1:** Overview of applied methods.

Method	Key parameter	Sample type	Conclusion Type	Experimental Chapters
TEM; Cryo-TEM	Large structure (1 to approx. 1000 nm).	Dried solution for TEM; vitreous frozen for Cryo-TEM.	Direct Structure	3, 4, 5, 6
SAXS	Large to internal structure (1 to 100 nm).	Solutions or gels.	Direct Structure, Modelled Structure	3, 4, 5, 6
CD	Secondary structure (0.15-0.6 nm).	Solution or gels.	Direct Structure	3, 4, 5, 6
UV Absorbance	Environmental effects; complexation potential.	Solutions and gels.	Direct Structure	5, 6
Zeta Potential	Charge of Particle and by extension stability of particle.	Solutions.	Direct Solution Charges	5, 6
CAC	Concentration of self-assembly.	Solutions.	Indirect Structure (CAC)	3
BODIPY TR	Complexation potential to LPS.	Solutions.	Indirect Structure	5

### 3. Effects of Lipidation of PYY<sub>3-36</sub>

This chapter was published in part in the paper, for which the full reference is as follows: Hutchinson, J. A.; Burholt, S.; Hamley, I. W.; Lundback, A.-K.; Uddin, S.; Gomes dos Santos, A.; Reza, M.; Seitsonen, J.; Ruokolainen, J., The Effect of Lipidation on the Self-Assembly of the Gut-Derived Peptide Hormone PYY<sub>3-36</sub>. *Bioconjugate Chem.* 2018, 29 (7), 2296-2308.

#### 3.1 Introduction to Peptide Hormone PYY<sub>3-36</sub> and 17PYY<sub>3-36</sub>

This chapter's work relates to the lipidated form of PYY<sub>3-36</sub> as a potential peptide hormone drug. As it will be referred to throughout this chapter and beyond, 17PYY<sub>3-36</sub> is a 34 amino acid peptide based on PYY<sub>3-36</sub> with a palmitoyl chain coupled at position 17 on the peptide chain. Three lipidated versions have been synthesised (Chapter 2.1), following the same amino acid replacement method but at position 11 (11PYY<sub>3-36</sub>), 17 (17PYY<sub>3-36</sub>) and 23 (23PYY<sub>3-36</sub>). This chapter's work also compares the specific conformational changes between the native peptide PYY<sub>3-36</sub> and that of the 17PYY<sub>3-36</sub>. Further studies within this thesis have been devoted to understanding any self-assembled structures that are formed by 17PYY<sub>3-36</sub>; specifically, their stability, structure, and morphology.

By referring to Figure 19 of 17PYY<sub>3-36</sub>, it can be seen that an arginine amino acid at residue 17 was replaced with a Lys- $\gamma$  Glu Spacer-Palmitoyl Group (Figure 19). From an electrostatic viewpoint this has replaced a positively charged amino acid with a longer neutral and hydrophobic moiety. Combining this electrostatic change with the incorporation of the lipid chain into the end section of the  $\alpha$ -helical section of the peptide chain will have a destabilising effect on the peptide's overall helical content and peptide structure, reducing hydrogen bonding effects and adding steric bulk. This addition will also dramatically change the overall amphiphilicity of the molecule, potentially hindering its ability to self-assemble. The native PYY<sub>3-36</sub>, although highly hydrophilic, has a secondary structure that protects a hydrophobic pocket, this can be seen in the previous Figure 6, with the PP fold.<sup>271, 275, 333</sup> Both of these aspects will be probed further in following sections (Chapters 3, 4 and 5) of this thesis that will set out to investigate their overall structure, the constraints that define these structures, their internal secondary structure, and finally the concentrations at which these structures are formed.

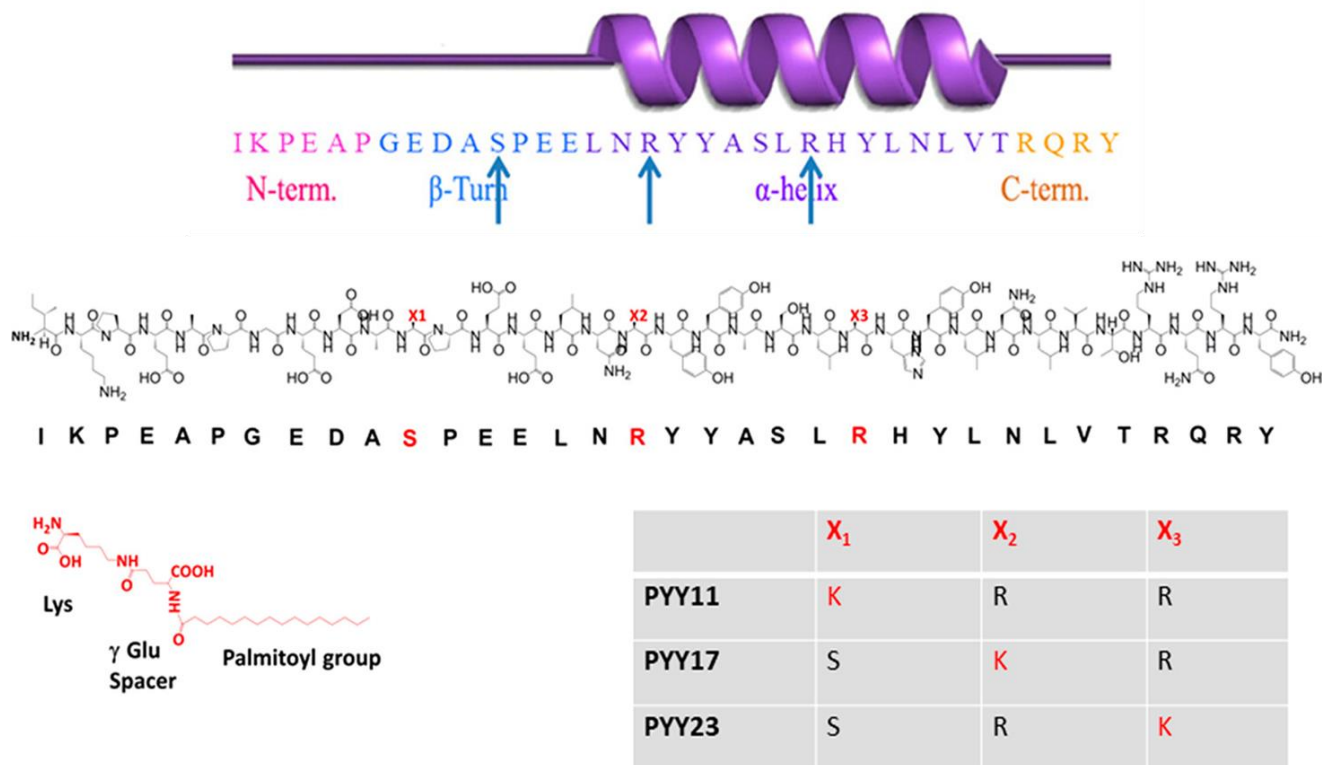


**Figure 19:** Full Structure of PYY<sub>3-36</sub> and linker unit, with locations of lipidations. Top: Chemical structure with positions of lipitation on the amino acid chain shown by the arrows. Left to right of the arrow positions being 11PYY<sub>3-36</sub>, 17PYY<sub>3-36</sub>, and finally 23PYY<sub>3-36</sub>. Bottom: Amino acid sequence of native PYY<sub>3-6</sub> with all three positions noted by X1, 2, and 3. A table of amino acids for that location and K being the Lys- $\gamma$  Glu Spacer-Palmitoyl Group replacement. Amended from authored paper 4.<sup>305</sup>

### 3.2 Cryo-TEM, Visualising Self-Assembled Structures

Cryo-TEM allows *in situ* visualisation of self-assembled structures.<sup>178, 186, 309, 334-337</sup> The first step was to observe if any self-assembly occurred. Second, the type of self-assembly was also verified by Cryo-TEM. Detailed information regarding the sample preparation, methodology and analysis are given in section 2.1.2 and 2.2.1, respectively. As mentioned previously in Chapter 2.1.2, all efforts to make sure the concentration and pH values studied are as precise as possible.

The simple addition of PYY<sub>3-36</sub> to ultrapure water (Chapter 2.1.2) can be seen in Figure 20 C, which shows twisted tape like structures at high concentrations. This is an extremely interesting and novel observation, as the self-assembly properties of this amphiphilic peptide has not been investigated before. Although the primary, secondary and tertiary structures of PYY<sub>3-36</sub> have been defined multiple times previously (Chapter 1.13), the larger self-assembled structure has

not been investigated.<sup>87, 338-343</sup> With this hormone peptide being of interest as a potential drug, this larger nano-scale structure is important to investigate, as all levels of the self-assembled structure can affect a drug's clearance from the body, its efficacy and its stability.

Different pH values were investigated with pH 2, 4, 6 and 8 being selected as this range covers most the human body's pH values.<sup>344</sup> As this peptide could be potentially used as a new drug molecule, administered by ingestion, injection, or inhalation, the effect of this biological pH range on PYY<sub>3-36</sub> is extremely important to be investigated and understood.

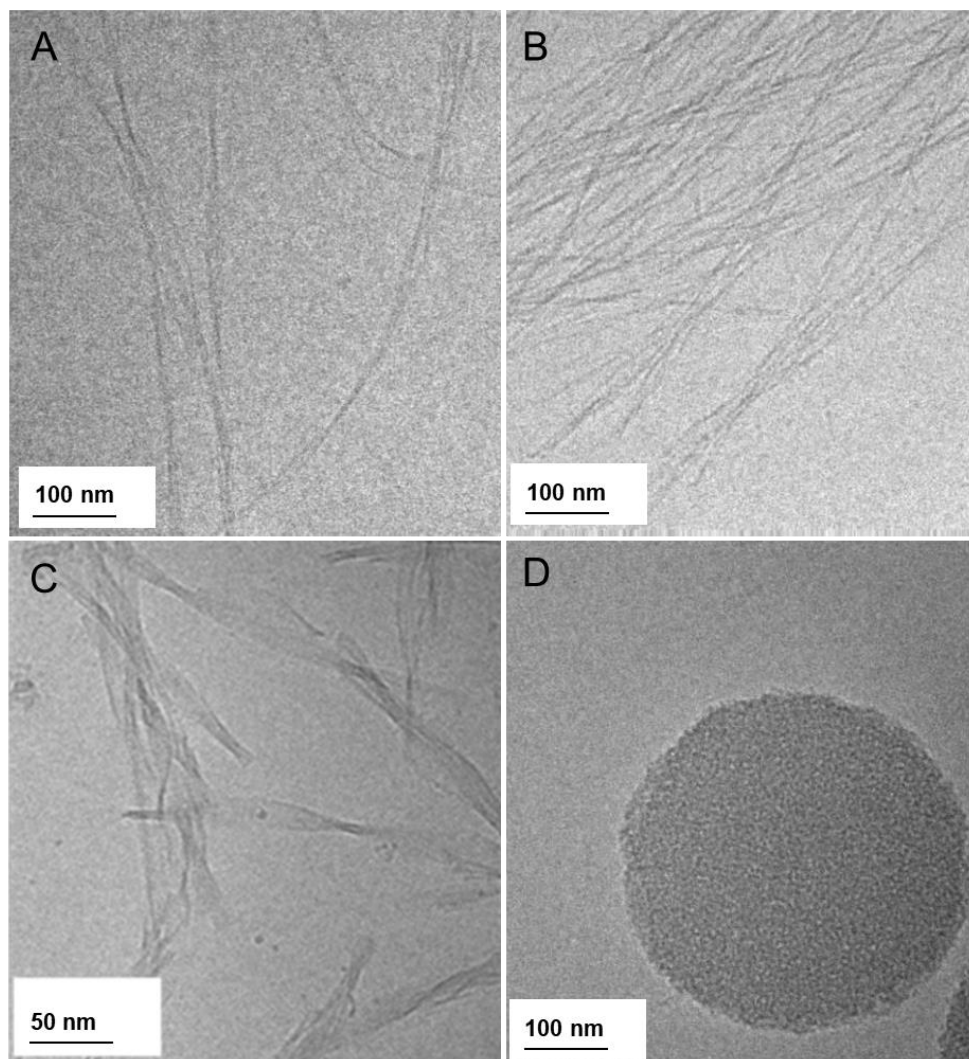


**Figure 20:** Cryo-TEM images showing the twisted sheet self-assembled structures of 0.5 wt% PYY<sub>3-36</sub> prepared in H<sub>2</sub>O at pH 2 (A), 4 (B), 6 (C), and 8 (D). Key observations include twisted sheets for A, B, and C, with a large disc structure formed for pH 8. The change in pH values clearly changes the overall self-assembled structures, with thinner twisted sheets for 2 and 4, with a complete structural change at pH 8.

At pH 2 and 4 the self-assembled PYY<sub>3-36</sub> structure changes from around a 4 nm to around 1 nm thin fibres. Although being thinner, compared to the pH 6 PYY<sub>3-36</sub> fibres, it can still be seen to have the similar, but less intense twist to them. This is just noticeable in the bottom of Figure

20 A, where a flat area of the twist can be seen. The size change of the fibres can be attributed to the change in pH increasing the positive charge throughout the amino acids within the peptide, making them less likely to aggregate and increasing the enthalpy of aggregation, compared to structure at pH 6. pH 8 on the other hand shows a large flat aggregation that is disk like and uniform. This is a much larger structure of 400 nm in diameter. As TEM is limited in its resolution, any internal structure of this disk, if present, could not be determined.

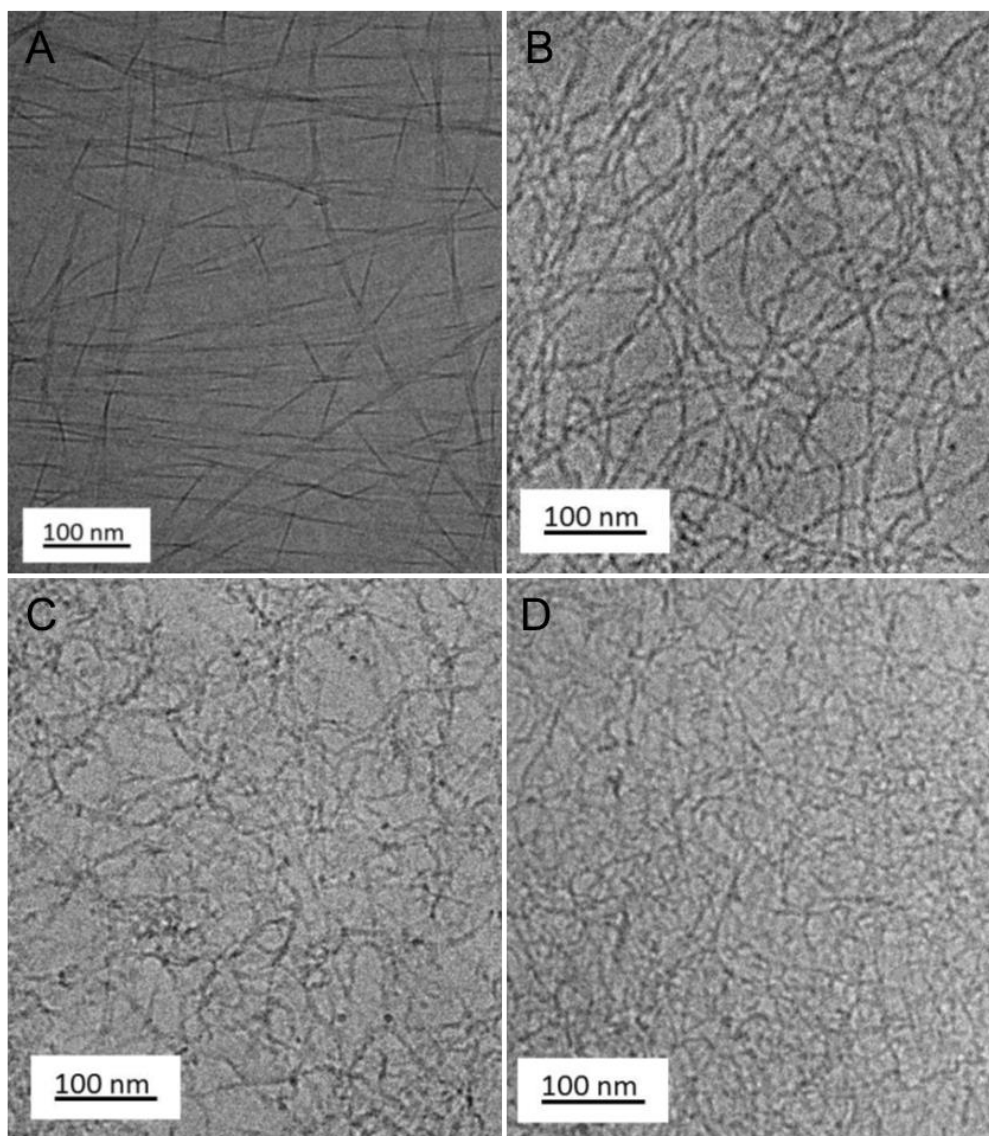


**Figure 21:** Cryo-TEM Images showing the self-assembled elongated fibre structures of 17PYY<sub>3-36</sub>, in water, at pH 2 (A), pH 4 (B), pH 6 (C) and pH 8 (D).

The same concentrations and pH ranges were used for 17PYY<sub>3-36</sub> and all pH values showed thin highly elongated entangled fibres, clearly seen in Figure 21. The presence of these thin fibres is in stark contrast to the native, unlipidated, peptide, showing that the addition of the lipid has changed the self-assembled structure.

The diameter of the fibres was found to be consistently about 4 nm. The fibres were also elongated with lengths well over 1  $\mu\text{m}$ . The pH changes can also be seen to not have as much of an effect on the structures formed, unlike with pH 8 for PYY<sub>3-36</sub> (Figure 20 D). pH 2 does show straighter and “crisp” fibres, without the entanglement that the other three pH values show. Without knowing the internal structure of this pH 2 structure it is difficult to suggest a reason for this observation, but the high positive charge at pH 2 could be limiting the flexibility of the peptide. This effect could potentially lock the peptide into a specific orientation, thus producing very linear and rigid fibres.

With regards to the three other pH values, 4, 6 and 8, it was mentioned earlier in this section that a change in pH would affect the enthalpy of aggregation. This would allow different structures to form, but it seems here that the lipid and the hydrophobic effect are driving the assembly. If one factor overwhelmingly drives the assembly, it would make all subsequent structures similar in macrostructure and density regardless of changes in pH value.

The elongated and entangled nature of the fibres is one of a few key factors that can cause fibrillar gel formation.<sup>222, 309, 345</sup> This potential gel formation, as mentioned earlier, means that a gel formed from a peptide drug could be slow releasing and would be of great interest for drug formulation and drug delivery. These fibres do in fact form gels and their structures are explored in greater detail in Chapter 4.

Cryo-TEM confirmed self-assembly of both the native (Figure 20) and lipidated (Figure 21) forms of PYY<sub>3-36</sub>. Now that these structures have been identified they should be investigated further, as the limitations of Cryo-TEM mean further methods, such as SAXS and CD, are needed to give these structures better definition and probe the internal structure that have assembled to form these observed macro-assemblies.

### 3.3 Small Angle X-Ray Scattering of PYY<sub>3-36</sub> and 17PYY<sub>3-36</sub> Structures

Small Angle X-ray Scattering (SAXS) is a highly versatile, non-invasive technique applied in soft matter science as well in other fields<sup>307, 310, 346-355</sup> and is able to probe the internal structure of a multitude of materials and samples. SAXS was used to provide detailed information regarding the shape, size, thickness, density and orientation of PYY<sub>3-36</sub> and 17PYY<sub>3-36</sub> aggregates using form factor fitting (Chapter 2.2.2). The sample preparation, measurement protocols and analysis methods, including form factor fitting are summarised in the sections 2.2.1 and 2.2.2.

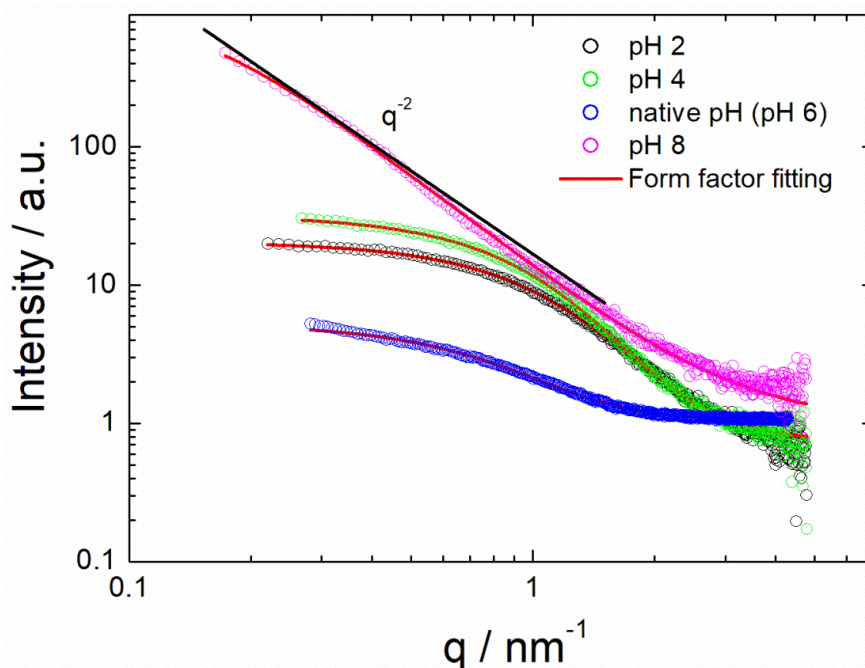


**Figure 22:** All SAXS curves and form factor fitting curves for PYY<sub>3-36</sub> at four different pH values (2, 4, 6 and 8). All samples were prepared in H<sub>2</sub>O at room temperature. Figure taken from authored paper 4.<sup>305</sup>

For the three pH values 2, 4 and 6 the SAXS curves were all fitted to a generalised Gaussian coil form factor model (see 2.2.2, Eq. 4), this is a good approximation for a twisted sheet (Figure 20 C). On the other hand, the pH 8 SAXS sample showed large flat circular assemblies and as such was fitted to a Gaussian bilayer model form factor (Figure 20 D and 2.2.2 Eq. 5). Using  $q$  scaling, as mentioned at the end of Chapter 2.2.2, and superimposed, as shown in Figure 22, has confirmed the suggested 2D-planar structure by a  $q^{-2}$  scaling in the low  $q$  range. The form factor parameters used for these four fits at pH 2, 4, 6 and 8 can be seen below in Table 2, with sketches of the models present in Chapter 2.2.2.

**Table 2:** Gaussian coil and gaussian bilayer form factor fitting parameters for the PYY<sub>3-36</sub> samples at pH values 2, 4, 6 and 8.

Sample Parameter (Gaussian coil model)	0.5 wt% PYY <sub>3-36</sub> pH 2	0.5 wt% PYY <sub>3-36</sub> pH 4	0.5 wt% PYY <sub>3-36</sub> pH 6	Sample Parameter (Gaussian bilayer model)	0.5 wt% PYY <sub>3-36</sub> pH 8
<b>BG</b>	0.70	0.75	0.021	<b>BG</b>	2.09
<b>N / arb. units</b>	0.10	0.15	1.01	<b>N / arb. units</b>	1.39
<b>Rg / nm</b>	1.69	1.87	22.12	<b><math>\sigma</math> / nm</b>	1.74
<b><math>\nu</math></b>	0.28	0.25	0.29	<b>t</b>	3.19
<b>I<sub>0</sub></b>	197.65	204.85	0.084	<b><math>p_{out}</math></b>	0.597
				<b><math>b_{out}</math></b>	0.00086
				<b><math>p_{core}</math></b>	3.59
				<b><math>b_{core}</math></b>	-0.000135
				<b>D / nm</b>	1000

BG – Background. N - Scaling Factor. Rg - Radius of Gyration.  $\nu$  – Flory Exponent. I<sub>0</sub> – Forward Scattering.  $\sigma$  - Gaussian Width. t - Bilayer Thickness.  $p_{out}$  - Electron density of the Outer Gaussians.  $b_{out}$  - Width of Outer Gaussians.  $p_{core}$  - Electron density of the Inner Gaussian.  $b_{core}$  - Width of Inner Gaussians D - Diameter of Disc (constrained parameter, as a large disk was seen in cryo-TEM).

From these SAXS fittings the pH 6 fitting parameters showed a large radius of gyration,  $R_g$ , of 22 nm compared to the other pH values. This is comparable to the results from the cryo-TEM that also showed that pH 6 contained wider sheets, compared to the other values. pH values 2 and 4 also confirmed a smaller radius ranging from 1.7-1.9 nm, which again is confirmed by the structures seen in cryo-TEM. pH 6, can now be confirmed to form larger, and potentially more stable aggregates, compared to the other pH values. The reason for this observation is that more stable self-assemblies normally have a low threshold to assembly, such as enthalpy (high charges), or entropy (small shape) that then allows for more to assemble, and stay assembled favourably. This is the first fitted SAXS data for the self-assembled structure of PYY<sub>3-36</sub>, making this a great addition to cumulative data surrounding the investigation of this molecule.

Although the PYY<sub>3-36</sub> samples formed in pH 8 water were circular and planar in shape (Figure 20 D), the SAXS fitting (Chapter 2.2.2 Bilayer Gaussian) showed a similar bilayer thickness of 1.74 nm to samples of PYY<sub>3-36</sub> formed at pH 2 and 4. This shows that the bilayer of pH 8 PYY<sub>3-36</sub> is as thick the two layers of similar fibres seen in pH 2, 4. Further work on this observation would be useful as the process by which these planar disks are formed cannot be determined by these cryo-TEM and CD results.

17PYY<sub>3-36</sub>, as shown using Cryo-TEM, formed thin fibres and this has been confirmed through SAXS as well. When creating the pH 6 17PYY<sub>3-36</sub> it was seen to produce a precipitate, as such it was not possible to complete SAXS analysis as the automated sample system could not retrieve the particulates from the bottom of the sample vial. Circular Dichroism has been used however to investigate this observation together with similar pH studies to understand this significant change. Following this methodology showed a total loss of secondary structure for pH 6, implying this was the isoelectric point for 17PYY<sub>3-36</sub> (discussed more in Chapter 3.4).

Three other pH values have been investigated, pH 2, 4 and 8. SAXS has shown 17PYY<sub>3-36</sub> formed thin fibres of extremely long length and that is consistent with the entangled elongated fibres seen previously using Cryo-TEM (Figure 21).

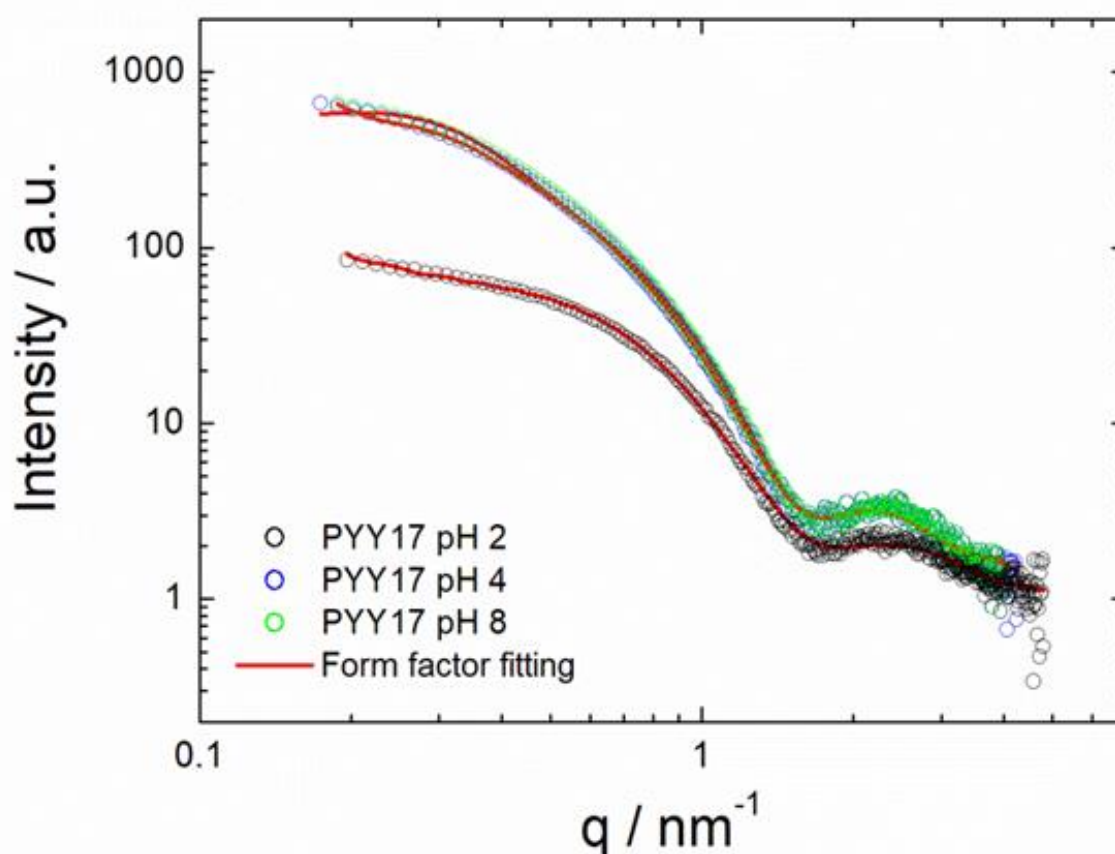


**Figure 23:** SAXS curves for 17PYY<sub>3-36</sub> at three different pH values, prepared in H<sub>2</sub>O, 2, 4 and 8 including the long cylinder shell fitted curves. All samples were in water and at room temperature. Figure taken from authored paper 4.<sup>305</sup>

The SAXS patterns can be seen in Figure 23 with constraints in Table 3. The parameters shown in Table 3 show a clear consistency through-out the pH values, compared to that of the native PYY<sub>3-36</sub> that varied considerably. A small change can be seen in the radius values, but this can be explained with the sample being in a highly positively charged environment at pH 2.

**Table 3:** Shows the fitting parameters used to fit the long cylinder shell model for the 3 different pH samples of 17PYY<sub>3-36</sub>.

Parameter	0.5 wt% PYY17 pH 2	0.5 wt% PYY17 pH 4	0.5 wt% PYY17 pH 8
<b>BG</b>	0.9	0.9	0.8
<b>N / arb. units</b>	0.258	0.267	0.286
<b><math>\sigma</math> / nm</b>	0.286	0.321	0.347
<b>R / nm</b>	1.273	1.63	1.45
<b>DR / nm</b>	0.113	0.151	0.271
<b>L / nm</b>	500	500	500
<b><math>p_{core}</math></b>	0.0357	0.0408	0.0469
<b><math>p_{shell}</math></b>	0.312	0.241	0.165
<b><math>p_{solv}</math></b>	0.0314	0.0185	0.0266

BG - Background. N - Scaling Factor.  $\sigma$  - Gaussian Width. R - Inner Radius. DR - Shell Thickness. L - Length of cylinder.  $p_{core}$  - Electron density of the core.  $p_{shell}$  - Electron density of the shell.  $p_{solv}$  - Electron density of the solvent.

The values obtained above compare extremely well with the Cryo-TEM images of the lipidated peptide. They show a small radius value that was seen throughout the pH values. This contrasts with the native peptide that at pH 2 and 4 changed to thin fibres and at pH 8 showed large planar, while for the lipidated version they were all fibres, and this was enforced by SAXS fitting as well. Cryo-TEM also showed the loss of a twisted structure by lipidation and again, SAXS has confirm this loss for all the pH values, asides from pH 6 which precipitated. The fits also show that these fibres are low scattering cores of 1.3 - 1.6 nm, but more heavily scattering shells of between 0.113 – 0.271 nm. This is a helpful observation as the fibres seen in cryo-TEM did not visibly show this inner core or an obvious outer shell. It would be difficult to determine the structure of these shells, as before with the native peptide, as more of the internal structure of the fibres is needed to be known. It is unknown if the inner core is just a hydrophobic pocket of the lipid chains or more solvent based (the values for scattering density are higher, suggesting the first, but this cannot be fully confirmed).

In summary, the distinct change seen in the cryo-TEM results (for the pH values and lipidation) can be confirmed with SAXS as well. Further to this, SAXS has allow for more detailed parameters for the structures to be gleaned, such as the radius of the lipidated peptide fibres range from 1.3 to 1.6 nm. With cryo-TEM it is only possible to deduce these parameters by visual observation of the cryo-TEM image. The length of these fibres however was too long to be confirmed as SAXS is limited by the detector distance from the sample (which determines the observation of larger structures, such as 1000 nm fibre lengths). Though, in the above fits

the values (L) were constrained pre-emptively, before fitting, to 500 nm that gives a reasonable expectation of a long-extended fibre.

### **3.4 Secondary Structure Investigation of 17PYY<sub>3-36</sub> by Circular Dichroism**

A useful technique for enantiomer identification and for secondary structure investigation is Circular Dichroism spectroscopy (CD).<sup>309, 343, 356-362</sup> For a detailed explanation of this technique and the process by which the data was recorded and analysed, please see section 2.2.3. One of the key observations that be been obtained from CD is if  $\alpha$ -helical and  $\beta$ -sheet secondary structure is present.  $\alpha$ -helical structure when present in a molecule present two minima at around 205 and 225 nm.  $\beta$ -sheets on the other hand only show one minimum around 215 nm. This allows for simple characterisation of the secondary structure and the observation of any changes from one to the other.

In a first set of experiments CD was applied to investigate the effect of the lipidation on the secondary structure, followed by tests probing the unlipidated and lipidated peptide's secondary structure's stability to pH change. As mentioned previously in Chapter 2.1.2, all efforts to make sure the concentration and pH values studied are as precise as possible.

Three pH values around 4, 6 and 8 were selected for the lipopeptide as the scope of this project was for drug formulation and these are three of the most common pH values found throughout the body. This also correlates well to the range mentioned earlier in Chapter 3.2<sup>344</sup>, the reason being that for injectable or consumables purposes formulations above or below these values were not given to patients, so only this pH range was studied as it had biological relevance.

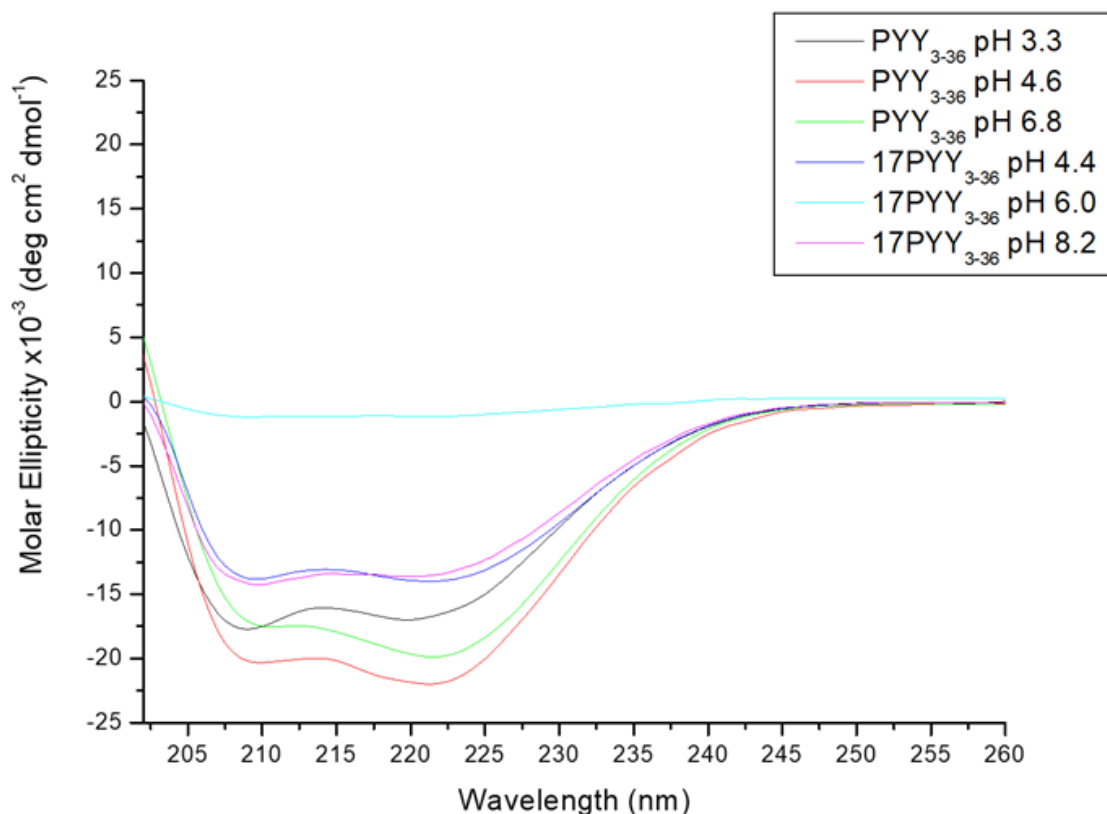


**Figure 24:** CD spectrum comparing 0.5 wt% PYY<sub>3-36</sub> at pH 3.3, 4.6, and 6.8 to 17PYY<sub>3-36</sub> at pH values, 4.4, 6.0, and 8.2. 17PYY<sub>3-36</sub> at pH 6.0 shows no secondary structure as this pH is its isoelectric point and precipitated out of solution, native PYY<sub>3-36</sub> did not show this effect at any selected pH. All samples prepared in water and at room temperature. All run at room temperature.

The first observation from Figure 24 is in keeping with the previous studies mentioned in the introduction (Chapter 1.13) and showed that PYY<sub>3-36</sub> (black, red and green in Figure 25) contained  $\alpha$ -helical secondary structure at all pH values. The second observation for the native peptide here is that pH 4.6 has the largest content of  $\alpha$ -helical secondary structure, estimated 45% (red), then the two other pH values investigated for it, 35% content at pH 6.8 (green) and 30% content at pH 3.3 (black). These percentages coming from the comparison with a 100%  $\alpha$ -helical peptide of a similar length, as mentioned within the CD method Chapter 2.2.3. The percentage  $\alpha$ -helical content of PYY<sub>3-36</sub> is 45%, which is more than double previous studies estimates, which showed PYY<sub>3-36</sub> having 24% content.<sup>341</sup> Interestingly, the previous study (by Keire et al.)<sup>341</sup> also estimated the percentage of  $\alpha$ -helical content of PYY to be 45%, which is closer to that was observed in these studies.

The loss of  $\alpha$ -helical content is not uncommon in peptide secondary structures as both  $\alpha$ -helices and  $\beta$ -sheets rely heavily on hydrogen bonding motifs that are impacted by pH changes.<sup>146, 310, 363-366</sup>

The lipidated peptide 17PYY<sub>3-36</sub> also shows  $\alpha$ -helical content similar to the native peptide, however its  $\alpha$ -helical content is reduced when compared to its unlipidated form. This was hypothesised at the beginning of this chapter as the placement of the lipid for 17PYY<sub>3-36</sub> is within the beginning of the  $\alpha$ -helical coil (Chapter 3.1 Figure 19).

pH 6.0 for 17PYY<sub>3-36</sub> can be seen to have created no secondary structure as it has produced a spectrum without any large minima. This was because when the sample was changed to pH 6.0 the solution turned cloudy, and a precipitate formed which fell out of solution. An aliquot with these precipitates were gathered and the CD light blue results of these precipitates can be seen in Figure 24. The results seem to suggest that the precipitate has lost all secondary structure when at this pH value, pointing to evidence of this being 17PYY<sub>3-36</sub>'s isoelectric point (the point of the molecule having zero charge). This isoelectric point would make sense that the secondary structure is lost as most secondary structure ( $\alpha$ -helical and  $\beta$ -sheets) requires charged amino acid interactions, and in this case, there are none, so the structure does not form. This precipitation affect at the pI is common and found throughout peptide and other chemistry fields.<sup>8, 367-370</sup> Although a loss of secondary structure is possible at the pI, it is also highly probable that with the precipitation at the pI there would be no peptide present to be able to record a CD spectrum. The specific collection of the precipitate, and the thin (0.1mm) pathlength, should have alleviated this outcome, but this collection process is not infallible and therefore further CD and pI experiments would be needed to rule out the effect of precipitation at the pI.

A more significant observation, from a drug delivery perspective, relates to the differences in the stability of the native and lipidated forms. The CD shows that the native peptide's  $\alpha$  helical structure is reduced when not at pH 4.6. Aside from the precipitation at pH 6.0, the  $\alpha$ -helical content of the lipidated peptide at pH 4.4, estimated to be 35% content (dark blue), and pH 8.2 with 32.6% content (Pink) are extremely similar. This suggests that the lipidation has helped limit the interaction of pH on the secondary structure, although the  $\alpha$ -helical content of the lipopeptide was lower than that of the native peptide.

In a second set of experiments, temperature studies were completed to probe both PYY<sub>3-36</sub> and 17PYY<sub>3-36</sub> secondary structure stability to temperature changes. This was completed for temperatures 20 °C to 60/70 °C, taking measurements every 5 °C or 10 °C, allowing the sample to equilibrate for 5 minutes. A cooling step was also completed and another 20 °C measurement was completed. This cooling experiment provided an understanding if the secondary structure

recovered fully or if the temperature had affected the secondary structure. Further information regarding these temperature experiments can be found in the methodology CD-section 2.2.3.

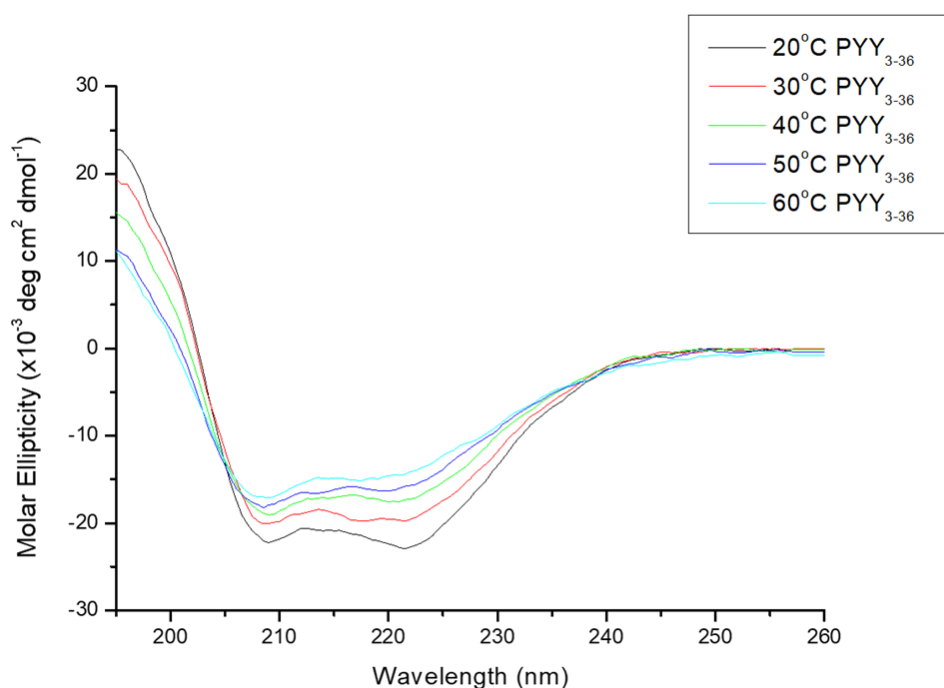


**Figure 25:** CD spectra for a 0.5 wt% PYY<sub>3-36</sub> sample prepared in H<sub>2</sub>O at pH 4.6. Temperature study of 20-60 °C.

A temperature CD experiment for PYY<sub>3-36</sub> was completed first and, as there are many previous secondary structure characterisation studies of PYY<sub>3-36</sub>, it was only completed on a sample at pH 4.6, using 10 °C temperature steps.<sup>271, 275, 280</sup> The main observation from Figure 25 is that the  $\alpha$ -helical structure of the peptide decreases as the temperature increases, from 45% to 22.5%. This is to be expected as the hydrogen bonds within  $\alpha$ -helices are affected by changes in temperature. As temperature increases, the kinetic energy of the hydrogen bond components increase. This energy increase will reduce the interactions of the donating and accepting hydrogen bond moieties and subsequently reduce the overall bond stability. This reduction in stability reduces the chances of an interaction between the two moieties and gives further kinetic energy to the bond to dissociate, further reducing the duration of a stable hydrogen bond. Again, in a similar way to that of pH, this effect can be seen across all hydrogen bonding complexes.<sup>371-375</sup>

Three pH values, 4.4, 6.0 and 8.2, were used to complete temperature studies for 17PYY<sub>3-36</sub>. The temperature steps for these experiments were 5 °C because, as a novel molecule, a more

detailed temperature experiment is needed to help fully characterise the molecule and to avoid overlooking any possible changes that might occur because of temperature change.

As seen in Figure 26 A, a similar effect of temperature on the self-assembled  $\alpha$ -helix can be seen to that of 17PYY<sub>3-36</sub> for pH 4.4, with an overall reduction in the  $\alpha$ -helical content presented by the two minima of 205 and 225 nm. This effect can also be seen to be reversible, back to around 32.5% content, although not back to its original 35%  $\alpha$ -helical content at 20 °C (A – black line). This reversibility (A – dark green line) seems to only reach structure comparable to its content at the 35 °C measurement (32.5% content) (A - dark blue). Most notably, 17PYY<sub>3-36</sub> at pH 4.4 retains an  $\alpha$ -helical structure throughout the temperature ramps. This is important information for drug formulation as large changes in secondary structure can inhibit activity, induce gelation, and affect the removal of the peptide hormone from the body.<sup>359, 376-382</sup>

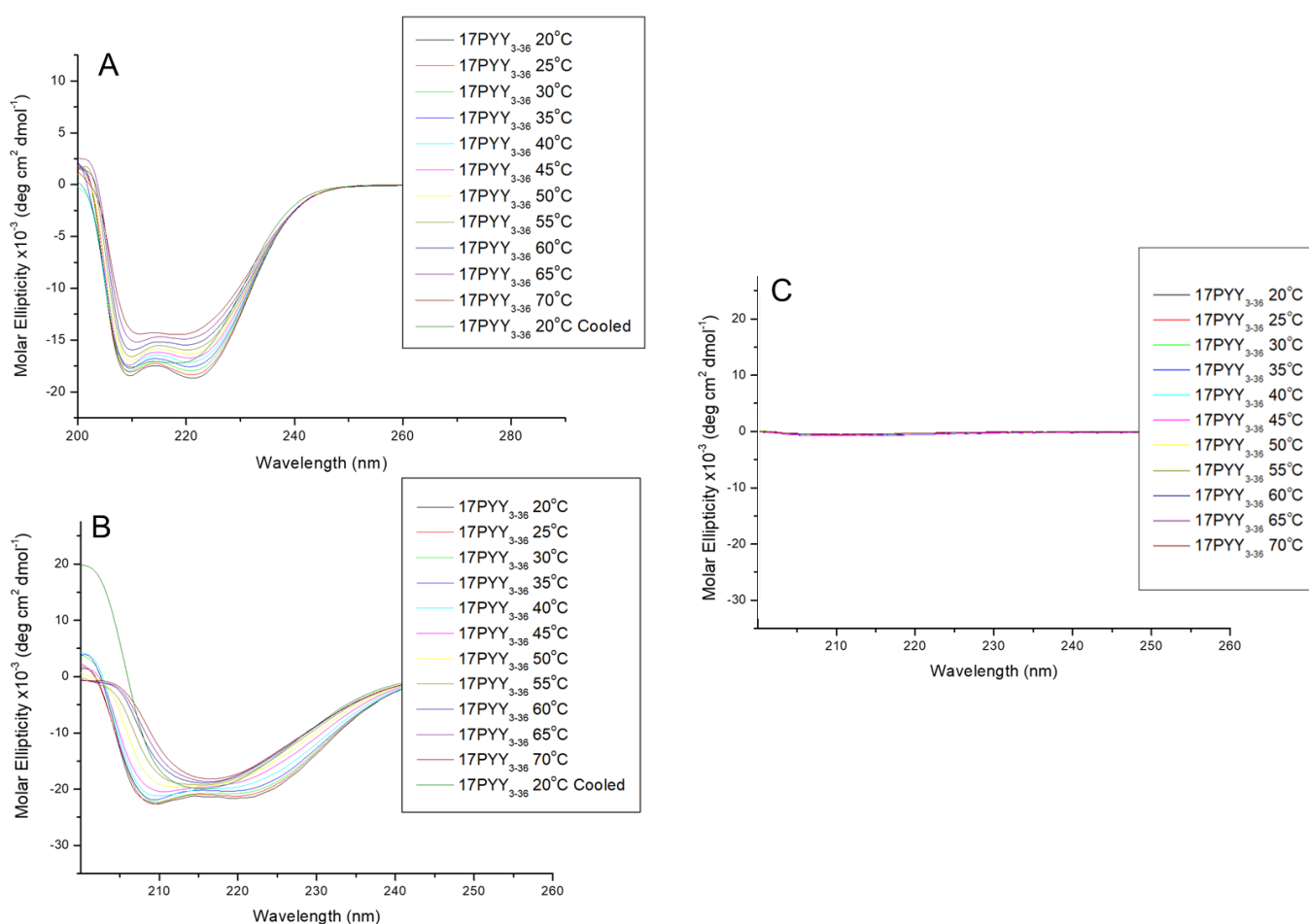


**Figure 26:** pH-dependent CD spectra of 17PYY<sub>3-36</sub> observed from 20-70 °C. A - CD spectra for 0.5 wt% 17PYY<sub>3-36</sub>, pH 4.4 H<sub>2</sub>O. B - CD spectra for 0.5 wt% 17PYY<sub>3-36</sub>, pH 8.2 H<sub>2</sub>O. C - CD study of 0.5 wt% 17PYY<sub>3-36</sub> pH 6.0, showing the lack of secondary structure of the precipitate formed (graph scaled to be similar to A and B).

A similar observation can be seen in Figure 26 B for the pH 8.20 17PYY<sub>3-36</sub> sample for the first 30 °C increase (Bright Yellow – Figure 26 B). A reduction in  $\alpha$ -helical content can be seen for

the first few temperature points, from 32.5% to around 25%, but after temperature 55 °C this has transformed into a  $\beta$ -sheet type structure with the characteristic one minimum at 215 nm.<sup>336, 383-391</sup> This change can be seen to be slowly forming at 50 °C. This  $\beta$ -sheet structure can also be seen to dominate the structure even after cooling back to 20 °C.

At 200 nm and after cooling (Figure 26 B), an observable increase between the 70 °C result and that of the cooled 20 °C result was produced. There are two potential reasons for this. The first being a time factor, as the sample will take time to cool down from 70 to 20 °C this could provide time for the  $\beta$ -sheet structure to continue forming. In this case, the  $\beta$ -sheet structure seen to be forming around 50-55 °C could have continued to arrange, producing a larger CD signal. The second reason behind this observation is that some of the  $\alpha$ -helical structure was reformed during cooling, but in this case the structure remained predominately  $\beta$ -sheet with the only part of the spectrum to observe this  $\alpha$ -helical reformation being at the 200 nm wavelength. A maxima at 200 nm is one of the characteristics of  $\alpha$ -helical secondary structure, as seen in the other experiments in this chapter (Figure 24, 25, and 26). It is unknown which of these potential reasons caused this effect, but the  $\beta$ -sheet structure is slightly more difficult to form than that of  $\alpha$ -helix, requiring inter (between strands) and intramolecular bonding (within strands) unlike  $\alpha$ -helical which only requires intramolecular bonding.<sup>392-394</sup> This would suggest that the  $\alpha$ -helix structure reforms while cooling and represents a more favourable hypothesis at these higher temperature ranges. To help substantiate this hypothesis a selection of known alpha-helical peptides could be subjected to the same temperature denaturing to enable a fuller comparison. Examples of well characterised alpha-helical peptides include Melittin (bee-sting component peptide) and Pardaxins (fish produced shark repellent).

The results for pH 5.99 are shown in Figure 26 C, for completeness, but the experiment showed no secondary structure at all, as previously mentioned in this chapter. 17PYY<sub>3-36</sub> has an isoelectric point at this value and precipitated out of solution. A single room temperature result can be seen in Figure 24, and this pH 5.99 17PYY<sub>3-36</sub> experiment was then continued for all temperature values showing no changes and no structure. This “loss” of structure, as mentioned earlier, was attributed to the isoelectric point with the lipopeptide falling out of solution at, or close to, neutral charge. The graph was scaled to that of A and B to give a useful understanding of the amount of structure that was present in relation to the other pH values. The results again show little structure, neither  $\alpha$ -helical nor  $\beta$ -sheet. This effect was commented on earlier and is related to the impact of the charge removing the possibility of there being charged amino acids and hence reducing the formation of secondary structures.

The most valuable observation from these temperature studies has been the transition of the lipidated 17PYY<sub>3-36</sub> from a dominant  $\alpha$ -helical secondary structure to that of a strong  $\beta$ -sheet structure.  $\beta$ -sheet secondary structure, when combined with that of the fibre macro-structure seen in cryo-TEM and SAXS, invited an investigation into the potential for gelation to occur (Chapter 4).  $\beta$ -sheets have been known to be highly favourable for gelation as well as for elongated and entangled fibres.<sup>23, 142, 206, 222, 309, 363, 385-387, 395-407</sup> This is hypothesised to be due to the ability of self-assembled  $\beta$ -sheets to form repeating structures.  $\alpha$ -helical structure is limited in structure in one dimension, along the helix, but  $\beta$ -sheets can form tubes, sheets and “cross link” between strands to form a much more rigid and expansive network than compared to that of just  $\alpha$ -helix structures. This is not to say all hydrogels are  $\beta$ -sheet as some have been formed from  $\alpha$ -helices.<sup>408-411</sup> In Chapter 4 the question of gelation with this peptide hormone, PYY<sub>3-36</sub>, and lipopeptides 11, 17, and 23PYY<sub>3-36</sub> is dealt with and have been found to form elongated fibre structured hydrogels.

### **3.5 Critical Aggregation Concentration (CAC) Determination of 17PYY<sub>3-36</sub> Self-Assembled Structures**

Using Cryo-TEM, SAXS and CD the macromolecular structure of 17PYY<sub>3-36</sub> has been confirmed and the internal structure investigated, the next question is that of aggregation. Aggregation can be identified by a variety of methods all of which measure different physical factors such as surface tension, conductivity and fluorescence to determine a critical aggregation concentration (CAC). The critical aggregation concentration is defined as when the surfactant is no longer suspended as free molecules and the point at which they form aggregates, which sometimes are well ordered. One of the CAC methods uses pyrene as a fluorescence probe. This method uses the intensities of two characteristic pyrene emission bands, after being excited using light of 339 nm, to determine the surfactant’s concentration point of aggregation. Pyrene’s emission peaks at 373 nm and 383 nm are sensitive to its environment, which means a hydrophobic or hydrophilic environment will change the emission pattern that is measured. In particular, the  $I_{383}/I_{373}$  intensity ratio can be plotted against the surfactant concentration revealing a “break point” at which the pyrene changes from a hydrophilic to hydrophobic environment. A more in-depth explanation can be found in the methodology section 2.2.6.

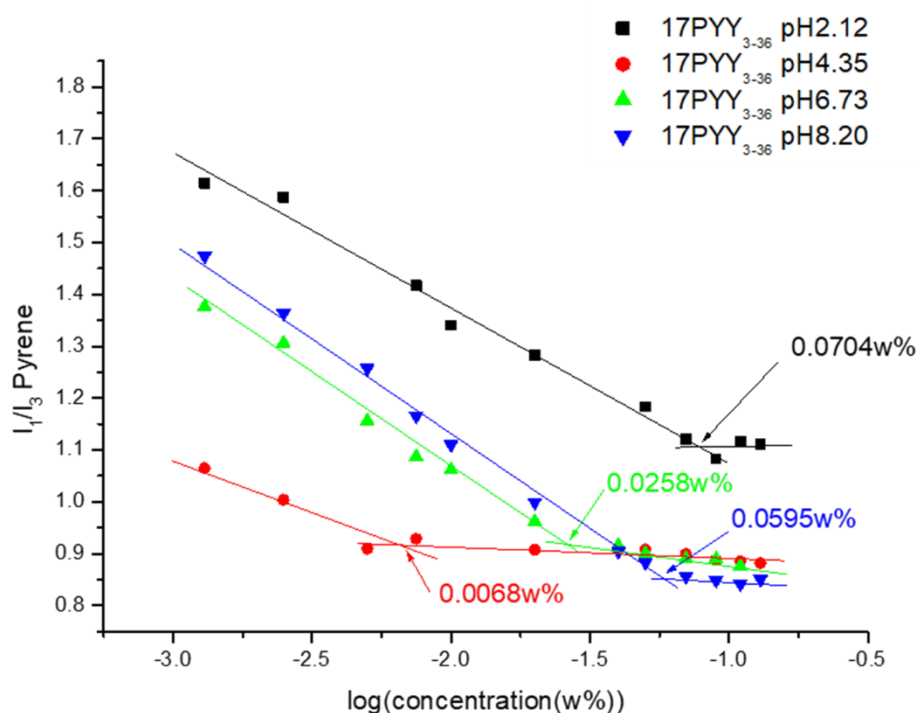


**Figure 27:** Pyrene fluorescence vs. concentration of 17PYY<sub>3-36</sub> at pH 2.12, 4.35, 6.73 and 8.21. I<sub>1</sub> and I<sub>3</sub> being Pyrene vibronic bands at 373 nm and 383 nm, respectively. The intersection of linear fits defines the CAC.

Previous studies have focused on PYY<sub>3-36</sub> but they have been solely focused on physiological effects and receptor binding.<sup>74, 412-422</sup> To understand the self-assembly structure of the lipidated peptides when injected or consumed, a CAC study at different pH values has been completed on the lipidated peptide. These pH values are like those found throughout the body and are important to study, as previously mentioned in the CD and SAXS sections. The values of 4 to 8 pH are also relevant for drug administration as these are safe injectable pH values. Any changes to aggregation, structure and bioactivity due to these pH values would therefore be of use for understanding potential drug applications. The most significant observation seen from Figure 27 is the increase in the critical aggregation concentration away from pH 4.35 (formed by the simple addition of the lipopeptide to pH 7 water). At pH 4.35 17PYY<sub>3-36</sub> showed an extremely low CAC of 0.0068 wt%. This low critical aggregation concentration shows that the assembling concentration of the lipopeptide is highly affected by the lipid addition. Any increases or decreases in pH value show an increase in the CAC at which the fibres form (Figure 21). pH 6.73 shows an almost 4 times greater increase in the CAC as compared to the pH 4.35 concentration. This increases further for pH 2.12 and pH 8.20 by almost 10-fold. This was not unexpected as increases to pH affect the enthalpy of assembly and, as the lipopeptide has charged amino acids, this will change the charges on them. The larger increase in CAC, as

seen in Figure 27, is caused by the two “extremes” of the pHs tested. This result indicates that changes in pH on the charged moieties have caused the molecules to repel each other with greater force that, will in turn, reduce the ability of the molecules to aggregate.

These observations conclude that the pH of the environment does affect 17PYY<sub>3-36</sub>'s self-assembling properties. Changes in pH also show that the charges of the peptide are an extremely important requirement for the fibre formation of this lipopeptide. This affect is clearly one of the critical methods of self-assembly, via charged motifs and moieties (as previously mentioned in the introduction Chapter 1.8). Furthermore, these pH values show injection or consumption of the lipopeptide within the human body, with its varied pH values, will affect the critical aggregation concentration, as well as the assembly properties already highlighted by CD, SAXS and cryo-TEM. An awareness of this impact of pH on 17PYY<sub>3-36</sub> will be an important consideration for 17PYY<sub>3-36</sub> drug formulation, manufacture and delivery. As mentioned previously in Chapter 2.1.2, all efforts to make sure the concentration and pH values studied are as precise as possible.

### **3.6 Comparison of 17PYY<sub>3-36</sub>, 11PYY<sub>3-36</sub> and 23PYY<sub>3-36</sub>**

As part of this study, and as mentioned previously, three lipidated forms of the peptide hormone PYY<sub>3-36</sub> were prepared. These were 11PYY<sub>3-36</sub>, 17PYY<sub>3-36</sub> and 23PYY<sub>3-36</sub>. 17PYY<sub>3-36</sub>, each of which have been investigated within this report. 11PYY<sub>3-36</sub> and 23PYY<sub>3-36</sub> were investigated separately by a fellow PhD student of the Hamley group, Jessica Hutchinson. This collaboration has allowed for a faster completion of the methods and has provided a comparison of the three lipopeptides. The comparison between the three lipopeptides has proved valuable as it added to the lipidation and peptide scientific understanding of the characteristics and differences in the self-assembled structures between the different lipidated positioned lipopeptides. This has led to an improvement in the understanding of the implications of the lipidation of larger (36 amino acids) peptides.

A summary is provided below but for the full data on 11PYY<sub>3-36</sub> and 23PYY<sub>3-36</sub> please refer to the authored paper referenced at the beginning of this chapter.<sup>305</sup> This paper has also been referenced (paper number 4) in the publications chapter of this thesis. This published paper gives a greater and more in-depth comparison of the three lipopeptides.<sup>305</sup> At pH 4 all lipopeptides (11, 17 and 23) formed fibres, but when the pH was changed to pH 2 both 11PYY<sub>3-36</sub> and 23PYY<sub>3-36</sub> formed micelles. This was at odds with 17PYY<sub>3-36</sub> that showed the formation

of fibres at all pH values (Figure 20). This is a clear change that can be assigned to the difference in lipidation position.

SAXS fitting applied a spherical shell form factor to both the 11PYY<sub>3-36</sub> and 23PYY<sub>3-36</sub>, resulting micellar radii of about 2 nm. The secondary structure of these micelles was confirmed to be  $\alpha$ -helical in secondary structure, which is the same secondary structure found for the fibres at pH 2, 4, 6 and 8 values.

11 and 23PYY<sub>3-36</sub> showed similar increases in critical aggregation concentrations for higher and lower pH values when compared to the CACs that arose following the simple addition of each of the lipopeptides to water. This was a 3-to-4-fold increases from pH values around 4.5, 11 being 0.013 wt% and 23 being 0.0093 wt%, to that of pH 2 and 8, resulting in 0.038 and 0.033 wt% for 11 and 23PYY<sub>3-36</sub> respectively. This is consistent with the charge of the solution having a large effect on the aggregation concentration, seen similarly with 17PYY<sub>3-36</sub>, and explained earlier in Chapter 3.5.

The precipitation affects seen at around pH 6 for 17PYY<sub>3-36</sub> was also seen at around pH 6 for the other two lipidated peptides. This effect was investigated further, by PhD student Jessica Hutchinson, using an acid titration experiment with the addition of small amounts of dilute HCl to 2 wt% samples of the three lipopeptides. Starting at pH 10 and ending at pH 2, it was observed at around pH 5.5 a pH plateau formed even with multiple additions of HCl, indicating an isoelectric point (pI). This precipitation effect for the other two lipopeptides 11 and 23 showed similar effects in the form of a cloudy sample and precipitation to that of 17PYY<sub>3-36</sub> at pH 6. This lends evidence to all three lipopeptides being at zero charge at around pH 6.

CD of all the lipopeptides showed  $\alpha$ -helical secondary structure for all pH values (2-8) even with the above self-assembly structure change (fibre to micelle).

As shown previously, temperature ramps of 20-70 °C were completed on 17PYY<sub>3-36</sub> as well as the other lipopeptides. Interestingly, both 17 and 23PYY<sub>3-36</sub>, at pH 6 or 8, showed a  $\beta$ -sheet transformation at around 45-55 °C, but 11PYY<sub>3-36</sub> does not. This, akin to the micelle formation at pH 2, shows that the difference in the lipidation anchor-point is decisive for the formation of distinct macro-structures as well as important for the conservation of secondary structures in these three lipopeptides. Table 4 summarises all the findings.

**Table 4:** Summary of self-assembly structures. Secondary structures are colour coded:  $\alpha$ -helix (light orange background) and  $\beta$ -sheet (grey-blue background). Temperature of the experiment is at room temperature, unless otherwise stated.

	11PYY <sub>3-36</sub>	17PYY <sub>3-36</sub>	23PYY <sub>3-36</sub>
<b>pH 2</b>	micelles	fibres	micelles
<b>pH 4 (Native)</b>	fibres	fibres	fibres
<b>pH 8</b>	fibres	fibres	fibres
<b>pH 6/8: 20-40 °C</b>	fibres	fibres	fibres
<b>pH 6/8: 40-50 °C</b>	fibres	fibres	fibres
<b>pH 6/8: 50-70 °C</b>	fibres	fibres	fibres

### 3.7 Conclusions of the Lipidation of PYY<sub>3-36</sub> at Position 17

PYY<sub>3-36</sub> has an extremely valuable potential use as a peptide drug.<sup>281-282, 423-425</sup> for obesity or for eating disorders. The larger self-assembled aggregates of PYY<sub>3-36</sub> have not been shown before, with many studies limiting themselves to drug binding or secondary structure studies.<sup>271, 273, 333, 338, 340-342, 426-432</sup>

Within this thesis it has been demonstrated for the first time that PYY<sub>3-36</sub> forms twisted tape-like structures, with small changes in structure when the pH is changed. 17PYY<sub>3-36</sub>, a novel lipopeptide, has been characterised from its macrostructure to its secondary structure together with its critical aggregation concentrations. The experiments and subsequent analysis have shown a change in 17PYY<sub>3-36</sub>'s self-assembly structure from twisted tapes to fibres. The secondary structure, although  $\alpha$ -helical like the native peptide, was reduced by 10%. This finding is consistent with the incorporation of the palmitoyl functional group, as its location disrupts the beginning of the helix (Figure 19). The studies carried out with pH changes and temperature ranges have also shown a secondary structure change, from  $\alpha$ -helical to  $\beta$ -sheet, at around 45 °C. The macro-structure is still of a fibre like nature, but an internal rearrangement has occurred allowing for this secondary structure change. Once changed to  $\beta$ -sheet, 17PYY<sub>3-36</sub> remains with this structure when cooled back to 20 °C. It was also observed through a comparison between the three lipopeptides 11PYY<sub>3-36</sub>, 17PYY<sub>3-36</sub> and 23PYY<sub>3-36</sub> that they show different macrostructure and secondary structural differences. Each lipopeptide, although based on the same peptide backbone show similarities and differences when exposed to the same environments and processes.

These observations demonstrate two things; firstly although lipidation, with its bio-acceptance and slow release qualities, is seen as a good route to overcome current drug delivery and formulation draw backs, the lipidation point on a large peptide requires careful consideration. Secondly, if the lipidation of PYY<sub>3-36</sub> does not affect the efficacy, these three lipopeptides (11, 17, and 23PYY<sub>3-36</sub>) could improve overall drug delivery, as lipidation has been shown to reduce clearing, lower degradation and improve drug release characteristics.

## 4. Lipopeptide PYY<sub>3-36</sub> Gels

This chapter was published in part in the paper: Hutchinson, J. A.; Burholt, S.; Hamley, I. W.; Lundback, A.-K.; Uddin, S.; Gomes dos Santos, A.; Reza, M.; Seitsonen, J.; Ruokolainen, J., The Effect of Lipidation on the Self-Assembly of the Gut-Derived Peptide Hormone PYY<sub>3-36</sub>. *Bioconjugate Chem.* 2018, 29 (7), 2296-2308.

### 4.1 Introduction to Lipopeptide and Peptide Gels

Gels, as mentioned previously in the Introduction (Chapter 1.11), are solvent swollen highly extended assembled networks of polymeric molecules.<sup>142, 309, 363, 395, 403, 406, 408, 433-441</sup> These large networks of polymeric molecules are normally formed through intra-molecular bonding mechanisms, such as hydrogen bonding or  $\pi$ - $\pi$  interactions, but can also be formed by intermolecular bonding such as cross-linking.<sup>96, 231, 442-446</sup> Many dispersion mediums can be used to form these gels from water or other organic molecules, such as hexane or petrol.<sup>231, 406, 433, 436, 447-448</sup> There are many defining attributes for gels, including; charge, type of monomers, monomeric or co-polymeric networks, and their organisation such as amorphous or crystalline.<sup>32, 150, 208, 335, 345, 349, 449-457</sup>

Peptides and lipopeptides can form self-assembled structures capable of hydrogel formation.<sup>363, 395, 458-459</sup> Studies of these have included both the drug (peptide or lipopeptide) itself forming the gel network, as well as the peptide or lipopeptide network allowing encapsulation and retention of drug molecules.<sup>213, 241, 460-464</sup> Both methods lead to different advantages, but the formation of a hydrogel can be difficult, especially for gels formed from the drug molecule.

The intention of this project was to investigate these lipopeptides for drug delivery and formulation. For this reason, hydrogels, specifically gels formed using water as the swelling solvent, were to be investigated. This section provides details of their preparation and characterisation.

## 4.2 Formation of Hydrogels

The  $\beta$ -sheet formation, and their stability to temperature, seen in Chapter 3.4 prompted a further investigation into hydrogels. Many  $\beta$ -sheet forming gels are formed from peptides or lipopeptides by using charges and temperatures.<sup>23, 178, 386, 396, 398</sup> This was seen in the previous chapter at 45 °C and pH 8 when both 17 and 23PYY<sub>3-36</sub> transitioned to that of  $\beta$ -sheet, which is highly beneficial to gel formation (Chapter 3.4 Figure 26 B for 17PYY<sub>3-36</sub>). 11PYY<sub>3-36</sub> did not show this transition; neither did studies of native PYY<sub>3-36</sub>. These two significant observations indicate the most important changes caused by lipidation and the position of lipidation. Even without showing the  $\beta$ -sheet secondary structure transition, both 11 and native PYY<sub>3-36</sub> were tested for hydrogel formation for completeness.

Samples were made using the dehydration method (Chapter 2.1.2 Gel Sample Preparations). The potential critical gelation concentration (CGC), the concentration at which the sample gelled, was unknown for these novel lipopeptides, which is why a dehydration experiment would help define the concentration and probe the potential gel formation properties. By using the method within Chapter 2.1.2 gels were readily formed of 11, 17, and 23PYY<sub>3-36</sub>. The gels were confirmed by the inverted vial test (inverting a vial and visually observing a lack of movement and rigidity characteristics of a gel like network). Photos of the clear gels that were tested can be observed in Figure 28.

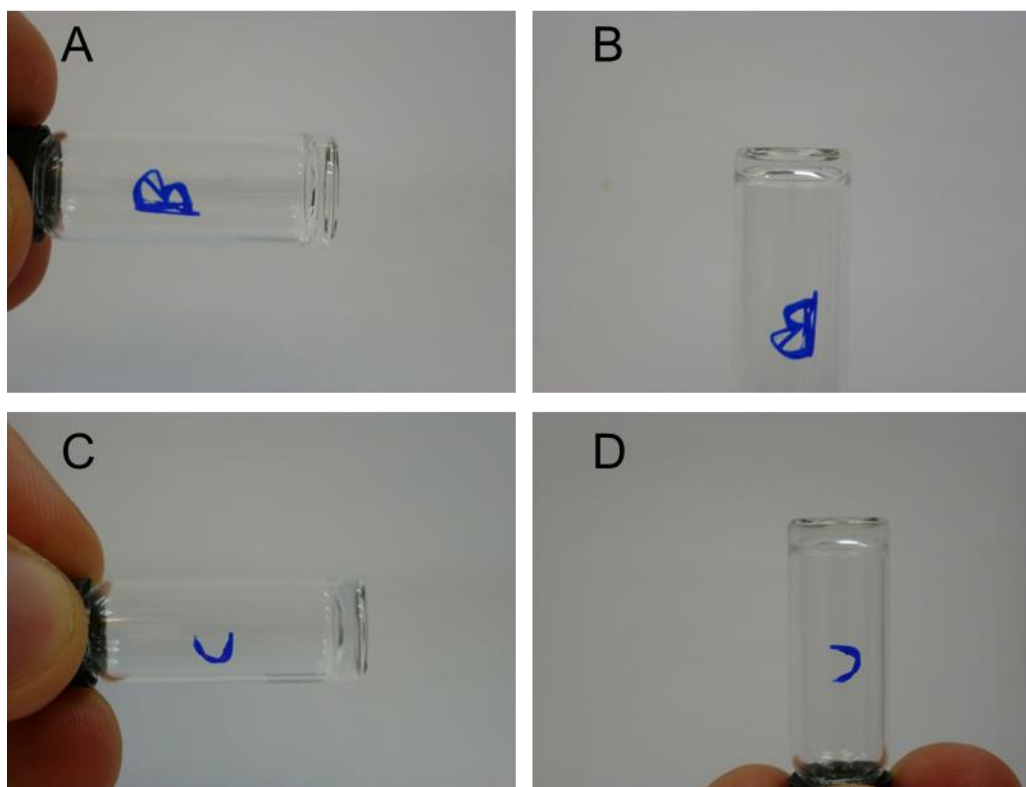


**Figure 28:** Four photos demonstrating the inverted vial tests for gel formation. A, B - Hydrogel B formed from 17PYY<sub>3-36</sub> at pH 8.88, C, D – Another hydrogel formed from 23PYY<sub>3-36</sub> at pH 6.09.

Once the singular gel formation had been observed a variety of different pH values were experimented with. The range of 4 – 8 was used, as previously stated (Chapter 3.2), because this is within the limits of injectable as well as consumable medication (i.e. pills and tablets). To make these studies more biologically relatable the pH values were kept within this boundary. A separation of 1 pH per gel was used to help provide a good range to observe any trends from the formation. Some gels were remade at specific pHs known to form gels, so multiple close values around one pH value can be seen. A full table of the formed gels can be seen in Table 5 below. From Table 5, it can be observed that gels were not made with pH values around pH 4 – 5.8, at which the solutions showed precipitation or cloudy solutions. pH 5.0 – 6 values are linked heavily to the pI observation in the previous chapter (Chapter 3.1 to 3.7), making the failure to form gels understandable with zero charge and precipitation.

The most critical observation was seen when trying to make a gel using the native PYY<sub>3-36</sub> peptide. All attempts at making a gel with the native, un-lipidated, peptide failed, this shows that the lipidation is of key importance for the potential for gel formation.

**Table 5:** Summary of lipidated PYY<sub>3-36</sub> samples that formed gels for given pH values. Error being  $\pm 0.01$ .

<b>11PYY<sub>3-36</sub></b>	<b>17PYY<sub>3-36</sub></b>	<b>23PYY<sub>3-36</sub></b>
8.47	3.80	3.19
8.76	7.35	6.09
	7.77	6.11
	8.67	6.56
	8.88	7.16
		8.57
<b>No gels formed from un-lipidated PYY<sub>3-36</sub>.</b>		

Suggested future work that would improve the confidence in the gel formation hypothesis would be to compare the three lipopeptide gels to a range of well-known standard gel forming chemicals. Suggested examples include cellulose, collagen, chitosan, or synthetic poly(ethylene glycol), or poly(vinyl alcohol), all of which would add more information into what is causing the structural change and gel formation.

#### **4.3 Gel Concentration Determination using A280 nm.**

After confirming the conditions needed to form them, the next step in investigating these gels was to characterise their macro and internal structure. This experiment would help address how and why these gels form. As the gel formation is completed by dehydrating the sample it was not clear what the end concentration of the gels would be. Again, dehydration and gel formation could be highly varied so a range of concentrations would be useful to understand. For this, two simple methods were used, namely a weighing method and by the use of a Nanodrop spectrometer. The weighing method was extremely simple, by weighing the sample before and after dehydration an overall mass loss of water could be calculated and then a concentration determined. This method showed around a 1.7 wt% for the gels tested. The second methodology, explained in more detail in the Materials and Methodology Chapter 2.2.4, was the A280 nm peptide method used by the Nanodrop spectrometer. This A280 nm method uses the wavelength 280 nm to measure the aromatic amino acids in the peptide, explained further in Chapter 2.2.4. Fortunately, in PYY<sub>3-36</sub> and the lipopeptides, there are multiple tyrosine's that can be detected using this method (Chapter 2.2.4). With the absorbance value obtained this can be used to calculate the concentrations of the gels (Chapter 2.2.4 Eq. 10). A benefit of using the Nanodrop spectrometer is that it requires around 2  $\mu$ L of sample so that the formed gel could be used for further experiments (Chapter 2.2.4 Fig. 15).

The weighing method showed a concentration of 1.7 wt%, showing a loss of around 80  $\mu\text{L}$  of water by dehydration. The Nanodrop experiment produced a range of concentrations from 1.6 wt% to 2.4 wt%. This range is rather large (0.8 wt%) confirming what was mentioned earlier that this dehydration method produces a variety of concentrations, but is shown to be around 2 wt%.

#### 4.4 Transmission Electron Microscopy to Visualise Hydrogel Structure

With the concentration investigated an examination of the internal structure of the gel is now needed. Transmission Electron Microscopy (TEM) is a powerful microscopy technique used to probe thin layers of material for structure. This method, explained in greater detail in the Methodology Chapter 2.2.1, and is capable of visualising self-assembled structures.<sup>156, 186, 297, 334, 465-466</sup> Two methods were used for preparation for the gels, the first spin coating on silicon nitride membrane grids (Chapter 2.2.1 Fig 9 D and E): the other breaking the gel up and using a standard TEM preparation method (Chapter 2.2.1), but with a higher viscosity sample.

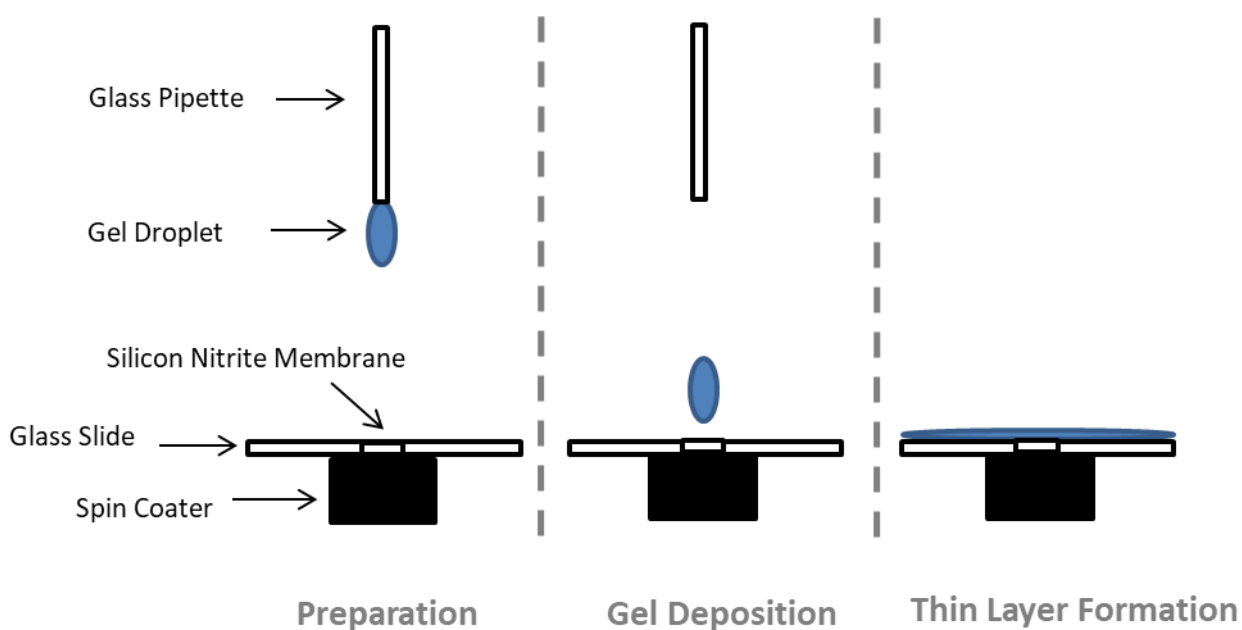


**Figure 29:** Overall diagram showing the method of thin layer gel formation, showing the preparation (left), deposition (middle) and layer (right) formation.

The spin coating method requires dropping a droplet of the gel from a height onto a rotating silicon nitride membrane on a glass slide (as seen in Figure 29). These grids were then allowed to dry and be stained, if needed, using uranyl acetate, which is a heavy metal staining agent used to create a higher contrast.

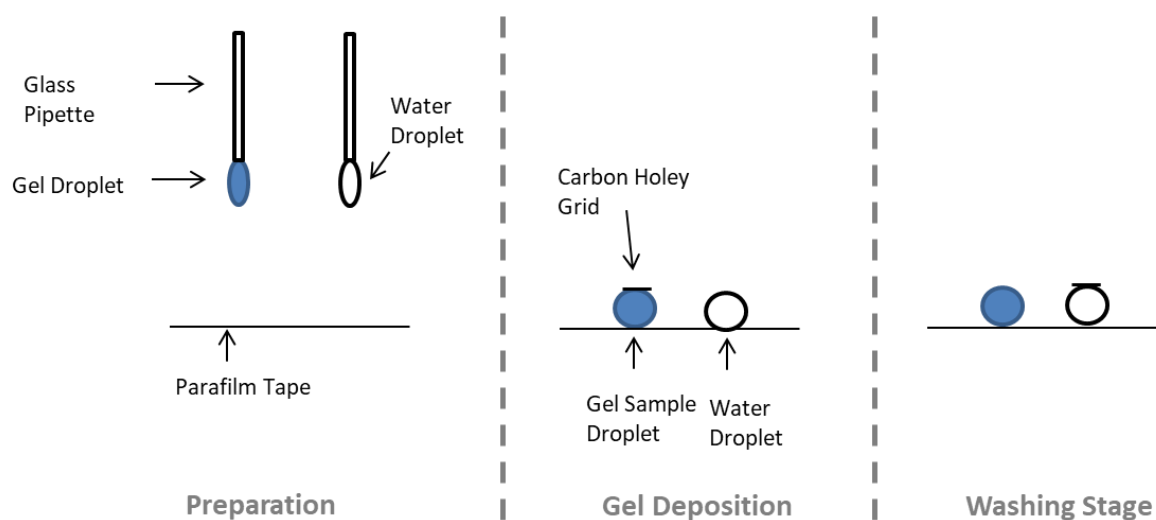
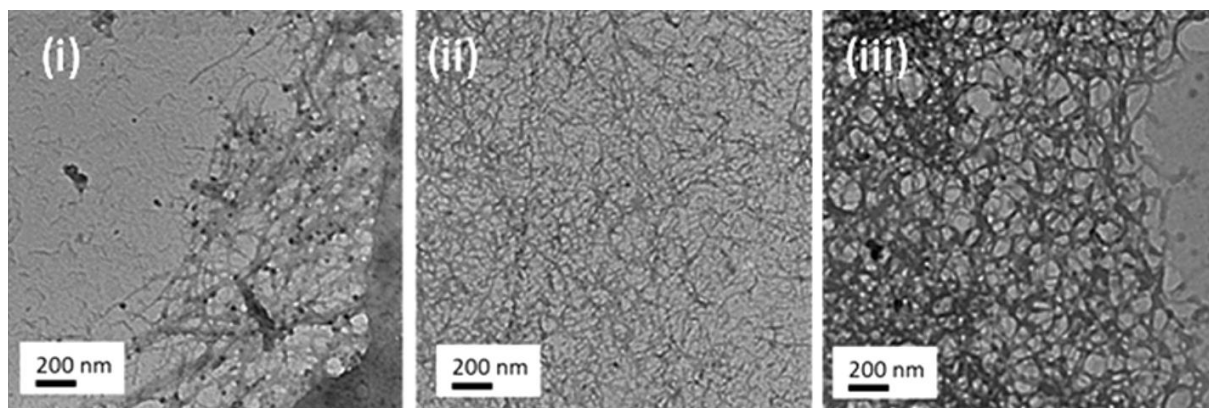


**Figure 30:** Drop coating method used for gel TEM. Left – Preparation stage by dispensing a gel and water droplet onto a parafilm tape, center – deposition stage that was transferring some of the hydrogel onto the holey grid by surface contact, and finally right – the washing stage with the gel covered TEM grid in surface contact with the water droplet. This was used to remove excess hydrogel from the grid, reducing the thickness of the gel, thus not limiting the scattering of electrons (as mentioned within Chapter 2.2.1).

For the second methodology, small amounts of the gel were transferred out of their vials and placed onto para-film tape with a droplet of ultrapure water (Figure 30). A carbon holey grid (Chapter 2.2.1 Fig. 9 B), the physical vehicle for the TEM, was placed on top of the droplet for 1 minute to allow for gel deposition onto the grid. This grid was then taken and placed on top of the water droplet for 30 seconds to allow for a washing step. This step is mainly used during staining as well to remove any unused uranyl acetate. In this case the washing step is used because gels can deposit heavily onto the grid and the structures cannot be seen. Washing reduces this effect, allowing for easier TEM visualisation. This is also the reason the gels were not stained as the uranyl acetate increases the contrast between the structure and the background but now, with a heavily concentrated gel structure, the structure is harder to interpret. Unless otherwise stated all further TEM photos are not stained. After each methodology, spin or drop, the sample is dried for a few minutes and then placed into the TEM for imaging.

Transmission Electron Microscopy allows for the visualisation of the structure of the gels, but only if the constraints of concentration, thickness, water content, contrast and stability are met. In this case 11, 17 and 23PYY<sub>3-36</sub> were all prepared for TEM in a way that produced the best visualisations. The pH of the TEM samples was also kept to around pH 8 as all lipidated PYY<sub>3-</sub>

36 versions readily produced gels at this pH. Other pH values were investigated such as pH 7 and 3. These all showed the same structure seen at pH 8.



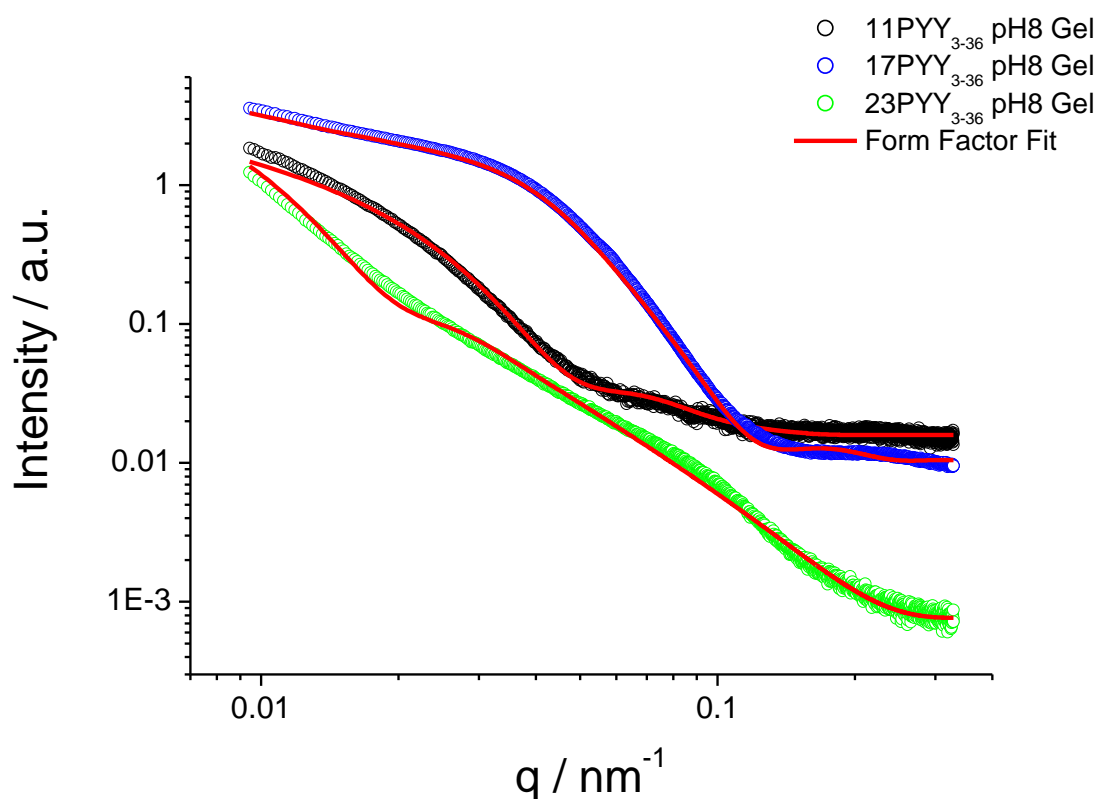
**Figure 31:** Three TEM Images showing highly elongated and entwined fibres from different lipopeptides hydrogels at pH 8. i) 11PYY<sub>3-36</sub> ii) 17PYY<sub>3-36</sub> iii) 23PYY<sub>3-36</sub>. Figure taken from paper referenced at the beginning of the chapter, and in the publication chapter, paper numbered 4.<sup>305</sup>

Figure 31 shows that all the pH 8 gels, for all the lipopeptides (11, 17 and 23), produced thin, roughly 10-20 nm, fibre like structures. These are extremely structurally similar to that of the pre-gel samples of the lipopeptides (17PYY<sub>3-36</sub> fibres seen in Chapter 3.2 Figure 21), though larger in diameter. The lipopeptides remain very entangled and elongated. The TEM images do not show any intermolecular structure such as repeating sheets or crystal-like structures. As mentioned earlier these grids were not stained so the contrast shown here is produced from the molecules and the structures themselves. Although cryo-TEM/TEM results are more visual and easier to be interpreted than other scientific methods, it is suggested that two comparison molecules were investigated to provide additional experimental insight into the fibres seen (Figure 31). Large fibrous hydrogel Gelatine, and the extended fibres of Cellulose, would be the two comparison molecules that would be suggested for this use.

## 4.5 Small Angle X-Ray Scattering Investigation into Hydrogel Fibres

To assign more parameters to these fibres, Small Angle X-ray Scattering (SAXS) was completed. SAXS, as previously mentioned in Chapter 3.3 before and in the Methodology Chapter 2.2.2, allows for assigning structures as well understanding their parameters based on their sample scattering patterns.

As the samples for the SAXS analysis were gels, the regular high-throughput system was not used as this normally requires low viscosity samples that can be drawn up via needle under pressure. Further information on this technique can be found within Chapter 2.2.2 and as mentioned there, a specific “Gel Cell”, designed by Charlotte Edwards-Gayle, was used for these samples of gels (see further details in methodology Chapter 2.2.2).



**Figure 32:** Small Angle X-Ray Scattering comparison graph showing at pH 8 gels of 11, 17 and 23PYY<sub>3-36</sub>. All fitted with a long cylindrical shell model (Chapter 2.2.2 Eq 2).

It was interesting to observe that all three gels showed different structures even with the TEM images showing similar structures of long entangled fibres and with their pre-gel samples showing a similar SAXS pattern (Chapter 3.3 Figure 23). The red lines in the graph above indicate the separate form factor fits that were applied to each of the gel scattering patterns. The applied fits show a close relationship to their scattering patterns, having a residuum chi square of 0.8 – 0.9 (Chapter 2.2.2 Eq. 6). A long cylindrical shell model was used for all three gel fits. The cylindrical shell model was primarily used because the TEM showed fibres and

the models allow for a variety of inner radii and shell thicknesses, which can be viewed in the Table 6. In comparison with hydrogel structures already found in scientific literature, this entangled fibre or long cylinder shell structure is found to be extremely common amongst different hydrogelator compounds.<sup>23, 387, 396, 453</sup>

**Table 6:** Summary of all three long cylindrical shell models (Chapter 2.2.2 Eq. 2) with fitting parameters resulting from the 11, 17 and 23PYY<sub>3-36</sub> hydrogels SAXS patterns.

<b>Parameters</b>	<b>11PYY<sub>3-36</sub> pH 8.5</b> <b>2 wt%</b>	<b>17PYY<sub>3-36</sub> pH 8.2</b> <b>2 wt%</b>	<b>23PYY<sub>3-36</sub> pH 7.2</b> <b>2 wt%</b>
<b>Background</b>	0.00158	0.0102	$8.26 \cdot 10^{-6}$
<b>N / arb. units</b>	$5.37 \cdot 10^{-9}$	$1.01 \cdot 10^{-5}$	$1.447 \cdot 10^{-7}$
<b><math>\sigma</math> / nm</b>	12.96	23.12	14.75
<b>R / nm</b>	22.59	30.01	55.21
<b>DR / nm</b>	28.05	48.55	6.55
<b>L / nm</b>	5000	1000	5000
<b><math>p_{\text{core}}</math> / nm</b>	$-3.677 \cdot 10^{-5}$	$2.70 \cdot 10^{-4}$	$1.098 \cdot 10^{-3}$
<b><math>p_{\text{shell}}</math> / nm</b>	$-5.49 \cdot 10^{-4}$	$-6.91 \cdot 10^{-5}$	$3.57 \cdot 10^{-3}$
<b><math>p_{\text{solv}}</math> / nm</b>	$2.00 \cdot 10^{-4}$	0.00	$5.90 \cdot 10^{-4}$

BG = Background, N = Scaling Factor,  $\sigma$  = Gaussian Width, R = Inner Radius, DR = Shell Thickness, L = Length of Cylinder,  $p_{\text{core}}$  = electron density of core,  $p_{\text{shell}}$  = electron density of shell and  $p_{\text{solv}}$  = electron density of the solvent. L was constrained to 5000 for 11/23, and 1000 for 17, to simulate elongated fibres.

The SAXS fitting parameters show that, although they all have the same structural design, the internal structure of the fibres differs. 23PYY<sub>3-36</sub> seems to show the greatest change with the inner radius being almost twice the size of the other lipidated peptides, from 22.59/30.01 nm to 55.21 nm. 23PYY<sub>3-36</sub> also has a much smaller shell thickness with 6.55 nm compared to 28.05/48.55 nm for 11 and 17PYY<sub>3-36</sub>. These large radii are seen in the TEM images that seem to show smaller fibres of 10-20 nm in radius, however this could be an issue related to the drying effect of the TEM. The fibres seen in the TEM maybe be “solvent removed” due to the high vacuum levels used, whereas the SAXS results are showing fibres that remain solvent swelled, which would explain the larger radii observed. The changes in structure, with differences in location of lipidation on the peptide, is clear within Table 6. Each of these model fits show differences that were not noticeable in the TEM images. It was also good to confirm the hydrated radius of the gels as TEM does suffer from the dehydration of the sample, thus potentially changing the sample’s structure.

The internal structure of these fibres was investigated by Circular Dichroism (CD). Combined with the previous solution studies this technique can give a good insight into the internal structure of the fibres. As all gels are formed via the same process, all methodologies can be compared, however there is a natural variability in gel concentrations that will need to be considered before a final comparison between the methodologies is made.

#### 4.6 Secondary Structure Investigation of Fibres using Circular Dichroism

Circular Dichroism has been mentioned before in the Methodology Chapter 2.2.3 as well as the Chapter 3.4 about PYY<sub>3-36</sub>. The method of sample preparation was similar to that of the solutions but instead of a small quantity of solution (20  $\mu$ L), a small quantity of gel was removed and pressed between the two plates (Chapter 2.2.3). The plates were then placed into the sample chamber as normal.

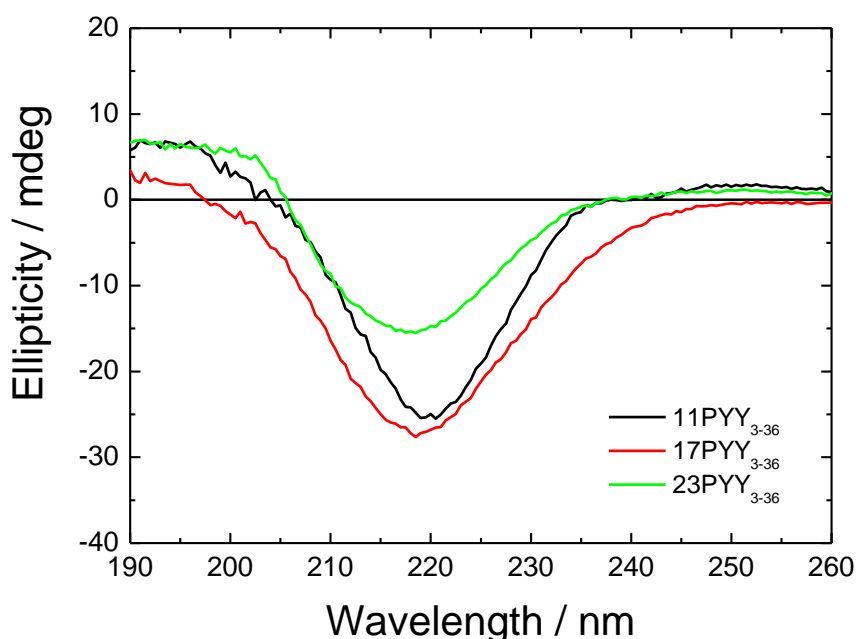


**Figure 33:** CD Spectra for 11, 17 and 23PYY<sub>3-36</sub> hydrogels at pH 8. All hydrogels show varied amounts of  $\beta$ -sheet secondary structure (with minima around 220 nm) with 17PYY<sub>3-36</sub> having the highest content, and 23 having the lowest.

CD showed  $\beta$ -sheet structure with a minimum ellipticity appearing at around 220 nm, characteristic for this secondary structure.<sup>180</sup> This secondary structure is like the  $\beta$ -sheet structure seen for the solutions (17 PYY<sub>3-36</sub> shown previously in Chapter 3.4 Figure 26 B) when heated and the pH changed. This secondary structure change, from  $\alpha$ -helical to  $\beta$ -sheet, does seem to be indicative of gel formation as none of the gels that were tested showed an  $\alpha$ -helical structure. Gels from  $\alpha$ -helical peptides have however been evidenced in scientific literature.<sup>408,</sup>

<sup>467</sup> 11PYY<sub>3-36</sub> and 17PYY<sub>3-36</sub> showed higher  $\beta$ -sheet concentration compared to that of

23PYY<sub>3-36</sub>. This can be compared to what was seen in the SAXS. SAXS showed a larger but thinner cylindrical shell model that seems to be formed from a less structured secondary environment, as informed by CD. As mentioned earlier, a more detailed analysis is needed of these gels to really probe the differences between them, but as CD shows around a 50% decrease in  $\beta$ -sheet secondary structure between 11, 17 and 23PYY<sub>3-36</sub> this indicates a large structural difference. This change could be due to a concentration difference between samples, but as this decrease is as much as 50%, some of this could be due to concentration variance, though this is a rather large decrease to be solely related to concentration alone.

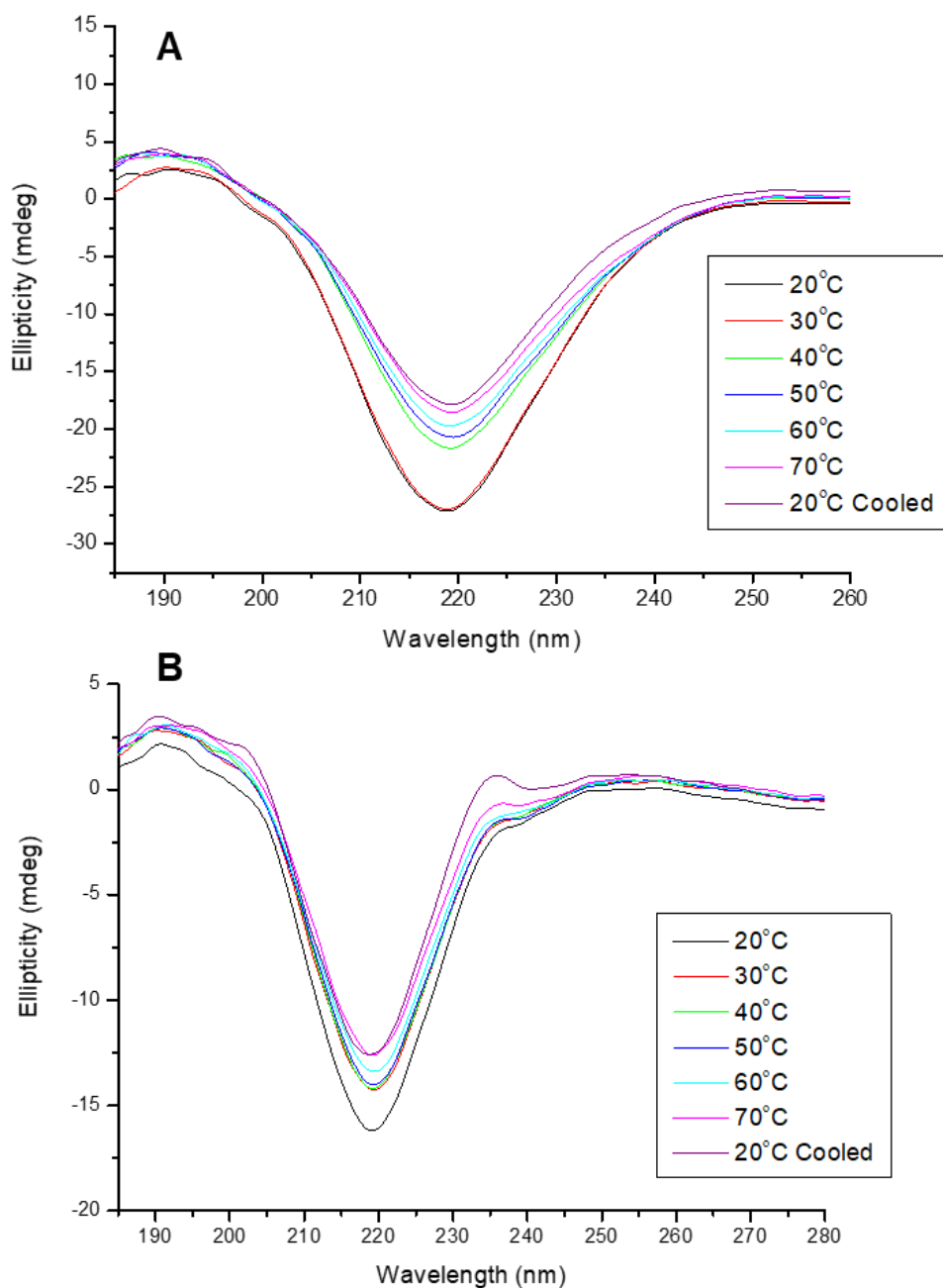


**Figure 34:** Temperature CD studies on the 17PYY<sub>3-36</sub> pH 8 gel (A) and on the 23PYY<sub>3-36</sub> pH 8 gel (B) from 20-70 °C. Both show the visual loss of  $\beta$ -sheet secondary structure as temperature increases. This loss is then shown to be permanent with the 20 °C cooled measurement showing similar structure to the 70 °C measurement.

Further studies were completed to investigate the gel's stability to temperature. Previously, it has been shown (in Chapter 3.4) that even after cooling back to 20 °C the  $\beta$ -sheet structure of 17PYY<sub>3-36</sub> is still retained and does not revert. These gels were put through the same test with a temperature ramp from 20 to 70 °C with a cooling run after the sample had cooled back down.

This sheet formation trend can be seen again in the temperature CD studies of two of the gels. 17PYY<sub>3-36</sub> shows a loss of structure but only after the jump to 40 °C. After this temperature jump the loss is consistent up to 70 °C. This shows that the secondary structure is weak to temperature and once the structure is removed it is not reversible. Similar effects can be seen with temperature increases for the 23PYY<sub>3-36</sub> gel with a loss of  $\beta$ -sheet structure with an increase in temperature up to 70 °C yet with no secondary structure reforming after cooling.

It should be noted that all gel CD spectra have been reported in Ellipticity (mdeg) and, although a concentration between 1.1 – 2.1 wt% was calculated, a precise concentration of each of these gels is not possible to determine as the concentration varied by  $\pm 0.4$  wt% from gel sample to gel sample made. Furthermore, molar ellipticity requires a reliable concentration to be able to compare spectra (Chapter 2.2.3 Eq. 9). This would mean that a gel made with the same lipopeptide, at the same pH, and starting concentration could produce different final gel concentrations. As multiple gels were made to run these experiments, the concentration values cannot be transferred between all the experiments but can provide a rough concentration range.

A gel sample of 11PYY<sub>3-36</sub> was also studied by temperature range using CD by another PhD student within the group, Jessica Hutchinson. The experiment however did not set out to understand 11PYY<sub>3-36</sub>'s stability to temperature but to understand the gel's formation. It was known that the  $\beta$ -sheet structure formation is incredibly important and that the samples would not form gels of  $\alpha$ -helical structures, as seen in the native peptide with other pH values failing to gel. This experiment was to show that these two events,  $\beta$ -sheet formation and gelation happens coherently. As seen in paper 4 (referenced at the beginning of this chapter), gel formation was related to the increase in  $\beta$ -sheet formation and a loss of  $\alpha$ -helical structure<sup>305</sup> after a pH change and as CD was taken at 5 °C steps of increase in temperature.

#### **4.7 11, 17 and 23PYY<sub>3-36</sub> Gel Conclusions**

In conclusion, the novel lipopeptides 11PYY<sub>3-36</sub>, 17PYY<sub>3-36</sub> and 23PYY<sub>3-36</sub> can form gels by simple dehydration at different pH values, expect at that of their pIs. It has been shown that without lipidation PYY<sub>3-36</sub> does not form gels at any pH value. This shows clear evidence that the lipidation has enabled the formation of gels, although lipidation did result in a decrease of the overall secondary structure (Chapter 3.4).

The gels analysed have been characterised through a multitude of experiments, including TEM, SAXS, CD and Fluorescence. It was shown that these gels have an average concentration of

1.7 wt% with a variance of  $\pm 0.4$  wt%. Their overall network was seen by TEM to be large, with entangled networks of long fibre like structures and with a variety of radii from 20 to 50 nm, similar to, but much larger than, those seen for their solution counterparts.

An investigation into these fibres enabled the fibres to be defined, using SAXS, to give radii and radius thicknesses, combined with circular dichroism spectroscopy to show a  $\beta$ -sheet secondary structure. These gels were also tested for temperature stability that showed a loss of structure upon heating that was not regained upon cooling. It was also shown that this transition from  $\alpha$ -helical to  $\beta$ -sheet is the driving factor for the gel formation, as no gels were formed under the same conditions with  $\alpha$ -helical secondary structure fibres. Further support for this observation is that the gel transition occurred at the same transition point for  $\beta$ -sheet formation.

As lipidation is a common method for elongating a drug's half-life and helps in reducing degradation pathways in the body, this analysis will add valuable information to the research field of lipidation and gel formation. If these findings are applied to other peptide and non-peptide drugs the potential for the application of lipidation could make for an extremely important area for further investigation. It would also be of interest to the gel research field as the formation of a gel using only the drug component could be highly valuable in saving research costs, excipients and allow for simpler, bio-friendly and longer lasting gel delivery systems.

## 5. 17PYY<sub>3-36</sub>, PYY<sub>3-36</sub> and A9R interactions with Lipopolysaccharide

### 5.1 Introduction to A9R and LPS

Peptide self-assembly has been an ever-growing, mainly academically focused, field that is now gaining interest in their use in biomedical applications through drug treatment, delivery, and formulation.<sup>152, 468-471</sup> Many parameters can affect the process of assembly, stability, and structure of the self-assembled system. These include temperature; pH, ionic strengths, concentration, and excipients.<sup>307, 472-474</sup> Peptide YY<sub>3-36</sub> (PYY<sub>3-36</sub>) (as mentioned in the previous Chapter 1.13 and 3.1) is a 36 amino-acid peptide hormone produced from the cleavage of another stomach hormone Peptide YY (PYY) by the enzyme DDP4.<sup>475</sup>

Lipopolysaccharide (LPS) is a large amphiphilic molecule originating from the outer membrane of bacteria, also known as an endotoxin.<sup>476</sup> LPS is formed of two sections, polysaccharide and lipid. The polysaccharide section has three parts, O antigen, outer and inner cores. Bacteria use LPS to support the cell membrane and to protect against attack from foreign bodies. For this reason, LPS's exhibit strong immune responses in animals as they are found on various disease-causing bacteria. The human immune system uses LPS as a detector molecule.<sup>477</sup> Similar to PYY<sub>3-36</sub>, LPS has also been studied extensively with a focus on structure and biological activity.<sup>478-495</sup> Current studies focus heavily on bioactivity, with many studying inhibitor effects, such as cationic peptides, or cationic metals.<sup>254, 486, 496-502</sup> Only a few studies include self-assembly or co-assembly of LPS with other peptides or lipopeptides.<sup>482, 497, 503-504</sup>

Papers and reviews have commented on the potential for positively charged peptides to be used as an antibacterial target or for complexation with LPS.<sup>94, 195, 230</sup> A9R is a nine alanine amino acids then one arginine in a positively charged peptide that has also been shown to have antibacterial properties (Figure 39).<sup>505</sup> As A9R potentially interacts with the bacterial cell wall it makes for an useful comparison molecule for LPS complexation and as such will help give further information on complexation experiments with PYY<sub>3-36</sub> and 17PYY<sub>3-36</sub>.<sup>505</sup> This LPS complexation is of interest to drug companies as this effect can cause a reduced activity of a drug molecule or can cause issues with side interactions with bacteria.<sup>486</sup>

## 5.2 17PYY<sub>3-36</sub> complexation to LPS Cryo-TEM Observations

A preliminary test of a mixture of 1:1 weight ratio of 17PYY<sub>3-36</sub>: LPS was completed in tandem with other experiments (Chapters 3 and 4). This experiment was undertaken to visualise any useful observations occurring from the complexation. After simply mixing the two compounds it formed a white precipitate that would fall to the bottom of the sample tube after a few hours. Photos of the samples can be seen in Figure 35 with the change in turbidity clearly seen.



**Figure 35:** Visual turbidity from the mixing of LPS and 17PYY<sub>3-36</sub>. Left to right: 0.5 wt% LPS, mix 0.5:0.5 wt% LPS:17PYY<sub>3-36</sub> and 0.5 wt% 17PYY<sub>3-36</sub>. All samples and mix in water, at room temperature, and pH unchanged.

This result caused an interest in what was being formed, as these lipidated peptides are novel and any potential co-assembly would be useful to characterise. For the precipitate to be visualised the samples were sent off for Cryo-TEM analysis with instructions to mix the sample vials before they were sampled. Through this approach it was hoped to “capture” the precipitate for visualisation. All three vials were visualised to allow for comparison between the separate molecules and the mixture.

Firstly the 0.5 wt% sample of 17PYY<sub>3-36</sub> can be seen in Figure 36 A. This showed the same type of structure similar to that seen in the previous Chapters 3.2 and 4.4. The fibre nature can be seen to be thin radius, elongated and entangled with length greater than 1000 nm.

Previous LPS studies have shown the self-assembled structure to be short fibre like assemblies. These structures can be seen in Figure 36 B showing similar properties to those shown previously in scientific literature.<sup>501, 506</sup> Another interesting observation from this experiment is the seemingly regular spacing between the fibre like structures. This is starkly different to that of 17PYY<sub>3-36</sub>, which shows a tangled fibre like nature.

As the LPS used for this thesis has an inherently high variance in molecular weight, caused by it being manufactured using bacteria and its purification by phenol extraction, it is not possible to provide a precise view on the actual molecular weight of the LPS used. However, by using the typical average molecular weight of 1,000,000 g/mol (1000 kilodaltons) for LPS, this would produce a molarity of 5  $\mu$ mol for the LPS in this experiment. As the molecular weight of the

17PYY<sub>3-36</sub> and PYY<sub>3-36</sub> used in this experiment is 4047.07 and 4387.32 g/mol, the molarity will be 1.235 and 1.140 mmol, respectively. As can be seen there are, in broad terms, 250 times as many peptide/lipopeptide molecules than LPS molecules in the mixtures. As proposed later in this chapter, 17PYY<sub>3-36</sub> and PYY<sub>3-36</sub> are physically interacting with LPS via co-assembly (FIGURE 36 and 37). With the difference in the estimated molarities, this is likely to mean that the peptide/lipopeptide is in higher concentration, and thus has a higher impact on the co-assembly process. However, it is worth remembering that as self-assembly and aggregation does not necessarily require a 1:1 bonding of the components, the calculation of a ratio of molecules can only, at best, be an estimate.

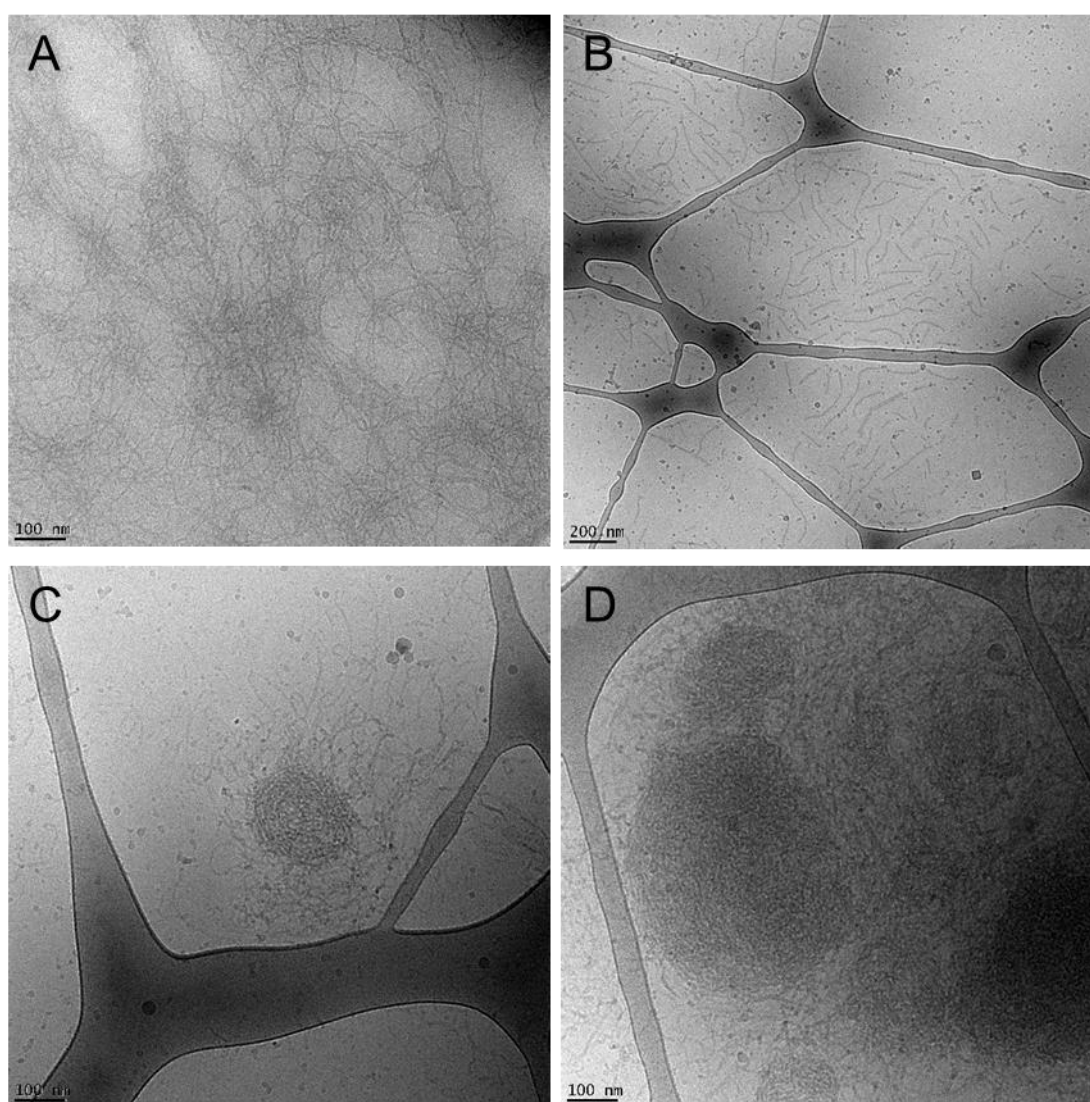


**Figure 36:** Cryo-TEM images showing the odd co-assembly of 17PYY<sub>3-36</sub> and the bacteria endotoxin LPS. A – The first comparison image showing 0.5 wt% 17PYY<sub>3-36</sub> in H<sub>2</sub>O scaled at 100 nm to visualise the thin elongated fibres, structure similar to that seen previously in Chapters 3 and 4. B – The second comparison image of 0.5 wt% LPS in H<sub>2</sub>O, with the short fibre like structure, and with regular spacing between. C, D – The various sized large aggregates

of the mixture 0.5:0.5 wt% (250:1 estimated molarity) 17PYY<sub>3-36</sub>: LPS in H<sub>2</sub>O, C showing a smaller one, and D larger ones, both at 100 nm scale.

The mixture of these two compounds showed a similar fibular nature but rather than being short and regularly spaced, such as LPS (Figure 36 B), or entangled and lengthy such as 17PYY<sub>3-36</sub> (Figure 36 A), Figures 35 C and D show “circular” aggregates of fibres. These aggregates are of different sizes, from 400 – 100 nm diameters, but regardless of size, they all seem to show the same type of aggregation. It is unclear what the underlying effects of these aggregations are. Although what is noticeably clear is that there is an interaction between the two molecules. Studies about the aggregation of peptides, specifically AMPs, with LPS, have not reached a consensus on why some peptides promote aggregation and others negate LPS aggregation.<sup>486, 507-512</sup>

### 5.3 SAXS Investigation of 17PYY<sub>3-36</sub>/LPS Aggregation Structures

To investigate these aggregates, small samples were taken for SAXS measurements. SAXS, as mentioned previously, can obtain more precise parameters for the structures formed. The first thing that can be noticed from the scattering patterns of the samples (Figure 37) is that each showed different structures are being formed.

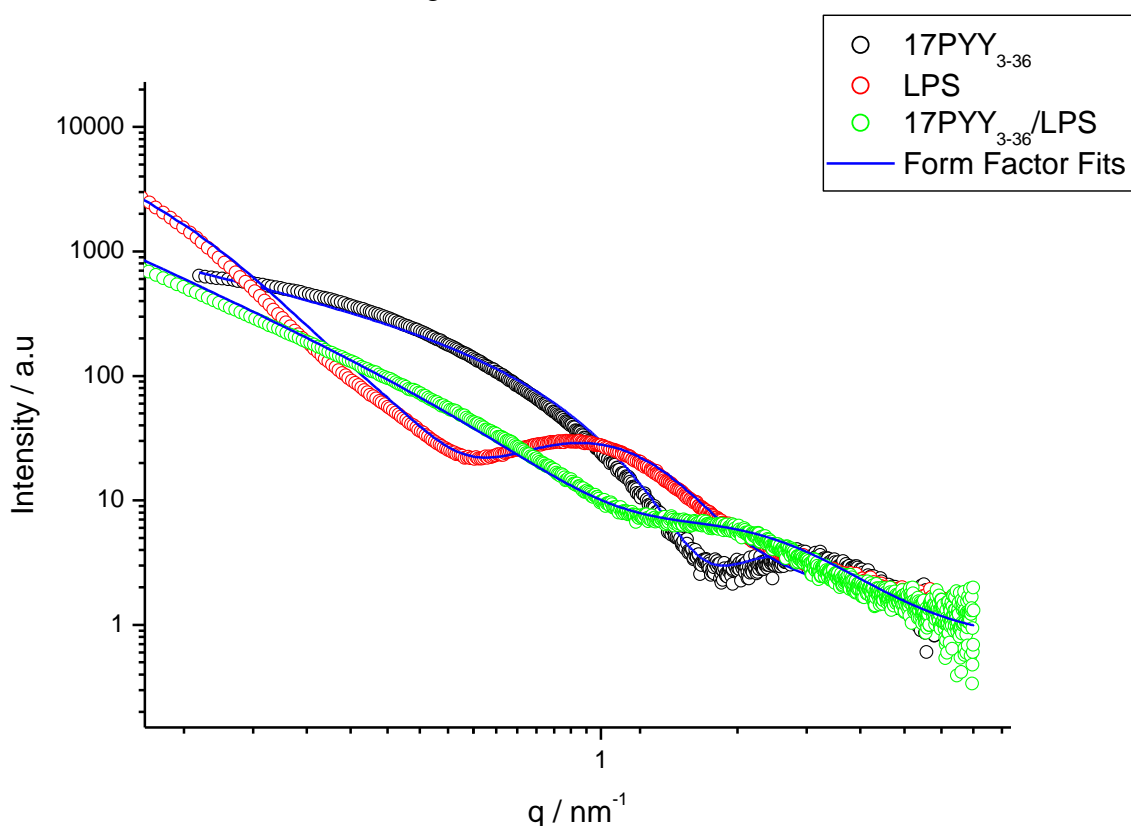


**Figure 37:** Comparison spectrum of SAXS patterns for 17PYY<sub>3-36</sub>, fitted with a long cylindrical shell (2.2.2 Eq. 2), LPS, fitted with a bilayer and long cylindrical model (2.2.2 Eq 2 and 5 and

1:1 wt% (250:1 estimated molarity ratio) mixture, which was fitted with a bilayer model (2.2.2 Eq 5). All samples are 0.5 wt% with H<sub>2</sub>O as the solvent.

17PYY<sub>3-36</sub> has been fitted to a long cylindrical shell model, as seen in Figure 23 of the previous Chapter 3.3. Lipopolysaccharide showed a different scattering pattern, with a peak at around 1 nm<sup>-1</sup> compared to that of 17PYY<sub>3-36</sub> (1.4 nm<sup>-1</sup>). A form factor of bilayer gaussian (2.2.2 Eq. 5) combined with a long cylindrical shell model (2.2.2 Eq. 2) showed to fit the experimental scattering pattern for LPS. The parameters for this fitting are shown in the Table 7. The mixture of LPS and 17PYY<sub>3-36</sub> showed a further different scattering pattern, indicating the formation of a different structure. This finding adds information to academic research and helps confirm the co-assembly of LPS and 17PYY<sub>3-36</sub>. A bilayer gaussian form factor was used to fit the SAXS pattern of the 1:1 wt% ratio 17PYY<sub>3-36</sub> and LPS mixture (250:1 estimate molarity ratio) as can be seen in Figure 37. This result also showed a good correlation to the data of 0.8 – 0.9 chi square residuum fit. This gaussian bilayer form factor is similar to that used for LPS but showed some differences in parameters, particularly in the bilayer thickness (around 0.5 nm for the mixture, and LPS is around 1.2 nm using cylinder inner radius and shell thickness).

**Table 7:** SAXS form factor fitting parameters for LPS, 17PYY<sub>3-36</sub> and a 0.5:0.5 wt% (250:1 estimate molarity ratio) mixture. All samples are in H<sub>2</sub>O.

N - scaling factor.  $\sigma$  - gaussian width. R = radius of core, t = thickness of shell, L = length of cylinder, q = scattering vector,  $\rho_{core}$  = electron density of the core,  $\rho_{shell}$  = electron density of the shell,  $\rho_{solv}$  = electron density of the solvent.  $\sigma_{out}$  = scattering length of outer gaussians.

Sample	17PYY <sub>3-36</sub>	LPS	17PYY <sub>3-36</sub> + LPS (250:1 estimated molarity ratio)
	<b>Long Cylinder Shell Model</b>	<b>Gaussian Bilayer and Long Cylinder Shell Model</b>	<b>Gaussian Bilayer Model</b>
<b>N / arb. units</b>	0.294	0.000645	0.000551
<b><math>\sigma</math> / nm</b>	0.347	3.32	1.13
<b>Long Cylinder Shell Parameters</b>			
<b>R / nm</b>	1.45	1	
<b>DR / nm</b>	0.271	0.2	
<b>L / nm</b>	500	1000	
<b><math>\rho_{core}</math></b>	0.0567	0.023	
<b><math>\rho_{shell}</math></b>	0.165	-0.03	
<b><math>\rho_{solv}</math></b>	0.0354	0.002	
<b>Gaussian Bilayer Parameters</b>			
<b><math>\sigma_{out}</math></b>		0.455	0.282
<b><math>p_{out}</math></b>		0.0376	0.094
<b><math>\sigma_{core}</math></b>		0.342	0.590
<b><math>p_{core}</math></b>		-0.0154	-0.0328
<b>t / nm</b>		-0.03	0.50
<b>D / nm</b>		1000	1000

$p_{out}$  = electron density of the outer gaussians.  $\sigma_{core}$  = scattering length of inner gaussian,  $p_{core}$  = electron density of inner gaussians. t = bilayer thickness. D = diameter of disc (defines the unit cell).

Predictably, the form factors for the fitted SAXS data showed that three different structures formed. This was expected from the cryo-TEM images (Figure 36) as the incorporation of the LPS into the 17PYY<sub>3-36</sub> fibres would change the structure of the fibres. In this case it seems that the radius of the fibres is the major affected parameter.

All three form factors have had their length or the diameter of the disk constrained to that of 500 nm for 17PYY<sub>3-36</sub>, or 1000 nm for the LPS and mixture models. This is because they all show an elongated structure. Both the LPS and 17PYY<sub>3-36</sub> also show similar radii with 1 nm and 1.45 nm respectively. This can be seen to be reduced by looking at the bilayer thickness

value ( $t$ ) for the mixture which shows a value of 0.5 nm. The other values change as well, but what is clear to see is that these structures, aside from their length, have changed scattering densities ( $\sigma_{out}, \rho_{out}, \sigma_{core}, \rho_{core}$ ) as well as the width values of the self-assembled structures.

#### 5.4 Circular Dichroism Study of 17PYY<sub>3-36</sub> and LPS Aggregates

The previous Chapters 3 and 4 show that 17PYY<sub>3-36</sub> has a reduced  $\alpha$ -helical secondary structure compared to that of the unlipidated form (Figure 24).<sup>305</sup> Lipopolysaccharide has also been shown to form self-assembled structures (Figure 36 B). A simple mixing experiment, using a wt% ratio, allowed for the secondary structure of the un-mixed molecules to be further confirmed.

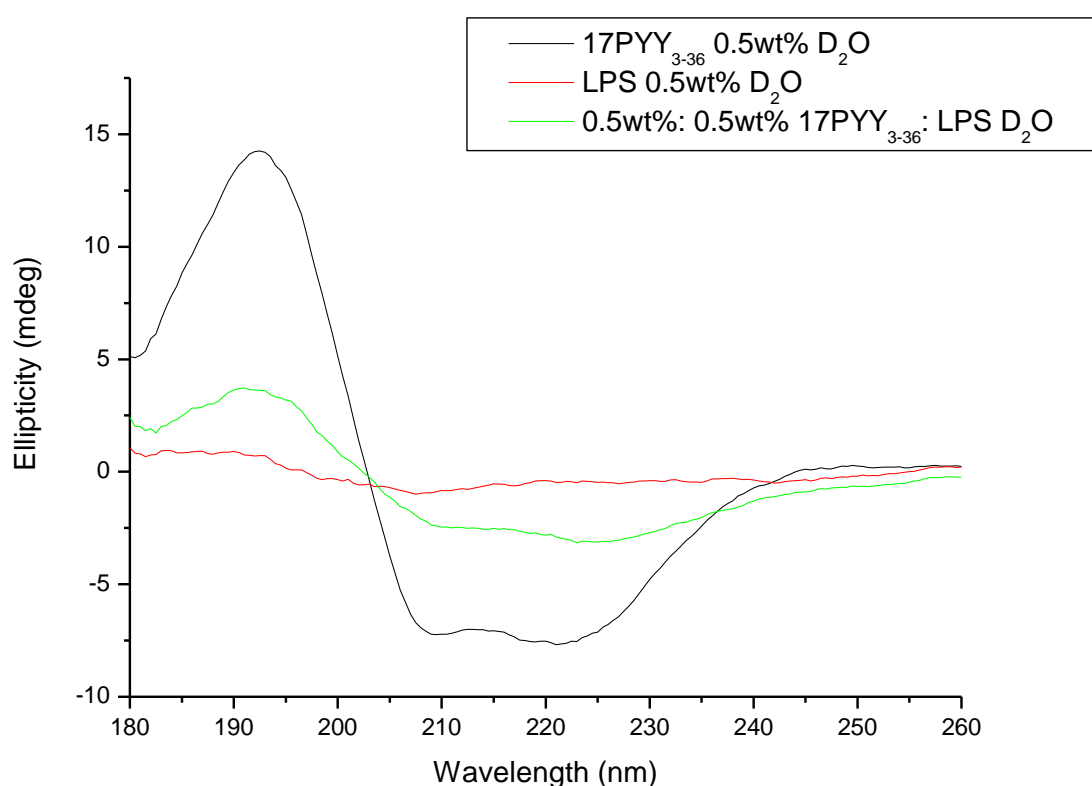


**Figure 38:** CD spectrum of 0.5 wt% 17PYY<sub>3-36</sub> (black), 0.5 wt% LPS (red), and a 1:1 wt% ratio (250:1 estimated molarity ratio) mixture of the two samples (green). All samples and mixtures were made in D<sub>2</sub>O. The mixture shows reduced  $\alpha$ -helical secondary content. LPS showed no secondary structure.

The CD spectra, see Figure 38, shows a further reduced  $\alpha$ -helical nature for the mixture. This was to be expected as an incorporation of a large molecule without secondary structure reduces the overall solution's ellipticity. Therefore, the reduced  $\alpha$ -helical secondary structure can be either caused by the presence of both self-assembled structures or through the incorporation of the LPS into the 17PYY<sub>3-36</sub> self-assembled structure, which would reduce its overall secondary structure, and in doing so reduce the recorded ellipticity. Unlike for 17PYY<sub>3-36</sub> at pH 6 this

reduction in  $\alpha$ -helical content was not caused by precipitation, as the solution became cloudy but did not settle out of solution, this effect can be seen in the Figure 35.

CD by itself would not have given a clear view of the reason behind the  $\alpha$ -helical reduction as the results could have occurred from the averaging out of two samples where no co-assembly had occurred. However, as it has been evidenced before by cryo-TEM (Figure 36), co-self-assembly has occurred. It can be deduced therefore that this reduction in  $\alpha$ -helical content is due to the incorporation of LPS into the fibres. The radius of the fibre, as measured by SAXS, has been seen to reduce to 0.5 nm compared to the original 1.5 nm. This compacting effect could be produced by LPS incorporation, along with the denaturing of the  $\alpha$ -helical content.

### 5.5 Further Investigations with PYY<sub>3-36</sub> and A9R Complexing to LPS

Even with these observations, which are seen from the fitting of the SAXS parameters and Cryo-TEM, a complexation effect cannot be fully confirmed. Small Angle X-Ray Scattering takes an average “shot” of the solution, so if, as seen in the Cryo-TEM, the observation could be an interaction between the two self-assembled structures and not a complexation for the two molecules into a distinctly different structure. This is a difficult theory to investigate as it requires specific molecules that show binding to LPS or PYY<sub>3-36</sub> that can also be quantified.

Further experiments with A9R were suggested to complement these studies for two reasons. Firstly, to experiment with the reason for complexation. A9R is a different molecule in terms of size (10 amino acids vs. 33) and charge and overall function (anti-bacterial vs. hormone). A9R is a 10 amino acid chain, with only one charged group, arginine. A9R has also been shown to have anti-bacterial properties and, given the presence of LPS on the cell wall of bacteria, the interaction between the two molecules would be of further interest to anti-bacterial drug research.<sup>505</sup>

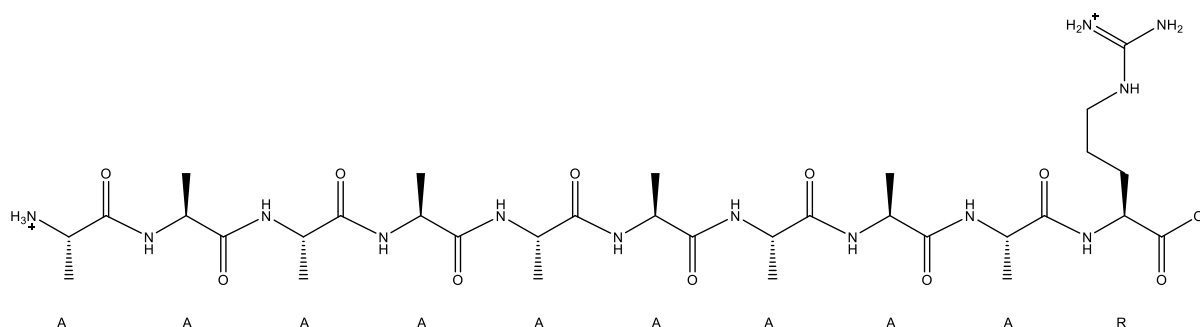


**Figure 39:** Chemical Structure of A9R. A9R is a known anti-bacterial peptide and readily self-assembles and forms gels.

120 mg of 17PYY<sub>3-36</sub> was originally supplied for the experimentation for this thesis; however, 17PYY<sub>3-36</sub> is expensive and as a result of budget constraints, no further supplies could be acquired. This meant that, after only a small number of experiments, further studies into the interactions between 17PYY<sub>3-36</sub> and LPS, and its complexations, had to be suspended. The potential work that could have been completed with further amounts of 17PYY<sub>3-36</sub> has been suggested for future work (Chapter 7.2).

The use of the available 17PYY<sub>3-36</sub> was however focussed on the aforementioned studies into the characterisation and gelation of 17PYY<sub>3-36</sub> that are contained within this thesis. In addition, a selection of LPS studies were completed using the available quantity of 17PYY<sub>3-36</sub>.

To enable to continuation of the LPS studies, native PYY<sub>3-36</sub> was used as a substitute for 17PYY<sub>3-36</sub>. The replacement with PYY<sub>3-36</sub> was chosen as it has a similar 34 amino acid peptide chain, similar charged and uncharged groups, size and secondary structure. This approach allowed for more information to be gathered on the observations seen to occur between 17PYY<sub>3-36</sub> and LPS in the Cryo-TEM.

To follow the molarity estimation from before, using A9R's mr of 814 gmol<sup>-1</sup>, for the following experiments LPS is still at 5 µmol, while A9R is 6.142 mmol. This means there is a ratio of around 1:1228 of LPS to A9R. As proposed earlier in this chapter, 17PYY<sub>3-36</sub> and PYY<sub>3-36</sub> are physically interacting with LPS via co-assembly (FIGURE 36 and 37). With the difference in the estimated molarities, this means that A9R is in a much higher concentration, and thus has a higher impact on the co-assembly process. Again however, it is worth remembering that as self-assembly and aggregation does not necessarily require a 1:1 molarity bonding of the components, the calculation of a ratio of molecules can only, at best, be an estimate.

## **5.6 Cryo-TEM Investigation of the interaction between A9R and LPS**

The first step in observing an interaction between the two molecules is to complete Cryo-TEM. This approach would allow for comparison to that of 17PYY<sub>3-36</sub> and LPS, which did show an interaction. Investigation into whether it is the lipid or the peptide that is responsible for the co-assembly effects seen in cryo-TEM, CD and SAXS would need to be undertaken. A9R has been studied before, by PhD student Charlotte Edwards-Gayle, and has been confirmed to have a fibular like structure.<sup>505</sup> The structure of LPS has also been seen to be fibular in nature, as seen in the previous Cryo-TEM images (Figure 36 B).

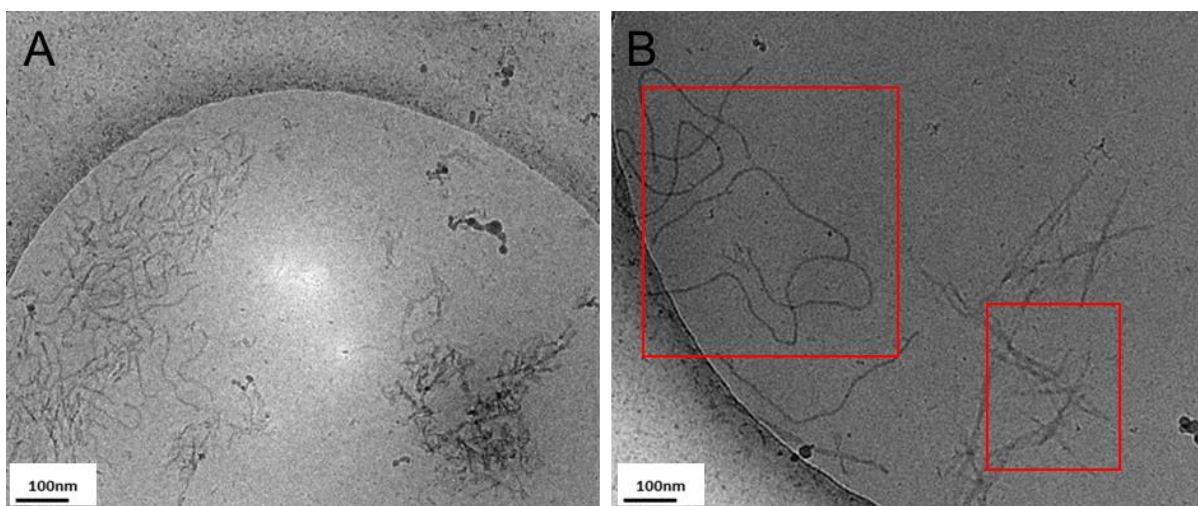


**Figure 40:** Cryo-TEM showing the formation of two distinct self-assembly structures of 0.5 wt% : 0.5 wt% (1228:1 estimated molarity ratio) A9R: LPS in H<sub>2</sub>O. Both A and B belonging to the same sample and are at the same magnification. Red squares on B are indicating the different structures formed, left fibres for LPS, and right being A9R fibres (similar to previous A9R structures seen<sup>505</sup>).

The first observation, in Figure 40, is that there are two visually different self-assembled structures formed within the same sample. The first structure is highly similar to that of LPS, seen previously as being fibre like, but these fibres are shown to be longer and not as dispersed as before (seen in Figure 36 B). The second self-assembled structure seen is that of short fibres “sharp or needle like” in nature.

These structures are similar to that seen in a paper to be published by the Professor Ian Hamley group on A9R with bacterial studies.<sup>505</sup> This separation between the two structures clearly shows no interaction when compared to that of 17PYY<sub>3-36</sub> and LPS. As cryo-TEM is limited in resolution the internal structure of these two fibres is unknown. This limitation of cryo-TEM means further experiments are required to probe the internal structure to determine if any self-assembly incorporation has occurred.

## 5.7 A9R with LPS, SAXS Investigation

As seen with other studies (Chapter 3 and 4), small angle X-ray scattering analysis has been carried out to probe the formed self-assembled structures (Chapter 3.3). As SAXS produces an average scattering pattern of a sample, it is not easy to accurately determine the individual structures contained within these mixtures of A9R and LPS. It is however known that A9R and LPS have formed separately, as seen in cryo-TEM Figure 40. This in turn means that any SAXS scattering patterns from the mixtures would only be the average view of both structures.

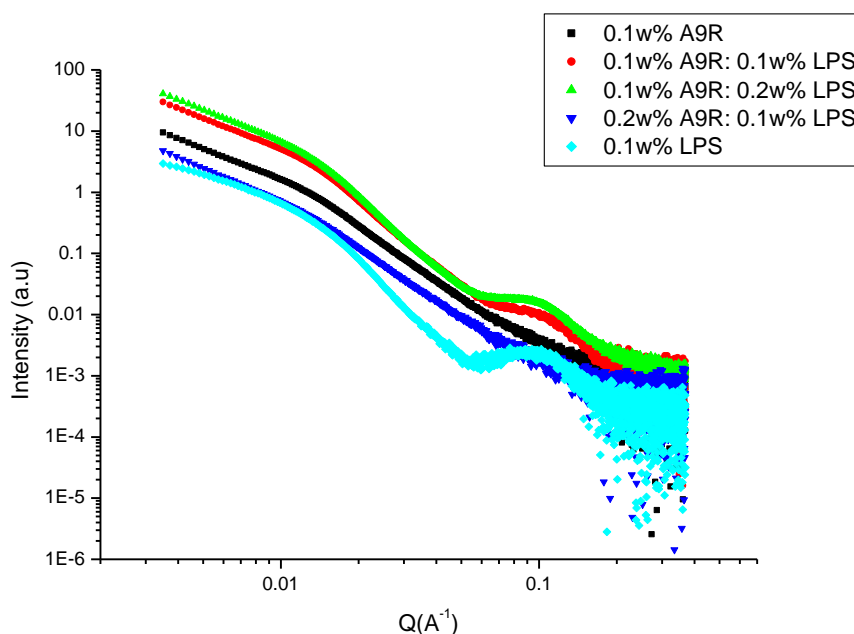


**Figure 41:** SAXS patterns for 0.1 wt% A9R, 0.1 wt% LPS and 0.1: 0.1 (1228:1 estimated molarity ratio), 0.2: 0.1 (2456:1 estimated molarity ratio), 0.1: 0.2 wt% (614:1 estimated molarity ratio) mixtures in H<sub>2</sub>O. All these samples were run on B21 at Diamond (Chapter 2.2.2). Samples and mixtures with LPS showed a peak for 0.1 A<sup>-1</sup> and very similar scattering patterns, A9R did not show this 0.1 A<sup>-1</sup> peak but showed similar patterns to each other.

This averaging effect seen in SAXS was confirmed by the spectra shown above in Figure 41. A 0.1 wt% sample of A9R showed a fibre type scattering pattern with little features within (black - Figure 41). This scattering pattern has been reported before, and was fitted to a long cylindrical shell model.<sup>513</sup> The 0.1 wt% LPS sample did show a similar pattern to previous experiments, which can be attributed to that of a fibre-like self-assembly structure (Figure 37). The concept of an average scattering pattern can be clearly seen in the mixtures used (red, green, and dark blue). The SAXS pattern for 0.1 wt%: 0.1 wt% (1228:1 estimated molarity ratio) A9R: LPS showed a small structural feature at 0.1 A<sup>-1</sup>. This feature is attributed to that of the 0.1 wt% LPS sample, which showed a similar profile (Figure 37). This feature can also be seen in the 0.1 wt%: 0.2 wt% A9R: LPS sample (614:1 estimated molarity ratio), showing similar scattering patterns between the 1228:1 and 614:1 estimated molarity samples (green

and dark blue). The  $0.1 \text{ A}^{-1}$  LPS structural feature was lost in the 0.2 wt%: 0.1 wt% (2456:1 estimated molarity ratio) A9R: LPS sample (dark blue). This shows a specific issue with SAXS where the average picture of the sample is taken and, even with a 2456:1 molarity ratio sample, the structures cannot be fully accessed, identified, or separated.

If we compare these A9R: LPS SAXS patterns to the difference seen in the mixing of just 250:1 (estimated molarity) of 17PYY<sub>3-36</sub> and LPS it is very clear that the structure's shape changed upon mixing (Figure 36), which was not seen with A9R and LPS (Figure 40). This was also confirmed by the cryo-TEM images of the 250:1 molarity mixture, with 17PYY<sub>3-36</sub> and LPS, showing a clear aggregation effect (Figure 35) while A9R and LPS show clear separation of self-assembly (Figure 39).

### **5.8 Circular Dichroism Study PYY<sub>3-36</sub> and A9R with LPS**

As PYY<sub>3-36</sub> and 17PYY<sub>3-36</sub> both contain an  $\alpha$ -helix segment, circular dichroism spectroscopy was used again to investigate the effect of potential LPS incorporation on this  $\alpha$ -helical section. A9R does form a  $\beta$ -sheet structure at high weight percentages, (1 wt% - to higher), which could be investigated by CD spectroscopy.<sup>505</sup> As the weight percentages under investigation were lower than this (0.5 wt%), the CD spectra for A9R incorporation with LPS showed minimal structure at low concentrations. For this reason, the A9R and LPS spectra will not be commented on as it did not add any valuable information to the investigation, besides from showing a loss in the minimal  $\beta$ -sheet structure seen. This is consistent with an averaging effect expected from the CD process.

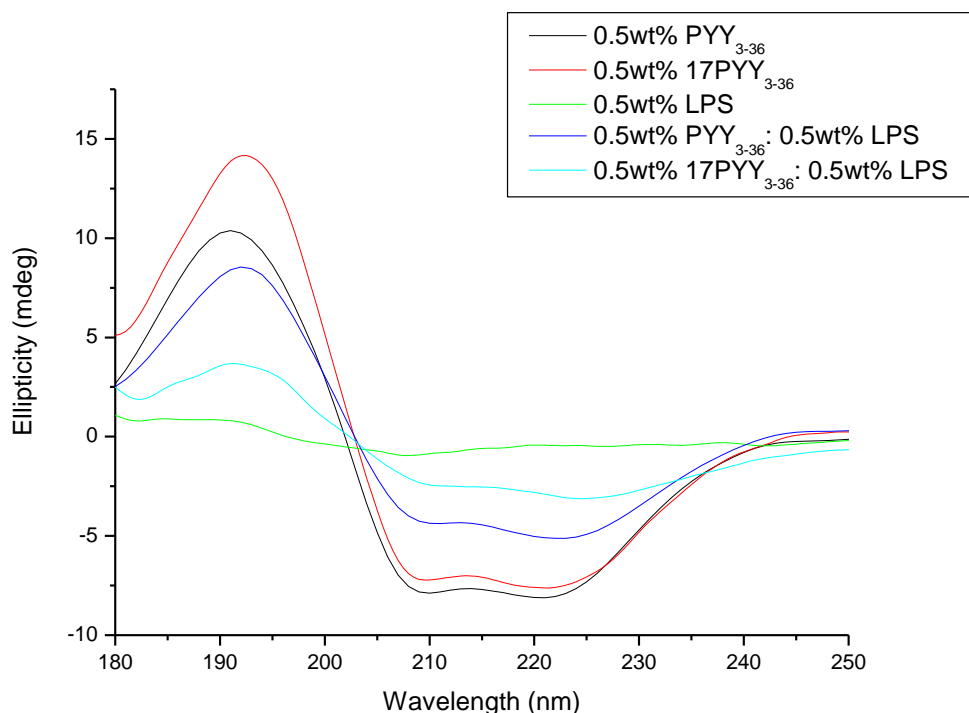


**Figure 42:** Comparison CD spectra of PYY<sub>3-36</sub>, 17PYY<sub>3-36</sub> and mixtures with LPS. All samples prepared in D<sub>2</sub>O, at room temperature, and ratios are in wt%. Both convert to around 250:1 in molarity ratios. Data smoothed using FTT smooth fit by 5 points, and kept in mdeg as mixtures can not be converted to molar ellipticity.

A study comparing PYY<sub>3-36</sub> with LPS and 17PYY<sub>3-36</sub> with LPS was completed to investigate the use of PYY<sub>3-36</sub> as a good replacement molecule for the studies, as seen in Figure 42.

A few observations can be gathered just from viewing this CD spectrum. Firstly, LPS shows little secondary structure that has been confirm in previous CD experiments (Figure 38). This means any changes in secondary structure can be attributed to that of either PYY<sub>3-36</sub> or 17PYY<sub>3-36</sub>.

Secondly, to highlight the actual changes in secondary structure and compare the two mixtures and their separate components, the ellipticities at key wavelengths have been noted. These values are specific to the  $\alpha$ -helical secondary structure of PYY<sub>3-36</sub> and have been used to compare the loss of structure upon LPS addition, which can be seen in Table 8 and 9 below.

**Table 8:** Ellipticities values at 190, 210 and 222 nm wavelength for CD spectrums of 0.5 wt% PYY<sub>3-36</sub>, 17PYY<sub>3-36</sub>, LPS and estimated 250:1 mixtures. All values are in mdeg, errors are the last number recorded ( $\pm 0.01$  mdeg).

Wavelength	PYY <sub>3-36</sub>	17PYY <sub>3-36</sub>	LPS	PYY <sub>3-36</sub> /LPS	17PYY <sub>3-36</sub> /LPS
190	10.25	13.26	0.84	8.06	3.57
210	-7.88	-7.22	-0.86	-4.37	-2.43
222	-8.05	-7.59	-0.45	-5.13	-2.99

**Table 9:** Difference in ellipticities values at 190, 210 and 222 nm wavelength for CD spectrums of PYY<sub>3-36</sub>, 17PYY<sub>3-36</sub>, LPS and estimated 250:1 mixture. All values are in mdeg, errors are the last number recorded ( $\pm 0.01$  mdeg).

Wavelength	PYY <sub>3-36</sub> to Mixture	17PYY <sub>3-36</sub> to Mixture
190	2.19	9.69
210	-3.51	-4.79
222	-2.92	-4.60

The wavelengths of 190, 210 and 222 nm have been chosen because both PYY<sub>3-36</sub> and 17PYY<sub>3-36</sub> have  $\alpha$ -helical structure, which will have reduced upon the addition of LPS and will not change to a different structure upon addition. This  $\alpha$ -helical structure has three key data points, a large positive maximum at around 190 nm and then two minima at around 210 and 222 nm. These three points can be clearly seen in Figure 42.

From Figure 42 and Table 9 above it can be seen that there is a much larger decrease in structure when LPS is added to that of 17PYY<sub>3-36</sub> over PYY<sub>3-36</sub>. This observation indicates that the lipid of 17PYY<sub>3-36</sub> is important to the potential binding or co-aggregation that was found within these samples.

Finally, although PYY<sub>3-36</sub> does not show to the fullest extent the reduction of the  $\alpha$ -helix compared to 17PYY<sub>3-36</sub>, it still shows a reduction. This has then confirmed PYY<sub>3-36</sub> as a reasonably good potential replacement molecule for further studies of this interaction.

## 5.9 A280 and A200 Absorbance Studies of PYY<sub>3-36</sub> and A9R with LPS

PYY<sub>3-36</sub> and 17PYY<sub>3-36</sub> both contain tyrosine amino acid groups that, as shown in Figure 19 in Chapter 3.1, can be used, thanks to their absorbance at 280 nm, to work out the concentration of a sample (Chapter 2.2.4). The environment of the tyrosine, as with pyrene, can be used to identify if the tyrosine is in a hydrophobic or hydrophilic environment. If a protein denatures, for example upon the addition of a certain metal ion, this can be shown as a decrease of absorbance at the 280 nm wavelength with the concentration of the protein being kept constant, indicating that the hydrophobic pocket has been lost, reducing the intensity.

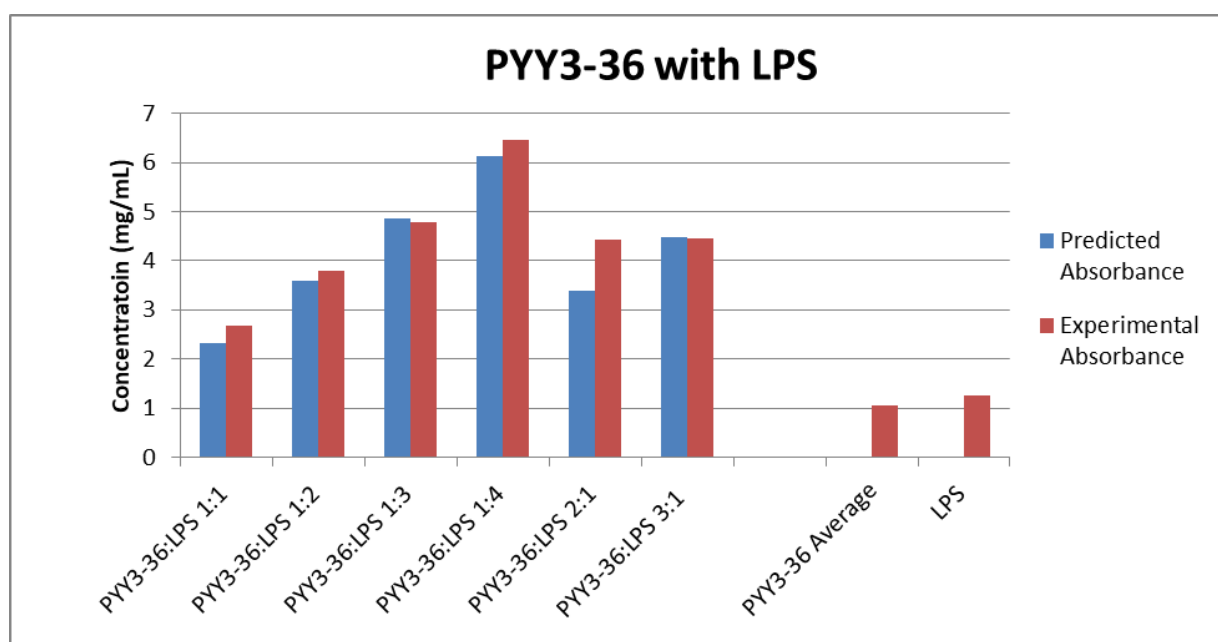


**Figure 43:** UV absorbance experiment showing the A280 Nanodrop concentration results combined with the predicted results. The predicted results using results from the starting materials, PYY<sub>3-36</sub> and LPS, to predict the combined absorbance, when mixed. All samples were in H<sub>2</sub>O, and ratios given in wt%. The ratios convert to 250:1, 500:1, 750:1, 125:1, and 75:1 estimated molarity ratios, respectively.

The first observation that can be seen from Figure 43 is the increase in the A280 absorbance, which is related to the mg/mL, when LPS is added to PYY<sub>3-36</sub>. To study this effect the PYY<sub>3-36</sub> average and the LPS absorbance were used to predict the mg/mL value of the other samples. The experimental values recorded can be seen to be either similar, or larger than their predicted values. This would suggest a shift in the tyrosine environment that only occurs from the interaction with LPS.

LPS did show an absorbance value that given LPS's lack of aromaticity, was not expected (Figure 43). Investigation into the extraction methods of LPS (from bacteria) used in this study showed that the samples had been extracted using the phenol method, contaminating the sample with several peptides and proteins. LPS, without these peptides or proteins, can be obtained but

only by more expensive and time-consuming methods. The data showed that our sample, purchased through Sigma Aldrich, contained around a 1 mg/mL concentration of proteins and/or peptides (Chapter 2.1).

When working out the actual difference between the predicted and measured values, there does not appear to be any consistent effect which happens with the addition of LPS (Figure 43). An increase in absorbance is what would have been hypothesised, as the tyrosine residues would be “shielded” further within a hydrophobic pocket. This effect would also be seen even if the tyrosine residues were to be “shielded” from the solution by the larger LPS molecules. In this case, this method has not shown a clear result, with some mixtures showing an increase while others shown little to none.

This method works for absorbance studies for aromatic amino acids, such as tyrosine, phenylalanine, or tryptophan, but as A9R is also under investigation another method needs to be used to try and understand if there are any binding interactions. Another absorbance of 205 nm was used to work out the concentration of peptides using the peptide backbone as an identifying aspect (Chapter 2.2.4). This wavelength is the specific absorbance value for the peptide bond so can be related to the concentration of the peptide in solution (Chapter 2.2.4). Therefore, given no other absorbance method an experiment with this wavelength, 205 nm, was completed to see if the absorbance value would change upon the addition of LPS.

After completing the study and processing it in a similar way to that of the 280 nm study completed earlier, this 205 nm study did not show a consistent change in absorbance with increasing mixture ratios. This was to be expected as the peptide bond is not being changed, necessarily by the action of mixing.

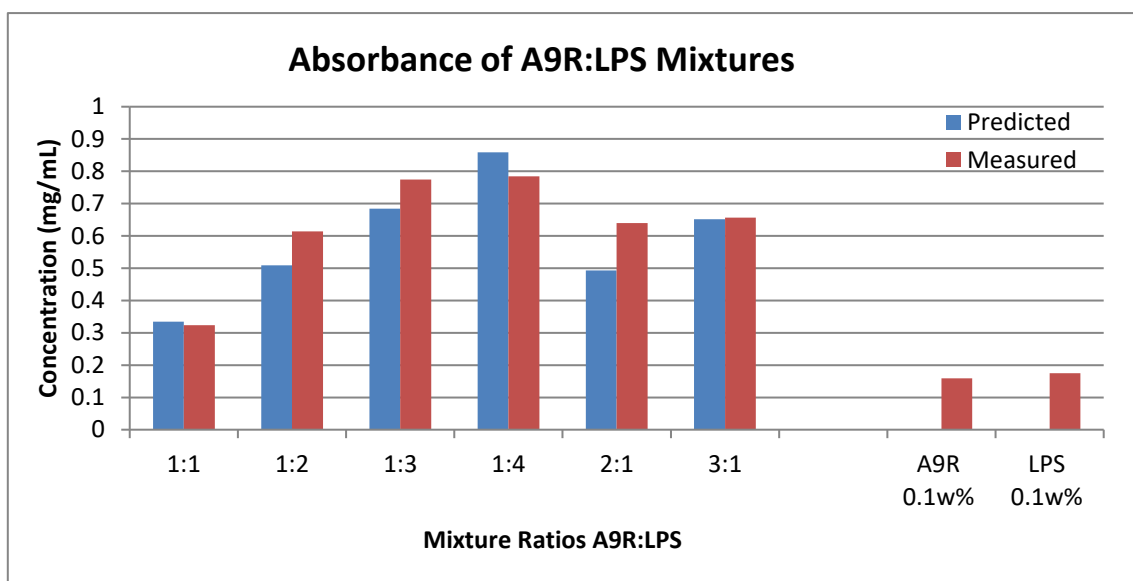


**Figure 44:** Showing the results for the A205 nm experiment on the Nanodrop. All samples are prepared with water, and ratios are in wt%. Blue being the predicted values calculated using the separate results from the singular samples (A9R, and LPS). Ratios convert to 1228:1, 618:1, 309:1, 2456:1, and 3864:1 in estimated molarity, respectively.

It can be seen in Figure 44 above that even though some of the complexes show an increased concentration; others show negative or minimal differences which make this technique similar in result to that of the 280 nm study. These inconclusive results suggest that another approach is needed to ascertain if complexation does occur, such as the LPS specific dye BODIPY TR.

### 5.10 LPS Specific Dye Absorbance Study using PYY<sub>3-36</sub> and A9R

A dye called BODIPY<sup>TM</sup> TR Cadaverine was found to be a specific dye that complexes to the Lipid A segment of the LPS. This complex then allows for a highly sensitive and robust fluorescent displacement assay (Chapter 2.2.7). This dye allows for a substitution experiment to be completed where a small amount of PYY<sub>3-36</sub> or A9R is added and if the absorbance of the sample increases this indicates a release of the BODIPY<sup>TM</sup> TR Cadaverine molecule, thus showing a complexation between these molecules and LPS. The methodology behind this experiment has been explained in larger detail in the Methodology Chapter 2.2.7, including concentrations, specific volumes and parameters used. The chemical structure of BODIPY<sup>TM</sup> TR Cadaverine can be seen in Figure 45.

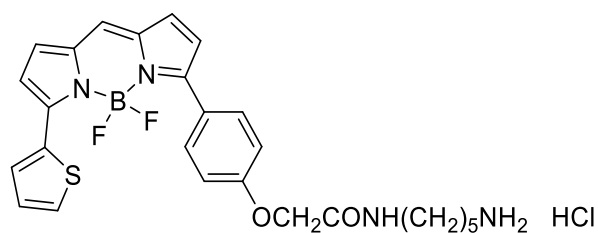


**Figure 45:** Chemical structure drawing of BODIPY<sup>TM</sup> TR cadaverine.

An interesting observation seen during the preparation was a colour change between the prepared BODIPY<sup>TM</sup> TR Cadaverine solution and when mixed with LPS from a bright pink solution to one of a blue solution after addition. Images were taken to show this contrast and can be seen in the materials and methods section (Figure 45 and Section 2.2.7).

BODIPY<sup>TM</sup> TR Cadaverine has an excitation wavelength of 580 nm and has a specific emission wavelength of 620 nm. For this study, the intensity of this wavelength was plotted against the addition of the excipient, PYY<sub>3-36</sub> or A9R, with additions of 10  $\mu$ L (20  $\mu$ M). Both the PYY<sub>3-36</sub> and A9R sample have been made to the same concentration of 20  $\mu$ M, with all samples (A9R, PYY and LPS + BODIPY) being made to the previous study's concentrations.

A clear increase in the intensity at 620 nm was seen (Figure 46) with the addition of the PYY<sub>3-36</sub> solution. After each 10  $\mu$ L addition the intensity at 620 nm increased. This increase can be attributed to the substitution of the BODIPY<sup>TM</sup> TR Cadaverine from the LPS with PYY<sub>3-36</sub> giving rise to an increase in this specific wavelength.

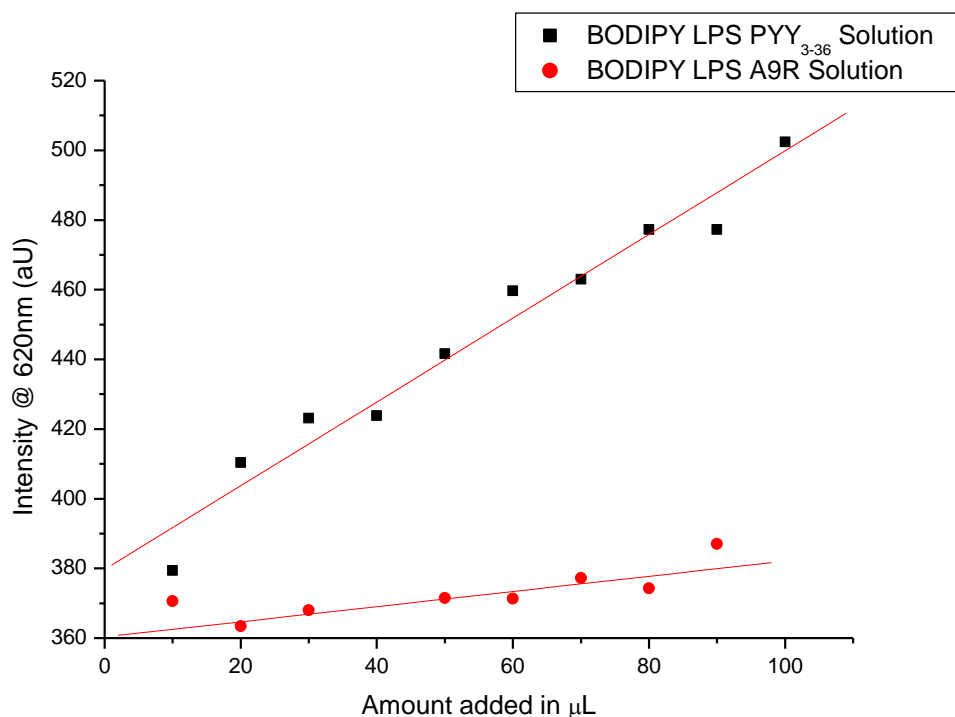


**Figure 46:** Comparison of BODIPY<sup>TM</sup> TR cadaverine release with complexation of A9R and PYY<sub>3-36</sub> to Lipopolysaccharide. Intensity values at 620 nm were recorded with the addition of 10  $\mu\text{L}$  (20  $\mu\text{M}$ ) of each solution. Both solutions were the same molarity. The intensity values were then fitted linearly to show a trend line and help show the gradient of increase.

This adds evidence to the complexation of the 17PYY<sub>3-36</sub> with LPS as even the unlipidated form, PYY<sub>3-36</sub>, complexes to LPS. The addition of the lipid chain would benefit the complexation as the dye used BODIPY TR is shown to specifically complex to the Lipid A section of LPS. The Lipid A section of LPS is highly hydrophobic and could help complexation or aggregation of a lipopeptide, such as 17PYY<sub>3-36</sub>, via the hydrophobic effect.

Without a clear reference the PYY<sub>3-36</sub> and LPS result seen cannot be stated to be useful as this could be the action of BODIPY TR and LPS regardless of the additional molecule. To test this an antimicrobial peptide A9R is also tested to see if it complexes in the same way as PYY<sub>3-36</sub> shown above in Figure 46. As mentioned previously all concentrations were kept the same to allow for comparison. If A9R does complexes to LPS, this could be helpful in determining its mode of action against bacteria, however this area is still under investigation.<sup>505</sup> Complexation to LPS could be of importance as this result shows that LPS is critical in A9R's anti-bacterial pathway.

Between the two molecules there is a clear difference in the intensity at 620 nm for the two samples over the 10  $\mu\text{L}$  additions. The graph (Figure 46) suggests that A9R does not, or does

in an extremely limited way, interact with LPS. This is clear as the slope of the A9R data is shallow and suggests little displacement of the BODIPY<sup>TM</sup> TR Cadaverine dye. PYY<sub>3-36</sub> shows the opposite with a larger gradient and having large increases in intensity from one 10  $\mu$ L addition.

A control was not run for this experiment, if it had been the control would have been in the form of the addition of 10  $\mu$ L of ultra-pure water to the LPS-BODIPY TR complex solution to observe any intensity changes. It can be assumed that if this LPS-BODIPY TR complex is stable, then the solution will become more dilute, thus reducing the intensity value over the additions (Eq. 8). Although this is the most logical outcome, without completing this control experiment, the above data should not be taken as clear evidence of complexation but could be used as evidence for further experiments.

In conclusion, these LPS specific dye experiments have shown, to a limited effect that PYY<sub>3-36</sub> does interact with the Lipid A section of LPS, while A9R, a known anti-bacterial, does not interact. This means A9R's interaction with bacteria could be by other methods, and that 17PYY<sub>3-36</sub>'s interaction, as seen earlier, is related to the Lipid A section. Fundamentally, these observations are of extreme interest and potential value in developing alternative forms of drug delivery, however further tests are needed, including a control experiment and the carrying out of a comparison with other molecules of interest.

### **5.11 Zeta Potentials of A9R or PYY<sub>3-36</sub> and LPS Complexes**

A further study to try and understand the complexation of A9R and PYY<sub>3-36</sub> with LPS is to measure the zeta potential of the complexed samples compared to their separate molecules. As with many of these experiments the full methodology can be found within the Methodology Chapter 2.2.5. Zeta potential is, simplistically, the measurement of the charge of the molecules within the sample. This method can be used for many reasons from self-assembly, charged species, coordination chemistry and neutralisation experiments.<sup>90, 514-521</sup> In this case it is being used to understand the charges that are part of the self-assembled structures of A9R, PYY<sub>3-36</sub> and LPS.

In Table 10, both PYY<sub>3-36</sub> and A9R showed a large positive value that is consistent with a stable self-assembled structure, both being above positive 20. Values of above a positive or negative 5 have been shown to represent stable, large, structures in solution.<sup>522-523</sup> LPS shows a negative value of -5, which shows a weaker structure, compared to that of PYY<sub>3-36</sub> and A9R. The ratio's

zeta potentials findings are set out below, also with the comparing of theoretical and measured findings of zeta potentials. The three main observations seen from Table 10 is;

1. The addition of LPS to PYY<sub>3-36</sub> markedly changed the charge of the sample even after 1:1 (250:1 PYY<sub>3-36</sub>: LPS estimated molarity) addition (from 25.5 to -0.6848), which is still seen for A9R (25.5 to 12.3) but not as severe.
2. The 2:1 (and 3:1 ratio of PYY<sub>3-36</sub> showed a continued near zero value but the ratios of the A9R showed higher values, indicating similar charged species to the 1:1 ratio. This effect can also be seen in the mobility results.
3. The final effect seen is that the mixtures of PYY<sub>3-36</sub> and LPS, after the 1:1 ratio, are more negative that suggests these structures are slightly more stable compared to the similar A9R: LPS ratios. These results do not add much information to the reason for complexation. They do suggest that PYY<sub>3-36</sub> and LPS do complex, furthermore the structures are reasonably stable. The differences in the 2:1 (500:1 molarity) and 3:1 (750:1) ratio between the two molecules is of further interest and an area that could be investigated further.

**Table 10:** Zeta potential, Mobility, and Conductivity results for PYY<sub>3-36</sub>, A9R and estimated ratio of mixtures with LPS. Errors being last value,  $\pm 0.001$ . Theoretical zetapotential values calculated from the separate samples (PYY, A9R, and LPS).

Sample	ZP (mV)	Mob ( $\mu\text{mcm/Vs}$ )	Cond (mS/cm)	TheoZeta Value (mV)
<b>PYY<sub>3-36</sub>: LPS 250:1</b>	-0.648	-0.051	0.217	19.907
<b>PYY<sub>3-36</sub>: LPS 125:1</b>	-4.053	-0.317	0.198	14.680
<b>PYY<sub>3-36</sub>: LPS 83:1</b>	-3.807	-0.298	0.230	9.453
<b>PYY<sub>3-36</sub>: LPS 65:1</b>	-2.673	-0.210	0.293	4.227
<b>PYY<sub>3-36</sub>: LPS 500:1</b>	0.172	0.013	0.192	45.040
<b>PYY<sub>3-36</sub>: LPS 750:1</b>	-0.344	-0.344	0.213	70.173
<b>A9R: LPS 1228:1</b>	12.367	0.969	0.242	17.340
<b>A9R: LPS 614:1</b>	-0.349	-0.027	0.206	12.113
<b>A9R: LPS 409:1</b>	-0.905	-0.071	0.271	6.887
<b>A9R: LPS 307:1</b>	-0.675	-0.053	0.271	1.660
<b>A9R: LPS 2456:1</b>	13.000	1.020	0.439	39.907
<b>A9R: LPS 3684:1</b>	14.667	1.150	0.609	62.473
<b>PYY<sub>3-36</sub></b>	25.133	1.971	0.119	
<b>A9R</b>	22.567	1.769	0.212	
<b>LPS</b>	-5.227	-0.410	0.048	

ZP = Zeta potential, Mob = Mobility, Cond = Conductivity and TheoZeta = Theoretical Zeta value given separate sample values.

## 5.12 Conclusion of LPS interaction with comparison of 17PYY<sub>3-36</sub> and A9R

All these studies have investigated an unusual observation of precipitation and large “aggregation” between 17PYY<sub>3-36</sub> fibres and the short LPS structures. Cryo-TEM confirmed the presence of these aggregates. Further studies used A9R for comparison and PYY<sub>3-36</sub> for similarity.

Using SAXS and CD it was shown that a mixture of 17PYY<sub>3-36</sub> and LPS reduced the  $\alpha$ -helical structure of the peptide. SAXS analysis of the same mixture showed a shift of form factor from fibre to bilayer gaussian. This shift shows a significant change in self-assembled structure, but to confirm this, further studies are needed.

Cryo-TEM of A9R and LPS, in comparison, showed two separate self-assembled structures being formed. This was seen again through SAXS, but as the technique is an average of values, it only showed an average of the scattering patterns.

A study of the fluorescent amino acids within PYY<sub>3-36</sub>, using the 280 nm wavelength, did not show any trends, as the residues are not affected by the co-self-assembly. This was also the case with A9R and LPS as the 205 nm wavelength did not show any change, or trend, from the mixtures.

The specific study using BODIPY<sup>TM</sup> TR Cadaverine, which is a specific dye that complexes to the Lipid A section of LPS, was undertaken. This dye showed a large increase in intensity with the addition of PYY<sub>3-36</sub>, which is an indicator of BODIPY release, and PYY<sub>3-36</sub> complexation to LPS. A9R on the other hand, showed a reduced gradient, but nowhere near as marked as PYY<sub>3-36</sub>. Upon further reflection, carrying out a control experiment, and expanding the molecules investigated, would help to provide further confirmation of the above BODIPY TR dye hypothesis.

The final study with Zeta-potential showed a few notable observations with A9R or PYY<sub>3-36</sub> and LPS with the most noticeable being the difference in charge that can be seen between the two mixtures of PYY: LPS and A9R: LPS at 1:1 wt% ratios. Further studies and controls using well characterised short peptide chains would be needed to add to these experiments and further probe this complexation. A<sub>9</sub>R analogues, such as RA<sub>9</sub>R, or AR<sub>9</sub>, or modified A<sub>9</sub>R with different amino acids such as Glutamic Acid (E), or Phenylalamine (F), would be suggested to be used as control peptides. Further complexation tests with cyclic lipopeptides, such as the

antibiotic Fusaricidin, would also be of interest to explore whether the cyclic nature of the peptide might hinder the LPS complexation.

## 6. Synthesis and Inclusion Potential for Polysaccharides with PYY<sub>3-36</sub> using $\beta$ -cyclodextrin.

### 6.1 Introduction to Synthesis and Inclusion of PYY<sub>3-36</sub> with $\beta$ -cyclodextrin.

In previous chapters lipidation has been the key factor in either causing different forms of self-assembly and changes in secondary structure (Chapter 3 and 4). Lipidation has been used by many other research groups for this reason, with the aim of making useful 3D networked structures for use in different fields of science.<sup>108, 191, 472</sup> Polysaccharides, which are multiple sugar units bonded together (as seen in Figure 47), are also a potentially useful molecule for gel formation and self-assembly as they contain multiple hydroxyl groups that can facilitate hydrogen bonding. This characteristic creates the potential for the addition of a polysaccharide chain to PYY<sub>3-36</sub> to create a novel conjugate. The addition of polysaccharides would be beneficial as they are bio-recognised, easily broken down within the body and the potential resultant hydrogen bonding that occurs could readily form a gel.

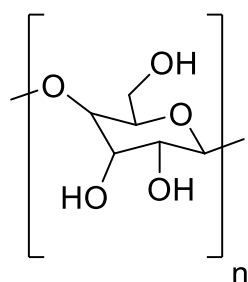


**Figure 47:** Example saccharide unit,  $n$  denoting chain possibility.  $n=1$  is glucose,  $n=2$  disaccharide,  $n>3$  oligosaccharides,  $n>5$  polysaccharides.

Within the literature many conjugates have been formed between PYY or PYY<sub>3-36</sub> and other species, these include the conjugation with Vitamin B-12 and Albumin with both conjugates (Vitamin B-12 and Albumin) influencing food intake.<sup>342, 426, 524-525</sup> The conjugation of a 7 membered polysaccharide to PYY<sub>3-36</sub> has not been found within the literature, so this synthesis experiment would be of interest from a drug formulation perspective, as well as providing the potential for further drug conjugates to be explored.

For this novel conjugate synthesis, a readily found sugar  $\beta$ -cyclodextrin was used as the starting point. This sugar is formed of a 7 membered ring of glucose units (Figure 47). The polysaccharide ring formation has characteristics worth exploring when included with PYY<sub>3-36</sub> such as its internal hydrophobic cavity within the ring and its orientated hydroxyl groups

with a primary and secondary hydroxyl group. Previous studies have used the internal cavity to produce self-assembled structures with surfactants, such as SDS.<sup>32, 451, 518, 526-530</sup> Further studies have shown the incorporation of small drug molecules within the  $\beta$ -cyclodextrin structure that showed delayed release profiles.<sup>518, 531-541</sup>

The experimental methodology used was found within a previous paper that detailed the use of thiol-ene click chemistry.<sup>542</sup> This paper proposed the use of  $\beta$ -cyclodextrin as the starting material, breaking it with acid to form the 7 membered oligosaccharide, named Maltoheptaose, which could then, with simple chemical modifications, be functionalised with an alkene group.

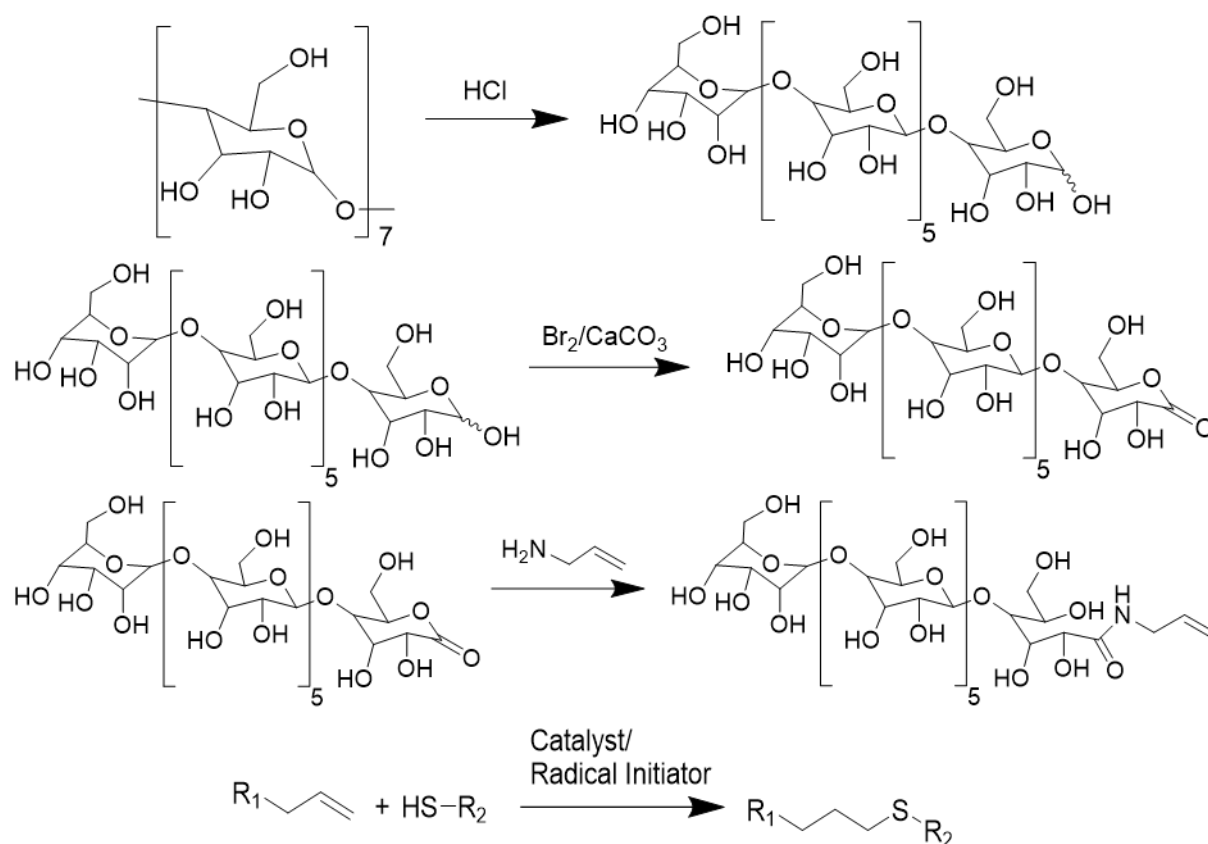


**Figure 48:** First reaction: Simplistic ring opening using HCl. Found in paper reference<sup>542</sup> Second reaction step: oxidation of anomeric hydroxyl. Third reaction stage: Adding the alkene functionality to the polysaccharide. Final reaction step: thio-ene click reaction.  $\text{R}_1$  and  $\text{R}_2$  being additional functionality.

This alkene functional group would then be used in the thiol-ene click reaction with a sulphur containing group, in this case, a cysteine function group can be incorporated into the peptide chain during synthesis. A simplified thiol-ene click reaction can be seen in Figure 48. The thiol-ene click reaction has become an extensive research field with many groups utilising this

selective and highly useful reaction for gel formation, lipid addition and further functionality.<sup>111, 543-545</sup>

In addition to creating this synthetic target it would be useful to investigate the mixing effects of  $\beta$ -cyclodextrin with native PYY<sub>3-36</sub> as this could provide insight into the complexation possibilities. The possibility stems from the hydrophobic pocket found within the  $\beta$ -cyclodextrin that could interact with the peptide or part of the chain.

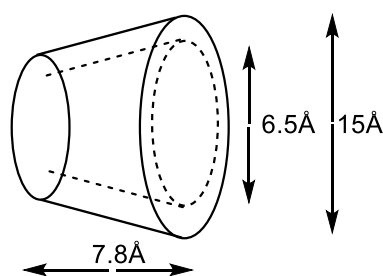


**Figure 49:** Mesh diagram of  $\beta$ -cyclodextrin showing pocket formed by the 7 membered ring.

## 6.2 Polysaccharide Conjugate Synthesis

Using the cheaper starting product,  $\beta$ -cyclodextrin, and breaking it with the use of HCl, proved to be more difficult than first suggested in the paper.<sup>542</sup> The issue stemmed from the problem of selectively controlling the acid hydrolysis. It was suggested through the paper that a solution of 0.1M HCl was used to break down the cyclic polysaccharide.<sup>542</sup> Multiple experiments were completed under different reaction conditions yet the breaking down of the cyclic polysaccharide was difficult to achieve and, as such, the synthetic pathway purposed in the introduction above could only produce Maltoheptaose in quantities too small for experimental and measurement purposes.

To attempt to break  $\beta$ -cyclodextrin, experiments were completed at higher temperatures, under more concentrated acid conditions and by changing the acids used. Under milder acidic conditions (such as 0.1M HCl) a mixture of compounds was found by thin layer chromatography (TLC). These compounds were determined to be the 7 different possible products from an acid hydrolysis (1 to 7 polysaccharide). As there is no way to properly control the selectivity of the ring opening and hydrolysis, the method produced all 7 different polysaccharides. Further difficulties were found in the amount of Maltoheptaose that was produced, as the acid hydrolysis produced a higher percentage of glucose (1) compared to very little or none of the maltoheptaose. This then became the main issue for the synthesis route, as

even starting with a large amount of the  $\beta$ -cyclodextrin, only a very small amount of the specific 7 membered ring opened product was available. The 7 different polysaccharide products identified were found when completing a timed TLC experiment. Attempts at separating these 7 products by column chromatography failed to separate these compounds as they are extremely similar in polarity.

To continue the project a small amount of the 7 membered polysaccharide, Maltoheptaose, was purchased and the oxidation was then attempted (Chapter 2.1). Further complications were found with this step as the method suggesting the use of bromine and calcium carbonate (Figure 48) showed limited success. An attempt to use NMR to identify a single hydrogen loss in the oxidation reaction product was carried out however, with such a large molecule and such a small change, NMR was unable to differentiate between the two molecules. Another issue was found to relate to the impurities introduced during its manufacturing process. The purchased Maltoheptaose was rated at 60% purity which negatively impacted the oxidation reaction outcome and made any subsequent NMR analysis more difficult to achieve than originally hypothesised. Due to the complexities that were experienced and the danger that the project would encounter a significant overrun (by at least 4 months), it was decided that the synthesis section of this work should be halted and that the complexation studies using the hydrophobic pocket were focused on instead. Synthesis of these novel polysaccharide conjugates to PYY<sub>3-36</sub> remains of high interest particularly to drug formation and self-assembly science fields as  $\beta$ -cyclodextrin is a cheap material that could help facilitate PYY<sub>3-36</sub> drug delivery or improve PYY<sub>3-36</sub> circulation times. It is suggested therefore that the level of work required would make it a suitable for a project with a longer timeframe in the future.

### **6.3 Circular Dichroism for Complexation of PYY<sub>3-36</sub> and $\beta$ -cyclodextrin**

Before continuing with CD, and following the same molarity estimations from before, using  $\beta$ -cyclodextrin's  $m_r$  of  $814 \text{ gmol}^{-1}$ , for the following experiments PYY<sub>3-36</sub> is 2.469 mmol, while  $\beta$ -cyclodextrin is 8.811 mmol. This means there is a ratio of around 1:3.6 of  $\beta$ -cyclodextrin to PYY<sub>3-36</sub>. With this difference in the molarities, this means that  $\beta$ -cyclodextrin is in a slightly higher concentration, and thus could have a greater impact on the co-assembly process. Again however, it is worth remembering that as self-assembly and aggregation does not necessarily require a 1:1 bonding of the components, and here for example there could be a 1:3 co-assembly.

PYY<sub>3-36</sub>, as shown in all the other chapters contains a segment of  $\alpha$ -helical structure (Chapters 3.1, 3.4, 5.4, and 5.8). This was shown in the circular dichroism results with further studies showing the disruption of this secondary structure by lipidation (Chapter 3.4). To test the possibility for complexation CD was completed on  $\beta$ -cyclodextrin with PYY<sub>3-36</sub>. Application of this method would show if the  $\beta$ -cyclodextrin interacts with the secondary structure of the peptide.

The study that was carried out, Figure 50, showed no specific interaction between PYY<sub>3-36</sub> and  $\beta$ -cyclodextrin.  $\beta$ -cyclodextrin showed no secondary structure or ellipticity which is as expected as the molecule itself does not self-assemble (no secondary structure) or have any specific chirality (R/S). Both the 1 wt% PYY<sub>3-36</sub> and the 1:1 mixture (1:3.6 molarity) showed similar ellipticity values, clearly showing the  $\alpha$ -helical structure of the native peptide is still present and at the same intensity in the mixture. This experiment does not fully show that there is no interaction as the  $\beta$ -cyclodextrin could still interact with the hydrophilic or hydrogen bonding amino acids on the outer edges of the peptide, or even the self-assembled twisted fibres PYY<sub>3-36</sub> forms. Further studies are needed to confirm or remove this possibility.

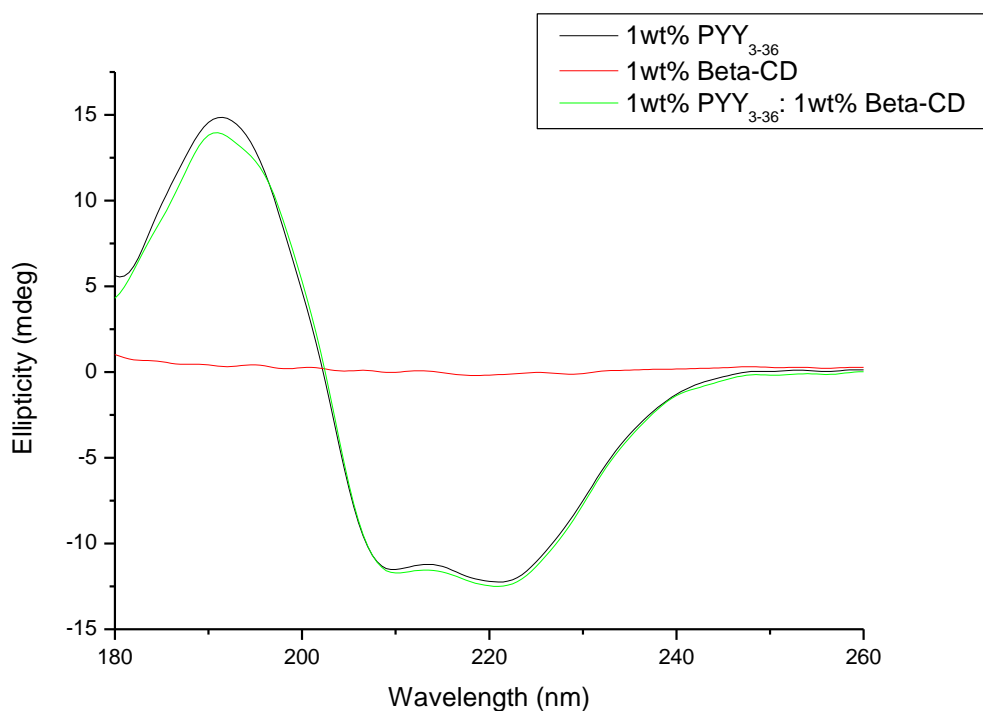


**Figure 50:** Circular Dichroism comparison of PYY<sub>3-36</sub>,  $\beta$ -cyclodextrin and a 1:1 wt% mixture (1:3.6 molarity). Data has been smoothed by Fast Fourier Transform (5 points). All samples were prepared in H<sub>2</sub>O. PYY<sub>3-36</sub> and mixture showing the same  $\alpha$ -helical content, showing a lack of interaction with the  $\alpha$ -helix of PYY<sub>3-36</sub>.

#### 6.4 Small Angle X-ray Scattering Study of PYY<sub>3-36</sub> with $\beta$ -cyclodextrin

A technique that could provide information on the aggregation at the outer edges of the peptide is small angle X-ray scattering. As the aggregation occurs the diameter and/or the structure will change which, in turn, could give rise to a different SAXS pattern. In this experiment, reduced concentrations were used to preserve the amount of sample used and to reduce the possibility of affecting the thin capillary used in the high-throughput SAXS experiments (see Chapter 2.2.2). Other ratios of 1:2 wt% (1:7.2 molarity) and 2:1 wt% (1:1.8 molarity) were used in addition to the similar ratio of 1:1 wt% PYY<sub>3-36</sub>:  $\beta$ -cyclodextrin (1:3.6 molarity) to probe the effect of higher concentrations of PYY<sub>3-36</sub> or  $\beta$ -cyclodextrin on potential aggregation.

The results of this experiment can be seen in Figure 51. The first observation to make is that diluted samples have made the scattering patterns become more defused, making fitting and experimental observations difficult to make. 0.1 wt% PYY<sub>3-36</sub> can be seen to have little structure as evidenced by the different slope from 0.005 to 0.02  $\text{\AA}^{-1}$  and compared to that of the 0.2 wt% PYY<sub>3-36</sub> pattern (Figure 51, see black vs. dark blue spread). This slope is similar to a 1 wt% sample of PYY<sub>3-36</sub> (see Chapter 3.3) indicating a bilayer formation. This bilayer formation has been shown to be a twisted sheet structure in previous chapters using Cryo-TEM (Chapter 3.2).

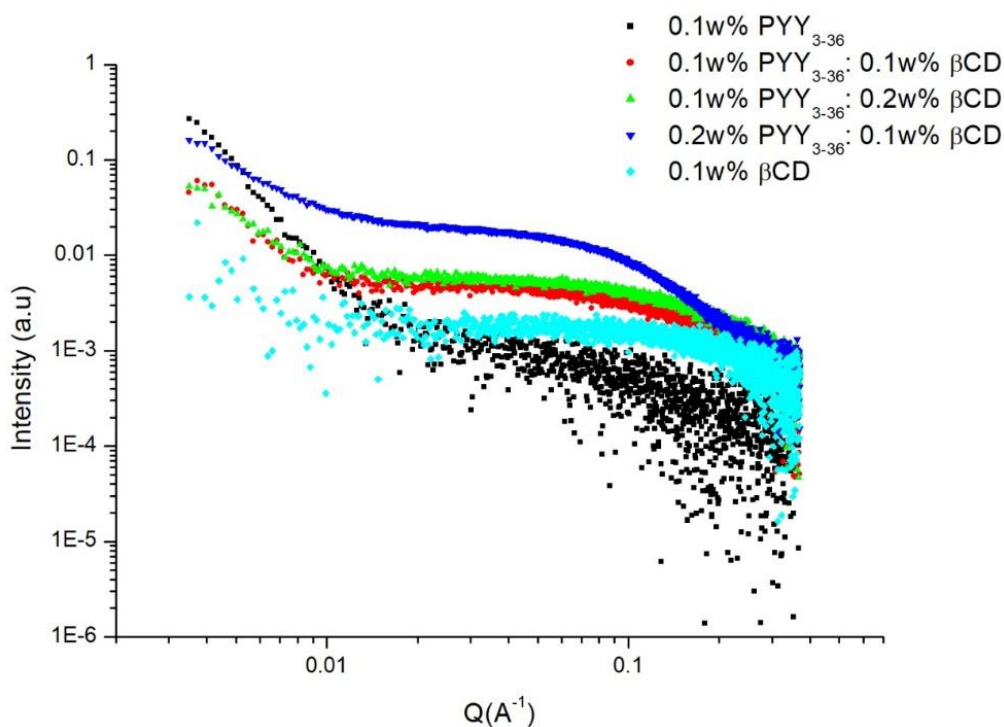


**Figure 51:** SAXS patterns comparing PYY<sub>3-36</sub>,  $\beta$ -cyclodextrin, and 1:1 wt% (1:3.6 molarity), 1:2 wt% (1:7.2 molarity), and 2:1 wt% (1:1.8 molarity) ratios. All samples were made in water. These scattering curves are relatively the same, with PYY<sub>3-36</sub> showing the same patterns seen in the previous Chapter 3.3.

The  $\beta$ -cyclodextrin pattern can be seen to have a monomeric pattern as suggested by the increased randomness and the shape of the curve of the data (see Figure 51). This result is not unexpected as the hydroxyl covered polysaccharide would only be hydrophilic and, as such, would not self-assemble. The two other main observations are that 0.1 wt% PYY<sub>3-36</sub>: 0.1 wt%  $\beta$ -cyclodextrin (1:3.6 molarity) and 0.1 wt% PYY<sub>3-36</sub>: 0.2 wt%  $\beta$ -cyclodextrin (1:7.2 molarity) have very similar scattering patterns. Secondly, the increased intensity of the 0.2 wt% PYY<sub>3-36</sub>: 0.1 wt%  $\beta$ -cyclodextrin (1:1.8 molarity) sample was compared to the other ratios that showed that they generated a similar scattering pattern. This increased intensity for the 0.2 wt% PYY<sub>3-36</sub> sample is not surprising as it suggests the formation of more twisted sheets as seen in the Cryo-TEM in the previous Chapter 3.2. Overall, SAXS does show some change in structure from monomeric or gaussian coil type due the presence of similar scattering patterns, however, as the samples were dilute, not many conclusions can be drawn from this study. Consequently, SAXS experiments with higher concentrations are needed to investigate the interactions between these two molecules.

### **6.5 Cryo-TEM Visualisation of PYY<sub>3-36</sub> with $\beta$ -cyclodextrin**

Small Angle X-ray Scattering did not provide any insight into what was occurring between the twisted fibres of PYY<sub>3-36</sub> and that of the monomeric  $\beta$ -cyclodextrin. Another method that has been used throughout the previous chapters is Cryo-TEM (Chapters 3.2, 4.4, and 5.2). This method could be used to visualise any changes to the conformations of the twisted sheets or could show the formation of new self-assembled structures that keep the  $\alpha$ -helical structure seen in circular dichroism. A similar twisted sheet structure of PYY<sub>3-36</sub> can be seen again in Cryo-TEM (Figure 52). This was expected as these samples were imaged using a higher concentration of PYY<sub>3-36</sub> (1 wt%) that was used to increase the possibility of seeing any complexation or self-assembly.

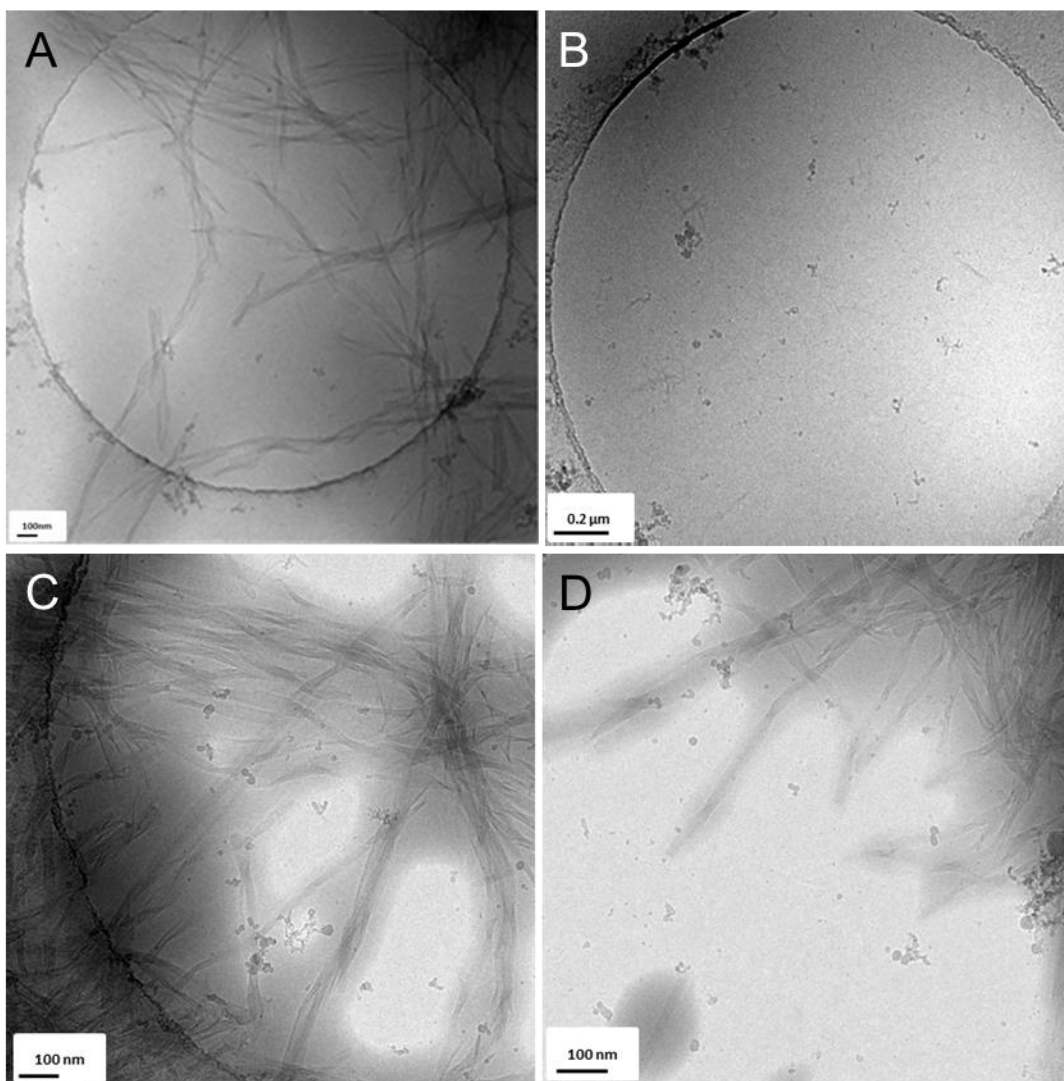


**Figure 52:** Cryo-TEM images showing the  $\beta$ -cyclodextrin aggregation around that of the  $\alpha$ -helical twisted sheets of PYY<sub>3-36</sub>. A – A comparison image of 1 wt% PYY<sub>3-36</sub> in H<sub>2</sub>O, showing the twisted sheets as seen before in Chapter 3. The scale is 100 nm to allow the twisted sheets to be better visualised. B – A second comparison cryo-TEM image of  $\beta$ -cyclodextrin in H<sub>2</sub>O, to show that  $\beta$ -cyclodextrin does not form any structures. This was completed at 0.2  $\mu$ m scale, to help visualise any large structure formation, but there was none. C, D – Two images showing the aggregation of  $\beta$ -cyclodextrin around that of the clear twisted sheets of PYY<sub>3-36</sub> in a 1:1 mixture of 1 wt% PYY<sub>3-36</sub> and 1 wt%  $\beta$ -cyclodextrin (1:3.6 molarity), in H<sub>2</sub>O. Two images are shown to show the nonuniformity of the aggregation, at the same scale.

Using circular dichroism,  $\beta$ -cyclodextrin has previously been shown to have no chirality or secondary structure that means that no self-assembled structures were expected to be seen in the cryo-TEM investigations (Chapter 6.3 Figure 50).

Only one mixture of 1 wt% PYY<sub>3-36</sub> and 1 wt%  $\beta$ -cyclodextrin (1:3.6 molarity) mixture was imaged as this was the key mixture of interest and allowed a comparison of it to the results from the Circular Dichroism and SAXS analysis. Taking this approach would therefore give a clear indication if there was complexation or self-assembly going on. The analysed mixture

showed large, clouded sections surrounding the self-assembled structure of the twisted tapes of PYY<sub>3-36</sub>, which can be seen in Figure 52.

The contrast seen in Cryo-TEM (Figure 52) shows the aggregation between the PYY<sub>3-36</sub> fibres and  $\beta$ -cyclodextrin. The areas of high contrast, in this particular case, are very specific and seem to be highly aggregated around the fibres. The fibres still show the same structure as seen in the previous pictures and as also seen in the previous Chapters 3.2 and 5.2. This observed structure includes twisted as well as the elongated structures with lengths over 1000 nm. Aggregation with  $\beta$ -cyclodextrin has not disrupted this structure, as seen from Figure 52 and CD, which lends evidence to an interaction between the edges of the fibres and the cyclodextrin ring.

This observation needs other studies to add further evidence to fully conclude that the interaction between  $\beta$ -cyclodextrin and PYY<sub>3-36</sub> is limited due to the charged or hydrophilic amino acid residues on the outside of the fibres.

### 6.6 A280 nm Study of $\beta$ -cyclodextrin aggregation with PYY<sub>3-36</sub>

A similar study to the one completed in the previous chapter is to study the aromatic groups on the arginine amino acids found within the PYY<sub>3-36</sub> peptide. Although this does not cover the charged groups interactions it could lend evidence to an aromatic interaction.

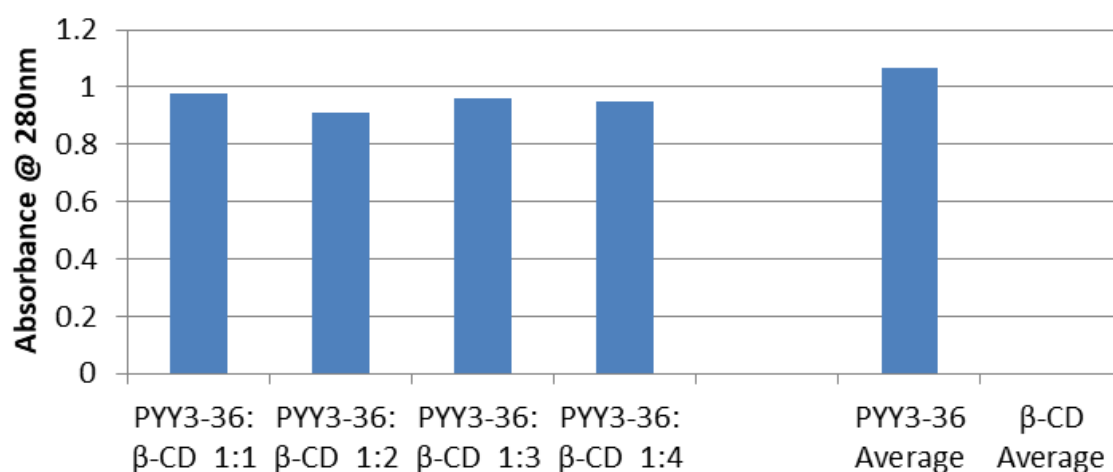


**Figure 53:** Absorbance values for mixtures of PYY<sub>3-36</sub> and  $\beta$ -cyclodextrin. All samples were made up in H<sub>2</sub>O and ratio is in wt%, translated to 1:3.6, 1:7.2, 1:10.8, and 1:14.4 molarity respectively. Each absorbance value is an average of 3 separate readings. PYY<sub>3-36</sub> and  $\beta$ -cyclodextrin have also been included to allow for comparison.

The results from this experiment also confirm the circular dichroism results (Figure 49) of no interaction between the hydrophobic, aromatic, amino acids and the  $\beta$ -cyclodextrin. It also

confirms that there is also no conformational change of the peptide with the addition of  $\beta$ -cyclodextrin as the hydrophobic environment has not changed. Even with increasing the ratio, 1:1 (1:3.6 molarity) to 1:4 (1:14.4 molarity), there was no change in the absorbance value. Further to that, all the solutions containing 1 wt% PYY<sub>3-36</sub> showed similar absorbance values and  $\beta$ -cyclodextrin showed no absorbance, which was expected as it has no aromatic groups (Figure 49).

Overall, this experiment added evidence to the CD data previously gathered (Figure 50) and showed there was no conformational change and no interaction between the CD and the peptide chain. This means that the high density, seen selectively around the PYY<sub>3-36</sub> fibres (Figure 52), is occurring by a hydrophilic charged interaction. It also seems to show that this is more of an aggregation to the charged moieties rather than a co-assembly.

Aggregation has been used before to describe self-assembly or a grouping of monomers, but in this study, it refers to a loose proximity, formed by weaker interactions, rather than co-assembly.

### **6.7 Zeta Potentials of PYY<sub>3-36</sub> and $\beta$ -cyclodextrin Ratios.**

To add evidence to the theory of charged aggregation, solutions of different ratios were prepared similar to the A280 nm experiment above and were then analysed by a Zetasizer to measure the charges of molecules within the solution. As mentioned previously, a charge of more than plus or minus 5 indicates a molecule that has a stable structure. Anything between these values is deemed to be either unstable or unformed.

The study was carried out to compare the differences in the aromatic and charged species. It should be noted, as stated before in Chapter 2.2.5, zeta potential is a measure of the electrokinetic potential of the particles, if present, within the sample. More information on this can be found within Chapter 2.2.5. In this study the zeta potential is used to measure the charge of the twisted sheets seen in Cryo-TEM. This study, it is hoped, will show a loss of charge as the sheets become shielded by  $\beta$ -cyclodextrin.

As seen in Table 14 the results showed a reduction in zeta potential from the native solution of PYY<sub>3-36</sub> to a mixture of 1:1 (1:3.6 molarity) with  $\beta$ -cyclodextrin. This reduction is around 5 mV, but the solution still has a zeta potential of 20 mV that indicates that it is still a stable colloid.<sup>522-523</sup>

**Table 11:** Zeta potentials for Various Ratios of PYY<sub>3-36</sub> and  $\beta$ -cyclodextrin. All solutions were made up in H<sub>2</sub>O, measured using the same sample cell, and are in wt%. Error values for each measurement are  $\pm 0.1\%$ .

Sample Name and Ratio	Zeta Potential (mV)	Mobility ( $\mu\text{cm/Vs}$ )	Conductivity (mS/cm)
<b>PYY<sub>3-36</sub>: <math>\beta</math>-cyclodextrin 1:1 (1:3.6 molarity)</b>	20.6000	1.6147	0.0685
<b>PYY<sub>3-36</sub>: <math>\beta</math>-cyclodextrin 1:2 (1:7.2 molarity)</b>	0.2504	0.0196	0.0272
<b>PYY<sub>3-36</sub>: <math>\beta</math>-cyclodextrin 1:3 (1:10.8 molarity)</b>	-0.0050	-0.0004	0.0083
<b>PYY<sub>3-36</sub>: <math>\beta</math>-cyclodextrin 1:4 (1:14.4 molarity)</b>	-0.0662	-0.0052	0.0046
<b>PYY<sub>3-36</sub></b>	25.1333	1.9707	0.1187
<b><math>\beta</math>-cyclodextrin</b>	0.2253	0.0177	0.0070

When the ratio was increased from 1:1 (1:3.6 molarity) to 1:2 (1:7.2 molarity) and beyond, there was a total loss of charge observed that lends evidence to a loss of stability. These ratios have not been studied using Cryo-TEM due to time limitations on the thesis, so the stability of these structures cannot be determined for certain.

A small reduction was seen in the mobility and conductivity values at 1:1 addition of  $\beta$ -cyclodextrin, however, at molarity ratios 1:10.8 and 1:14.4 there was a greater reduction in these values. These reductions suggest a loss of stability, as identified by other authors' Zeta-Potential experiments,<sup>546-548</sup> however the structures seen in cryo-TEM (Figure 52) suggest there could be a shielding effect being caused by the  $\beta$ -cyclodextrin surrounding the PYY<sub>3-36</sub> fibres.

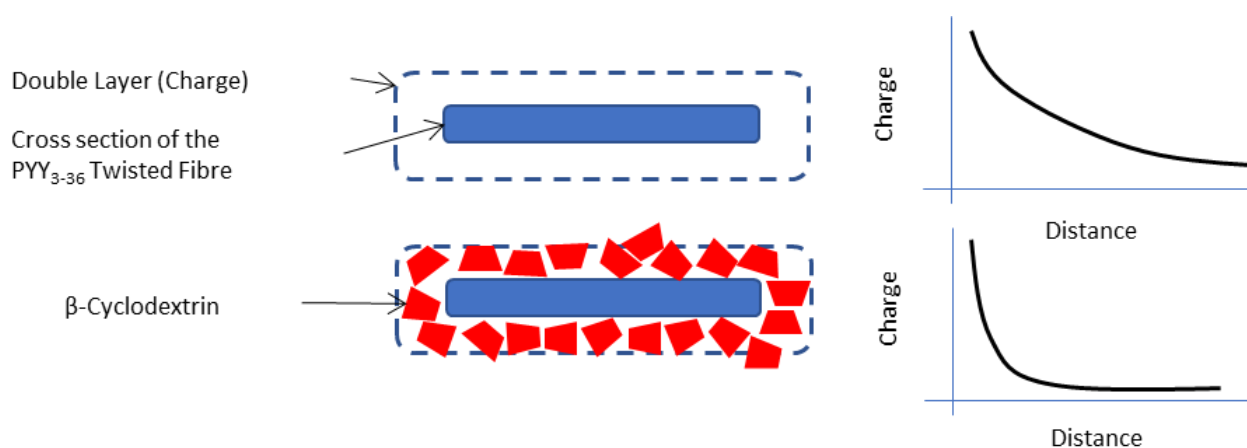


**Figure 54:** Zeta-potential diagram explaining the possible shielding effects of  $\beta$ -cyclodextrin on the charged twisted sheet structure of PYY<sub>3-36</sub>.

The potential shielding effect has been noted in other zeta potential studies, specifically with the use of metal ions.<sup>517, 549-551</sup> A simplistic view of the suggested aggregation can be seen in Figure 53 with the charge of the fibre dropping significantly as  $\beta$ -cyclodextrin aggregates around the fibre. As this shielding and aggregation effect can only be seen with molarity ratios

of 1:3.2, it is suggested that further ratios need to be researched to evidence these stable self-assembled structures and not the destabilised monomers that zeta potential suggests.

## 6.8 Conclusions of PYY<sub>3-36</sub> with $\beta$ -cyclodextrin

This chapter set out to analyse two aspects of the synthesis and inclusion potential for polysaccharides with PYY<sub>3-36</sub> using  $\beta$ -cyclodextrin. However, only the potential of  $\beta$ -cyclodextrin and PYY<sub>3-36</sub> co-assembly was fully investigated as the proposed synthesis route of  $\beta$ -cyclodextrin proved problematic, with the work required being beyond the timeframes of this thesis. The largest and most problematic issue was found to be the acid hydrolysis of the  $\beta$ -cyclodextrin that produced unusably small quantities of the required product.

After this synthesis obstacle was encountered a different experiment was proposed, namely an aggregation experiment with  $\beta$ -cyclodextrin and PYY<sub>3-36</sub>. This experiment was considered of interest as other molecules such as SDS, azomethine, and pipemidic acid (HPPA), having shown complexation with PYY<sub>3-36</sub> could be of use in the field of drug delivery for PYY<sub>3-36</sub>.<sup>518, 552-553</sup>

To investigate the potential of the aggregation the secondary structure was probed by using circular dichroism techniques. The CD showed that a 1:1 ratio of PYY<sub>3-36</sub> and  $\beta$ -cyclodextrin complex caused no secondary structural change.

Small Angle X-Ray Scattering showed structural differences between the 1:1 wt% ratio (1:3.6 molarity) of PYY<sub>3-36</sub> and  $\beta$ -cyclodextrin when compared to that of the separated molecules. This effect was seen with the higher ratios as well. In previous chapters, the structure of PYY<sub>3-36</sub> has been shown, through a range of techniques, to be twisted sheets (Chapter 3.3). The scattering pattern of the 1:3.2 molarity ratio was found to be of a different type that potentially indicates the formation of a different self-assembled structure.

To confirm if different structures were formed, cryo-TEM was used. This showed the presence of the original twisted sheets of PYY<sub>3-36</sub> in the 1:3.2 molarity  $\beta$ -cyclodextrin mixture. A high density of  $\beta$ -cyclodextrin was also seen specifically around these twisted sheets. This observation adds weight to the aggregation theory which suggests the aggregation is driven through the charged nature of the twisted sheets.

This observed effect of aggregation was further investigated by A280 nm and zeta potential experiments. A280 nm analysis showed limited to no interaction with the aromatic residues of

the PYY<sub>3-36</sub> peptide chain. Zeta potential analysis on the other hand, which measures the charged double layer of any charged species, showed a significant charge decrease from native PYY<sub>3-36</sub> to that of the 1:1 wt% (1:3.6 molarity) ratio. Combining the results from these methods showed a charged aggregation effect but one that was limited to the outer edge of the PYY<sub>3-36</sub> fibres and one that did not affect the aromatic residues found within the PYY<sub>3-36</sub> native structure itself. Further experiments using fluorescence would help probe the co-aggregation effect on the aromatic amino acids in more detail.

These experiments show an aggregation between the peptide hormone PYY<sub>3-36</sub> and the cyclic sugar,  $\beta$ -cyclodextrin. The observed aggregation is of a “weak” double layer effect that is formed by the charged residues on the outer edges of the self-assembled fibre of PYY<sub>3-36</sub>. The hydrophobic “pocket” found within  $\beta$ -cyclodextrin was shown to have no interaction with the peptide chain itself or, for that matter, with the hydrophobic aromatic residues on the peptide chain. Post experimentally, it was noted that, as the samples were not pH tested, the addition of  $\beta$ -cyclodextrin could have changed the pH which may in turn have affected the result findings.

These observations will have added new information for future  $\beta$ -cyclodextrin and PYY<sub>3-36</sub> inclusion experiments and related drug formulation research. As larger peptides, such as PYY<sub>3-36</sub>, have little inclusion research based on them, further research into the different ratios would be of interest as well as potentially looking into to the denaturing of the peptide chain (removing the secondary structure) to enable a “threading” type assembly to occur.<sup>101, 554-557</sup> Other variants of PYY<sub>3-36</sub> such as the lipopeptides studied in earlier Chapters, 3 and 4, could also be of interest to study in this regard. Further controls using cyclodextrin complexing molecules would be of interest to help delve deeper into what is occurring in the aggregation of  $\beta$ -cyclodextrin and PYY<sub>3-36</sub>. Small drug molecules (such as meropenem, or camptothecin), or larger surfactants such as SDS or dodecyltrimethylammonium bromide (DTAB) would be suggested for this purpose, as they all have been studied via similar characterisation methods.

## 7. Conclusions and Future Work

### 7.1 Thesis Conclusions

The conclusions of the experimental work contained within the four previous chapters will be summarised in this section.

The characterisation of the novel lipidated PYY molecule (17PYY<sub>3-36</sub>) was completed and further investigations were carried out into its potential to form a gel. 17PYY<sub>3-36</sub> showed a reduction in its  $\alpha$ -helical structure compared to that of the native peptide (Chapter 3.4). Although experimentation showed a reduction in  $\alpha$ -helical content, the lipopeptide itself showed a more stable response to pH and temperature changes (Chapter 3.4) than the native peptide, except at its pI when it precipitates out of solution. The pH values investigated were chosen to align with those found within the human body, from pH 2 in the stomach to pH 7.4 in the large intestine.<sup>344</sup> The observations demonstrated that if 17PYY<sub>3-36</sub> were given as a drug it would undergo less secondary structure changes, if kept away from its pI, which would potentially give it valuable increased stability.

Further experiments showed that the addition of the lipid causes a different self-assembly process, namely from twisted sheets to thin fibre structures (Chapter 3). The concentration at which 17PYY<sub>3-36</sub> molecule assembled was investigated, with greater acidic pH values (pH 2) leading to an increased critical aggregation concentration (Chapter 3.5). This observation showed that the charges of the surrounding solution affects the assembly process, giving weight to the hypothesis that the pH within the body will affect the assembly process as well.

Investigation into the secondary structure of the fibres showed them to be  $\alpha$ -helical in nature at lower temperatures (Chapter 3.4). This changed at 45 °C with the internal structure changing to a  $\beta$ -sheet structure (Chapter 3.4, Fig. 27 B). Although this temperature is slightly above the normal temperature for the human body, 37 °C, it does add information to the need for any 17PYY<sub>3-36</sub> related drug to be stored and transported under careful conditions. The  $\alpha$ -helical structure of the native peptide has been shown to be important for Y receptor recognition, so any change in the secondary structure could limit, if not inhibit, the drug's potency.<sup>271, 273, 333</sup>

Studies into the gels formed from these lipopeptides; 11, 17 and 23PYY<sub>3-36</sub>, showed that the ability to form a gel through dehydration was possible at different pH values (Chapter 4.2,

Table 5). Further studies showed the gels were formed because of the lipidation, as native PYY<sub>3-36</sub> did not form gels at the same pH values for lipidated versions.

The average gel concentration was found to be 1.7 wt% with circular dichroism spectroscopy showing them to have a secondary structure of  $\beta$ -sheet (Chapter 4.5). This was similar in structure to that seen in the previous studies of the lipopeptides above 45 °C. The  $\alpha$ -helical structure to  $\beta$ -sheet structural change was also shown to be extremely important for the formation of the gel (Chapter 4.6). Further studies, using TEM, allowed the visualisation of the entangled network of fibres which formed up the gel material (Chapter 4.4). These gels showed a loss of structure when heated after being formed, and this loss was also shown to be irreversible after cooling (Chapter 4.4, Fig. 35). So, again, this lends further importance to the need to control temperature when manufacturing or handling these gels.

This study has shown the potential for lipidation to create a gel from a peptide hormone, which could be extremely important from a drug delivery perspective. This process could allow for the reduction in additives and reduce research into formulation, ending up with simpler and safer delivery systems.

Other studies in this thesis investigated the lipidated 17PYY<sub>3-36</sub> and its interactions with another short self-assembled bio-important molecule, LPS. Another anti-bacterial short peptide A9R was used as a comparison peptide. Visual and cryo-TEM experiments showed the presence of aggregations, between 17PYY<sub>3-36</sub> and LPS, which consequently prompted further investigation (Chapter 5.2). A9R showed separate formation of structures with little cross-assembly (Chapter 5.6). Within this study it was shown that these LPS-17PYY<sub>3-36</sub> aggregates had a reduced  $\alpha$ -helical secondary structure compared to that of the native peptide (Chapter 5.4, Fig. 39). This change in structure was also confirmed by SAXS analysis, with a shift from fibre to bilayer formation being seen (Chapter 5.3, Fig. 38).

Due to organisation budgetary constraints only 120 mg of each lipopeptide were made available for this study. To overcome this problem and ensure that progress could be made experiments were completed with the cheaper non-lipidated native peptide PYY<sub>3-36</sub>. Studies using zeta potentials, LPS specific dyes and fluorescence showed that PYY<sub>3-36</sub> interacted heavily with LPS, whereas A9R did not (Chapter 5.11). This work did provide an insight into the importance and need to continue investigating how a peptide hormone like PYY<sub>3-36</sub> interacts with a molecule like LPS.

A different drug delivery method for PYY<sub>3-36</sub> was also suggested within this thesis, namely that of using the molecule  $\beta$ -cyclodextrin.  $\beta$ -cyclodextrin has been extensively studied for its ability to encapsulate smaller drug molecules and has also been shown to have the ability in complexation to form potentially useful self-assembled structures.<sup>558-565</sup>

Various ratios of PYY<sub>3-36</sub> and  $\beta$ -cyclodextrin, were investigated using a variety of spectroscopic techniques. Many of these experiments showed little to no co-self-assembly (Chapter 6). The most notable observation was that during SAXS analysis the complex showed a change in structure for the 1:1 wt% ratio (1:3.6 molarity ratio) complex as well as for higher ratios of  $\beta$ -cyclodextrin (Chapter 6.4). This effect was then further investigated and was shown to be an aggregation of the  $\beta$ -cyclodextrin molecules to the highly charged outer edge of the PYY<sub>3-36</sub> twisted tape like structure (Chapter 6.5, Fig. 53).

Further investigations, which used the aromatic residues of the peptide chain as indicators, showed no change in their environments when PYY<sub>3-36</sub> was mixed with  $\beta$ -cyclodextrin (Chapter 6.6). Measuring the overall charge of the molecules in solutions also produced similar results (Chapter 6.7). Both experiments lend even further evidence to there being no co-assembly of PYY<sub>3-36</sub> and  $\beta$ -cyclodextrin, but that there is solely aggregation between the charged aspects of both molecules.

In summary, 17PYY<sub>3-36</sub> was characterised in conditions close to biological pH values (2-8)<sup>344</sup> and within a wide range of temperatures (20-70 °C). The potential for the lipopeptides to form gels was investigated. Gels of 11, 17 and 23PYY<sub>3-36</sub> were then characterised, with their fibre parameters defined. Further studies investigating the interactions of 17PYY<sub>3-36</sub>, or native PYY<sub>3-36</sub> with LPS and  $\beta$ -cyclodextrin were completed. These studies have shown aggregation of LPS and  $\beta$ -cyclodextrin by observing the charge effects between the structures. Many of these results advance the study of large lipopeptides, from the characterisation of a novel bioactive peptide (17PYY<sub>3-36</sub>) to co-assembly studies with different excipients (LPS and  $\beta$ -cyclodextrin).

## 7.2 Future Work

High cost of the lipidated peptides (11, 17 and 23PYY<sub>3-36</sub>) meant that further syntheses of these lipopeptides limited the scope of these studies. With additional supplies of these lipopeptides, bacterial cell tests and biological receptor experiments would prove to be the most impactful as they would add more information to the effects of lipidation on the bioactivity of these

peptides. The other aspect of this biological based research would give further insights into the effect of self-assembly on the efficacy of a self-assembling drug molecule.

Further experiments into the effect of different solutions on the self-assembly of these lipopeptides would also determine if changing the solution medium (hydrophilic to hydrophobic) affects the secondary structure or overall macro-structures formed. Some drug formulations can rely on excipients, for example through the addition of ions or small molecules, and as such, further studies that investigate these excipients and their impact on macro-structures and the nature of their bonding would be beneficial to carry out. The kinetics of aggregation would also be useful to investigate, as these are important for drug formulation and delivery. Repeating the experiments with the use of buffer systems, such as a phosphate buffer that can be tailored to pH 5.8 to 8, or a Tris buffer that can pH 7.1 to 8.9, would provide further confidence in the results as this approach would help keep a consistent pH throughout the different experimental methods used.

With additional lipopeptide 11, 17 and 23PYY<sub>3-36</sub> further studies into the release profile of the gels would be of interest. In addition, these studies would add to the characterisation of the lipopeptide and the gels. Although this affect has been seen before for other gels it would be important to study this gelation effect and its property on drug delivery. Another important aspect of gels is their rheology profile or flow characteristics. This is important to investigate as certain viscous gels cannot be injected. The issue with this type of experiment is that it needs large quantities of sample and with the limited sample provided for this thesis, this area of investigation was not pursued. The fibrils formed by the gels are also closely related to the structure of the harmful amyloid fibrils, further experiments using a fibril specific dye, such as conga red, can probe this potential structural similarity.

Further studies relating to the complexation of LPS with 17PYY<sub>3-36</sub> and the effects on biological cells would also be of particular interest as this complexation potentially reduces the toxic effects of LPS on cells. Secondly, one could investigate the difference in complexation between the three lipidated PYY<sub>3-36</sub> and LPS. The previous experiments were only specific to that of 17PYY<sub>3-36</sub> (Chapter 5). It would be useful to see, if the lipidation position changes the LPS complexation affect, as was similarly seen in their characterisation analysis (Chapter 3 and 4). There are also further SAXS analytical methods that would help to probe the complexation of LPS and 17PYY<sub>3-36</sub>, such as using the absolute intensity method that would enable the determination of the volume fraction of each chemical in the mixture. This technique

would work extremely well with mixed samples and would enable individual shapes and volume fractions to be separated for each component of the mixture. With additional lipopeptide samples, future studies could be completed to enable a more detailed comparison of the separate samples of LPS and 17PYY<sub>3-36</sub> to the mixture of the two.

Another study that would be useful to complete, would be to investigate fragments of PYY<sub>3-36</sub> with LPS. This could show which segment, peptide (hydrophobic or hydrophilic) or lipid, is complexed to LPS, could have implications for other drug interactions. Adding other drugs, like that of A9R, in a complexation study could reveal other valuable observations with regards to interactions with LPS. The TAT peptide, or beta-amyloid, with well over 220,000 publications each (as of 2019) would appear to be a strong candidate for this comparison.

As mentioned within the conclusion of Chapter 6 the study of  $\beta$ -cyclodextrin and PYY<sub>3-36</sub> showed no co-aggregation. Other studies have shown  $\beta$ -cyclodextrin to have a “threading” affect with many other molecules, so this should still be followed up. The main area that should be investigated is, if the denatured peptide could thread within  $\beta$ -cyclodextrin, and once threaded, potentially co-assemble, locking  $\beta$ -cyclodextrin to the native peptide. As stated earlier, the pH of the mixed  $\beta$ -cyclodextrin and PYY<sub>3-36</sub> samples was not recorded, therefore repeating the experiments, whilst recording the pH value, would be of use to improve knowledge in this area, particularly as it is known that pH can be instrumental in self-assembly process.

Finally, a set of co-assembly experiments, using the lipidated forms 11, 17 and 23PYY<sub>3-36</sub>, with  $\beta$ -cyclodextrin, are also suggested as the results could yield valuable information on whether the co-assembly could limit, or even stop, self-assembly of the fibre-like structures through the “shielding” of the lipid from the other hydrophobic lipid environments. This proposed study may also reveal the formation of new self-assembled structures.

## References

1. NHS Obesity Conditions. <https://www.nhs.uk/conditions/obesity/>.
2. Baker, C. Obesity Statistics, Briefing Paper, Number 3336. <https://commonslibrary.parliament.uk/research-briefings/sn03336/>.
3. CDC, Data Brief - Overweight + Obese Survey. **2018**.
4. Organisation, W. H. Obesity in Adults. [https://www.who.int/gho/ncd/risk\\_factors/overweight\\_obesity/obesity\\_adults/en/](https://www.who.int/gho/ncd/risk_factors/overweight_obesity/obesity_adults/en/).
5. CDC Adult Obesity Causes. <https://www.cdc.gov/obesity/adult/causes.html>.
6. Tatemoto, K., Isolation and Characterization of Peptide Yy (Pyy), a Candidate Gut Hormone That Inhibits Pancreatic Exocrine Secretion. *P Natl Acad Sci-Biol* **1982**, 79 (8), 2514-2518.
7. Fujii, N.; Saito, T., Homochirality and life. *The Chemical Record* **2004**, 4 (5), 267-278.
8. Pergande, M. R.; Cologna, S. M., Isoelectric Point Separations of Peptides and Proteins. *Proteomes* **2017**, 5 (1).
9. Fasoli, E.; Castillo, B.; Santos, A.; Silva, E.; Ferrer, A.; Rosario, E.; Griebenow, K.; Secundo, F.; Barletta, G. L., Activation of subtilisin Carlsberg in organic solvents by methyl-beta-cyclodextrin: Lyoprotection versus substrate and product-complex effect. *J Mol Catal B-Enzym* **2006**, 42 (1-2), 20-26.
10. Norman, J. M.; Cohen, G. M.; Bampton, E. T. W., The in vitro cleavage of the hAtg proteins by cell death proteases. *Autophagy* **2010**, 6 (8), 1042-1056.
11. Kramer, R. A.; Zandwijken, D.; Egmond, M. R.; Dekker, N., In vitro folding, purification and characterization of Escherichia coli outer membrane protease OmpT. *Eur J Biochem* **2000**, 267 (3), 885-893.
12. Umate, P.; Tuteja, N.; Tuteja, R., Genome-wide comprehensive analysis of human helicases. *Commun. Integr. Biol.* **2011**, 4 (1), 118-137.
13. Wu, Y., Unwinding and rewinding: double faces of helicase? *J Nucleic Acids* **2012**, 2012, 140601-140601.
14. Hamley, I. W., Protein Assemblies: Nature-Inspired and Designed Nanostructures. *Biomacromolecules* **2019**, 20 (5), 1829-1848.
15. Saladin, K., *Anatomy & physiology: the unity of form and function*. 6th ed.
16. Ostergaard, L.; Frandsen, C. S.; Madsbad, S., Treatment potential of the GLP-1 receptor agonists in type 2 diabetes mellitus: a review. *Expert Rev. Clin. Pharmacol.* **2016**, 9 (2), 241-265.
17. Davis, P. N.; Ndefo, U. A.; Oliver, A.; Payton, E., Albiglutide: A once-weekly glucagon-like peptide-1 receptor agonist for type 2 diabetes mellitus. *Am. J. Health Syst. Pharm.* **2015**, 72 (13), 1097-1103.
18. Ryan, D.; Acosta, A., GLP-1 receptor agonists: Nonglycemic clinical effects in weight loss and beyond. *Obesity* **2015**, 23 (6), 1119-1129.
19. Grant, M.; Leone-Bay, A., Peptide therapeutics: it's all in the delivery. *Ther Deliv* **2012**, 3 (8), 981-96.
20. Holst, J. J., The Physiology of Glucagon-like Peptide 1. *Physiol. Rev.* **2007**, 87 (4), 1409-1439.
21. Huda, M. S.; Wilding, J. P.; Pinkney, J. H., Gut peptides and the regulation of appetite. *Obes. Rev.* **2006**, 7 (2), 163-82.
22. Drucker, D. J., Minireview: the glucagon-like peptides. *Endocrinology* **2001**, 142 (2), 521-7.
23. Saiani, A.; Mohammed, A.; Frielinghaus, H.; Collins, R.; Hodson, N.; Kielty, C. M.; Sherratt, M. J.; Miller, A. F., Self-assembly and gelation properties of alpha-helix versus beta-sheet forming peptides. *Soft Matter* **2009**, 5 (1), 193-202.

24. Mello, L. R.; Hamley, I. W.; Miranda, A.; Alves, W. A.; Silva, E. R., beta-sheet assembly in amyloidogenic glutamic acid nanostructures: Insights from X-ray scattering and infrared nanospectroscopy. *J Pept Sci* **2019**, e3170.
25. Jernigan, R. L.; Miyazawa, S.; Szu, S. C., Electrostatic interactions and secondary structures in proteins. *Biophys J* **1980**, *32* (1), 93-5.
26. Kanehisa, M. I.; Tsong, T. Y., Local hydrophobicity stabilizes secondary structures in proteins. *Biopolymers* **1980**, *19* (9), 1617-28.
27. Carlisle, E. A.; Holder, J. L.; Maranda, A. M.; de Alwis, A. R.; Selkie, E. L.; McKay, S. L., Effect of pH, urea, peptide length, and neighboring amino acids on alanine alpha-proton random coil chemical shifts. *Biopolymers* **2007**, *85* (1), 72-80.
28. Adhikari, B.; Palui, G.; Banerjee, A., Self-assembling tripeptide based hydrogels and their use in removal of dyes from waste-water. *Soft Matter* **2009**, *5* (18), 3452-3460.
29. Arnold, M. S.; Stupp, S. I.; Hersam, M. C., Tuning the optical properties of carbon nanotube solutions using amphiphilic self-assembly. *Quantum Sensing: Evolution and Revolution from Past to Future* **2003**, 4999, 238-248.
30. Perez, C. M. R.; Rank, L. A.; Chmielewski, J., Tuning the thermosensitive properties of hybrid collagen peptide-polymer hydrogels. *Chem. Commun.* **2014**, *50* (60), 8174-8176.
31. Tsonchev, S.; Niece, K. L.; Schatz, G. C.; Ratner, M. A.; Stupp, S. I., Phase diagram for assembly of biologically-active peptide amphiphiles. *J Phys Chem B* **2008**, *112* (2), 441-447.
32. Shen, J. L.; Xin, X.; Liu, G. K.; Pang, J. Y.; Song, Z. H.; Xu, G. Y.; Yuan, S. L., Fabrication of Smart pH-Responsive Fluorescent Solid-like Giant Vesicles by Ionic Self-Assembly Strategy. *J Phys Chem C* **2016**, *120* (48), 27533-27540.
33. Kar, T.; Mukherjee, S.; Das, P. K., Organogelation through self-assembly of low-molecular-mass amphiphilic peptide. *New J. Chem.* **2014**, *38* (3), 1158-1167.
34. Cornish-Bowden, A. J.; Koshland, D. E., Jr., The quaternary structure of proteins composed of identical subunits. *J Biol Chem* **1971**, *246* (10), 3092-102.
35. Langerman, N.; Sturtevant, J. M., Calorimetric studies of quaternary structure and ligand-binding hemerythrin. *Biochemistry-U.S.* **1971**, *10* (15), 2809-15.
36. Chulkova, T. M.; Orekhovich, V. N., On the quaternary structure of human thrombin. *Clin. Chim. Acta* **1971**, *34* (3), 493-4.
37. Fernandez, A., Therapeutically Targeted Destabilization of the Quaternary Structure of the Spike Protein in the Dominant G614 Strain of SARS-CoV-2. *ACS Pharmacol Transl Sci* **2020**, *3* (5), 1027-1029.
38. Hartmann-Petersen, R.; Tanaka, K.; Hendil, K. B., Quaternary structure of the ATPase complex of human 26S proteasomes determined by chemical cross-linking. *Arch. Biochem. Biophys.* **2001**, *386* (1), 89-94.
39. Garian, R., Prediction of quaternary structure from primary structure. *Bioinformatics* **2001**, *17* (6), 551-6.
40. Trombetta, E. S.; Fleming, K. G.; Helenius, A., Quaternary and domain structure of glycoprotein processing glucosidase II. *Biochemistry-U.S.* **2001**, *40* (35), 10717-22.
41. Bhandari, D.; Rafiq, S.; Gat, Y.; Gat, P.; Waghmare, R.; Kumar, V., A Review on Bioactive Peptides: Physiological Functions, Bioavailability and Safety. *Int. J. Pept. Res. Ther.* **2020**, *26* (1), 139-150.
42. Sánchez, A.; Vázquez, A., Bioactive peptides: A review. *Food Quality and Safety* **2017**, *1*, 29-46.
43. Daliri, E. B.-M.; Oh, D. H.; Lee, B. H., Bioactive Peptides. *Foods* **2017**, *6* (5), 32.
44. Olf, M.; Frijling, J. L.; Kubzansky, L. D.; Bradley, B.; Ellenbogen, M. A.; Cardoso, C.; Bartz, J. A.; Yee, J. R.; van Zuiden, M., The role of oxytocin in social bonding, stress

regulation and mental health: An update on the moderating effects of context and interindividual differences. *Psychoneuroendocrino* **2013**, *38* (9), 1883-1894.

45. McCormack, S. E.; Blevins, J. E.; Lawson, E. A., Metabolic Effects of Oxytocin. *Endocr. Rev.* **2020**, *41* (2), 121-145.
46. Pompella, A.; Visvikis, A.; Paolicchi, A.; Tata, V. D.; Casini, A. F., The changing faces of glutathione, a cellular protagonist. *Biochem. Pharmacol.* **2003**, *66* (8), 1499-1503.
47. Wu, G.; Fang, Y.-Z.; Yang, S.; Lupton, J. R.; Turner, N. D., Glutathione Metabolism and Its Implications for Health. *The Journal of Nutrition* **2004**, *134* (3), 489-492.
48. Huang, X. Q., Somatostatin: Likely the most widely effective gastrointestinal hormone in the human body. *World J Gastroentero* **1997**, *3* (4), 201-204.
49. Gomes-Porras, M.; Cárdenas-Salas, J.; Álvarez-Escolá, C., Somatostatin Analogs in Clinical Practice: a Review. *Int. J. Mol. Sci.* **2020**, *21* (5), 1682.
50. Scatena, R., Bivalirudin: a new generation antithrombotic drug. *Expert Opin Inv Drug* **2000**, *9* (5), 1119-1127.
51. Rousselle, C.; Clair, P.; Smirnova, M.; Kolesnikov, Y.; Pasternak, G. W.; Gac-Breton, S.; Rees, A. R.; Scherrmann, J. M.; Tamsamani, J., Improved brain uptake and pharmacological activity of dalargin using a peptide-vector-mediated strategy. *J Pharmacol Exp Ther* **2003**, *306* (1), 371-376.
52. Reardon, D. A.; Nabors, L. B.; Stupp, R.; Mikkelsen, T., Cilengitide: an integrin-targeting arginine-glycine-aspartic acid peptide with promising activity for glioblastoma multiforme. *Expert Opin Inv Drug* **2008**, *17* (8), 1225-1235.
53. Riedel, M. J.; Kieffer, T. J., Treatment of diabetes with glucagon-like peptide-1 gene therapy. *Expert Opin. Biol. Ther.* **2010**, *10* (12), 1681-1692.
54. Rosenstock, J.; Stewart, M. W., ALBIGLUTIDE Glucagon-Like Peptide GLP-1 Receptor Agonist Treatment of Type 2 Diabetes. *Drug Future* **2010**, *35* (9), 701-712.
55. Joffe, D., Liraglutide: A once-daily human glucagon-like peptide-1 analogue for type 2 diabetes mellitus. *Am. J. Health Syst. Pharm.* **2010**, *67* (16), 1326-1336.
56. Craik, D. J.; Fairlie, D. P.; Liras, S.; Price, D., The Future of Peptide-based Drugs. *Chemical Biology & Drug Design* **2013**, *81* (1), 136-147.
57. Petersen, A. B.; Knop, F. K.; Christensen, M., Lixisenatide for the Treatment of Type 2 Diabetes. *Drug Today* **2013**, *49* (9), 537-553.
58. McCormack, P. L., Exenatide Twice Daily: A Review of Its Use in the Management of Patients with Type 2 Diabetes Mellitus. *Drugs* **2014**, *74* (3), 325-351.
59. Muscogiuri, G.; Gastaldelli, A., Albiglutide for the Treatment of Type 2 Diabetes. *Drug Today* **2014**, *50* (10), 665-678.
60. Sharma, A. K.; Thanikachalam, P. V.; Rajput, S. K., Albiglutide: Is a better hope against diabetes mellitus? *Biomed. Pharmacother.* **2016**, *77*, 120-128.
61. Steenbergen, J. N.; Alder, J.; Thorne, G. M.; Tally, F. P., Daptomycin: a lipopeptide antibiotic for the treatment of serious Gram-positive infections. *J. Antimicrob. Chemother.* **2005**, *55* (3), 283-8.
62. Mohr, J. F.; Friedrich, L. V.; Yankelev, S.; Lamp, K. C., Daptomycin for the treatment of enterococcal bacteraemia: results from the Cubicin (R) Outcomes Registry and Experience (CORE). *Int. J. Antimicrob. Agents* **2009**, *33* (6), 543-548.
63. Lam, H. Y.; Gaarden, R. I.; Li, X. C., A Journey to the Total Synthesis of Daptomycin. *Chemical Record* **2014**, *14* (6), 1086-1099.
64. Pogliano, J.; Pogliano, N.; Silverman, J. A., Daptomycin-mediated reorganization of membrane architecture causes mislocalization of essential cell division proteins. *J. Bacteriol.* **2012**, *194* (17), 4494-504.
65. Kirkham, S.; Castelletto, V.; Hamley, I. W.; Inoue, K.; Rambo, R.; Reza, M.; Ruokolainen, J., Self-Assembly of the Cyclic Lipopeptide Daptomycin: Spherical Micelle

Formation Does Not Depend on the Presence of Calcium Chloride. *Chemphyschem* **2016**, *17* (14), 2118-2122.

66. Howard, B., Bacitracin. In *xPharm: The Comprehensive Pharmacology Reference*, Enna, S. J.; Bylund, D. B., Eds. Elsevier: New York, 2007; pp 1-4.

67. Lei, J.; Sun, L.; Huang, S.; Zhu, C.; Li, P.; He, J.; Mackey, V.; Coy, D. H.; He, Q., The antimicrobial peptides and their potential clinical applications. *Am J Transl Res* **2019**, *11* (7), 3919-3931.

68. Levine, J. F., Vancomycin: A Review. *Med. Clin. North Am.* **1987**, *71* (6), 1135-1145.

69. Dinu, V.; Lu, Y.; Weston, N.; Lithgo, R.; Coupe, H.; Channell, G.; Adams, G. G.; Torcello Gómez, A.; Sabater, C.; Mackie, A.; Parmenter, C.; Fisk, I.; Phillips-Jones, M. K.; Harding, S. E., The antibiotic vancomycin induces complexation and aggregation of gastrointestinal and submaxillary mucins. *Sci. Rep.* **2020**, *10* (1), 960.

70. Nakatsuji, T.; Gallo, R. L., Antimicrobial peptides: old molecules with new ideas. *The Journal of investigative dermatology* **2012**, *132* (3 Pt 2), 887-895.

71. Lee, S. S.; Huang, B. J.; Kaltz, S. R.; Sur, S.; Newcomb, C. J.; Stock, S. R.; Shah, R. N.; Stupp, S. I., Bone regeneration with low dose BMP-2 amplified by biomimetic supramolecular nanofibers within collagen scaffolds. *Biomaterials* **2013**, *34* (2), 452-459.

72. Chen, J.; Chen, X. Y.; Yang, X. Y.; Han, C. M.; Gao, C. Y.; Gou, Z. R., Bioactive glasses-incorporated, core-shell-structured polypeptide/polysaccharide nanofibrous hydrogels. *Carbohydr. Polym.* **2013**, *92* (1), 612-620.

73. Drucker, D. J., The biology of incretin hormones. *Cell Metab* **2006**, *3* (3), 153-65.

74. Huda, M. S. B.; Wilding, J. P. H.; Pinkney, J. H., Gut peptides and the regulation of appetite. *Obes. Rev.* **2006**, *7* (2), 163-182.

75. Morin, V.; Hozer, F.; Costemale-Lacoste, J. F., The effects of ghrelin on sleep, appetite, and memory, and its possible role in depression: A review of the literature. *Encephale* **2018**, *44* (3), 256-263.

76. Neal, J. M., *How the Endocrine System Works*. 2nd ed.; Wiley-Blackwell: 2016.

77. Schjoldager, B.; Mortensen, P. E.; Myhre, J.; Christiansen, J.; Holst, J. J., Oxyntomodulin from distal gut. Role in regulation of gastric and pancreatic functions. *Dig. Dis. Sci.* **1989**, *34* (9), 1411-9.

78. Wren, A. M.; Bloom, S. R., Gut Hormones and Appetite Control. *Gastroenterology* **2007**, *132* (6), 2116-2130.

79. Drucker, D. J.; Nauck, M. A., The incretin system: glucagon-like peptide-1 receptor agonists and dipeptidyl peptidase-4 inhibitors in type 2 diabetes. *The Lancet* **368** (9548), 1696-1705.

80. Schepp W, D. K., Riedel T, Schmidtler J, Schaffer K, Classen M, Oxyntomodulin: a cAMP-dependant stimulus of rat parietal cell function via the receptor for glucagon-like peptide-1 (7-36)NH<sub>2</sub>. *Digestion* **1996**, *57*, 398-405.

81. Anini Y, J. C., Chariot J, Nagain C, Oxyntomodulin inhibits pancreatic secretion through the nervous system in rats. *Pancreas* **2000**, *20*, 348-360.

82. K. Siddle, J. C. H., *Peptide Hormone Secretion/Peptide Hormone Action: A Practical Approach*. Oxford University Press: 1991.

83. Hans-Rudolf Berthoud, C. M., The Brain, Appetite, and Obesity. *The Annual Review of Psychology* **2008**, *59*, 55-92.

84. Kuehl, P. J.; Boyden, T.; Dobry, D. E.; Doyle-Eisele, M.; Friesen, D. T.; McDonald, J. D.; Murri, B. G.; Vodak, D. T.; Lyon, D. K., Inhaled PYY(3-36) dry-powder formulation for appetite suppression. *Drug Dev. Ind. Pharm.* **2016**, *42* (1), 150-156.

85. Degen, L.; Oesch, S.; Casanova, M.; Graf, S.; Ketterer, S.; Drewe, J.; Beglinger, C., Effect of peptide YY3-36 on food intake in humans. *Gastroenterology* **2005**, *129* (5), 1430-6.

86. Klok, M. D.; Jakobsdottir, S.; Drent, M. L., The role of leptin and ghrelin in the regulation of food intake and body weight in humans: a review. *Obes. Rev.* **2007**, *8* (1), 21-34.
87. Keire, D. A.; Mannon, P.; Kobayashi, M.; Walsh, J. H.; Solomon, T. E.; Reeve, J. R., Primary structures of PYY, [Pro(34)]PYY, and PYY-(3-36) confer different conformations and receptor selectivity. *Am J Physiol-Gastr L* **2000**, *279* (1), G126-G131.
88. Bernkop-Schnuerch, A.; Duennhaupt, S., Chitosan-based drug delivery systems. *European Journal of Pharmaceutics and Biopharmaceutics* **2012**, *81* (3), 463-469.
89. Hamman, J. H., Chitosan Based Polyelectrolyte Complexes as Potential Carrier Materials in Drug Delivery Systems. *Marine Drugs* **2010**, *8* (4), 1305-1322.
90. Win, K. Y.; Feng, S. S., Effects of particle size and surface coating on cellular uptake of polymeric nanoparticles for oral delivery of anticancer drugs. *Biomaterials* **2005**, *26* (15), 2713-2722.
91. Lin, Y.-H.; Sonaje, K.; Lin, K. M.; Juang, J.-H.; Mi, F.-L.; Yang, H.-W.; Sung, H.-W., Multi-ion-crosslinked nanoparticles with pH-responsive characteristics for oral delivery of protein drugs. *Journal of Controlled Release* **2008**, *132* (2), 141-149.
92. Thunemann, A. F.; Muller, M.; Dautzenberg, H.; Joanny, J. F. O.; Lowen, H., Polyelectrolyte complexes. In *Polyelectrolytes with Defined Molecular Architecture II*, Schmidt, M., Ed. 2004; Vol. 166, pp 113-171.
93. He, W.; Parowatkin, M.; Mailander, V.; Flechtner-Mors, M.; Graf, R.; Best, A.; Koynov, K.; Mohr, K.; Ziener, U.; Landfester, K.; Crespy, D., Nanocarrier for Oral Peptide Delivery Produced by Polyelectrolyte Complexation in Nanoconfinement. *Biomacromolecules* **2015**, *16* (8), 2282-2287.
94. Han, H.; Gopal, R.; Park, Y., Design and membrane-disruption mechanism of charge-enriched AMPs exhibiting cell selectivity, high-salt resistance, and anti-biofilm properties. *Amino Acids* **2016**, *48* (2), 505-522.
95. Janes, K. A.; Calvo, P.; Alonso, M. J., Polysaccharide colloidal particles as delivery systems for macromolecules. *Advanced Drug Delivery Reviews* **2001**, *47* (1), 83-97.
96. Berger, J.; Reist, M.; Mayer, J. M.; Felt, O.; Peppas, N. A.; Gurny, R., Structure and interactions in covalently and ionically crosslinked chitosan hydrogels for biomedical applications. *European Journal of Pharmaceutics and Biopharmaceutics* **2004**, *57* (1), 19-34.
97. Berger, J.; Reist, M.; Mayer, J. M.; Felt, O.; Gurny, R., Structure and interactions in chitosan hydrogels formed by complexation or aggregation for biomedical applications. *European Journal of Pharmaceutics and Biopharmaceutics* **2004**, *57* (1), 35-52.
98. Torchilin, V. P., Micellar Nanocarriers: Pharmaceutical Perspectives. *Pharm. Res.* **2006**, *24* (1), 1-16.
99. Accardo A, T. D., Mangiapia D, Pedone C, Morelli G, Nanostructures by self-assembly peptide amphiphile as potential selective drug carriers. *J. Pept. Sci.* **2006**, *88*, 115-121.
100. Mazza, M.; Notman, R.; Anwar, J.; Rodger, A.; Hicks, M.; Parkinson, G.; McCarthy, D.; Daviter, T.; Moger, J.; Garrett, N.; Mead, T.; Briggs, M.; Schatzlein, A. G.; Uchegbu, I. F., Nanofiber-Based Delivery of Therapeutic Peptides to the Brain. *Acs Nano* **2013**, *7* (2), 1016-1026.
101. Karim, A. A.; Loh, X. J., Design of a micellized alpha-cyclodextrin based supramolecular hydrogel system. *Soft Matter* **2015**, *11* (27), 5425-5434.
102. Binello, A.; Cravotto, G.; Nano, G. M.; Spagliardi, P., Synthesis of chitosan-cyclodextrin adducts and evaluation of their bitter-masking properties. *Flavour Fragrance J.* **2004**, *19* (5), 394-400.
103. Sivakumaran, D.; Maitland, D.; Hoare, T., Injectable Microgel-Hydrogel Composites for Prolonged Small-Molecule Drug Delivery. *Biomacromolecules* **2011**, *12* (11), 4112-4120.

104. Choi, S.; Baudys, M.; Kim, S. W., Control of Blood Glucose by Novel GLP-1 Delivery Using Biodegradable Triblock Copolymer of PLGA-PEG-PLGA in Type 2 Diabetic Rats. *Pharm. Res.* **2004**, *21* (5), 827-831.
105. Kim, K. S.; Park, S. J.; Yang, J. A.; Jeon, J. H.; Bhang, S. H.; Kim, B. S.; Hahn, S. K., Injectable hyaluronic acid–tyramine hydrogels for the treatment of rheumatoid arthritis. *Acta Biomater.* **2011**, *7* (2), 666-674.
106. Wu, J.; Zeng, F.; Huang, X.-P.; Chung, J. C. Y.; Konecny, F.; Weisel, R. D.; Li, R.-K., Infarct stabilization and cardiac repair with a VEGF-conjugated, injectable hydrogel. *Biomaterials* **2011**, *32* (2), 579-586.
107. Makovitzki, A.; Baram, J.; Shai, Y., Antimicrobial lipopolypeptides composed of palmitoyl di- and tricationic peptides: In vitro and in vivo activities, self-assembly to nanostructures, and a plausible mode of action. *Biochemistry-Us* **2008**, *47* (40), 10630-10636.
108. Castelletto, V.; Hamley, I. W.; Whitehouse, C.; Matts, P. J.; Osborne, R.; Baker, E. S., Self-assembly of palmitoyl lipopeptides used in skin care products. *Langmuir* **2013**, *29* (29), 9149-55.
109. Giddi, H. S.; Arunagirinathan, M. A.; Bellare, J. R., Self-assembled surfactant nanostructures important in drug delivery: a review. *Indian J. Exp. Biol.* **2007**, *45* (2), 133-59.
110. Mnif, I.; Ghribi, D., Review lipopeptides biosurfactants: Mean classes and new insights for industrial, biomedical, and environmental applications. *Peptide Science* **2015**, *104* (3), 129-147.
111. Kowalczyk, R.; Harris, P. W. R.; Williams, G. M.; Yang, S. H.; Brimble, M. A., Peptide Lipidation - A Synthetic Strategy to Afford Peptide Based Therapeutics. *Adv Exp Med Biol* **2017**, *1030*, 185-227.
112. Bech, E. M.; Pedersen, S. L.; Jensen, K. J., Chemical Strategies for Half-Life Extension of Biopharmaceuticals: Lipidation and Its Alternatives. *Acs Med Chem Lett* **2018**, *9* (7), 577-580.
113. Menacho-Melgar, R.; Decker, J. S.; Hennigan, J. N.; Lynch, M. D., A review of lipidation in the development of advanced protein and peptide therapeutics. *J. Control. Release* **2019**, *295*, 1-12.
114. Stupp, S. I.; LeBonheur, V.; Walker, K.; Li, L. S.; Huggins, K. E.; Keser, M.; Amstutz, A., Supramolecular materials: Self-organized nanostructures. *Science* **1997**, *276* (5311), 384-389.
115. Cui, H.; Muraoka, T.; Cheetham, A. G.; Stupp, S. I., Self-Assembly of Giant Peptide Nanobelts. *Nano Letters* **2009**, *9* (3), 945-951.
116. Hamley, I. W., Self-assembly of amphiphilic peptides. *Soft Matter* **2011**, *7* (9), 4122-4138.
117. Song, Z.; Chen, X.; You, X.; Huang, K.; Dhinakar, A.; Gu, Z.; Wu, J., Self-assembly of peptide amphiphiles for drug delivery: the role of peptide primary and secondary structures. *Biomater Sci* **2017**, *5* (12), 2369-2380.
118. Das, U. N., Essential Fatty acids - a review. *Curr. Pharm. Biotechnol.* **2006**, *7* (6), 467-82.
119. Yashodhara, B. M.; Umakanth, S.; Pappachan, J. M.; Bhat, S. K.; Kamath, R.; Choo, B. H., Omega-3 fatty acids: a comprehensive review of their role in health and disease. *Postgrad. Med. J.* **2009**, *85* (1000), 84.
120. Shahidi, F.; Senanayake, S. P. J. N., Fatty Acids. In *International Encyclopedia of Public Health*, Heggenhougen, H. K., Ed. Academic Press: Oxford, 2008; pp 594-603.
121. Liu, X.; Mallapragada, S., Bioinspired Synthesis of Organic/Inorganic Nanocomposite Materials Mediated by Biomolecules. 2011.

122. Palmer, L. C.; Newcomb, C. J.; Kaltz, S. R.; Spoerke, E. D.; Stupp, S. I., Biomimetic Systems for Hydroxyapatite Mineralization Inspired By Bone and Enamel. *Chem. Rev.* **2008**, *108* (11), 4754-4783.
123. Bensaude-Vincent, B., Self-Assembly, Self-Organization: Nanotechnology and Vitalism. *NanoEthics* **2009**, *3*, 31-42.
124. Bancroft, J. B.; Hills, G. J.; Markham, R., A study of the self-assembly process in a small spherical virus. Formation of organized structures from protein subunits in vitro. *Virology* **1967**, *31* (2), 354-79.
125. Armspach, D.; Ashton, P.; Moore, C. P.; Spencer, N.; Stoddart, J. F.; Wear, T. J.; Williams, D. J., The Self-Assembly of Catenated Cyclodextrins. *Angew Chem Int Edit* **1993**, *32* (6), 854-858.
126. Stupp, S. I., Self-assembly of rodcoil molecules. *Current Opinion in Colloid & Interface Science* **1998**, *3* (1), 20-26.
127. Pralle, M. U.; Whitaker, C. M.; Braun, P. V.; Stupp, S. I., Molecular variables in the self-assembly of supramolecular nanostructures. *Macromolecules* **2000**, *33* (10), 3550-3556.
128. Hartgerink, J. D.; Beniash, E.; Stupp, S. I., Self-assembly and mineralization of peptide-amphiphile nanofibers. *Science* **2001**, *294* (5547), 1684-1688.
129. Li, L. M.; Zubarev, E. R.; Acker, B. A.; Stupp, S. I., Chemical structure and nonlinear optical properties of polar self-assembling films. *Macromolecules* **2002**, *35* (7), 2560-2565.
130. Messmore, B. W.; Hulvat, J. F.; Sone, E. D.; Stupp, S. I., Synthesis, self-assembly, and characterization of supramolecular polymers from electroactive dendron rodcoil molecules. *J. Am. Chem. Soc.* **2004**, *126* (44), 14452-14458.
131. Stupp, S. I., Biomaterials for regenerative medicine. *MRS Bull.* **2005**, *30* (7), 546-553.
132. Sone, E. D.; Zubarev, E. R.; Stupp, S. I., Supramolecular templating of single and double nanohelices of cadmium sulfide. *Small* **2005**, *1* (7), 694-697.
133. Stupp, S. I., Self-assembly of wires and helices. *Abstr Pap Am Chem S* **2006**, 231.
134. Guler, M. O.; Stupp, S. I., A self-assembled nanofiber catalyst for ester hydrolysis. *J. Am. Chem. Soc.* **2007**, *129* (40), 12082-+.
135. Stupp, S. I., POLY 30-Self-assembly of macromolecules and small molecules across the scales. *Abstr Pap Am Chem S* **2007**, 234.
136. Sargeant, T. D.; Oppenheimer, S. M.; Dunand, D. C.; Stupp, S. I., Titanium foam-bioactive nanofiber hybrids for bone regeneration. *J. Tissue Eng. Regen. Med.* **2008**, *2* (8), 455-462.
137. Palmer, L. C.; Stupp, S. I., Molecular Self-Assembly into One-Dimensional Nanostructures. *Acc. Chem. Res.* **2008**, *41* (12), 1674-1684.
138. Rajagopal, K.; Lamm, M. S.; Haines-Butterick, L. A.; Pochan, D. J.; Schneider, J. P., Tuning the pH Responsiveness of beta-Hairpin Peptide Folding, Self-Assembly, and Hydrogel Material Formation. *Biomacromolecules* **2009**, *10* (9), 2619-2625.
139. Shera, J. N.; Sun, X. S., Effect of peptide sequence on surface properties and self-assembly of an amphiphilic pH-responsive peptide. *Biomacromolecules* **2009**, *10* (9), 2446-50.
140. Cui, H.; Webber, M. J.; Stupp, S. I., Self-Assembly of Peptide Amphiphiles: From Molecules to Nanostructures to Biomaterials. *Biopolymers* **2010**, *94* (1), 1-18.
141. Stupp, S. I., Self-Assembly and Biomaterials. *Nano Letters* **2010**, *10* (12), 4783-4786.
142. Huang, R. L.; Qi, W.; Feng, L. B.; Su, R. X.; He, Z. M., Self-assembling peptide-polysaccharide hybrid hydrogel as a potential carrier for drug delivery. *Soft Matter* **2011**, *7* (13), 6222-6230.
143. Newcomb, C. J.; Bitton, R.; Velichko, Y. S.; Snead, M. L.; Stupp, S. I., The Role of Nanoscale Architecture in Supramolecular Templating of Biomimetic Hydroxyapatite Mineralization. *Small* **2012**, *8* (14), 2195-2202.

144. Stupp, S. I.; Zha, R. H.; Palmer, L. C.; Cui, H. G.; Bitton, R., Self-assembly of biomolecular soft matter. *Faraday Discuss.* **2013**, *166*, 9-30.
145. Glassman, M. J.; Chan, J.; Olsen, B. D., Reinforcement of Shear Thinning Protein Hydrogels by Responsive Block Copolymer Self-Assembly. *Adv. Funct. Mater.* **2013**, *23* (9), 1182-1193.
146. Dehsorkhi, A.; Castelletto, V.; Hamley, I. W., Self-assembling amphiphilic peptides. *J Pept Sci* **2014**, *20* (7), 453-67.
147. Mandal, D.; Nasrolahi Shirazi, A.; Parang, K., Self-assembly of peptides to nanostructures. *Org Biomol Chem* **2014**, *12* (22), 3544-61.
148. Weingarten, A. S.; Kazantsev, R. V.; Palmer, L. C.; McClendon, M.; Koltonow, A. R.; Samuel, A. P. S.; Kiebal, D. J.; Wasielewski, M. R.; Stupp, S. I., Self-assembling hydrogel scaffolds for photocatalytic hydrogen production. *Nat. Chem.* **2014**, *6* (11), 964-970.
149. Stupp, S. I.; Palmer, L. C., Supramolecular Chemistry and Self-Assembly in Organic Materials Design. *Chem. Mater.* **2014**, *26* (1), 507-518.
150. Nguyen, M. K.; Alsberg, E., Bioactive factor delivery strategies from engineered polymer hydrogels for therapeutic medicine. *Prog. Polym. Sci.* **2014**, *39* (7), 1235-1265.
151. Wang, J. W.; Song, L. F.; Zhao, J.; Yuan, X. B., Polymer Hydrogels Based on Peptide Structure. *Prog Chem* **2015**, *27* (4), 373-384.
152. Shen, L. L.; Zhao, L. Z.; Qu, R.; Huang, F.; Gao, H. J.; An, Y. L.; Shi, L. Q., Complex micelles with the bioactive function of reversible oxygen transfer. *Nano Res* **2015**, *8* (2), 491-501.
153. Liu, G.; Chen, X. I.; Zhou, W. U.; Yang, S.; Ye, S.; Cao, F.; Liu, Y. I.; Xiong, Y., Preparation of a novel composite nanofiber gel-encapsulated human placental extract through layer-by-layer self-assembly. *Exp. Ther. Med.* **2016**, *11* (4), 1447-1452.
154. Hamley, I. W.; Hutchinson, J.; Kirkham, S.; Castelletto, V.; Kaur, A.; Reza, M.; Ruokolainen, J., Nanosheet Formation by an Anionic Surfactant-like Peptide and Modulation of Self-Assembly through Ionic Complexation. *Langmuir* **2016**, *32* (40), 10387-10393.
155. Lu, S.; Li, M.; Liu, D.; Yang, Y.; Yang, P., Self-Assembly of Au Nanoparticles and Quantum Dots by Functional Sol-Gel Silica Layers. *J Nanosci Nanotechnol* **2018**, *18* (1), 288-295.
156. Castelletto, V.; Barnes, R. H.; Karatzas, K. A.; Edwards-Gayle, C. J. C.; Greco, F.; Hamley, I. W.; Seitsonen, J.; Ruokolainen, J., Restructuring of Lipid Membranes by an Arginine-Capped Peptide Bolaamphiphile. *Langmuir* **2019**, *35* (5), 1302-1311.
157. Hutchinson, J. A.; Hamley, I. W.; Edwards-Gayle, C. J. C.; Castelletto, V.; Piras, C.; Cramer, R.; Kowalczyk, R.; Seitsonen, J.; Ruokolainen, J.; Rambo, R. P., Melanin production by tyrosinase activity on a tyrosine-rich peptide fragment and pH-dependent self-assembly of its lipidated analogue. *Org Biomol Chem* **2019**, *17* (18), 4543-4553.
158. Albert, J. N.; Epps III, T. H., Self-assembly of block copolymer thin films. *Mater. Today* **2010**, *13* (6), 24-33.
159. Bowerman, C. J.; Nilsson, B. L., Review self-assembly of amphipathic  $\beta$ -sheet peptides: insights and applications. *Peptide Science* **2012**, *98* (3), 169-184.
160. Chaudhary, A.; Yadav, R. D., A review on virus protein self-assembly. *J. Nanopart. Res.* **2019**, *21* (11), 254.
161. Bishop, K. J.; Wilmer, C. E.; Soh, S.; Grzybowski, B. A., Nanoscale forces and their uses in self-assembly. *Small* **2009**, *5* (14), 1600-1630.
162. Jain, N.; Trabelsi, S.; Guillot, S.; McLoughlin, D.; Langevin, D.; Letellier, P.; Turmine, M., Critical Aggregation Concentration in Mixed Solutions of Anionic Polyelectrolytes and Cationic Surfactants. *Langmuir* **2004**, *20* (20), 8496-8503.
163. Wang, D.; Dong, R.; Long, P.; Hao, J., Photo-induced phase transition from multilamellar vesicles to wormlike micelles. *Soft Matter* **2011**, *7* (22), 10713.

164. Kirkham, S.; Hamley, I. W.; Smith, A. M.; Gouveia, R. M.; Connon, C. J.; Reza, M.; Ruokolainen, J., A self-assembling fluorescent dipeptide conjugate for cell labelling. *Colloids and Surfaces B: Biointerfaces* **2015**.
165. Lowik, D. W.; Leunissen, E. H.; van den Heuvel, M.; Hansen, M. B.; van Hest, J. C., Stimulus responsive peptide based materials. *Chem Soc Rev* **2010**, *39* (9), 3394-412.
166. Gouveia, R. M.; Castelletto, V.; Hamley, I. W.; Connon, C. J., New self-assembling multifunctional templates for the biofabrication and controlled self-release of cultured tissue. *Tissue Eng Part A* **2015**, *21* (11-12), 1772-84.
167. Melo, E. P.; Aires-Barros, M. R.; Cabral, J. M. S., Reverse micelles and protein biotechnology. In *Biotechnol. Ann. Rev.*, Elsevier: 2001; Vol. 7, pp 87-129.
168. Alexandridis, P.; Andersson, K., Reverse Micelle Formation and Water Solubilization by Polyoxyalkylene Block Copolymers in Organic Solvent. *The Journal of Physical Chemistry B* **1997**, *101* (41), 8103-8111.
169. Sandoval, C.; Ortega, A.; Sanchez, S. A.; Morales, J.; Gunther, G., Structuration in the Interface of Direct and Reversed Micelles of Sucrose Esters, Studied by Fluorescent Techniques. *Plos One* **2015**, *10* (4), e0123669.
170. Xu, Z. G.; Liu, S. Y.; Liu, H.; Yang, C. J.; Kang, Y. J.; Wang, M. F., Unimolecular micelles of amphiphilic cyclodextrin-core star-like block copolymers for anticancer drug delivery. *Chem. Commun.* **2015**, *51* (87), 15768-15771.
171. Arnold, M. S.; Guler, M. O.; Hersam, M. C.; Stupp, S. I., Encapsulation of carbon nanotubes by self-assembling peptide amphiphiles. *Langmuir* **2005**, *21* (10), 4705-4709.
172. Arnold, M. S.; Green, A. A.; Hulvat, J. F.; Stupp, S. I.; Hersam, M. C., Sorting carbon nanotubes by electronic structure using density differentiation. *Nat Nanotechnol* **2006**, *1* (1), 60-65.
173. Hamley, I. W.; Burholt, S.; Hutchinson, J.; Castelletto, V.; da Silva, E. R.; Alves, W.; Gutfreund, P.; Porcar, L.; Dattani, R.; Hermida-Merino, D.; Newby, G.; Reza, M.; Ruokolainen, J.; Stasiak, J., Correction to Shear Alignment of Bola-Amphiphilic Arginine-Coated Peptide Nanotubes. *Biomacromolecules* **2017**, *18* (5), 1660.
174. Hamley, I. W.; Burholt, S.; Hutchinson, J.; Castelletto, V.; da Silva, E. R.; Alves, W.; Gutfreund, P.; Porcar, L.; Dattani, R.; Hermida-Merino, D.; Newby, G.; Reza, M.; Ruokolainen, J.; Stasiak, J., Shear Alignment of Bola-Amphiphilic Arginine-Coated Peptide Nanotubes. *Biomacromolecules* **2017**, *18* (1), 141-149.
175. Meegan, J. E.; Aggeli, A.; Boden, N.; Brydson, R.; Brown, A. P.; Carrick, L.; Ansell, R. J., EFTEM investigation of silica nanotubes produced using designed self assembling beta-sheet peptide fibrils as templates. *Inst Phys Conf Ser* **2004**, (179), 475-478.
176. Han, Y.; He, C.; Cao, M.; Huang, X.; Wang, Y.; Li, Z., Facile disassembly of amyloid fibrils using gemini surfactant micelles. *Langmuir* **2010**, *26* (3), 1583-7.
177. Ikeda, K.; Okada, T.; Sawada, S.; Akiyoshi, K.; Matsuzaki, K., Inhibition of the formation of amyloid beta-protein fibrils using biocompatible nanogels as artificial chaperones. *Febs Lett* **2006**, *580* (28-29), 6587-6595.
178. Krysmann, M. J.; Castelletto, V.; Kelarakis, A.; Hamley, I. W.; Hule, R. A.; Pochan, D. J., Self-assembly and hydrogelation of an amyloid peptide fragment. *Biochemistry-Us* **2008**, *47* (16), 4597-4605.
179. Qahwash, I. M.; Boire, A.; Lanning, J.; Krausz, T.; Pytel, P.; Meredith, S. C., Site-specific effects of peptide lipidation on beta-amyloid aggregation and cytotoxicity. *J Biol Chem* **2007**, *282* (51), 36987-97.
180. Segers-Nolten, I.; van Raaij, M.; Subramaniam, V., 2.19 Biophysical Analysis of Amyloid Formation. In *Comprehensive Biomaterials II*, Ducheyne, P., Ed. Elsevier: Oxford, 2017; pp 438-451.

181. Gershfeld, N. L., Phospholipid surface bilayers at the air-water interface. III. Relation between surface bilayer formation and lipid bilayer assembly in cell membranes. *Biophys J* **1986**, *50* (3), 457-61.
182. Gruenewald, B.; Frisch, W.; Holzwarth, J. F., The kinetics of the formation of rotational isomers in the hydrophobic tail region of phospholipid bilayers. *Biochim Biophys Acta* **1981**, *641* (2), 311-9.
183. Boni, L. T.; Stewart, T. P.; Alderfer, J. L.; Hui, S. W., Lipid-polyethylene glycol interactions: II. Formation of defects in bilayers. *J. Membr. Biol.* **1981**, *62* (1-2), 71-7.
184. Schindler, H., Formation of planar bilayers from artificial or native membrane vesicles. *Febs Lett* **1980**, *122* (1), 77-9.
185. Lee, H. K.; Soukasene, S.; Jiang, H. Z.; Zhang, S. M.; Feng, W. C.; Stupp, S. I., Light-induced self-assembly of nanofibers inside liposomes. *Soft Matter* **2008**, *4* (5), 962-964.
186. Gustafsson, J.; Arvidson, G.; Karlsson, G.; Almgren, M., Complexes between cationic liposomes and DNA visualized by cryo-TEM. *Biochim Biophys Acta* **1995**, *1235* (2), 305-12.
187. Jones, R. R.; Castelletto, V.; Connon, C. J.; Hamley, I. W., Collagen stimulating effect of peptide amphiphile C16-KTTKS on human fibroblasts. *Mol. Pharm.* **2013**, *10* (3), 1063-9.
188. Dehsorkhi, A.; Castelletto, V.; Hamley, I. W., Self-assembling amphiphilic peptides. *Journal of peptide science : an official publication of the European Peptide Society* **2014**, *20* (7), 453-467.
189. Pakalns, T.; L. Haverstick, K.; Fields, G. B.; McCarthy, J. B.; L. Mooradian, D.; Tirrell, M., Cellular recognition of synthetic peptide amphiphiles in self-assembled monolayer films. *Biomaterials* **1999**, *20* (23), 2265-2279.
190. Guo, J.; Su, H.; Zeng, Y.; Liang, Y.-X.; Wong, W. M.; Ellis-Behnke, R. G.; So, K.-F.; Wu, W., Reknitting the injured spinal cord by self-assembling peptide nanofiber scaffold. *Nanomed. Nanotechnol. Biol. Med.* **2007**, *3* (4), 311-321.
191. Hamley, I. W., Lipopeptides: from self-assembly to bioactivity. *Chem Commun (Camb)* **2015**, *51* (41), 8574-83.
192. Zhang, P.; Cheetham, A. G.; Lin, Y. A.; Cui, H., Self-assembled Tat nanofibers as effective drug carrier and transporter. *ACS Nano* **2013**, *7* (7), 5965-77.
193. Daptomycin (Cubicin) for skin and soft tissue infections. *Med. Lett. Drugs Ther.* **2004**, *46* (1175), 11-12.
194. New molecular entities - Cubicin - Daptomycin for injection - CUBIST - First approval in a new class of antibiotics. *Formulary* **2003**, *38* (10), 571-572.
195. Azmi, F.; Elliott, A. G.; Marasini, N.; Ramu, S.; Ziora, Z.; Kavanagh, A. M.; Blaskovich, M. A. T.; Cooper, M. A.; Skwarczynski, M.; Toth, I., Short cationic lipopeptides as effective antibacterial agents: Design, physicochemical properties and biological evaluation. *Biorg. Med. Chem.* **2016**, *24* (10), 2235-2241.
196. Baltz, R. H.; Miao, V.; Wrigley, S. K., Natural products to drugs: daptomycin and related lipopeptide antibiotics. *Nat. Prod. Rep.* **2005**, *22* (6), 717-41.
197. Chuang, Y. C.; Wang, J. T.; Lin, H. Y.; Chang, S. C., Daptomycin versus linezolid for treatment of vancomycin-resistant enterococcal bacteremia: systematic review and meta-analysis. *BMC Infect. Dis.* **2014**, *14*.
198. Taylor, R.; Butt, K.; Scott, B.; Zhang, T. H.; Muraih, J. K.; Mintzer, E.; Taylor, S.; Palmer, M., Two successive calcium-dependent transitions mediate membrane binding and oligomerization of daptomycin and the related antibiotic A54145. *Bba-Biomembranes* **2016**, *1858* (9), 1999-2005.
199. Budovich, A.; Blum, S.; Berger, B., Daptomycin-induced hyperkalemia in a patient with normal renal function. *Am. J. Health Syst. Pharm.* **2014**, *71* (24), 2137-2141.
200. Durante-Mangoni, E.; Andini, R.; Parrella, A.; Mattucci, I.; Cavezza, G.; Senese, A.; Trojaniello, C.; Caprioli, R.; Diana, M. V.; Utili, R., Safety of treatment with high-dose

- daptomycin in 102 patients with infective endocarditis. *Int. J. Antimicrob. Agents* **2016**, *48* (1), 61-68.
201. McCormack, P. L.; Perry, C. M., Caspofungin. *Drugs* **2005**, *65* (14), 2049-2068.
202. Brajtburg, J.; Powderly, W. G.; Kobayashi, G. S.; Medoff, G., Amphotericin B: current understanding of mechanisms of action. *Antimicrob. Agents Chemother.* **1990**, *34* (2), 183-188.
203. Giuliani, A.; Pirri, G.; Nicoletto, S., Antimicrobial peptides: an overview of a promising class of therapeutics. *Open Life Sciences* **2007**, *2* (1), 1-33.
204. Pirri, G.; Giuliani, A.; Nicoletto, S.; Pizzuto, L.; Rinaldi, A., Lipopeptides as anti-infectives: a practical perspective. *Open Life Sciences* **2009**, *4* (3), 258-273.
205. Allahyari, M.; Mohit, E., Peptide/protein vaccine delivery system based on PLGA particles. *Hum. Vaccin. Immunother.* **2016**, *12* (3), 806-828.
206. Altunbas, A.; Pochan, D. J., Peptide-Based and Polypeptide-Based Hydrogels for Drug Delivery and Tissue Engineering. *Peptide-Based Materials* **2012**, *310*, 135-167.
207. Cai, Y. E.; Zhang, W. J.; Chen, Z. R.; Shi, Z.; He, C. W.; Chen, M. W., Recent insights into the biological activities and drug delivery systems of tanshinones. *International Journal of Nanomedicine* **2016**, *11*, 121-130.
208. Chaturvedi, K.; Ganguly, K.; Nadagouda, M. N.; Aminabhavi, T. M., Polymeric hydrogels for oral insulin delivery. *Journal of Controlled Release* **2013**, *165* (2), 129-138.
209. Chen, X. C.; Chen, H. M.; Tripisciano, C.; Jedrzejewska, A.; Rummeli, M. H.; Klingeler, R.; Kalenczuk, R. J.; Chu, P. K.; Borowiak-Palen, E., Carbon-Nanotube-Based Stimuli-Responsive Controlled-Release System. *Chem-Eur J* **2011**, *17* (16), 4454-4459.
210. Guler, M. O.; Hsu, L.; Soukasene, S.; Harrington, D. A.; Hulvat, J. F.; Stupp, S. I., Presentation of RGDS epitopes on self-assembled nanofibers of branched peptide amphiphiles. *Biomacromolecules* **2006**, *7* (6), 1855-1863.
211. Hutchinson, J. A.; Burholt, S.; Hamley, I. W., Peptide hormones and lipopeptides: from self-assembly to therapeutic applications. *J Pept Sci* **2017**, *23* (2), 82-94.
212. Ito, T.; Saito, M.; Uchino, T.; Senna, M.; Iafisco, M.; Prat, M.; Rimondini, L.; Otsuka, M., Preparation of injectable auto-forming alginate gel containing simvastatin with amorphous calcium phosphate as a controlled release medium and their therapeutic effect in osteoporosis model rat. *J. Mater. Sci. Mater. Med.* **2012**, *23* (5), 1291-7.
213. Kim, J. K.; Anderson, J.; Jun, H. W.; Repka, M. A.; Jo, S., Self-Assembling Peptide Amphiphile-Based Nanofiber Gel for Bioresponsive Cisplatin Delivery. *Mol. Pharm.* **2009**, *6* (3), 978-985.
214. Kim, J. Y.; Lee, H.; Oh, K. S.; Kweon, S.; Jeon, O. C.; Byun, Y.; Kim, K.; Kwon, I. C.; Kim, S. Y.; Yuk, S. H., Multilayer nanoparticles for sustained delivery of exenatide to treat type 2 diabetes mellitus. *Biomaterials* **2013**, *34* (33), 8444-8449.
215. Kojima, C.; Nishisaka, E.; Suehiro, T.; Watanabe, K.; Harada, A.; Goto, T.; Magata, Y.; Kono, K., The synthesis and evaluation of polymer prodrug/collagen hybrid gels for delivery into metastatic cancer cells. *Nanomed-Nanotechnol* **2013**, *9* (6), 767-775.
216. Kojima, C.; Suehiro, T.; Watanabe, K.; Ogawa, M.; Fukuhara, A.; Nishisaka, E.; Harada, A.; Kono, K.; Inui, T.; Magata, Y., Doxorubicin-conjugated dendrimer/collagen hybrid gels for metastasis-associated drug delivery systems. *Acta Biomater.* **2013**, *9* (3), 5673-5680.
217. Kreuter, J., Nanoparticulate systems for brain delivery of drugs. *Advanced Drug Delivery Reviews* **2012**, *64*, 213-222.
218. Lalatsa, A.; Lee, V.; Malkinson, J. P.; Zloh, M.; Schatzlein, A. G.; Uchegbu, I. F., A Prodrug Nanoparticle Approach for the Oral Delivery of a Hydrophilic Peptide, Leucine(5)-enkephalin, to the Brain. *Mol. Pharm.* **2012**, *9* (6), 1665-1680.
219. Lattin, J. R.; Belnap, D. M.; Pitt, W. G., Formation of eLiposomes as a drug delivery vehicle. *Colloids Surf. B. Biointerfaces* **2012**, *89*, 93-100.

220. Li, Y.; Shao, M. X.; Zheng, X. M.; Kong, W. L.; Zhang, J. N.; Gong, M., Self-Assembling Peptides Improve the Stability of Glucagon-like Peptide-1 by Forming a Stable and Sustained Complex. *Mol. Pharm.* **2013**, *10* (9), 3356-3365.
221. Lu, X. Y.; Gao, H.; Li, C.; Yang, Y. W.; Wang, Y. N.; Fan, Y. G.; Wu, G. L.; Ma, J. B., Polyelectrolyte complex nanoparticles of amino poly(glycerol methacrylate)s and insulin. *Int. J. Pharm.* **2012**, *423* (2), 195-201.
222. Matson, J. B.; Newcomb, C. J.; Bitton, R.; Stupp, S. I., Nanostructure-templated control of drug release from peptide amphiphile nanofiber gels. *Soft Matter* **2012**, *8* (13), 3586-3595.
223. Matson, J. B.; Stupp, S. I., Drug release from hydrazone-containing peptide amphiphiles. *Chem. Commun.* **2011**, *47* (28), 7962-7964.
224. Zhang, P.; Cheetham, A. G.; Lin, Y.-A.; Cui, H., Self-assembled Tat nanofibers as effective drug carrier and transporter. *ACS nano* **2013**, *7* (7), 5965-5977.
225. Gray, P. E. A., A 5th type of hypersensitivity reaction: Does incidental recruitment of autoreactive effector memory T-cells in response to minute amounts of PAMPs or DAMPs, underlie inflammatory episodes in the seronegative arthropathies and acute anterior uveitis? *Med. Hypotheses* **2009**, *73* (3), 284-291.
226. Boekhoven, J.; Stupp, S. I., 25th Anniversary Article: Supramolecular Materials for Regenerative Medicine. *Adv. Mater.* **2014**, *26* (11), 1642-1659.
227. Kreuter, J.; Shamenkov, D.; Petrov, V.; Range, P.; Cychutek, K.; Koch-Brandt, C.; Alyautdin, R., Apolipoprotein-mediated transport of nanoparticle-bound drugs across the blood-brain barrier. *J. Drug Targeting* **2002**, *10* (4), 317-325.
228. Kreuter, J., Application of nanoparticles for the delivery of drugs to the brain. *Drug Transport(ers) and the Diseased Brain* **2005**, *1277*, 85-94.
229. Kreuter, J.; Alyautdin, R. N.; Kharkevich, D. A.; Ivanov, A. A., Passage of Peptides through the Blood-Brain-Barrier with Colloidal Polymer Particles (Nanoparticles). *Brain Res* **1995**, *674* (1), 171-174.
230. Liu, L. H.; Xu, K. J.; Wang, H. Y.; Tan, P. K. J.; Fan, W. M.; Venkatraman, S. S.; Li, L. J.; Yang, Y. Y., Self-assembled cationic peptide nanoparticles as an efficient antimicrobial agent. *Nat Nanotechnol* **2009**, *4* (7), 457-463.
231. Hudson, S. P.; Langer, R.; Fink, G. R.; Kohane, D. S., Injectable in situ cross-linking hydrogels for local antifungal therapy. *Biomaterials* **2010**, *31* (6), 1444-1452.
232. Wang, J. Q.; Sun, Y. J.; Dai, J. R.; Zhao, Y. R.; Cao, M. W.; Wang, D.; Xu, H., Effects of Alkyl Chain Length and Peptide Charge Distribution on Self-Assembly and Hydrogelation of Lipopeptide Amphiphiles. *Acta Phys-Chim Sin* **2015**, *31* (7), 1365-1373.
233. Mellati, A.; Dai, S.; Bi, J.; Jin, B.; Zhang, H., A biodegradable thermosensitive hydrogel with tuneable properties for mimicking three-dimensional microenvironments of stem cells. *Rsc Adv* **2014**, *4* (109), 63951-63961.
234. Thorburn Burns, D.; Lewis, R. J.; Bridges, J., Systematic approach to the identification of water-gel explosives. *Anal. Chim. Acta* **1998**, *375* (3), 255-260.
235. Mi, S. L.; Khutoryanskiy, V. V.; Jones, R. R.; Zhu, X. P.; Hamley, I. W.; Connon, C. J., Photochemical cross-linking of plastically compressed collagen gel produces an optimal scaffold for corneal tissue engineering. *Journal of Biomedical Materials Research Part A* **2011**, *99a* (1), 1-8.
236. Gouveia, R. M.; Jones, R. R.; Hamley, I. W.; Connon, C. J., The bioactivity of composite Fmoc-RGDS-collagen gels. *Biomater Sci-Uk* **2014**, *2* (9), 1222-1229.
237. Ahmed, E. M., Hydrogel: Preparation, characterization, and applications: A review. *Journal of Advanced Research* **2015**, *6* (2), 105-121.
238. Ahmed, T. A.; Alharby, Y. A.; El-Helw, A. R.; Hosny, K. M.; El-Say, K. M., Depot injectable atorvastatin biodegradable in situ gel: development, optimization, in vitro, and in vivo evaluation. *Drug Des. Devel. Ther.* **2016**, *10*, 405-15.

239. Shekhawat, M.; Surti, Z.; Surti, N., Biodegradable in situ Gel for Subcutaneous Administration of Simvastatin for Osteoporosis. *Indian J. Pharm. Sci.* **2018**, *80*, 395-399.
240. Smith, D. K., Lost in translation? Chirality effects in the self-assembly of nanostructured gel-phase materials. *Chemical Society Reviews* **2009**, *38* (3), 684-694.
241. Gao, X.; Huang, Y. X.; Makhov, A. M.; Epperly, M.; Lu, J. Q.; Grab, S.; Zhang, P. J.; Rohan, L.; Xie, X. Q.; Wipf, P.; Greenberger, J.; Li, S., Nanoassembly of Surfactants with Interfacial Drug-Interactive Motifs as Tailor-Designed Drug Carriers. *Mol. Pharm.* **2013**, *10* (1), 187-198.
242. Yan, X.; Xu, D.; Chi, X.; Chen, J.; Dong, S.; Ding, X.; Yu, Y.; Huang, F., A multiresponsive, shape-persistent, and elastic supramolecular polymer network gel constructed by orthogonal self-assembly. *Adv. Mater.* **2012**, *24* (3), 362-9.
243. Srinivasan, S.; Babu, P. A.; Mahesh, S.; Ajayaghosh, A., Reversible self-assembly of entrapped fluorescent gelators in polymerized styrene gel matrix: erasable thermal imaging via recreation of supramolecular architectures. *J. Am. Chem. Soc.* **2009**, *131* (42), 15122-3.
244. Coates, I. A.; Smith, D. K., Controlled self-assembly-synthetic tunability and covalent capture of nanoscale gel morphologies. *Chemistry (Easton)* **2009**, *15* (26), 6340-4.
245. Wu, J.; Yi, T.; Xia, Q.; Zou, Y.; Liu, F.; Dong, J.; Shu, T.; Li, F.; Huang, C., Tunable gel formation by both sonication and thermal processing in a cholesterol-based self-assembly system. *Chemistry (Easton)* **2009**, *15* (25), 6234-43.
246. Nithitanakool, S.; Pithayanukul, P.; Bourgeois, S.; Fessi, H.; Bavovada, R., The development, physicochemical characterisation and in vitro drug release studies of pectinate gel beads containing Thai mango seed kernel extract. *Molecules* **2013**, *18* (6), 6504-20.
247. Jansen, M. M.; Verzijl, J. M.; Burger, D. M.; Hekster, Y. A., Controlled release of morphine from a poloxamer 407 gel. *Int. J. Pharm.* **2013**, *452* (1-2), 266-9.
248. Akash, M. S.; Rehman, K.; Sun, H.; Chen, S., Assessment of release kinetics, stability and polymer interaction of poloxamer 407-based thermosensitive gel of interleukin-1 receptor antagonist. *Pharm. Dev. Technol.* **2014**, *19* (3), 278-84.
249. Florczyk, S. J.; Leung, M.; Jana, S.; Li, Z.; Bhattarai, N.; Huang, J. I.; Hopper, R. A.; Zhang, M., Enhanced bone tissue formation by alginate gel-assisted cell seeding in porous ceramic scaffolds and sustained release of growth factor. *J. Biomed. Mater. Res. A* **2012**, *100* (12), 3408-15.
250. Simsek, S.; Canter, H. I.; Konas, E.; Korkusuz, P.; Demir, D.; Oner, F.; Unsal, I.; Mavili, M. E., A new concept in treatment of burn injury: controlled slow-release granulocyte-monocyte colony-stimulating factor chitosan gel system. *Ann. Plast. Surg.* **2011**, *67* (6), 583-8.
251. Hedegaard, S. F.; Cardenas, M.; Barker, R.; Jorgensen, L.; van de Weert, M., Lipidation Effect on Surface Adsorption and Associated Fibrillation of the Model Protein Insulin. *Langmuir* **2016**, *32* (28), 7241-9.
252. Gatto, E.; Mazzuca, C.; Stella, L.; Venanzi, M.; Toniolo, C.; Pispisa, B., Effect of peptide lipidation on membrane perturbing activity: a comparative study on two trichogin analogues. *J Phys Chem B* **2006**, *110* (45), 22813-8.
253. Sparks, D. L.; Frank, P. G.; Braschi, S.; Neville, T. A.; Marcel, Y. L., Effect of apolipoprotein A-I lipidation on the formation and function of pre-beta and alpha-migrating LpA-I particles. *Biochemistry-Us* **1999**, *38* (6), 1727-35.
254. Mohanram, H.; Bhattacharjya, S., beta-Boomerang Antimicrobial and Antiendotoxic Peptides: Lipidation and Disulfide Bond Effects on Activity and Structure. *Pharmaceuticals (Basel)* **2014**, *7* (4), 482-501.
255. Endocrine Peptides Website. <https://pacbio.com/news-media/white-paper/incretins-gastrointestinal-hormones/>.

256. Baltaci, A. K.; Mogulkoc, R.; Baltaci, S. B., Review: The role of zinc in the endocrine system. *Pak. J. Pharm. Sci.* **2019**, *32* (1), 231-239.
257. Tang, M. W.; Garcia, S.; Gerlag, D. M.; Tak, P. P.; Reedquist, K. A., Insight into the Endocrine System and the Immune System: A Review of the Inflammatory Role of Prolactin in Rheumatoid Arthritis and Psoriatic Arthritis. *Front. Immunol.* **2017**, *8*, 720.
258. Poddar, M.; Chetty, Y.; Chetty, V. T., How does obesity affect the endocrine system? A narrative review. *Clin Obes* **2017**, *7* (3), 136-144.
259. Bauer, D. G., Review of the endocrine system. *Medsurg Nurs.* **2005**, *14* (5), 335-7.
260. Grodzenskii, D. E., [Radiation effects & the endocrine system; review of experimental data]. *Med. Radiol. (Mosk.)* **1959**, *4* (5), 77-83.
261. Cummings, D. E.; Overduin, J., Gastrointestinal regulation of food intake. *J Clin Invest* **2007**, *117* (1), 13-23.
262. Coll, A. P.; Farooqi, I. S.; O'Rahilly, S., The hormonal control of food intake. *Cell* **2007**, *129* (2), 251-62.
263. Klok, M. D.; Jakobsdottir, S.; Drent, M. L., The role of leptin and ghrelin in the regulation of food intake and body weight in humans: a review. *Obes. Rev.* **2007**, *8* (1), 21-34.
264. Anderson, S. L.; Trujillo, J. M., Lixisenatide in type 2 diabetes: latest evidence and clinical usefulness. *Therapeutic advances in chronic disease* **2016**, *7* (1), 4-17.
265. Fala, L., Trulicity (Dulaglutide): A New GLP-1 Receptor Agonist Once-Weekly Subcutaneous Injection Approved for the Treatment of Patients with Type 2 Diabetes. *American health & drug benefits* **2015**, *8* (Spec Feature), 131-4.
266. Bond, A., Exenatide (Byetta) as a novel treatment option for type 2 diabetes mellitus. *Proc. (Bayl. Univ. Med. Cent.)* **2006**, *19* (3), 281-284.
267. Gallagher, J. Obesity: Appetite drug could mark 'new era' in tackling condition. <https://www.bbc.co.uk/news/health-56011979>.
268. RI, H., The pancreatic polypeptide (PP-fold) family: gastrointestinal, vascular, and feeding behavioural implication. *Exp. Biol. Med.* **1993**, *203*, 44-63.
269. McTigue, D. M.; Rogers, R. C., Pancreatic polypeptide stimulates gastric motility through a vagal-dependant mechanism in rats. *Neurosci Lett* **1995**, *188*, 93-96.
270. Troke, R. C.; Tan, T. M.; Bloom, S. R., The future role of gut hormones in the treatment of obesity. *Therapeutic advances in chronic disease* **2014**, *5* (1), 4-14.
271. Nygaard, R.; Nielbo, S.; Schwartz, T. W.; Poulsen, F. M., The PP-fold solution structure of human polypeptide YY and human PYY3-36 as determined by NMR. *Biochemistry-Us* **2006**, *45* (27), 8350-7.
272. Cabrele, C.; Beck-Sickinger, A. G., Molecular characterization of the ligand-receptor interaction of the neuropeptide Y family. *J Pept Sci* **2000**, *6* (3), 97-122.
273. Larhammar, D., Structural diversity of receptors for neuropeptide Y, peptide YY and pancreatic polypeptide. *Regul Peptides* **1996**, *65* (3), 165-174.
274. Albertsen, L.; Andersen, J. J.; Paulsson, J. F.; Thomsen, J. K.; Norrild, J. C.; Stromgaard, K., Design and Synthesis of Peptide YY Analogues with C-terminal Backbone Amide-to-Ester Modifications. *Acs Med Chem Lett* **2013**, *4* (12), 1228-32.
275. Germain, N.; Minnion, J. S.; Tan, T.; Shillito, J.; Gibbard, C.; Ghatei, M.; Bloom, S., Analogs of pancreatic polypeptide and peptide YY with a locked PP-fold structure are biologically active. *Peptides* **2013**, *39*, 6-10.
276. De Silva, A.; Salem, V.; Long, C. J.; Makwana, A.; Newbould, R. D.; Rabiner, E. A.; Ghatei, M. A.; Bloom, S. R.; Matthews, P. M.; Beaver, J. D.; Dhillon, W. S., The gut hormones PYY 3-36 and GLP-1 7-36 amide reduce food intake and modulate brain activity in appetite centers in humans. *Cell Metab* **2011**, *14* (5), 700-6.

277. Gendall, K. A.; Kaye, W. H.; Altemus, M.; McConaha, C. W.; La Via, M. C., Leptin, neuropeptide Y, and peptide YY in long-term recovered eating disorder patients. *Biol Psychiat* **1999**, *46* (2), 292-299.
278. Hoentjen, F.; Hopman, W. P. M.; Maas, M. I. M.; Jansen, J. B. M. J., Role of circulating peptide YY in the inhibition of gastric acid secretion by dietary fat in humans. *Scand J Gastroentero* **2000**, *35* (2), 166-171.
279. Batterham, R. L.; Cowley, M. A.; Small, C. J.; Herzog, H.; Cohen, M. A.; Dakin, C. L.; Wren, A. M.; Brynes, A. E.; Low, M. J.; Ghatei, M. A.; Cone, R. D.; Bloom, S. R., Gut hormone PYY(3-36) physiologically inhibits food intake. *Nature* **2002**, *418* (6898), 650-4.
280. Batterham, R. L.; Bloom, S. R., The gut hormone peptide YY regulates appetite. *Ann Ny Acad Sci* **2003**, *994*, 162-168.
281. Tschop, M.; Castaneda, T. R.; Joost, H. G.; Thone-Reineke, C.; Ortmann, S.; Klaus, S.; Hagan, M. M.; Chandler, P. C.; Oswald, K. D.; Benoit, S. C.; Seeley, R. J.; Kinzig, K. P.; Moran, T. H.; Beck-sickinger, A. G.; Koglin, N.; Rodgers, R. J.; Blundell, J. E.; Ishii, Y.; Beattie, A. H.; Holch, P.; Allison, D. B.; Raun, K.; Madsen, K.; Wulff, B. S.; Stidsen, C. E.; Birringer, M.; Kreuzer, O. J.; Schindler, M.; Arndt, K.; Rudolf, K.; Mark, M.; Deng, X. Y.; Whitcomb, D. C.; Halem, H.; Taylor, J.; Dong, J.; Datta, R.; Culler, M.; Craney, S.; Flora, D.; Smiley, D.; Heiman, M. L., Physiology: does gut hormone PYY3-36 decrease food intake in rodents? *Nature* **2004**, *430* (6996), 1 p following 165; discussion 2 p following 165.
282. Batterham, R. L.; Cohen, M. A.; Ellis, S. M.; Le Roux, C. W.; Withers, D. J.; Frost, G. S.; Ghatei, M. A.; Bloom, S. R., Inhibition of food intake in obese subjects by peptide YY3-36. *N. Engl. J. Med.* **2003**, *349* (10), 941-8.
283. Chelikani, P. K.; Haver, A. C.; Reidelberger, R. D., Dose-dependent effects of peptide YY(3-36) on conditioned taste aversion in rats. *Peptides* **2006**, *27* (12), 3193-201.
284. Hurtado, M. D.; Sergeev, V. G.; Acosta, A.; Spegele, M.; La Sala, M.; Waler, N. J.; Chiriboga-Hurtado, J.; Currlin, S. W.; Herzog, H.; Dotson, C. D.; Gorbatyuk, O. S.; Zolotukhin, S., Salivary peptide tyrosine-tyrosine 3-36 modulates ingestive behavior without inducing taste aversion. *J Neurosci* **2013**, *33* (47), 18368-80.
285. Scott, V.; Kimura, N.; Stark, J. A.; Luckman, S. M., Intravenous peptide YY3-36 and Y2 receptor antagonism in the rat: effects on feeding behaviour. *J. Neuroendocrinol.* **2005**, *17* (7), 452-7.
286. Robinson, A. L., Electron Microscope Inventors Share Nobel Physics Prize: Ernst Ruska built the first electron microscope in 1931; Gerd Binnig and Heinrich Rohrer developed the scanning tunneling microscope 50 years later. *Science* **1986**, *234* (4778), 821-2.
287. Ten Hove, J. B.; van Oosterom, M. N.; van Leeuwen, F. W. B.; Velders, A. H., Nanoparticles reveal Extreme Size-Sorting and Morphologies in Complex Coacervate Superstructures. *Sci. Rep.* **2018**, *8* (1), 13820.
288. Beveridge, T. J., Understanding the shapes of bacteria just got more complicated. *Mol. Microbiol.* **2006**, *62* (1), 1-4.
289. Braun, H. G.; Cardoso, A. Z., Self-assembly of Fmoc-diphenylalanine inside liquid marbles. *Colloid Surface B* **2012**, *97*, 43-50.
290. Harris, P. TEM Presentation. <https://www.reading.ac.uk/EMLab/EventsandOutreach/ElectronMicroscopy/EMLab-Workshop-PDF-presentation.aspx>.
291. Williams, D. B., Electron Microscopy: Transmission. In *Encyclopedia of Materials: Science and Technology*, Buschow, K. H. J.; Cahn, R. W.; Flemings, M. C.; Ilshner, B.; Kramer, E. J.; Mahajan, S.; Veyssi re, P., Eds. Elsevier: Oxford, 2001; pp 2577-2584.
292. Warner, D.; Branam, R.; Hargus, W.; Goebel, D., *Low Current Cerium Hexaboride and Lanthanum Hexaboride Hollow Cathodes*. 2008.

293. Eaton, P.; Quaresma, P.; Soares, C.; Neves, C.; de Almeida, M. P.; Pereira, E.; West, P., A direct comparison of experimental methods to measure dimensions of synthetic nanoparticles. *Ultramicroscopy* **2017**, *182*, 179-190.
294. Golding, C. G.; Lamboo, L. L.; Beniac, D. R.; Booth, T. F., The scanning electron microscope in microbiology and diagnosis of infectious disease. *Sci. Rep.* **2016**, *6* (1), 26516.
295. Cho, H.-J.; Hyun, J.-K.; Kim, J.-G.; Jeong, H.; Park, H.; You, D.-J.; Jung, H., Measurement of ice thickness on vitreous ice embedded cryo-EM grids: investigation of optimizing condition for visualizing macromolecules. *Journal of Analytical Science and Technology* **2013**, *4*.
296. Ted Pella, I. Pelco Silicon Aperture Frames (without support film). [https://www.tedpella.com/grids\\_html/silicon-aperture.htm](https://www.tedpella.com/grids_html/silicon-aperture.htm) (accessed 25/05/2019).
297. Franken, L. E.; Boekema, E. J.; Stuart, M. C. A., Transmission Electron Microscopy as a Tool for the Characterization of Soft Materials: Application and Interpretation. *Advanced Science* **2017**, *4* (5), 1600476.
298. Newcomb, C. J.; Moyer, T. J.; Lee, S. S.; Stupp, S. I., Advances in cryogenic transmission electron microscopy for the characterization of dynamic self-assembling nanostructures. *Current Opinion in Colloid & Interface Science* **2012**, *17* (6), 350-359.
299. Lee, J.; Saha, A.; Pancera, S. M.; Kempter, A.; Rieger, J.; Bose, A.; Tripathi, A., Shear free and blotless cryo-TEM imaging: a new method for probing early evolution of nanostructures. *Langmuir* **2012**, *28* (9), 4043-6.
300. Attia, J.; Remita, S.; Jonic, S.; Lacaze, E.; Faure, M. C.; Larquet, E.; Goldmann, M., Radiation-induced synthesis and cryo-TEM characterization of silver nanoshells on linoleate spherical micelles. *Langmuir* **2007**, *23* (19), 9523-6.
301. Sone, E. D.; Weiner, S.; Addadi, L., Biomineralization of limpet teeth: a cryo-TEM study of the organic matrix and the onset of mineral deposition. *J. Struct. Biol.* **2007**, *158* (3), 428-44.
302. Ferreira, D. A.; Bentley, M. V.; Karlsson, G.; Edwards, K., Cryo-TEM investigation of phase behaviour and aggregate structure in dilute dispersions of monoolein and oleic acid. *Int. J. Pharm.* **2006**, *310* (1-2), 203-12.
303. Murata, K.; Wolf, M., Cryo-electron microscopy for structural analysis of dynamic biological macromolecules. *Biochimica et Biophysica Acta (BBA) - General Subjects* **2018**, *1862* (2), 324-334.
304. Lodge, T. P.; Maxwell, A. L.; Lott, J. R.; Schmidt, P. W.; McAllister, J. W.; Morozova, S.; Bates, F. S.; Li, Y.; Sammler, R. L., Gelation, Phase Separation, and Fibril Formation in Aqueous Hydroxypropylmethylcellulose Solutions. *Biomacromolecules* **2018**, *19* (3), 816-824.
305. Hutchinson, J. A.; Burholt, S.; Hamley, I. W.; Lundback, A. K.; Uddin, S.; Gomes Dos Santos, A.; Reza, M.; Seitsonen, J.; Ruokolainen, J., The Effect of Lipidation on the Self-Assembly of the Gut-Derived Peptide Hormone PYY3-36. *Bioconjug. Chem.* **2018**, *29* (7), 2296-2308.
306. Boge, L.; Bysell, H.; Ringstad, L.; Wennman, D.; Umerska, A.; Cassisa, V.; Eriksson, J.; Joly-Guillou, M. L.; Edwards, K.; Andersson, M., Lipid-Based Liquid Crystals As Carriers for Antimicrobial Peptides: Phase Behavior and Antimicrobial Effect. *Langmuir* **2016**, *32* (17), 4217-4228.
307. Matson, J. B.; Navon, Y.; Bitton, R.; Stupp, S. I., Light-Controlled Hierarchical Self-Assembly of Polyelectrolytes and Supramolecular Polymers. *Acs Macro Lett* **2015**, *4* (1), 43-47.
308. Baral, A.; Basak, S.; Basu, K.; Dehsorkhi, A.; Hamley, I. W.; Banerjee, A., Time-dependent gel to gel transformation of a peptide based supramolecular gelator. *Soft Matter* **2015**, *11* (24), 4944-4951.

309. Cheng, G.; Castelletto, V.; Jones, R. R.; Connon, C. J.; Hamley, I. W., Hydrogelation of self-assembling RGD-based peptides. *Soft Matter* **2011**, *7* (4), 1326-1333.
310. Zubarev, E. R.; Sone, E. D.; Stupp, S. I., The molecular basis of self-assembly of dendron-rod-coils into one-dimensional nanostructures. *Chem-Eur J* **2006**, *12* (28), 7313-7327.
311. Edwards-Gayle, C. J. C.; Khunti, N.; Hamley, I. W.; Inoue, K.; Cowieson, N.; Rambo, R., Design of a multipurpose sample cell holder for the Diamond Light Source high-throughput SAXS beamline B21. *Journal of Synchrotron Radiation* **2021**, *28* (1).
312. Basham, M.; Filik, J.; Wharmby, M.; Chang, P.; El Kassaby, B.; Gerring, M.; Aishima, J.; Levik, K. E.; Pulford, B.; Sikharulidze, I.; Sneddon, D.; Webber, M.; Dhesi, S.; Maccherozzi, F.; Svensson, O.; Brockhauser, S.; Náray, G.; Ashton, A., Data Analysis WorkbeNch (DAWN). *Journal of Synchrotron Radiation* **2015**, *22*.
313. Förster, S.; Apostol, L.; Bras, W., Scatter: software for the analysis of nano- and mesoscale small-angle scattering. *J. Appl. Crystallogr.* **2010**, *43* (3), 639-646.
314. Livsey, I., Neutron scattering from concentric cylinders. Intraparticle interference function and radius of gyration. *Journal of the Chemical Society, Faraday Transactions 2: Molecular and Chemical Physics* **1987**, *83* (8), 1445-1452.
315. Onsager, L., THE EFFECTS OF SHAPE ON THE INTERACTION OF COLLOIDAL PARTICLES. *Ann. N.Y. Acad. Sci.* **1949**, *51* (4), 627-659.
316. Porod, G., Theorie der diffusen Röntgenkleinwinkelstreuung an kolloiden Systemen. *Zeitschrift für Naturforschung A* **1949**, *4* (6), 401-414.
317. Hammouda, B., Form Factors for Branched Polymers with Excluded Volume. *J. Res. Natl. Inst. Stand. Technol.* **2016**, *121*, 139+.
318. Hammouda, B., Small-Angle Scattering From Branched Polymers. *Macromol. Theory Simul.* **2012**, *21* (6), 372-381.
319. Pabst, G.; Rappolt, M.; Amenitsch, H.; Laggner, P., Structural information from multilamellar liposomes at full hydration: full q-range fitting with high quality x-ray data. *Physical review. E, Statistical physics, plasmas, fluids, and related interdisciplinary topics* **2000**, *62* (3 Pt B), 4000-9.
320. Pabst, G.; Koschuch, R.; Pozo-Navas, B.; Rappolt, M.; Lohner, K.; Laggner, P., Structural analysis of weakly ordered membrane stacks. *J. Appl. Crystallogr.* **2003**, *36* (6), 1378-1388.
321. Wei, Y.; Thyparambil, A.; A Latour, R., Protein Helical Structure Determination Using CD Spectroscopy for Solutions with Strong Background Absorbance from 190-230 nm. *Biochim Biophys Acta* **2014**, *1844*.
322. Yost, M.; Bremner, F. J.; Helmer, R. J.; Chino, M.-E. C., The effect of smoothing functions on data obtained from a FFT. *Behav. Res. Methods Instrum. Comput.* **1986**, *18* (2), 263-266.
323. Inouye, T.; Harper, T.; Rasmussen, N. C., Application of fourier transforms to the analysis of spectral data. *Nuclear Instruments and Methods* **1969**, *67* (1), 125-132.
324. Kosarev, E. L.; Pantos, E., Optimal smoothing of 'noisy' data by fast Fourier transform. *Journal of Physics E: Scientific Instruments* **1983**, *16* (6), 537-543.
325. Anthis, N. J.; Clore, G. M., Sequence-specific determination of protein and peptide concentrations by absorbance at 205 nm. *Protein science : a publication of the Protein Society* **2013**, *22* (6), 851-858.
326. Scopes, R. K., Measurement of protein by spectrophotometry at 205 nm. *Anal Biochem* **1974**, *59* (1), 277-282.
327. NanoDrop:How it works.  
<https://www.thermofisher.com/uk/en/home/industrial/spectroscopy-elemental-isotope-analysis/molecular-spectroscopy/ultraviolet-visible-visible-spectrophotometry-uv-vis-vis/uv->

[vis-vis-instruments/nanodrop-microvolume-spectrophotometers/nanodrop-products-guide/nanodrop-how-it-works.html](http://vis-vis-instruments/nanodrop-microvolume-spectrophotometers/nanodrop-products-guide/nanodrop-how-it-works.html) (accessed 23/05/2019).

328. Kumar, A.; Dixit, C. K., 3 - Methods for characterization of nanoparticles. In *Advances in Nanomedicine for the Delivery of Therapeutic Nucleic Acids*, Nimesh, S.; Chandra, R.; Gupta, N., Eds. Woodhead Publishing: 2017; pp 43-58.
329. Greenwood, R.; Kendall, K., Selection of Suitable Dispersants for Aqueous Suspensions of Zirconia and Titania Powders using Acoustophoresis. *J. Eur. Ceram. Soc.* **1999**, *19* (4), 479-488.
330. Hanaor, D.; Michelazzi, M.; Leonelli, C.; Sorrell, C. C., The effects of carboxylic acids on the aqueous dispersion and electrophoretic deposition of ZrO<sub>2</sub>. *J. Eur. Ceram. Soc.* **2012**, *32* (1), 235-244.
331. J Wood, S.; A Miller, K.; A David, S., Anti-Endotoxin Agents. 1. Development of a Fluorescent Probe Displacement Method Optimized for the Rapid Identification of Lipopolysaccharide-Binding Agents. *Combinatorial Chem. High Throughput Screening* **2004**, *7*, 239-49.
332. Wood, S. J.; Miller, K. A.; David, S. A., Anti-endotoxin agents. 1. Development of a fluorescent probe displacement method optimized for the rapid identification of lipopolysaccharide-binding agents. *Combinatorial Chem. High Throughput Screening* **2004**, *7* (3), 239-249.
333. Xu, B.; Fallmar, H.; Boukharta, L.; Pruner, J.; Lundell, I.; Mohell, N.; Gutierrez-de-Teran, H.; Aqvist, J.; Larhammar, D., Mutagenesis and Computational Modeling of Human G-Protein-Coupled Receptor Y2 for Neuropeptide Y and Peptide YY. *Biochemistry-Us* **2013**, *52* (45), 7987-7998.
334. Swanson-Vethamuthu, M.; Dubin, P. L.; Almgren, M.; Li, Y., Cryo-TEM of Polyelectrolyte-Micelle Complexes. *J. Colloid Interface Sci.* **1997**, *186* (2), 414-9.
335. Moren, A. K.; Regev, O.; Khan, A., A Cryo-TEM Study of Protein-Surfactant Gels and Solutions. *J. Colloid Interface Sci.* **2000**, *222* (2), 170-178.
336. Hamley, I. W.; Castelletto, V.; Moulton, C.; Myatt, D.; Siligardi, G.; Oliveira, C. L. P.; Pedersen, J. S.; Abutbul, I.; Danino, D., Self-Assembly of a Modified Amyloid Peptide Fragment: pH-Responsiveness and Nematic Phase Formation. *Macromol. Biosci.* **2010**, *10* (1), 40-48.
337. McKenzie, B. E.; de Visser, J. F.; Portale, G.; Hermida-Merino, D.; Friedrich, H.; Bomans, P. H.; Bras, W.; Monaghan, O. R.; Holder, S. J.; Sommerdijk, N. A., The evolution of bicontinuous polymeric nanospheres in aqueous solution. *Soft Matter* **2016**, *12* (18), 4113-22.
338. Minakata, H.; Iwashita, T., Synthesis of analogues of peptide YY with modified N-terminal regions: relationships of amphiphilic secondary structures and activity in rat vas deferens. *Biopolymers* **1990**, *29* (1), 61-7.
339. Lerch, M.; Mayrhofer, M.; Zerbe, O., Structural similarities of micelle-bound peptide YY (PYY) and neuropeptide Y (NPY) are related to their affinity profiles at the Y receptors. *J Mol Biol* **2004**, *339* (5), 1153-1168.
340. Keire, D. A.; Kobayashi, M.; Solomon, T. E.; Reeve, J. R., Solution structure of monomeric peptide YY supports the functional significance of the PP-fold. *Biochemistry-Us* **2000**, *39* (32), 9935-9942.
341. Keire, D. A.; Bowers, C. W.; Solomon, T. E.; Reeve, J. R., Structure and receptor binding of PYY analogs. *Peptides* **2002**, *23* (2), 305-321.
342. Henry, K. E.; Kerwood, D. J.; Allis, D. G.; Workinger, J. L.; Bonaccorso, R. L.; Holz, G. G.; Roth, C. L.; Zubieta, J.; Doyle, R. P., Solution Structure and Constrained Molecular Dynamics Study of Vitamin B12 Conjugates of the Anorectic Peptide PYY(3-36). *Chemmedchem* **2016**, *11* (9), 1015-21.

343. Hegefeld, W. A.; Kuczera, K.; Jas, G. S., Structural dynamics of neuropeptide hPYY. *Biopolymers* **2011**, *95* (7), 487-502.
344. Sciences, N.-M. L. pH in the Body. <https://www.news-medical.net/health/pH-in-the-Human-Body.aspx> (accessed 16/12/2020).
345. Greenfield, M. A.; Hoffman, J. R.; de la Cruz, M. O.; Stupp, S. I., Tunable Mechanics of Peptide Nanofiber Gels. *Langmuir* **2010**, *26* (5), 3641-3647.
346. Bitton, R.; Chow, L. W.; Zha, R. H.; Velichko, Y. S.; Pashuck, E. T.; Stupp, S. I., Electrostatic Control of Structure in Self-Assembled Membranes. *Small* **2014**, *10* (3), 500-505.
347. Hulvat, J. F.; Sofos, M.; Tajima, K.; Stupp, S. I., Self-assembly and luminescence of oligo(p-phenylene vinylene) amphiphiles. *J. Am. Chem. Soc.* **2005**, *127* (1), 366-372.
348. Leung, C. Y.; Palmer, L. C.; Qiao, B. F.; Kewalramani, S.; Sknepnek, R.; Newcomb, C. J.; Greenfield, M. A.; Vernizzi, G.; Stupp, S. I.; Bedzyk, M. J.; de la Cruz, M. O., Molecular Crystallization Controlled by pH Regulates Mesoscopic Membrane Morphology. *Acs Nano* **2012**, *6* (12), 10901-10909.
349. Palmer, L. C.; Leung, C. Y.; Kewalramani, S.; Kumthekar, R.; Newcomb, C. J.; de la Cruz, M. O.; Bedzyk, M. J.; Stupp, S. I., Long-Range Ordering of Highly Charged Self-Assembled Nanofilaments. *J. Am. Chem. Soc.* **2014**, *136* (41), 14377-14380.
350. Mortensen, H. G.; Jensen, G. V.; Hansen, S. K.; Vosegaard, T.; Pedersen, J. S., Structure of Phospholipid Mixed Micelles (Bicelles) Studied by Small-Angle X-ray Scattering. *Langmuir* **2018**, *34* (48), 14597-14607.
351. Liu, G. F.; Li, Y. W.; Wu, H. J.; Wu, X. B.; Xu, X. H.; Wang, W. H.; Zhang, R. G.; Li, N., Upgraded SSRF BL19U2 beamline for small-angle X-ray scattering of biological macromolecules in solution. *J. Appl. Crystallogr.* **2018**, *51*, 1633-1640.
352. Mrozowich, T.; McLennan, S.; Overduin, M.; Patel, T. R., Structural Studies of Macromolecules in Solution using Small Angle X-Ray Scattering. *Jove-J Vis Exp* **2018**, (141).
353. Lin, B.; Dobeli, M.; Mudie, S.; Hawley, A.; Hodgson, P.; Kong, L. X.; Spolenak, R.; Dumeé, L. F., An in-situ small angle x ray scattering analysis of nanopore formation during thermally induced chemical dealloying of brass thin foils. *Sci. Rep.* **2018**, *8*.
354. Gong, Y.; Du, R.; Mo, G.; Xing, X. Q.; Lu, C. X.; Wu, Z. H., Nanostructural heritability in polyacrylonitrile based fibers studied by small angle X-ray scattering. *Polymer* **2018**, *153*, 485-497.
355. Li, J. P.; Jiao, A. Q.; Chen, S.; Wu, Z. Z.; Xu, E. B.; Jin, Z. Y., Application of the small-angle X-ray scattering technique for structural analysis studies: A review. *J. Mol. Struct.* **2018**, *1165*, 391-400.
356. Suh, W. S.; Subedi, L.; Kim, S. Y.; Choi, S. U.; Lee, K. R., Bioactive lignan constituents from the twigs of *Sambucus williamsii*. *Bioorg. Med. Chem. Lett.* **2016**, *26* (8), 1877-1880.
357. Awasthi, S.; Anbanandam, A.; Rodgers, K. K., Structure of a TLR4-interacting SPA4 peptide. *Rsc Adv* **2015**, *5* (35), 27431-27438.
358. Ma, X. L.; Yu, Q.; Guo, X. Y.; Zeng, K. W.; Zhao, M. B.; Tu, P. F.; Jiang, Y., Nitric oxide inhibitory flavonoids from traditional Chinese medicine formula Baoyuan Decoction. *Fitoterapia* **2015**, *103*, 252-259.
359. Hamley, I. W.; Kirkham, S.; Dehsorkhi, A.; Castelletto, V.; Reza, M.; Ruokolainen, J., Toll-like receptor agonist lipopeptides self-assemble into distinct nanostructures. *Chem Commun (Camb)* **2014**, *50* (100), 15948-51.
360. Hamley, I. W.; Kirkham, S.; Dehsorkhi, A.; Castelletto, V.; Adamcik, J.; Mezzenga, R.; Ruokolainen, J.; Mazzuca, C.; Gatto, E.; Venanzi, M.; Placidi, E.; Bilalis, P.; Iatrou, H., Self-assembly of a model peptide incorporating a hexa-histidine sequence attached to an oligo-alanine sequence, and binding to gold NTA/nickel nanoparticles. *Biomacromolecules* **2014**, *15* (9), 3412-20.

361. Zhang, Y.; Wang, J. S.; Wang, X. B.; Gu, Y. C.; Wei, D. D.; Guo, C.; Yang, M. H.; Kong, L. Y., Limonoids from the Fruits of *Aphanamixis polystachya* (Meliaceae) and Their Biological Activities. *J Agr Food Chem* **2013**, *61* (9), 2171-2182.
362. Fry, H. C.; Garcia, J. M.; Medina, M. J.; Ricoy, U. M.; Gosztola, D. J.; Nikiforov, M. P.; Palmer, L. C.; Stupp, S. I., Self-Assembly of Highly Ordered Peptide Amphiphile Metalloporphyrin Arrays. *J. Am. Chem. Soc.* **2012**, *134* (36), 14646-14649.
363. Stendahl, J. C.; Rao, M. S.; Guler, M. O.; Stupp, S. I., Intermolecular forces in the self-assembly of peptide amphiphile nanofibers. *Adv. Funct. Mater.* **2006**, *16* (4), 499-508.
364. Arora, N.; Jayaram, B., Strength of hydrogen bonds in alpha helices. *J. Comput. Chem.* **1997**, *18* (9), 1245-1252.
365. Maccallum, P. H.; Poet, R.; Milnerwhite, E. J., Coulombic Interactions between Partially Charged Main-Chain Atoms Not Hydrogen-Bonded to Each Other Influence the Conformations of Alpha-Helices and Antiparallel Beta-Sheet - a New Method for Analyzing the Forces between Hydrogen-Bonding Groups in Proteins Includes All the Coulombic Interactions. *J Mol Biol* **1995**, *248* (2), 361-373.
366. Gray, T. M.; Matthews, B. W., Intrahelical Hydrogen-Bonding of Serine, Threonine and Cysteine Residues within Alpha-Helices and Its Relevance to Membrane-Bound Proteins. *J Mol Biol* **1984**, *175* (1), 75-81.
367. Rahmati, M.; Mozafari, M., Biocompatibility of alumina-based biomaterials-A review. *J. Cell. Physiol.* **2019**, *234* (4), 3321-3335.
368. Courtney, M.; Ren, C. L., Counterflow gradient electrophoresis for focusing and elution. *Electrophoresis* **2019**, *40* (5), 643-658.
369. Young, M. J.; Holder, A. M.; Musgrave, C. B., The Unified Electrochemical Band Diagram Framework: Understanding the Driving Forces of Materials Electrochemistry. *Adv. Funct. Mater.* **2018**, *28* (41).
370. Yamanaka, M., Supramolecular gel electrophoresis. *Polym. J.* **2018**, *50* (8), 627-635.
371. Tang, X. C.; Pikal, M. J.; Taylor, L. S., The effect of temperature on hydrogen bonding in crystalline and amorphous phases in dihydropyridine calcium channel blockers. *Pharm. Res.* **2002**, *19* (4), 484-90.
372. Ohtaki, H., Effects of Temperature and Pressure on Hydrogen Bonds in Water and in Formamide. *J. Mol. Liq.* **2003**, *103*, 3-13.
373. Bakó, I.; Pusztai, L.; Temleitner, L., Decreasing temperature enhances the formation of sixfold hydrogen bonded rings in water-rich water-methanol mixtures. *Sci. Rep.* **2017**, *7* (1), 1073.
374. Cooper, A., Heat capacity of hydrogen-bonded networks: an alternative view of protein folding thermodynamics. *Biophys. Chem.* **2000**, *85* (1), 25-39.
375. Mafy, N. N.; Afrin, T.; Rahman, M. M.; Mollah, M. Y. A.; Susan, M. A. B. H., Effect of temperature perturbation on hydrogen bonding in aqueous solutions of different urea concentrations. *Rsc Adv* **2015**, *5* (73), 59263-59272.
376. Joyce, P.; Dening, T. J.; Gustafsson, H.; Prestidge, C. A., Modulating the Lipase-Mediated Bioactivity of Particle-Lipid Conjugates Through Changes in Nanostructure and Surface Chemistry. *Eur. J. Lipid Sci. Technol.* **2017**, *119* (12).
377. Zhou, X. R.; Cao, Y. M.; Zhang, Q.; Tian, X. B.; Dong, H.; Chen, L.; Luo, S. Z., Self-assembly nanostructure controlled sustained release, activity and stability of peptide drugs. *Int. J. Pharm.* **2017**, *528* (1-2), 723-731.
378. Zha, R. H.; Sur, S.; Stupp, S. I., Self-assembly of Cytotoxic Peptide Amphiphiles into Supramolecular Membranes for Cancer Therapy. *Adv Healthc Mater* **2013**, *2* (1), 126-133.
379. Cavalieri, F.; Colone, M.; Stringaro, A.; Tortora, M.; Calcabrini, A.; Zhou, M. F.; Ashokkumar, M., Influence of the Morphology of Lysozyme-Shelled Microparticles on the

- Cellular Association, Uptake, and Degradation in Human Breast Adenocarcinoma Cells. *Particle & Particle Systems Characterization* **2013**, *30* (8), 695-705.
380. Jiang, B. B.; Li, B. Y., Tunable drug loading and release from polypeptide multilayer nanofilms. *International Journal of Nanomedicine* **2009**, *4* (1), 37-53.
381. Niece, K. L.; Czeisler, C.; Sahni, V.; Tysseling-Mattiace, V.; Pashuck, E. T.; Kessler, J. A.; Stupp, S. I., Modification of gelation kinetics in bioactive peptide amphiphiles. *Biomaterials* **2008**, *29* (34), 4501-4509.
382. Rajangam, K.; Arnold, M. S.; Rocco, M. A.; Stupp, S. I., Peptide amphiphile nanostructure-heparin interactions and their relationship to bioactivity. *Biomaterials* **2008**, *29* (23), 3298-3305.
383. Balaram, H.; Uma, K.; Balaram, P., Synthetic peptide models for protein secondary structures. Beta-sheet formation in acyclic cystine peptides. *Int. J. Pept. Protein Res.* **1990**, *35* (6), 495-500.
384. Behanna, H. A.; Rajangam, K.; Stupp, S. I., Modulation of fluorescence through coassembly of molecules in organic nanostructures. *J. Am. Chem. Soc.* **2007**, *129* (2), 321-327.
385. Frohm, B.; DeNizio, J. E.; Lee, D. S. M.; Gentile, L.; Olsson, U.; Malm, J.; Akerfeldt, K. S.; Linse, S., A peptide from human semenogelin I self-assembles into a pH-responsive hydrogel. *Soft Matter* **2015**, *11* (2), 414-421.
386. Wu, L. C.; Yang, J. Y.; Kopecek, J., Hybrid hydrogels self-assembled from graft copolymers containing complementary beta-sheets as hydroxyapatite nucleation scaffolds. *Biomaterials* **2011**, *32* (23), 5341-5353.
387. Zhou, M.; Smith, A. M.; Das, A. K.; Hodson, N. W.; Collins, R. F.; Ulijn, R. V.; Gough, J. E., Self-assembled peptide-based hydrogels as scaffolds for anchorage-dependent cells. *Biomaterials* **2009**, *30* (13), 2523-2530.
388. Berndt, K. D. 4.2.1 Circular dichroism spectroscopy. [http://www.cryst.bbk.ac.uk/PPS2/course/section8/ss-960531\\_21.html](http://www.cryst.bbk.ac.uk/PPS2/course/section8/ss-960531_21.html) (accessed 18-12-20).
389. Lees, J. G.; Miles, A. J.; Janes, R. W.; Wallace, B. A., Novel methods for secondary structure determination using low wavelength (VUV) circular dichroism spectroscopic data. *BMC Bioinformatics* **2006**, *7* (1), 507.
390. Greenfield, N. J., Using circular dichroism spectra to estimate protein secondary structure. *Nat. Protoc.* **2006**, *1* (6), 2876-2890.
391. Micsonai, A.; Wien, F.; Kernya, L.; Lee, Y.-H.; Goto, Y.; Réfrégiers, M.; Kardos, J., Accurate secondary structure prediction and fold recognition for circular dichroism spectroscopy. *Proceedings of the National Academy of Sciences* **2015**, *112* (24), E3095.
392. Kopeć, K.; Pędziwiatr, M.; Gront, D.; Sztatelman, O.; Sławski, J.; Łazicka, M.; Worch, R.; Zawada, K.; Makarova, K.; Nyk, M.; Grzyb, J., Comparison of  $\alpha$ -Helix and  $\beta$ -Sheet Structure Adaptation to a Quantum Dot Geometry: Toward the Identification of an Optimal Motif for a Protein Nanoparticle Cover. *ACS Omega* **2019**, *4* (8), 13086-13099.
393. Guo, J.; Harn, N.; Robbins, A.; Dougherty, R.; Middaugh, C. R., Stability of Helix-Rich Proteins at High Concentrations. *Biochemistry-Us* **2006**, *45* (28), 8686-8696.
394. Vijayakumar, S.; Vishveshwara, S.; Ravishanker, G.; Beveridge, D. L., Differential stability of beta-sheets and alpha-helices in beta-lactamase: a high temperature molecular dynamics study of unfolding intermediates. *Biophys J* **1993**, *65* (6), 2304-2312.
395. Behanna, H. A.; Donners, J. J. J. M.; Gordon, A. C.; Stupp, S. I., Coassembly of amphiphiles with opposite peptide polarities into nanofibers. *J. Am. Chem. Soc.* **2005**, *127* (4), 1193-1200.
396. Boothroyd, S.; Miller, A. F.; Saiani, A., From fibres to networks using self-assembling peptides. *Faraday Discuss.* **2013**, *166*, 195-207.
397. Guy, M. M.; Voyer, N., Structure and hydrogel formation studies on homologs of a lactoglobulin-derived peptide. *Biophys. Chem.* **2012**, *163*, 1-10.

398. Hamley, I. W.; Cheng, G.; Castelletto, V., A Thermoresponsive Hydrogel Based on Telechelic PEG End-Capped with Hydrophobic Dipeptides. *Macromol. Biosci.* **2011**, *11* (8), 1068-1078.
399. He, X.; Fan, J. W.; Zhang, F. W.; Li, R. C.; Pollack, K. A.; Raymond, J. E.; Zou, J.; Wooley, K. L., Multi-responsive hydrogels derived from the self-assembly of tethered allyl-functionalized racemic oligopeptides. *J Mater Chem B* **2014**, *2* (46), 8123-8130.
400. Matson, J. B.; Stupp, S. I., Self-assembling peptide scaffolds for regenerative medicine. *Chem. Commun.* **2012**, *48* (1), 26-33.
401. Matson, J. B.; Zha, R. H.; Stupp, S. I., Peptide self-assembly for crafting functional biological materials. *Curr Opin Solid St M* **2011**, *15* (6), 225-235.
402. Pashuck, E. T.; Cui, H. G.; Stupp, S. I., Tuning Supramolecular Rigidity of Peptide Fibers through Molecular Structure. *J. Am. Chem. Soc.* **2010**, *132* (17), 6041-6046.
403. Radu-Wu, L. C.; Yang, J.; Wu, K.; Kopecek, J., Self-Assembled Hydrogels from Poly[N-(2-hydroxypropyl)methacrylamide] Grafted with beta-Sheet Peptides. *Biomacromolecules* **2009**, *10* (8), 2319-2327.
404. Tian, Y. F.; Hudalla, G. A.; Han, H. F.; Collier, J. H., Controllably degradable beta-sheet nanofibers and gels from self-assembling decapeptides. *Biomater Sci-Uk* **2013**, *1* (10), 1037-1045.
405. Wang, W. J.; Wang, H. M.; Ren, C. H.; Wang, J. Y.; Tan, M.; Shen, J.; Yang, Z. M.; Wang, P. G.; Wang, L., A saccharide-based supramolecular hydrogel for cell culture. *Carbohydr. Res.* **2011**, *346* (8), 1013-1017.
406. Zhou, S. L.; Matsumoto, S.; Tian, H. D.; Yamane, H.; Ojida, A.; Kiyonaka, S.; Hamachi, I., pH-Responsive shrinkage/swelling of a supramolecular hydrogel composed of two small amphiphilic molecules. *Chem-Eur J* **2005**, *11* (4), 1130-1136.
407. De Leon Rodriguez, L.; Hemar, Y.; Cornish, J.; Brimble, M., Structure-mechanical property correlations of hydrogel forming  $\beta$ -sheet peptides. *Chem. Soc. Rev.* **2016**, *45*.
408. Banwell, E. F.; Abelardo, E. S.; Adams, D. J.; Birchall, M. A.; Corrigan, A.; Donald, A. M.; Kirkland, M.; Serpell, L. C.; Butler, M. F.; Woolfson, D. N., Rational design and application of responsive alpha-helical peptide hydrogels. *Nat Mater* **2009**, *8* (7), 596-600.
409. Ing, N. L.; Spencer, R. K.; Luong, S. H.; Nguyen, H. D.; Hochbaum, A. I., Electronic Conductivity in Biomimetic  $\alpha$ -Helical Peptide Nanofibers and Gels. *ACS Nano* **2018**, *12* (3), 2652-2661.
410. Skipper, L., PROTEINS | Overview. In *Encyclopedia of Analytical Science (Second Edition)*, Worsfold, P.; Townshend, A.; Poole, C., Eds. Elsevier: Oxford, 2005; pp 344-352.
411. Mehrban, N.; Abelardo, E.; Wasmuth, A.; Hudson, K. L.; Mullen, L. M.; Thomson, A. R.; Birchall, M. A.; Woolfson, D. N., Assessing cellular response to functionalized alpha-helical peptide hydrogels. *Adv Healthc Mater* **2014**, *3* (9), 1387-91.
412. Alhadeff, A. L.; Golub, D.; Hayes, M. R.; Grill, H. J., Peptide YY signaling in the lateral parabrachial nucleus increases food intake through the Y1 receptor. *Am J Physiol-Endoc M* **2015**, *309* (8), E759-E766.
413. Smith, R. M.; Klein, R.; Kruzliak, P.; Zulli, A., Role of Peptide YY in blood vessel function and atherosclerosis in a rabbit model. *Clin Exp Pharmacol P* **2015**, *42* (6), 648-652.
414. Chen, H.; Zhang, X.; Hao, J.; Chen, D. F.; Liu, J.; Gao, Y. D.; Zhu, J. Y.; Wu, H. W.; Lin, F. J.; Pu, Y. D.; Yuan, D. Y.; Wei, R. B.; Zhou, C. W.; Wang, T.; Li, Z. Q., Molecular cloning, expression analysis, and appetite regulatory effect of peptide YY in Siberian sturgeon (*Acipenser baerii*). *Gene* **2015**, *563* (2), 172-179.
415. Persaud, S. J.; Bewick, G. A., Peptide YY: more than just an appetite regulator. *Diabetologia* **2014**, *57* (9), 1762-1769.
416. Manning, S.; Batterham, R. L., The Role of Gut Hormone Peptide YY in Energy and Glucose Homeostasis: Twelve Years On. *Annu Rev Physiol* **2014**, *76*, 585-608.

417. La Sala, M. S.; Hurtado, M. D.; Brown, A. R.; Bohorquez, D. V.; Liddle, R. A.; Herzog, H.; Zolotukhin, S.; Dotson, C. D., Modulation of taste responsiveness by the satiation hormone peptide YY. *Faseb J* **2013**, *27* (12), 5022-5033.
418. Scheid, J. L.; Birch, L. L.; Williams, N. I.; Rolls, B. J.; De Souza, M. J., Postprandial peptide YY is lower in young college-aged women with high dietary cognitive restraint. *Physiol Behav* **2013**, *120*, 26-33.
419. Reidelberger, R.; Haver, A.; Chelikani, P. K., Role of peptide YY(3-36) in the satiety produced by gastric delivery of macronutrients in rats. *Am J Physiol-Endoc M* **2013**, *304* (9), E944-E950.
420. Greenberg, J. A.; Geliebter, A., Coffee, Hunger, and Peptide YY. *J Am Coll Nutr* **2012**, *31* (3), 160-166.
421. Li, J. B.; Asakawa, A.; Li, Y.; Cheng, K.; Inui, A., Effects of Exercise on the Levels of Peptide YY and Ghrelin. *Exp Clin Endocr Diab* **2011**, *119* (3), 163-166.
422. Boey, D.; Sainsbury, A.; Herzog, H., The role of peptide YY in regulating glucose homeostasis. *Peptides* **2007**, *28* (2), 390-395.
423. Renshaw, D.; Batterham, R. L., Peptide YY: A potential therapy for obesity. *Curr Drug Targets* **2005**, *6* (2), 171-179.
424. McGowan, B. M. C.; Bloom, S. R., Peptide YY and appetite control. *Curr Opin Pharmacol* **2004**, *4* (6), 583-588.
425. Tovar, S. A.; Seoane, L. M.; Caminos, J. E.; Nogueiras, R.; Casanueva, F. F.; Dieguez, C., Regulation of peptide YY levels by age, hormonal, and nutritional status. *Obes Res* **2004**, *12* (12), 1944-1950.
426. Ehrlich, G. K.; Michel, H.; Truitt, T.; Riboulet, W.; Pop-Damkov, P.; Goelzer, P.; Hainzl, D.; Qureshi, F.; Lueckel, B.; Danho, W.; Conde-Knape, K.; Konkar, A., Preparation and Characterization of Albumin Conjugates of a Truncated Peptide YY Analogue for Half-Life Extension. *Bioconjugate Chem* **2013**, *24* (12), 2015-2024.
427. Ehrlich, G. K.; Michel, H.; Truitt, T.; Riboulet, W.; Pop-Damkov, P.; Goelzer, P.; Hainzl, D.; Qureshi, F.; Lueckel, B.; Danho, W.; Conde-Knape, K.; Konkar, A., Preparation and characterization of albumin conjugates of a truncated peptide YY analogue for half-life extension. *Bioconjug. Chem.* **2013**, *24* (12), 2015-24.
428. Fallmar, H.; Sundstrom, G.; Lundell, I.; Mohell, N.; Larhammar, D., Neuropeptide Y/peptide YY receptor Y2 duplicate in zebrafish with unique introns displays distinct peptide binding properties. *Comp Biochem Phys B* **2011**, *160* (4), 166-173.
429. Fallmar, H.; Akerberg, H.; Gutierrez-de-Teran, H.; Lundell, I.; Mohell, N.; Larhammar, D., Identification of positions in the human neuropeptide Y/peptide YY receptor Y2 that contribute to pharmacological differences between receptor subtypes. *Neuropeptides* **2011**, *45* (4), 293-300.
430. Waegele, M. M.; Gai, F., Infrared Study of the Folding Mechanism of a Helical Hairpin: Porcine PYY. *Biochemistry-Us* **2010**, *49* (35), 7659-7664.
431. Ahn, J. S.; Nazarbaghi, R.; D'Souza, L. J.; Ghosh, S.; Jodka, C. M.; Lwin, A. N.; Levy, O. E., Synthesis & Biological Evaluation of PYY(3-36) Analogs Substituted with Alanine. *Adv Exp Med Biol* **2009**, *611*, 515-516.
432. le Roux, C. W.; Bloom, S. R., Peptide YY, appetite and food intake. *P Nutr Soc* **2005**, *64* (2), 213-216.
433. Dumitriu, S.; Magny, P.; Montane, D.; Vidal, P. F.; Chornet, E., Polyionic Hydrogels Obtained by Complexation between Xanthan and Chitosan - Their Properties as Supports for Enzyme Immobilization. *J. Bioact. Compatible Polym.* **1994**, *9* (2), 184-209.
434. Kopecek, J.; Tang, A. J.; Wang, C.; Stewart, R. J., De novo design of biomedical polymers: Hybrids from synthetic macromolecules and genetically engineered protein domains. *Macromolecular Symposia* **2001**, *174*, 31-42.

435. Liu, V. A.; Bhatia, S. N., Three-dimensional photopatterning of hydrogels containing living cells. *Biomed. Microdevices* **2002**, *4* (4), 257-266.
436. Mukhopadhyay, S.; Maitra, U.; Ira; Krishnamoorthy, G.; Schmidt, J.; Talmon, Y., Structure and dynamics of a molecular hydrogel derived from a tripodal cholamide. *J. Am. Chem. Soc.* **2004**, *126* (48), 15905-15914.
437. Plunkett, K. N.; Berkowski, K. L.; Moore, J. S., Chymotrypsin responsive hydrogel: Application of a disulfide exchange protocol for the preparation of methacrylamide containing peptides. *Biomacromolecules* **2005**, *6* (2), 632-637.
438. Yang, J. Y.; Xu, C. Y.; Kopeckova, P.; Kopecek, J., Hybrid hydrogels self-assembled from HEMA copolymers containing peptide grafts. *Macromol. Biosci.* **2006**, *6* (3), 201-209.
439. Stone, D. A.; Hsu, L.; Stupp, S. I., Self-assembling quinquethiophene-oligopeptide hydrogelators. *Soft Matter* **2009**, *5* (10), 1990-1993.
440. Kopecek, J., Hydrogels: From Soft Contact Lenses and Implants to Self-Assembled Nanomaterials. *J Polym Sci Pol Chem* **2009**, *47* (22), 5929-5946.
441. Hutchinson, J. A.; Hamley, I. W.; Edwards-Gayle, C. J. C.; Castelletto, V.; Piras, C.; Cramer, R.; Kowalczyk, R.; Seitsonen, J.; Ruokolainen, J.; Rambo, R. P., Melanin production by tyrosinase activity on a tyrosine-rich peptide fragment and pH-dependent self-assembly of its lipidated analogue. *Org Biomol Chem* **2019**.
442. Jayawarna, V.; Smith, A.; Gough, J. E.; Ulijn, R. V., Three-dimensional cell culture of chondrocytes on modified di-phenylalanine scaffolds. *Biochem. Soc. Trans.* **2007**, *35*, 535-537.
443. Adhikari, B.; Nanda, J.; Banerjee, A., Pyrene-Containing Peptide-Based Fluorescent Organogels: Inclusion of Graphene into the Organogel. *Chem-Eur J* **2011**, *17* (41), 11488-11496.
444. Haldar, S.; Maji, S. K., Spontaneous physical gelation from functionally modified tripeptides [C16-Ser(OBz)-X-Ser(OBz)-C16] via supramolecularly assisted polarophobic association in diverse organic media. *Colloid Surface A* **2013**, *430*, 65-75.
445. Hart, L. R.; Hunter, J. H.; Nguyen, N. A.; Harries, J. L.; Greenland, B. W.; Mackay, M. E.; Colquhoun, H. M.; Hayes, W., Multivalency in healable supramolecular polymers: the effect of supramolecular cross-link density on the mechanical properties and healing of non-covalent polymer networks. *Polym Chem-Uk* **2014**, *5* (11), 3680-3688.
446. Geng, H. M.; Zong, Q. Y.; You, J.; Ye, L.; Zhang, A. Y.; Shao, Z. Q.; Feng, Z. G., Gelation capability of cysteine-modified cyclo(L-Lys-L-Lys)s dominated by Fmoc and Trt protecting groups. *Science China-Chemistry* **2016**, *59* (3), 293-302.
447. Geng, H. M.; Ye, L.; Zhang, A. Y.; Li, J. B.; Feng, Z. G., Low-Molecular-Weight Organo- and Hydrogelators Based on Cyclo(L-Lys-L-Glu). *Langmuir* **2016**, *32* (18), 4586-4594.
448. Minakuchi, N.; Hoe, K.; Yamaki, D.; Ten-no, S.; Nakashima, K.; Goto, M.; Mizuhata, M.; Maruyama, T., Versatile Supramolecular Gelators That Can Harden Water, Organic Solvents and Ionic Liquids. *Langmuir* **2012**, *28* (25), 9259-9266.
449. Weingarten, A. S.; Kazantsev, R. V.; Palmer, L. C.; Fairfield, D. J.; Koltonow, A. R.; Stupp, S. I., Supramolecular Packing Controls H<sub>2</sub> Photocatalysis in Chromophore Amphiphile Hydrogels. *J. Am. Chem. Soc.* **2015**, *137* (48), 15241-15246.
450. McClendon, M. T.; Stupp, S. I., Tubular hydrogels of circumferentially aligned nanofibers to encapsulate and orient vascular cells. *Biomaterials* **2012**, *33* (23), 5713-5722.
451. Jiang, L. X.; Yan, Y.; Huang, J. B., Zwitterionic surfactant/cyclodextrin hydrogel: microtubes and multiple responses. *Soft Matter* **2011**, *7* (21), 10417-10423.
452. Malik, S.; Maji, S. K.; Banerjee, A.; Nandi, A. K., A synthetic tripeptide as organogelator: elucidation of gelation mechanism. *J Chem Soc Perk T 2* **2002**, (6), 1177-1186.

453. Nguyen, V. D.; Pal, A.; Snijkers, F.; Colomb-Delsuc, M.; Leonetti, G.; Otto, S.; van der Gucht, J., Multi-step control over self-assembled hydrogels of peptide-derived building blocks and a polymeric cross-linker. *Soft Matter* **2016**, *12* (2), 432-440.
454. Wang, C. R.; Chen, X. F.; Yao, X. M.; Chen, L.; Chen, X. S., Dual acid-responsive supramolecular nanoparticles as new anticancer drug delivery systems. *Biomater Sci-Uk* **2016**, *4* (1), 104-114.
455. Chu, T. W.; Feng, J. Y.; Yang, J. Y.; Kopecek, J., Hybrid polymeric hydrogels via peptide nucleic acid (PNA)/DNA complexation. *Journal of Controlled Release* **2015**, *220*, 608-616.
456. Yang, J. A.; Yeom, J.; Hwang, B. W.; Hoffman, A. S.; Hahn, S. K., In situ-forming injectable hydrogels for regenerative medicine. *Prog. Polym. Sci.* **2014**, *39* (12), 1973-1986.
457. Krishna, O. D.; Kiick, K. L., Protein- and Peptide-Modified Synthetic Polymeric Biomaterials. *Biopolymers* **2010**, *94* (1), 32-48.
458. Jing, P.; Rudra, J. S.; Herr, A. B.; Collier, J. H., Self-assembling peptide-polymer hydrogels designed from the coiled coil region of fibrin. *Biomacromolecules* **2008**, *9* (9), 2438-2446.
459. Tovar, J. D.; Claussen, R. C.; Stupp, S. I., Probing the interior of peptide amphiphile supramolecular aggregates. *J. Am. Chem. Soc.* **2005**, *127* (20), 7337-7345.
460. Soni, S.; Babbar, A. K.; Sharma, R. K.; Maitra, A., Delivery of hydrophobised 5-fluorouracil derivative to brain tissue through intravenous route using surface modified nanogels. *J. Drug Targeting* **2006**, *14* (2), 87-95.
461. Rawat, M.; Singh, D.; Saraf, S.; Saraf, S., Development and in vitro evaluation of alginate gel-encapsulated, chitosan-coated ceramic nanocores for oral delivery of enzyme. *Drug Dev. Ind. Pharm.* **2008**, *34* (2), 181-188.
462. Miao, B. L.; Ma, G. L.; Song, C. X., Synthesis, Characterization and Protein Drug Release of Temperature-Sensitive PCL-PEG-PCL Hydrogel. *Chem J Chinese U* **2009**, *30* (12), 2508-2513.
463. Wang, L.; Zeng, R.; Li, C.; Qiao, R. Z., Self-assembled polypeptide-block-poly(vinylpyrrolidone) as prospective drug-delivery systems. *Colloid Surface B* **2009**, *74* (1), 284-292.
464. Naskar, J.; Palui, G.; Banerjee, A., Tetrapeptide-Based Hydrogels: for Encapsulation and Slow Release of an Anticancer Drug at Physiological pH. *J Phys Chem B* **2009**, *113* (35), 11787-11792.
465. Danino, D.; Kaplun, A.; Lindblom, G.; Rilfors, L.; Oradd, G.; Hauksson, J. B.; Talmon, Y., Cryo-TEM and NMR studies of a micelle-forming phosphoglucolipid from membranes of *Acholeplasma laidlawii* A and B. *Chem. Phys. Lipids* **1997**, *85* (1), 75-89.
466. Kuvichkin, V. V.; Danev, R. S.; Shigematsu, H.; Nagayama, K., DNA-induced aggregation and fusion of phosphatidylcholine liposomes in the presence of multivalent cations observed by the cryo-TEM technique. *J. Membr. Biol.* **2009**, *227* (2), 95-103.
467. Mehrban, N.; Zhu, B.; Tamagnini, F.; Young, F. I.; Wasmuth, A.; Hudson, K. L.; Thomson, A. R.; Birchall, M. A.; Randall, A. D.; Song, B.; Woolfson, D. N., Functionalized alpha-Helical Peptide Hydrogels for Neural Tissue Engineering. *Acs Biomater Sci Eng* **2015**, *1* (6), 431-439.
468. Hamley, I. W.; Kirkham, S.; Kowalczyk, R. M.; Castelletto, V.; Reza, M.; Ruokolainen, J., Self-assembly of the anti-fungal polyene amphotericin B into giant helically-twisted nanotapes. *Chem Commun (Camb)* **2015**.
469. Zha, R. H.; Sur, S.; Boekhoven, J.; Shi, H. Y.; Zhang, M.; Stupp, S. I., Supramolecular assembly of multifunctional maspin-mimetic nanostructures as a potent peptide-based angiogenesis inhibitor. *Acta Biomater.* **2015**, *12*, 1-10.

470. Bury, M. I.; Fuller, N. J.; Meisner, J. W.; Hofer, M. D.; Webber, M. J.; Chow, L. W.; Prasad, S.; Thaker, H.; Yue, X.; Menon, V. S.; Diaz, E. C.; Stupp, S. I.; Cheng, E. Y.; Sharma, A. K., The promotion of functional urinary bladder regeneration using anti-inflammatory nanofibers. *Biomaterials* **2014**, *35* (34), 9311-9321.
471. Stephanopoulos, N.; Ortony, J. H.; Stupp, S. I., Self-assembly for the synthesis of functional biomaterials. *Acta Mater.* **2013**, *61* (3), 912-930.
472. Hutchinson, J. A.; Hamley, I. W.; Torras, J.; Aleman, C.; Seitsonen, J.; Ruokolainen, J., Self-Assembly of Lipopeptides Containing Short Peptide Fragments Derived from the Gastrointestinal Hormone PYY3-36: From Micelles to Amyloid Fibrils. *J Phys Chem B* **2019**, *123* (3), 614-621.
473. Xie, Y. Y.; Zhao, J.; Huang, R. L.; Qi, W.; Wang, Y. F.; Su, R. X.; He, Z. M., Calcium-Ion-Triggered Co-assembly of Peptide and Polysaccharide into a Hybrid Hydrogel for Drug Delivery. *Nanoscale Res Lett* **2016**, *11*.
474. Velichko, Y. S.; Mantei, J. R.; Bitton, R.; Carvajal, D.; Shull, K. R.; Stupp, S. I., Electric Field Controlled Self-Assembly of Hierarchically Ordered Membranes. *Adv. Funct. Mater.* **2012**, *22* (2), 369-377.
475. Eberlein, G. A.; Eysselein, V. E.; Schaeffer, M.; Layer, P.; Grandt, D.; Goebell, H.; Niebel, W.; Davis, M.; Lee, T. D.; Shively, J. E.; Reeve, J. R., A New Molecular-Form of Pyy - Structural Characterization of Human Pyy(3-36) and Pyy(1-36). *Peptides* **1989**, *10* (4), 797-803.
476. Singh, B. P.; Chauhan, R. S.; Singhal, L. K., Toll-like receptors and their role in innate immunity. *Curr. Sci.* **2003**, *85* (8), 1156-1164.
477. Henry, M. C. W.; Lawrence Moss, R., chapter 34 - NECROTIZING ENTEROCOLITIS. In *Ashcraft's Pediatric Surgery (Fifth Edition)*, Holcomb, G. W.; Murphy, J. P.; Ostlie, D. J., Eds. W.B. Saunders: Philadelphia, 2010; pp 439-455.
478. Zeitz, M.; Hopf, U.; Sieber, G.; Wust, B.; Galanos, C.; Moller, B.; Riecken, E. O., Disturbed Antibody-Response against Lipopolysaccharides (Lps) from Escherichia-Coli and Free Lipid a in Crohns-Disease (Cd). *Gastroenterology* **1985**, *88* (5), 1642-1642.
479. Mamat, U.; Rietschel, E. T.; Schmidt, G., Repression of Lipopolysaccharide Biosynthesis in Escherichia-Coli by an Antisense Rna of Acetobacter-Methanolicus Phage Acm1. *Mol. Microbiol.* **1995**, *15* (6), 1115-1125.
480. Brandenburg, K.; Koch, M. H.; Seydel, U., Biophysical characterisation of lysozyme binding to LPS Re and lipid A. *Eur J Biochem* **1998**, *258* (2), 686-95.
481. Bland, J. M.; De Lucca, A. J.; Jacks, T. J.; Vigo, C. B., All-D-cecropin B: Synthesis, conformation, lipopolysaccharide binding, and antibacterial activity. *Mol. Cell. Biochem.* **2001**, *218* (1-2), 105-111.
482. Ding, L.; Yang, L.; Weiss, T. M.; Waring, A. J.; Lehrer, R. I.; Huang, H. W., Interaction of antimicrobial peptides with lipopolysaccharides. *Biochemistry-Us* **2003**, *42* (42), 12251-12259.
483. Bito, R.; Shikano, T.; Kawabata, H., Isolation and characterization of denatured serum albumin from rats with endotoxycosis. *Bba-Proteins Proteom* **2003**, *1646* (1-2), 100-111.
484. Burke, J. P.; Cunningham, M. F.; Watson, R. W. G.; Docherty, N. G.; Coffey, J. C.; O'Connell, P. R., Bacterial lipopolysaccharide promotes profibrotic activation of intestinal fibroblasts. *Br. J. Surg.* **2010**, *97* (7), 1126-1134.
485. Wolfs, T. G. A. M.; Derikx, J. P. M.; Hodin, C. M. I. M.; Vanderlocht, J.; Driessen, A.; de Bruine, A. P.; Bevins, C. L.; Lasitschka, F.; Gassler, N.; van Gemert, W. G.; Buurman, W. A., Localization of the Lipopolysaccharide Recognition Complex in the Human Healthy and Inflamed Premature and Adult Gut. *Inflamm. Bowel Dis.* **2010**, *16* (1), 68-75.

486. Singh, S.; Papareddy, P.; Kalle, M.; Schmidtchen, A.; Malmsten, M., Importance of lipopolysaccharide aggregate disruption for the anti-endotoxic effects of heparin cofactor II peptides. *Bba-Biomembranes* **2013**, *1828* (11), 2709-2719.
487. Singh, S.; Kalle, M.; Papareddy, P.; Schmidtchen, A.; Malmsten, M., Lipopolysaccharide Interactions of C-Terminal Peptides from Human Thrombin. *Biomacromolecules* **2013**, *14* (5), 1482-1492.
488. Bruns, S.; Pastille, E.; Wirsdorfer, F.; Frisch, M.; Flohe, S. B., Lipopeptides rather than lipopolysaccharide favor the development of dendritic cell dysfunction similar to polymicrobial sepsis in mice. *Inflammation Res.* **2013**, *62* (6), 627-636.
489. Saleem, F.; Bjorn Dahl, T. C.; Ladner, C. L.; Perez-Pineiro, R.; Ametaj, B. N.; Wishart, D. S., Lipopolysaccharide induced conversion of recombinant prion protein. *Prion* **2014**, *8* (2), 221-232.
490. Anderson, S. T.; Commins, S.; Moynagh, P. N.; Coogan, A. N., Lipopolysaccharide-induced sepsis induces long-lasting affective changes in the mouse. *Brain Behavior and Immunity* **2015**, *43*, 98-109.
491. Durai, P.; Batool, M.; Choi, S., Structure and Effects of Cyanobacterial Lipopolysaccharides. *Marine Drugs* **2015**, *13* (7), 4217-4230.
492. Trussoni, C. E.; Tabibian, J. H.; Splinter, P. L.; O'Hara, S. P., Lipopolysaccharide (LPS)-Induced Biliary Epithelial Cell NRas Activation Requires Epidermal Growth Factor Receptor (EGFR). *Plos One* **2015**, *10* (4).
493. Fallarino, F.; Pallotta, M. T.; Matino, D.; Gargaro, M.; Orabona, C.; Vacca, C.; Mondanelli, G.; Allegrucci, M.; Boon, L.; Romani, R.; Talesa, V. N.; Puccetti, P.; Grohmann, U., LPS-conditioned dendritic cells confer endotoxin tolerance contingent on tryptophan catabolism. *Immunobiology* **2015**, *220* (2), 315-321.
494. Baek, M. H.; Kamiya, M.; Kushibiki, T.; Nakazumi, T.; Tomisawa, S.; Abe, C.; Kumaki, Y.; Kikukawa, T.; Demura, M.; Kawano, K.; Aizawa, T., Lipopolysaccharide-bound structure of the antimicrobial peptide cecropin P1 determined by nuclear magnetic resonance spectroscopy. *J. Pept. Sci.* **2016**, *22* (4), 214-221.
495. Mohammadi, F.; Rahimian, R.; Fakhræi, N.; Rezayat, S. M.; Javadi-Paydar, M.; Dehpour, A. R.; Afshari, K.; Mehr, S. E., Effect of glatiramer acetate on short-term memory impairment induced by lipopolysaccharide in male mice. *Fundam. Clin. Pharmacol.* **2016**, *30* (4), 347-356.
496. Chen, C. P.; Brock, R.; Luh, F.; Chou, P. J.; Larrick, J. W.; Huang, R. F.; Huang, T. H., The Solution Structure of the Active Domain of Cap18 - a Lipopolysaccharide-Binding Protein from Rabbit Leukocytes. *Febs Lett* **1995**, *370* (1-2), 46-52.
497. Chapple, D. S.; Hussain, R.; Joannou, C. L.; Hancock, R. E. W.; Odell, E.; Evans, R. W.; Siligardi, G., Structure and association of human lactoferrin peptides with Escherichia coli lipopolysaccharide. *Antimicrob. Agents Chemother.* **2004**, *48* (6), 2190-2198.
498. Gopal, R.; Park, J. S.; Seo, C. H.; Park, Y., Applications of Circular Dichroism for Structural Analysis of Gelatin and Antimicrobial Peptides. *Int. J. Mol. Sci.* **2012**, *13* (3), 3229-3244.
499. Kushibiki, T.; Kamiya, M.; Aizawa, T.; Kumaki, Y.; Kikukawa, T.; Mizuguchi, M.; Demura, M.; Kawabata, S.; Kawano, K., Interaction between tachyplesin I, an antimicrobial peptide derived from horseshoe crab, and lipopolysaccharide. *Bba-Proteins Proteom* **2014**, *1844* (3), 527-534.
500. Ryder, M. P.; Wu, X. M.; McKelvey, G. R.; McGuire, J.; Schilke, K. F., Binding interactions of bacterial lipopolysaccharide and the cationic amphiphilic peptides polymyxin B and WLBU2. *Colloid Surface B* **2014**, *120*, 81-87.

501. Bello, G.; Eriksson, J.; Terry, A.; Edwards, K.; Lawrence, M. J.; Barlow, D.; Harvey, R. D., Characterization of the aggregates formed by various bacterial lipopolysaccharides in solution and upon interaction with antimicrobial peptides. *Langmuir* **2015**, *31* (2), 741-51.
502. Datta, A.; Kundu, P.; Bhunia, A., Designing potent antimicrobial peptides by disulphide linked dimerization and N-terminal lipidation to increase antimicrobial activity and membrane perturbation: Structural insights into lipopolysaccharide binding. *J. Colloid Interface Sci.* **2016**, *461*, 335-345.
503. Shang, D. J.; Zhang, Q.; Dong, W. B.; Liang, H.; Bi, X. N., The effects of LPS on the activity of Trp-containing antimicrobial peptides against Gram-negative bacteria and endotoxin neutralization. *Acta Biomater.* **2016**, *33*, 153-165.
504. Falla, T. J.; Karunaratne, D. N.; Hancock, R. E. W., Mode of action of the antimicrobial peptide indolicidin. *J Biol Chem* **1996**, *271* (32), 19298-19303.
505. Castelletto, V.; Edwards-Gayle, C. J. C.; Hamley, I. W.; Barrett, G.; Seitsonen, J.; Ruokolainen, J., Peptide-Stabilized Emulsions and Gels from an Arginine-Rich Surfactant-like Peptide with Antimicrobial Activity. *ACS Appl Mater Interfaces* **2019**, *11* (10), 9893-9903.
506. Singh, S.; Papareddy, P.; Kalle, M.; Schmidtchen, A.; Malmsten, M., Importance of lipopolysaccharide aggregate disruption for the anti-endotoxic effects of heparin cofactor II peptides. *Biochim. Biophys. Acta* **2013**, *1828* (11), 2709-2719.
507. Tandon, A.; Harioudh, M. K.; Ishrat, N.; Tripathi, A. K.; Srivastava, S.; Ghosh, J. K., An MD2-derived peptide promotes LPS aggregation, facilitates its internalization in THP-1 cells, and inhibits LPS-induced pro-inflammatory responses. *Cell. Mol. Life Sci.* **2018**, *75* (13), 2431-2446.
508. Wang, J.; Li, Y.; Wang, X.; Chen, W.; Sun, H.; Wang, J., Lipopolysaccharide induces amyloid formation of antimicrobial peptide HAL-2. *Biochim. Biophys. Acta* **2014**, *1838* (11), 2910-2918.
509. Pulido, D.; Nogués, M. V.; Boix, E.; Torrent, M., Lipopolysaccharide Neutralization by Antimicrobial Peptides: A Gambit in the Innate Host Defense Strategy. *J. Innate Immun.* **2012**, *4* (4), 327-336.
510. Singh, S.; Kasetty, G.; Schmidtchen, A.; Malmsten, M., Membrane and lipopolysaccharide interactions of C-terminal peptides from S1 peptidases. *Bba-Biomembranes* **2012**, *1818* (9), 2244-2251.
511. Singh, S.; Papareddy, P.; Morgelin, M.; Schmidtchen, A.; Malmsten, M., Effects of PEGylation on Membrane and Lipopolysaccharide Interactions of Host Defense Peptides. *Biomacromolecules* **2014**, *15* (4), 1337-1345.
512. Sinha, S.; Zheng, L.; Mu, Y.; Ng, W. J.; Bhattacharjya, S., Structure and Interactions of A Host Defense Antimicrobial Peptide Thanatin in Lipopolysaccharide Micelles Reveal Mechanism of Bacterial Cell Agglutination. *Sci. Rep.* **2017**, *7* (1), 17795.
513. Castelletto, V.; Edwards-Gayle, C.; Hamley, I.; Barrett, G.; Seitsonen, J.; Ruokolainen, J., Peptide-Stabilized Emulsions and Gels from an Arginine-Rich Surfactant-Like Peptide with Antimicrobial Activity. *Acs Appl Mater Inter* **2019**, *11*.
514. Surfactants, not size or zeta-potential influence blood-brain barrier passage of polymeric nanoparticles. *European Journal of Pharmaceutics and Biopharmaceutics* **2014**, *87* (1), 19-29.
515. Cho, W. S.; Duffin, R.; Thielbeer, F.; Bradley, M.; Megson, I. L.; Macnee, W.; Poland, C. A.; Tran, C. L.; Donaldson, K., Zeta potential and solubility to toxic ions as mechanisms of lung inflammation caused by metal/metal oxide nanoparticles. *Toxicol Sci* **2012**, *126* (2), 469-77.
516. Choi, M. J.; Soottitawat, A.; Nuchuchua, O.; Min, S. G.; Ruktanonchai, U., Physical and light oxidative properties of eugenol encapsulated by molecular inclusion and emulsion-diffusion method. *Food Res. Int.* **2009**, *42* (1), 148-156.

517. Han, M. Y.; Ahn, H. J.; Shin, M. S.; Kim, S. R., The effect of divalent metal ions on the zeta potential of bubbles. *Water Sci. Technol.* **2004**, *50* (8), 49-56.
518. Li, Z.; Li, H. Y.; Wang, C. F.; Xu, J. H.; Singh, V.; Chen, D. W.; Zhang, J. W., Sodium dodecyl sulfate/beta-cyclodextrin vesicles embedded in chitosan gel for insulin delivery with pH-selective release. *Acta Pharmacol Sin B* **2016**, *6* (4), 344-351.
519. Pavan, C.; Turci, F.; Tomatis, M.; Ghiazza, M.; Lison, D.; Fubini, B., Zeta potential evidences silanol heterogeneity induced by metal contaminants at the quartz surface: Implications in membrane damage. *Colloids Surf. B. Biointerfaces* **2017**, *157*, 449-455.
520. Wyrzykowska, E.; Mikolajczyk, A.; Sikorska, C.; Puzyn, T., Development of a novel in silico model of zeta potential for metal oxide nanoparticles: a nano-QSPR approach. *Nanotechnology* **2016**, *27* (44), 445702.
521. Zhang, Q. F.; Yi, W. J.; Wang, B.; Zhang, J.; Ren, L. F.; Chen, Q. M.; Guo, L. D.; Yu, X. Q., Linear polycations by ring-opening polymerization as non-viral gene delivery vectors. *Biomaterials* **2013**, *34* (21), 5391-5401.
522. Shnoudeh, A. J.; Hamad, I.; Abdo, R. W.; Qadumii, L.; Jaber, A. Y.; Surchi, H. S.; Alkelany, S. Z., Chapter 15 - Synthesis, Characterization, and Applications of Metal Nanoparticles. In *Biomaterials and Bionanotechnology*, Tekade, R. K., Ed. Academic Press: 2019; pp 527-612.
523. Rajpoot, K.; Tekade, R. K., Chapter 10 - Microemulsion as drug and gene delivery vehicle: an inside story. In *Drug Delivery Systems*, Tekade, R. K., Ed. Academic Press: 2019; pp 455-520.
524. Hand, K. V.; Bruen, C. M.; O'Halloran, F.; Panwar, H.; Calderwood, D.; Giblin, L.; Green, B. D., Examining acute and chronic effects of short- and long-chain fatty acids on peptide YY (PYY) gene expression, cellular storage and secretion in STC-1 cells. *Eur J Nutr* **2013**, *52* (4), 1303-13.
525. Fazen, C. H.; Valentin, D.; Fairchild, T. J.; Doyle, R. P., Oral Delivery of the Appetite Suppressing Peptide hPYY(3-36) through the Vitamin B-12 Uptake Pathway. *Journal of Medicinal Chemistry* **2011**, *54* (24), 8707-8711.
526. Shen, J. L.; Song, L. F.; Xin, X.; Wu, D.; Wang, S. B.; Chen, R.; Xu, G. Y., Self-assembled supramolecular hydrogel induced by beta-cyclodextrin and ionic liquid-type imidazolium gemini surfactant. *Colloid Surface A* **2016**, *509*, 512-520.
527. Kang, Y. T.; Tang, X. Y.; Cai, Z. G.; Zhang, X., Supra-Amphiphiles for Functional Assemblies. *Adv. Funct. Mater.* **2016**, *26* (48), 8920-8931.
528. Petek, A.; Krajnc, M.; Petek, A., Study of host-guest interaction between -cyclodextrin and alkyltrimethylammonium bromides in water. *J. Incl. Phenom. Macrocycl. Chem.* **2016**, *86* (3-4), 221-229.
529. Zerkoune, L.; Angelova, A.; Lesieur, S., Nano-Assemblies of Modified Cyclodextrins and Their Complexes with Guest Molecules: Incorporation in Nanostructured Membranes and Amphiphile Nanoarchitectonics Design. *Nanomaterials-Basel* **2014**, *4* (3), 741-765.
530. Li, S. Y.; Xing, P. Y.; Hou, Y. H.; Yang, J. S.; Yang, X. Z.; Wang, B.; Hao, A. Y., Formation of a sheet-like hydrogel from vesicles via precipitates based on an ionic liquid-based surfactant and beta-cyclodextrin. *J. Mol. Liq.* **2013**, *188*, 74-80.
531. Chen, Z.; Wang, T.; Yan, X. F., Synthesis of an elastic beta-cyclodextrin hydrogel cage by hydroxyethyl cellulose. *J. Appl. Polym. Sci.* **2017**, *134* (2).
532. Yang, D. H.; Kim, H. J.; Kim, J. K.; Chun, H. J.; Park, K., Preparation of redox-sensitive beta-CD-based nanoparticles with controlled release of curcumin for improved therapeutic effect on liver cancer in vitro. *J Ind Eng Chem* **2017**, *45*, 156-163.
533. Rahimi, M.; Mobedi, H.; Behnamghader, A., In situ forming poly(lactic acid-co-glycolic acid) implants containing leuprolide acetate/beta-cyclodextrin complexes:

- preparation, characterization, and in vitro drug release. *Int J Polym Mater Po* **2016**, *65* (2), 75-84.
534. Liu, S. M.; Luo, W. C.; Huang, H. H., Characterization and behavior of composite hydrogel prepared from bamboo shoot cellulose and beta-cyclodextrin. *Int. J. Biol. Macromol.* **2016**, *89*, 527-534.
535. Li, R. C.; Zhang, X. T.; Zhang, Q. Y.; Liu, H. H.; Rong, J. H.; Tu, M.; Zeng, R.; Zhao, J. H., beta-cyclodextrin-conjugated hyaluronan hydrogel as a potential drug sustained delivery carrier for wound healing. *J. Appl. Polym. Sci.* **2016**, *133* (9).
536. Peng, K.; Tomatsu, I.; Korobko, A. V.; Kros, A., Cyclodextrin-dextran based in situ hydrogel formation: a carrier for hydrophobic drugs. *Soft Matter* **2010**, *6* (1), 85-87.
537. Swaminathan, S.; Pastero, L.; Serpe, L.; Trotta, F.; Vavia, P.; Aquilano, D.; Trotta, M.; Zara, G.; Cavalli, R., Cyclodextrin-based nanosponges encapsulating camptothecin: Physicochemical characterization, stability and cytotoxicity. *European Journal of Pharmaceutics and Biopharmaceutics* **2010**, *74* (2), 193-201.
538. Boulmedarat, L.; Piel, G.; Bochot, A.; Lesieur, S.; Delattre, L.; Fattal, E., Cyclodextrin-mediated drug release from liposomes dispersed within a bioadhesive gel. *Pharm. Res.* **2005**, *22* (6), 962-971.
539. Liu, Y. Y.; Fan, X. D., Preparation and characterization of a novel responsive hydrogel with a beta-cyclodextrin-based macromonomer. *J. Appl. Polym. Sci.* **2003**, *89* (2), 361-367.
540. Shieh, W. J.; Hedges, A. R., Properties and applications of cyclodextrins. *J Macromol Sci Pure* **1996**, *A33* (5), 673-683.
541. Solaro, R.; Dantone, S.; Bemporad, L.; Chiellini, E., New Polyfunctional Derivatives of Beta-Cyclodextrin Suited for the Formulation of Drug-Release Systems. *J. Bioact. Compatible Polym.* **1993**, *8* (3), 236-250.
542. Schatz, C.; Lecommandoux, S., Polysaccharide-Containing Block Copolymers: Synthesis, Properties and Applications of an Emerging Family of Glycoconjugates. *Macromol. Rapid Commun.* **2010**, *31* (19), 1664-1684.
543. Williams, E. T.; Harris, P. W. R.; Jamaluddin, M. A.; Loomes, K. M.; Hay, D. L.; Brimble, M. A., Solid-Phase Thiol-Ene Lipidation of Peptides for the Synthesis of a Potent CGRP Receptor Antagonist. *Angew. Chem. Int. Ed. Engl.* **2018**, *57* (36), 11640-11643.
544. Espeel, P.; Goethals, F.; Du Prez, F. E., One-Pot Multistep Reactions Based on Thiolactones: Extending the Realm of Thiol-Ene Chemistry in Polymer Synthesis. *J. Am. Chem. Soc.* **2011**, *133* (6), 1678-1681.
545. Rao, J. Y.; Zhang, Y. F.; Zhang, J. Y.; Liu, S. Y., Facile Preparation of Well-Defined AB(2) Y-Shaped Miktoarm Star Polypeptide Copolymer via the Combination of Ring-Opening Polymerization and Click Chemistry. *Biomacromolecules* **2008**, *9* (10), 2586-2593.
546. Bonventre, J. A.; Pryor, J. B.; Harper, B. J.; Harper, S. L., The impact of aminated surface ligands and silica shells on the stability, uptake, and toxicity of engineered silver nanoparticles. *J. Nanopart. Res.* **2014**, *16* (12), 2761.
547. Midekessa, G.; Godakumara, K.; Ord, J.; Viil, J.; Lättekivi, F.; Dissanayake, K.; Kopanchuk, S.; Rinken, A.; Andronowska, A.; Bhattacharjee, S.; Rinken, T.; Fazeli, A., Zeta Potential of Extracellular Vesicles: Toward Understanding the Attributes that Determine Colloidal Stability. *ACS Omega* **2020**, *5* (27), 16701-16710.
548. Kriegseis, S.; Vogl, A. Y.; Aretz, L.; Tonnesen, T.; Telle, R., Zeta potential and long-term stability correlation of carbon-based suspensions for material jetting. *Open Ceramics* **2020**, *4*, 100037.
549. Skoglund, S.; Hedberg, J.; Yunda, E.; Godymchuk, A.; Blomberg, E.; Odnevall Wallinder, I., Difficulties and flaws in performing accurate determinations of zeta potentials of metal nanoparticles in complex solutions-Four case studies. *Plos One* **2017**, *12* (7), e0181735.

550. Wang, N.; Hsu, C.; Zhu, L.; Tseng, S.; Hsu, J. P., Influence of metal oxide nanoparticles concentration on their zeta potential. *J. Colloid Interface Sci.* **2013**, *407*, 22-8.
551. Leong, Y. K., Yield stress and zeta potential of nanoparticulate silica dispersions under the influence of adsorbed hydrolysis products of metal ions--Cu(II), Al(III) and Th(IV). *J. Colloid Interface Sci.* **2005**, *292* (2), 557-66.
552. Iacovino, R.; Rapuano, F.; Caso, J. V.; Russo, A.; Lavorgna, M.; Russo, C.; Isidori, M.; Russo, L.; Malgieri, G.; Isernia, C.,  $\beta$ -Cyclodextrin inclusion complex to improve physicochemical properties of pipemidic acid: characterization and bioactivity evaluation. *Int. J. Mol. Sci.* **2013**, *14* (7), 13022-13041.
553. Sohora, M.; Mandić, L.; Basarić, N., [3 + 2] Cycloaddition with photogenerated azomethine ylides in  $\beta$ -cyclodextrin. *Beilstein J. Org. Chem.* **2020**, *16*, 1296-1304.
554. Aprahamian, I.; Miljanic, O. S.; Dichtel, W. R.; Isoda, K.; Yasuda, T.; Kato, T.; Stoddart, J. F., Clicked interlocked molecules. *Bull. Chem. Soc. Jpn.* **2007**, *80* (10), 1856-1869.
555. Fischer, M.; Ritter, H., Cyclodextrins in polymer synthesis: free radical polymerization of cyclodextrin complexes with oxazoline-functionalized vinyl monomers as guest molecules in aqueous medium. *Macromol. Rapid Commun.* **2000**, *21* (3), 142-145.
556. Jia, Y. G.; Malveau, C.; Mezour, M. A.; Perepichka, D. F.; Zhu, X. X., A Molecular Necklace: Threading beta-Cyclodextrins onto Polymers Derived from Bile Acids. *Angew Chem Int Edit* **2016**, *55* (39), 11979-11983.
557. Xue, M.; Su, Y. S.; Chen, C. F., Isomeric Squaraine-Based [2]Pseudorotaxanes and [2]Rotaxanes: Synthesis, Optical Properties, and Their Tubular Structures in the Solid State. *Chem-Eur J* **2010**, *16* (28), 8537-8544.
558. Zou, C. J.; Tang, Q. W.; Zhao, P. W.; Guan, E. D.; Wu, X.; Ye, H., Further study on the inclusion complex of 2-phosphonobutane-1,2,4-tricarboxylic acid with beta-cyclodextrin: A new insight of high inhibition efficiency for protecting steel corrosion. *J Petrol Sci Eng* **2013**, *103*, 29-35.
559. Zhang, G. L.; Liang, F.; Song, X. M.; Liu, D. L.; Li, M. J.; Wu, Q. H., New amphiphilic biodegradable beta-cyclodextrin/poly(L-leucine) copolymers: Synthesis, characterization, and micellization. *Carbohydr. Polym.* **2010**, *80* (3), 885-890.
560. Yong-Cun, Y.; Shao-Ming, C.; Hao, S.; Yong, Z.; Rong, H.; Hong-You, Z.; Yan, Z., Inclusion complexation of a novel diaminodiphenyl disulphide bridged bis(beta-cyclodextrin) with bile salts. *Phys. Chem. Liq.* **2011**, *49* (4), 482-492.
561. Yao, Q.; You, B.; Zhou, S. L.; Chen, M.; Wang, Y. J.; Li, W., Inclusion complexes of cypermethrin and permethrin with monochlorotriazinyl-beta-cyclodextrin: A combined spectroscopy, TG/DSC and DFT study. *Spectrochimica Acta Part a-Molecular and Biomolecular Spectroscopy* **2014**, *117*, 576-586.
562. Yan, J. C.; Dong, S. J., Self-assembly of the pre-formed inclusion complexes between cyclodextrins and alkanethiols on gold electrodes. *J. Electroanal. Chem.* **1997**, *440* (1-2), 229-238.
563. Xu, M. Y.; Wu, S. Z.; Zeng, F.; Yu, C. M., Cyclodextrin Supramolecular Complex as a Water-Soluble Ratiometric Sensor for Ferric Ion Sensing. *Langmuir* **2010**, *26* (6), 4529-4534.
564. Xu, D. D.; Wang, L. J.; Gourevich, D.; Kabha, E.; Arditti, F.; Athamna, M.; Cochran, S.; Melzer, A.; Gnaim, J. M., Synthesis and Inclusion Study of a Novel gamma-Cyclodextrin Derivative as a Potential Thermo-Sensitive Carrier for Doxorubicin. *Chem Pharm Bull* **2014**, *62* (7), 627-635.
565. Xin, J. Y.; Guo, Z. Z.; Chen, X. Y.; Jiang, W. F.; Li, J. S.; Li, M. L., Study of branched cationic beta-cyclodextrin polymer/indomethacin complex and its release profile from alginate hydrogel. *Int. J. Pharm.* **2010**, *386* (1-2), 221-228.